MECHANISMS OF ACUTE LEUKEMIA DISEASE INITIATION AND MAINTENANCE THROUGH MANIPULATION OF IGF1R AND RUNX FAMILY MEMBERS

by

Catherine Elfi Sarah Jenkins

B.Sc., The University of British Columbia, 2007

A THESIS SUBMITTED IN PARTIAL FULFILLMENT OF

THE REQUIREMENTS FOR THE DEGREE OF

DOCTOR OF PHILOSOPHY

in

THE FACULTY OF GRADUATE AND POSTDOCTORAL STUDIES

(Interdisciplinary Oncology)

THE UNIVERSITY OF BRITISH COLUMBIA

(Vancouver)

April 2017

Abstract

Characterization of new pathways in Acute Myeloid Leukemia and T-cell Acute Lymphoblastic Leukemia which contribute to oncogenesis is necessary to relieve dependence on conventional chemotherapy for treatment of these diseases. In this dissertation, I characterized the role of signaling molecules (IGF1R) and transcription factors (RUNX1, RUNX3, NOTCH1) in regulating mechanisms of leukemia initiation and maintenance. I discovered that committed myeloid progenitor cells with genetically reduced levels of IGF1R were less susceptible to myelogenous leukemogenic transformation due, at least in part, to a cell-autonomous defect in clonogenic activity. Genetic deletion of IGF1R by inducible Cre recombinase however had no effect on growth/survival of established leukemia cells. I raise the possibility that IGF1R inhibitors in clinical development may be acting through alternate/related pathways. Second, in a retroviral insertional mutagenesis study, I cloned retroviral integration sites from hNOTCH1ΔE mouse leukemias to find genes which collaborate with Notch signaling in T-ALL initiation. Common integration sites include the previously identified *Ikzf1*, and a novel potentially Notch-collaborating gene, *Runx3*. Using a multicistronic lentiviral system, I show that RUNX1A, RUNX1B and RUNX3 were able to collaborate with the ΔEΔL allele of NOTCH1 to initiate leukemia. Finally, I sought to understand how RUNX1 and RUNX3 contribute to the biology of established T-cell leukemias. I found that both RUNX1 and RUNX3 contribute to T-ALL cell proliferation and survival. Although RUNX3 can induce cell proliferation, RUNX1 expression is finely tuned with overexpression and knockdown resulting in negative growth phenotypes. This may be in part to regulation of *MYC*, *IL7R*, *IGF1R*, *and CDKN1B* as well as affecting genome-wide H3K27Ac. I found that RUNX1 expression was targeted by the CDK7 inhibitor, THZ1. RUNX1 and RUNX3 are mediators of Notch-directed regulation of PKCθ, and as such are indirect regulators of LIC-activity. Finally, I showed that RUNX1 and Notch signaling provide complimentary, additive signals for growth of T-ALL cells. These experiments provide insight into the role of *RUNX1* mutations in T-cell leukemia and point to a complementary role in supporting the Notch pathway.

Preface

The research described in Chapters 2-4 was done in Dr. Andrew Weng's laboratory in the Terry Fox Laboratory of the BC Cancer Agency by myself, Catherine Jenkins. I performed all of the experiments and analyzed the data with the exceptions listed below. Dr. Weng and I contributed equally to the experimental design.

A version of chapter 2 has been published in *Experimental Hematology*:

[Jenkins CR], Shevchuk OO, Giambra V, Lam SH, Carboni JM, Gottardis MM, Holzenberger M, Pollak M, Humphries RK, Weng AP. IGF signaling contributes to malignant transformation of hematopoietic progenitors by the MLL-AF9 oncoprotein. *Experimental Hematology*. 2012 Sep;40(9):715-723.e6. doi: 10.1016/j.exphem.2012.05.003. License: 4013180580620.

I wrote the manuscript and interpreted the results with Dr. Weng, planned the experiments with Dr. Weng and Vincenzo Giambra, and collected the data with assistance from Olena Shevchuk and Sonya Lam.

For Chapter 3, the experimental design was generated by Dr. Weng and I. With help from Olena Shevchuk, I performed the experiments, generated the data and interpreted the results.

Some of the data from Chapter 4 has previously been published in *Nature* (Figure 4.35), and *Nature Medicine* (Figure 4.37, Figure 4.38):

Kwiatkowski N, Zhang T, Rahl PB, Abraham BJ, Reddy J, Ficarro SB, Dastur A, Amzallag A, Ramaswamy S, Tesar B, [Jenkins CE], Hannett NM, McMillin D, Sanda T, Sim T, Kim ND, Look T, Mitsiades CS, Weng AP, Brown JR, Benes CH, Marto JA, Young RA, Gray NS. Targeting transcription regulation in cancer with a covalent CDK7

inhibitor. *Nature*. 2014 Jul 31;511(7511):616-20. doi: 10.1038/nature13393.

Giambra V, [Jenkins CR], Wang H, Lam SH, Shevchuk OO, Nemirovsky O, Wai C, Gusscott S, Chiang MY, Aster JC, Humphries RK, Eaves C, Weng AP. NOTCH1 promotes T cell leukemia-initiating activity by RUNX-mediated regulation of PKC-θ and reactive oxygen species. *Nat Med*. 2012 Nov;18(11):1693-8. doi: 10.1038/nm.2960. Epub 2012 Oct 21.

A version of the remainder of Chapter 4 is in preparation to be submitted for publication:

[Jenkins CE], Islam R, Shevchuk OO, Wong RAJ, Giambra V, Gusscott S, Rana G, Gray NS, Hirst M, Weng AP. RUNX1 promotes growth of established human T-ALL cells through regulation of key target genes.

I planned the experiments and wrote the manuscript with Dr. Weng. With the assistance of Olena Shevchuk, Rachel Wong and Gurneet Rana, I collected the data and interpreted the results. Vincenzo Giambra and Sam Gusscott discussed results and assisted with western blotting. Nathanael Gray developed and provided the THZ1 compound and gave advice towards experimental design.

The RNA-seq and ChIP-seq data in Chapter 4 represents a 50/50 shared contribution between myself and a graduate student from Dr. Martin Hirst's lab, Rashedul Islam (University of British Columbia, Bioinformatics Program, Department of Microbiology and Immunology). I conceived of the experimental design, generated the samples for the RNA-seq and ChIP-seq experiments and provided guidance for analysis. RNA-seq and ChIP-seq libraries were generated by Michelle Moksa and sequenced at Canada's Michael Smith Genome Sciences Centre and in Dr. Martin Hirst's lab. Rashedul Islam analyzed the data and generated figures.

All cell sorting was done in the Terry Fox Laboratory Flow Core by David Ko, Wenbo Xu and Gayle Thornbury.

All animals were housed in the BC Cancer Agency Animal Resource Centre under pathogen-free conditions and in compliance with protocols approved by the University of British Columbia Committee for Animal Care under protocols A09-0771, A09-0909, A13-0318 and A14-0098. Human patient-derived xenograft samples were handled according to ethics protocols H09-61292 and H13-02326 from the University of British Columbia - British Columbia Cancer Agency Research Ethics Board (UBC BCCA REB). Primary patient samples for research purposes were obtained by informed consent of patients or their legal guardians at initial diagnosis by institutional review board-approved protocols and by guidelines as set by the Declaration of Helsinki.

Table of Contents

List of Tables

List of Figures

List of Abbreviations

4-OHT: 4-hydroxytamoxifen

5-FU: 5-Fluorouracil

Ab: Antibody

Ac: Acetylation

AD: Activation Domain

AGM: aorta, gonads, and mesonephroi

ALL: Acute lymphoblastic leukemia

AML1: acute myeloid leukemia 1

ANOVA: Analysis of Variance

APC: Allophycocyanin

APML: Acute Promyelocytic Leukemia

ASXL1: additional sex combs like 1

ATRA: all-*trans* retinoic acid

B-ALL: B-cell precursor acute lymphoblastic leukemia

BCL11B: B-cell lymphoma/leukemia 11B

bHLH: basic helix-loop-helix

BM: bone marrow

BMI1: B cell-specific Moloney murine leukemia virus integration site 1

BMS: Bristol-Myers Squibb

BRD4: Bromodomain-containing protein 4

C/EBPα: CCAAT/enhancer binding protein α

CBF: core binding factor

CBFB: core binding factor beta

CBP: CREB-binding protein

CDK: cyclin-dependent kinase

CDKN1B: cyclin-dependent kinase inhibitor 1B

CDKN2A: cyclin-dependent kinase inhibitor 2A

CDKN2B: cyclin-dependent kinase inhibitor 2B

cDNA: complementary DNA

CEBPA: CCAAT/enhancer-binding protein alpha

CFC: Colony-forming cell

CFU-S: Colony-forming unit spleen

CHYSEL: *cis*-acting hydrolase elements

CIS: common insertion/integration site

CLP: common lymphoid progenitor

CNS: central nervous system

DAPI: 4',6-Diamidino-2-Phenylindole

DKO: double knockout

DL1: delta-like 1

DL4: delta-like 4

DMSO: Dimethyl sulfoxide

DN: Double negative ($CD4^-CD8^-$)

DN1: Double negative 1 ($CD4^-CD8^-CD44^+CD25^-$)

DN2: Double negative 2 ($CD4^-CD8^-CD44^+CD25^+$)

DN3: Double negative 3 ($CD4^-CD8^-CD44^-CD25^+$)

DN4: Double negative 4 ($CD4^-CD8^-CD44^-CD25^-$)

DNA: Deoxyribonucleic acid

DNMT3A: DNA (cytosine-5)-methyltransferase 3A

DOT1L: Disruptor of telomeric silencing 1-like

DP: Double positive ($CD4^+CD8^+$)

dsRNA: double-standed RNA

ERK: extracellular signal–regulated kinase

ETO: Eight Twenty One

ETP: early T-cell precursor

EZH2: Enhancer of zeste homolog 2

FA: Fanconi anemia

FAB: French-American-British classification system

FACS: Fluorescence activated cell sorting

FBS: Fetal bovine serum

FBXW7: F-box and WD repeat domain-containing 7

FITC: Fluorescein isothiocyanate

FLT3: fms like tyrosine kinase 3

FMDV: foot-and-mouth disease virus

FPD: Familial platelet disorder

FSC: forward light scatter

g: Gram

G-CSF: Granulocyte colony stimulating factor

GFP: green fluorescent protein

GM-CSF: Granulocyte macrophage colony stimulating factor

GMP: granulocyte-macrophage progenitor

GSI: gamma secretase inhibitor (γ-secretase inhibitor)

H3K4: Histone 3 Lysine 4

H3K27: Histone 3 Lysine 27

HA: Hemagglutinin

HAT: Histone acetyltransferases

HDAC: Histone deacetylases

HIPK2: Homeodomain-interacting protein kinase 2

HIV: human immunodeficiency virus

hN1: human NOTCH1

HOXA: Homeobox protein A

HSC: hematopoietic stem cell

HSPC: hematopoietic stem and progenitor cell

ICN: intracellular notch

ID: Inhibitory Domain

IDH: Isocitrate dehydrogenase

IGF: Insulin-like growth factor

IGH: Immunoglobulin heavy locus

Ikzf1: Ikaros

IMDM: Iscove's Modified Dulbecco's Medium

InsR: Insulin Receptor

IRES: Internal Ribosome Entry Site

IRS: Insulin Receptor Substrate

INK4: Inhibitors of CDK4

IL: Interleukin

JAG1: Jagged 1

JAK: janus kinase

Kb: Kilobase pairs

kDa: Kilodaltons

KMT2A: Histone-lysine N-methyltransferase 2A

KRAS: Kirsten rat sarcoma viral oncogene homolog

L: Litre

LIC: Leukemia initiating cell

LMO1: LIM domain only 1

LMO2: LIM domain only 2

LSK: $Lin^{-}Sca1^{+}c\text{-}kit^{+}$

LT-HSC: long-term hematopoietic stem cell

LTR: long terminal repeats

LYL1: Lymphoblastic leukemia derived sequence 1

μg: Microgram

μl: Microlitre

μM: Micromolar

M-CSF: Macrophage colony stimulating factor

mg: Milligram

miRNA: micro RNA

ml: Millilitre

mM: Millimolar

mRNA: Messenger ribonucleic acid

mAb: Monoclonal antibody

MDS: myelodysplastic syndrome

MDS-AML: MDS-related acute myeloid leukemia

MEK: Mitogen-activated protein kinase kinase

MEP: megakaryocyte-erythroid progenitors

MKL1: megakaryoblastic leukemia 1

MLL: mixed-lineage leukemia

MoMLV: Moloney Murine Leukemia Virus

MPD: Myeloproliferative disease

MSCV: Murine Stem Cell Virus

MTA: Material transfer agreement

MuLV: Murine Leukemia Virus

mw: molecular weight

MYB: myeloblastosis proto-oncogene

MYC: avian myelocytomatosis viral oncogene homolog

MYH11: myosin heavy chain 11

NOTCH1: Notch homolog 1, translocation-associated

NFAT: Nuclear factor of activated T-cells

ng: nanogram

NGFR: nerve growth factor receptor

NKX2: NK2 homeobox

NMTS: nuclear matrix targeting signal

NPM1: Nucleophosmin

NRAS: Neuroblastoma RAS viral oncogene homolog

NSG: NOD/Scid/*Il2rg–/–*

NUP214: Nucleoporin 214

P53: tumor protein 53

PBS: Phosphate-buffered saline

PCR: Polymerase chain reaction

PDX: patient-derived xenograft

PE: Phycoerythrin

PEBP2: polyomavirus enhancer-binding protein 2

PEI: polyethylenimine

PerCP: Peridinin chlorophyll

PI: propidium iodide

PI3K: Phosphatidylinositol-4,5-bisphosphate 3-kinase

PML: Promyelocytic leukemia protein

poly I:C: Polyinosinic:polycytidylic acid

PRC: polycomb repressive complex

PRKCQ: Protein Kinase C θ

PRMT: protein arginine methyl transferase

Py: pyrimidine

RARA: Retinoic acid receptor alpha

RBM: RNA binding protein

RNA: ribonucleic acid

RNAi: RNA interference

ROS: reactive oxygen species

RSV: Rous sarcoma virus

RTCGD: Retroviral Tagged Cancer Gene Database

RTK: Receptor Tyrosine Kinase

RT-PCR: reverse transcription-polymerase chain reaction

RUNX: Runt-related transcription factor

SCF: Stem Cell Factor (Steel Factor/kit ligand)

SCID: Severe combined immunodeficiency

shRNA: small hairpin RNA

shRX1: shRNA targeting RUNX1

shRUNX1: shRNA targeting RUNX1

siRNA: small interfering RNA

SIL: SCL-interrupting locus

SF3B1: Splicing factor 3B subunit 1

SP: single positive

SRSF2: Serine/arginine-rich splicing factor 2

SSC: Side light scatter

STAT: Signal transducers and activators of transcription

TAL1: T-cell acute lymphocytic leukemia 1

TAL2: T-cell acute lymphocytic leukemia 2

T-ALL: T-cell acute lymphoblastic leukemia

TAN-1: Translocation-Associated Notch Protein

TCR: T-cell receptor

TET2: Tet methylcytosine dioxygenase 2

TF: transcription factor

TGF: Transforming growth factor

TLE: Transducin-like enhancer

TLX: T-cell leukemia homeobox

TP53: Tumor protein p53

TrxG: trithorax group

TSS: Transcription start site

U2AF1: U2 small nuclear RNA auxiliary factor 1

UTR: untranslated region

WHO: world health organization

Wnt: int/Wingless

WT: Wild-type

WT1: Wilms tumor protein

ZRSR2: U2 small nuclear ribonucleoprotein auxiliary factor 35 kDa subunit-related protein 2

Acknowledgements

I want to thank my supervisor, Dr. Andrew Weng for his guidance, knowledge, and support in my studies and research. I will take forward an abundance of research skills and an ability to think critically about my research and the research of others thanks to his supervision.

I would also like to thank my thesis supervisory committee, Dr. Gregg Morin, Dr. Martin Hirst and Dr. Keith Humphries. Their direction and advice has greatly shaped and benefitted my research through their thoughtful encouragement and critique.

I received support from a CIHR Banting & Best Canada Graduate Scholarship Doctoral Award (CGS-D) and a UBC Four Year Fellowship. I was also supported by other funds from the Canadian Cancer Society Research Institute (CCSRI), the Canadian Institutes of Health Research (CIHR), The UBC Interdisciplinary Oncology Program, the Terry Fox Foundation and the Leukemia & Lymphoma Society of Canada.

I would like to thank Rachel Wong, Sneha Balani, Helen Shevchuk and Gurneet Rana for their experimental support, and emotional support; Sam Gusscott for his cloning advice, early mouse teachings and guidance in navigating the lab; Vincenzo Giambra for his early mentorship and helping me to think big about science; Courteney Lai for experimental discussions and advice; Sonya Lam for help in trying to achieve an admirable western blot. I would also like to thank all of the other past and present Weng Lab/Terry Fox Lab members who have provided assistance or discussed my research with me.

I would like to thank Dr. Nancy Speck, Dr. Takeshi Egawa and Dr. Martin Holzenberger for the gift of the *Runx1*$^{lox/lox}$, *Cbfb*$^{lox/lox}$ and *Igf1r*^{neo} mice, respectively. I would like to thank Dr. Nathanael Gray for the THZ1 compound. I would like to thank Dr. Scott Armstrong for the gift of the MLL-AF9 construct, Dr. Dixie Mager for providing cell lines, and Wenbo Xu, David Ko, Maura Gasparetto and Tobias Berg who assisted with FACS sorting. I would like to thank Dr. Michael Pollak, Dr. Jon Aster and Dr. Hongfang Wang for discussion of results.

I would also like to thank Dr. Angela Brooks-Wilson and the Interdisciplinary Oncology Program for their support in completing my thesis.

I would like to thank my family and friends, including but not limited to: Elfriede, Otto, Martha, Hal, Angelica, Evelin, Erika, David, David, Rick, Helen, Rachel, and Sneha. They have enriched my life and their support is immeasurable.

I would finally like to thank my parents, Elfi Jenkins and Robert Jenkins, for not only their unflinching love but also the emotional and financial support they have provided.

Dedication

This dissertation is dedicated to my mom and dad, my family, and to girls like us.

Chapter 1: General Introduction

1.1 Dissertation overview

Acute leukemias are a heterogeneous group of hematologic malignancy which are medical emergencies requiring immediate intervention. The first case of leukemia was described by Velpeau in 1827 but the first report of rational treatment of acute leukemia was carried out by Sidney Farber in 1948 using chemotherapy[1]. Despite incremental increases in survival, the treatment used to fight leukemia is non-specific and highly toxic. T-cell Acute Lymphoblastic Leukemia (T-ALL) and Acute Myeloid Leukemia (AML) are generally diseases of the very young and very old, respectively. Children are generally better at tolerating increasingly higher chemotherapy regimens with the caveat of relatively harsh side effects, while older adults are often unable to tolerate levels of chemotherapy required for cure. Thus, targeted therapies which are selective for the tumour cells are needed to reduce the burden on chemotherapy for treatment and thereby reduce treatment-associated side effects and achieve cure in a greater number of patients. The research outlined in this dissertation focused on mechanisms of leukemia initiation and maintenance through manipulation of IGF1R (in AML) and the RUNX family of transcription factors (in T-ALL).

Work in the Weng lab identified the receptor tyrosine kinase IGF1R to be necessary for both bulk tumour growth and leukemia stem cell activity in T-ALL[2]. Using both genetic and pharmacologic tools, I sought to extend these findings to AML to determine if IGF1R was a more broadly applicable drug target, or if it remained primarily relevant in T-cell neoplasms. Using an MLL-AF9 mouse model of AML and human AML cell lines, I tried to discover roles for IGF1R in leukemogenesis, clonogenic growth and bulk sensitivity to IGF1R inhibition.

Retroviral insertional mutagenesis screens have proven to be useful tools in uncovering potential oncogenes and tumour suppressors, and to discover collaboration between pathways that aid in the establishment of a leukemic clone. A previous screen in murine

T-ALL using an activated allele of the oncogene NOTCH1 had primarily uncovered mutations which serve to further augment Notch signaling[3]. As such I cloned insertion sites from leukemias generated using a more leukemogenic allele of NOTCH1 to find pathways outside of the Notch pathway that support oncogenesis in parallel.

Finally, *RUNX1* was recently been found to be mutated in T-ALL and had been hypothesized to have tumour suppressive activity in this context[4-6]. Contemporary studies described that RUNX1 was found near NOTCH1 and TAL1 in transcription complexes that supported an oncogenic gene expression programme[7-9]. To reconcile these differences, I performed experiments to determine the role of RUNX1 in established T-ALL cell growth and to find mediators of any phenotypes uncovered.

1.2 Acute Myeloid Leukemia

1.2.1 Clinical presentation and diagnosis

Acute Myeloid Leukemia (AML) is a clonal malignancy of developmentally arrested immature myeloid blast cells in the blood, bone marrow and other tissues. Unfortunately, this disease is primarily diagnosed in older adults and difficulties in tolerating therapy result in generally poor prognostic outcomes[10]. Diagnosis of AML is made based on blast cell morphology by blood smear, showing granular cytoplasm (with or without differentiation), and flow cytometry analysis of immunophenotype using various myeloid differentiation markers. Analysis of cytogenetics is used as a critical way to determine the subtype of AML, and is often associated with specific treatment plans and prognoses. In general, the initial treatment plan depends primarily on whether or not the patient can be given intensive induction chemotherapy or not, followed by consolidation therapy and salvage therapy. Standard induction chemotherapy involves continuous-infusion cytarabine with the addition of an anthracycline such as daunorubicin. Recently, the addition of an anti-CD33 monoclonal antibody which has been conjugated to calicheamicin (genmtuzumab ozogamicin) to induction regimens has been shown to reduce risk of relapse and has improved the rate of survival with certain lower risk groups[11]. Following induction of remission, patients are given either

further rounds of chemotherapy (cycles of cytarabine) or assessed for suitability for allogenic bone marrow transplantation based on a number of risk factors. Stem cell transplantation is typically favoured only in those that are expected to not achieve complete remission and as the graft-versus-leukemia effect may enhance eradication of tumour cells, has added benefits[12]. Older patients are often not able to withstand intensive induction or consolidation chemotherapy and as such, lower doses of cytarabine are often used in conjunction with hypomethylating agents such as decitabine and azacitidine, but concurrently other important factors which seek to preserve quality of life are factored in. Salvage therapy is critical in patients with relapsed disease, and the patient's health and wishes inform the process in attempt to achieve remission in order to perform allogeneic stem cell transplantation. AML remains a poorly cured disease and as chemotherapy remains difficult to tolerate in a large fraction of AML patients there is a need for targeted therapies to reduce the need for toxic chemotherapeutics.

1.2.2 Chromosomal translocations and point mutations

Acute Myeloid Leukemia frequently displays great cytogenetic diversity, with over 50 different patient subgroups[13]. For brevity, I will discuss only a subset of those described in the WHO Classification which have well-described clinical outcomes and pathology.

The t(8;21)(q22;q22) translocation creating the *RUNX1-RUNX1T1* (also known as *RUNX1-ETO*) fusion is found in about 12% of patients and has maturation of neutrophils, in the French-American-British (FAB) category M2[14]. It is hypothesized that the RUNX1-ETO protein acts in a dominant-negative fashion compared to wild-type RUNX1 function, causing a differentiation block and enhancing the self-renewal of hematopoietic progenitors[15-19]. The dimeric binding partner of *RUNX1*, *CBFB*, is also frequently rearranged in Acute myelomonocytic leukemia with eosinophilia (FAB category M4) in the *CBFB-MYH11* translocation [inv(16)(p13.1q22) or t(16;16)(p13.1;q22)] and is similarly thought to generate a protein which antagonizes wild-type RUNX1 functioning by forcing RUNX1 to interact with cytoplasmic actin or add repressive domains to CBFB[20-22]. The MLL-AF9 fusion protein is a result of the

t(9;11)(p22;q23) mutation, also known as *MLL-MLLT3*, and is typically associated with monocytic features of the M5 grouping of the FAB classification scheme and has an intermediate survival, but typically better outcome in comparison to other *MLL* translocations[23-25]. *MLL* translocations are discussed in further detail in Section 1.2.3.

The Cancer Genome Atlas Research Network identified nine functional categories of genes that are mutated based on analyzing the genomes from 200 *de novo* AML patients[26]. Among them are point mutations, copy number changes or other alterations affecting genes involved in [1] aberrant signaling (*FLT3*, *KIT, NRAS/KRAS*), [2] fusion proteins (*PML-RARA*, *MYH11-CBFB*) [3] tumour suppressors (*TP53,* WT1), [4] transcription factors (*RUNX1, CEBPA*), [5] epigenetic patterning (*EZH2, ASXL1, DOT1L, KMT2A, MLLT3*), [6] protein localization (*NPM1*), [7] CpG DNA methylation (*TET2*, *IDH1/IDH2*, *DNMT3A*), [7] the cohesin complex (*ASXL1*) and [8] the spliceosome (*SRSF2, SF3B1, U2AF1, ZRSR2*). These mutations underscore the heterogeneity of Acute Myeloid Leukemia and suggest that many molecular processes are dysregulated in this disease.

1.2.3 MLL fusion proteins.

MLL, a homologue of the *Drosophila melanogaster* gene trithorax is a member of the trithorax group (TrxG) protein family and catalyses the methylation of H3K4 (histone H3 lysine 4) which has been shown to correlate with gene expression[27]. The *MLL* gene is frequently found to participate in translocations with a variety of other genes in Acute Myeloid Leukemia, Acute Lymphoblastic Leukemia, and in close to all cases of Mixed Lineage Leukemia which lead to in-frame fusion proteins containing the first 8-13 exons of *MLL* (**Figure 1.1**). *MLL* translocations are found in the vast majority of pediatric leukemia, but are present less frequently in older children/adolescents and adults[28,29]. There are scores of fusion partners identified, however the most frequent are *MLL-AF4* [t(4;11)(q21;23)], *MLL-ENL* [t(11;19)(q23;p13.3)], *MLL-AF10* [t(10;11)(p12;q23)], *MLL-AF6* [t(6;11)(q27;q23)] and *MLL-AF9* [t(9;11)(p22;q23)][29,30]. A key aspect of MLL fusion proteins is their inability to methylate H3K4 due to the loss of the SET domain in the C-terminus of the wild-type *MLL* gene, but yet they remain able to regulate the expression

of genes including the HoxA cluster[31,32]. MLL-translocated leukemias represent an important subgroup of AML that deregulate gene expression in part through remodeling of the epigenome.

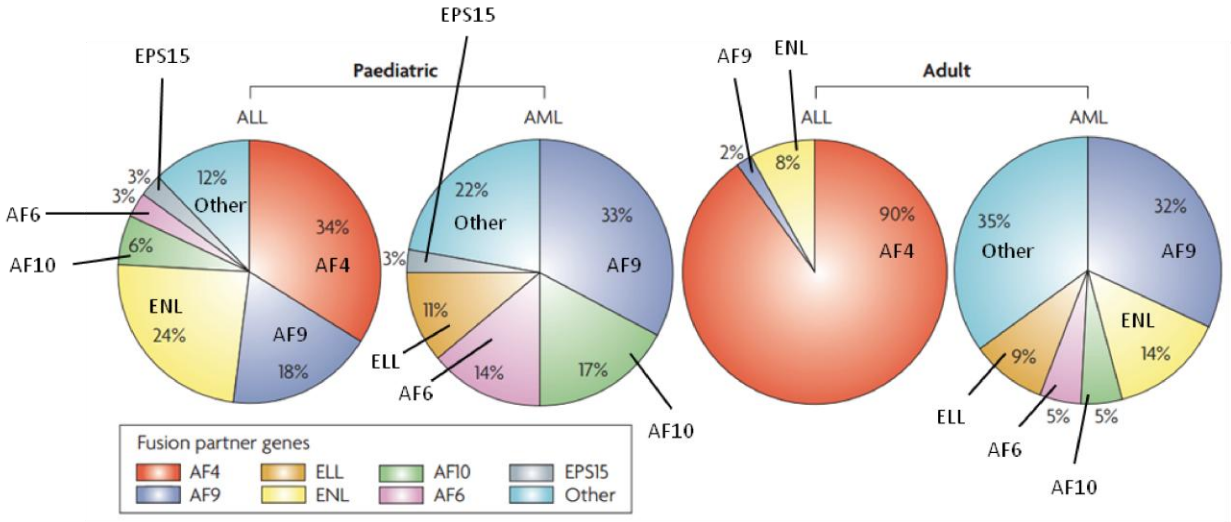

Figure 1.1 Distribution of major MLL fusion partner genes in *de novo* childhood and adult leukemias.

Mixed lineage leukemia (*MLL*) rearrangements are found in approximately 5% of acute lymphoblastic leukemias (ALL), approximately 5–10% of acute myeloid leukemias (AML) and virtually all cases of mixed lineage (or biphenotypic) leukemias (MLL)[29,30,33]. Major MLL fusion partner genes are AF4, which is predominantly found in ALL; AF9, which is predominantly found in AML; and ENL, which is found in both ALL and AML. Reprinted by permission from Macmillan Publishers Ltd: *Nature Reviews Cancer*. Figure from *MLL* translocations, histone modifications and leukemia stem-cell development (Krivtsov and Armstrong, 2007), doi:10.1038/nrc2253. © Nature Publishing group 2007, accessed December 2016.

1.3 T-cell Acute Lymphoblastic Leukemia

1.3.1 Clinical presentation and diagnosis

T-cell Acute Lymphoblastic Leukemia (T-ALL) is a clonal malignancy of developmentally arrested immature T-lymphoid blast cells that constitutes 20-25% of adult and 10-15% of childhood ALL[34,35]. Areas commonly infiltrated involve the blood, bone marrow, thymus (mediastinal mass), lymph nodes, spleen, liver and sometimes less commonly in other sites. T-ALL cells are small-medium sized with little cytoplasm and nuclei containing regions of condensed and dispersed chromatin and non-prominent nucleoli[36]. Diagnosis of T-ALL is informed by flow cytometric analysis of immunophenotype and microscopy to identify blast cell morphology[37]. Additional analysis of cytogenetics informs subtype analysis however whole genome analysis is expected to play a role as

it becomes more economical. Minimum residual disease following therapy is a powerful prognostic factor in disease and is determined by flow cytometry or PCR amplification of transcripts specific to disease subtypes. A subtype of T-ALL, early T-cell precursor acute lymphoblastic leukemia is particularly aggressive and has poor treatment and survival outcomes[38]. Recent studies have shown that this subtype is defined by perturbed expression of stem and myeloid markers as well as an immunophenotype similar to murine early thymic precursors[39]. T-ALL is usually treated using standard chemotherapy regimens used in three phases: induction therapy, consolidation therapy and maintenance therapy. Induction therapy involves high dose glucocorticoids (dexamethasone/prednisone), asparaginase, vincristine and at times an anthracycline. Consolidation therapy (also called intensification therapy) usually involves mercaptopurine and the anti-folate methotrexate (sometimes in combination with other therapies). Finally, maintenance therapy often entails 2 years of regular treatment with many of the above agents in order to eliminate any residual cancer cells. The central nervous system (CNS) can harbor cells which are not easily reached using intravenous delivery and so intra-thecal delivery of chemotherapy is used to prevent relapse from lurking residual cells and has proven to have great utility in comparison to the effective, but highly toxic prophylactic cranial irradiation which has a number of highly problematic side effects[37,40,41]. In high-risk patients, allogeneic stem cell transplants are considered advantageous and are often used in adult settings, while the use of higher-dose protocols often used in children may reduce the need for transplantation[37]. As treatment has generated improved survival, it has underscored the need for therapy which elicits fewer relatively harmful side effects.

1.3.2 Gross chromosomal lesions, point mutations and gene dysregulation

The Notch pathway was initially implicated in T-ALL due to the discovery of the t(7;9)(q34;q34.3) TAN-1 translocation by Leif Ellisen in Jeffrey Sklar's group which produces high levels of intracellular NOTCH1 (ICN) under the control of the *TCRβ* promoter[42]. Following this work, Warren Pear in David Baltimore's lab overexpressed truncated forms of NOTCH1 in HSPC-enriched populations of cells and found that it

was able to induce T-ALL in mice[43]. The pathway was widely considered a key player in T-cell leukemias after over 50% of T-ALL samples were found to have activating mutations in *NOTCH1*[44]. The Notch pathway is highly conserved and involved in critically important cell fate decisions which typically create divergent binary differentiation outcomes between the signal-sending cell (expressing Notch ligands such as DL1, DL4, JAG1) and the signal-receiving cells (expressing the Notch receptor). Notch drives T-cell lineage commitment and differentiation towards a burst of proliferation through β-selection after which cells become less dependent on Notch signaling[45-48]. Despite the availability of γ-secretase inhibitors which function to block Notch signaling, many T-ALL samples exhibit resistance and gut toxicity in patients is a key limitation[44,49].

The *CDKN2A* locus, encoding $p16^{INK4A}$ and $p14^{ARF}$ is deleted or repressed by BMI1 in the vast majority of T-ALL cells, promoting G_1-S cell cycle progression and resistance to apoptosis[50-53]. Additional tumour suppressor cell cycle regulators that are frequently deleted or silenced in T-cell leukemias are *RB1* (retinoblastoma 1) and *CDKN1B* ($p27^{KIP1}$)[54,55].

T-ALL cells typically have clonal T-cell receptor (TCR) gene rearrangements, but about 20% of cases also have rearrangements in *IGH* and in total, 50-70% of tumours have an abnormal karyotype[56-59]. A variety of genes are often rearranged to become juxtaposed with TCR loci, often with strong TCR promoters driving the expression of an oncogenic transcription factor. The most commonly implicated rearrangements involve *TCR* alpha and delta loci at 14q11.2, gamma locus at 7p14-15, and the beta locus at 7q35. LIM domain only (LMO) genes such as LMO1 and LMO2 were genes described originally as translocation partners with TCR[60,61]. *TAL1, TAL2* and *LYL1* are basic helix-loop-helix (bHLH) transcription factors which have been found to define expression profiles along with LMO family members[62-65] disrupted by TCR translocation or microdeletions which put the *TAL1* gene under control of the *SIL* promoter, or by mutation-directed *de novo* MYB-enhancer creation[66-68]. Interestingly, TAL1 participates in a feed-forward regulatory loop with RUNX1, GATA3 and MYB, and this loop can be

interrupted using a CDK7 inhibitor which inhibits the transcription of *RUNX1*[7,69]. *MYB* can be altered by translocation or focal amplification which serves to enhance cell proliferation and survival[70-72]. *MYC* is one of the most dysregulated genes in cancer, serving to amplify RNA levels and enhance proliferation across many different cell types[73-75]. MYC regulates T-cell development as well as T-cell leukemogenesis, primarily as a direct target of activated Notch signaling through regulation of a distal enhancer, and exogenous MYC overexpression can rescue Notch inhibition in some cell lines[76-81]. Of note, the ubiquitin ligase FBXW7 can target MYC and NOTCH1 for degradation and this gene is mutated in some cases of T-ALL, leading to reduced turnover of these proteins[82-85]. Recently, a new subgroup has been described in 5% of T-ALL defined by aberrant expression of the Hox family members *NKX2-1* and *NKX2-2*[65]. These genes can be expressed either through translocation or inversion of chromosomes. *HOXA9* or *HOXA10* are aberrantly expressed in a subset of T-ALL by TCR translocation, or through upstream mutations such as in *CALM-AF10* or *MLL*-translocation[86-90]. Additionally, a more commonly observed Hox aberration is the overexpression of *TLX1* and *TLX3*, two genes which can participate in translocations with the *TCRA* or *TCRD* loci (in the case of *TLX1*) or the *BCL11B* locus (in the case of *TLX3*), producing high levels of these transcription factors which can result in aberrant gene expression patterns[65,91-94]. While many subtypes of T-ALL have been uncovered through genomic and functional studies, there are still relatively few targeted therapies for this disease and for those that do exist, issues such as γ-secretase inhibitor resistance highlight the need for better understanding of the underlying molecular processes.

1.3.3 Runt-related (RUNX) transcription factors

1.3.3.1 RUNX paralogous family members

The Runt-related transcription factor (RUNX) family of genes have been conserved throughout all Metazoans and are thought to play roles in many biological processes[95]. Due to duplication events, mammals have three RUNX genes, *RUNX1*, *RUNX2*, and *RUNX3,* which are thought to play distinct but similar roles in cellular differentiation,

proliferation and survival. RUNX family member function depends largely on cell and tissue context and they have been found to work in concert with many other transcription factors and signaling molecules including the Notch[8,9,96], Wnt[97], Indian Hedgehog[98], YAP1/Hippo[99,100], TGFβ[101] pathways and receptor tyrosine kinase (RTK)[102] signaling. All of the RUNX family paralogs have links to cancer with most notably *RUNX1* implicated in leukemia, *RUNX2* in osteosarcoma, and *RUNX3* in gastric cancers.

1.3.3.2 RUNX protein structure and expression

The RUNX family of genes share common protein sequences and structure due to a gene duplication event in the evolutionary past which has conserved many of the same structural domains between the paralogs (**Figure 1.2**). The Runt domain contains peptide sequences shown to be involved in both DNA binding and interactions with the obligate heterodimeric partner for all RUNX gene products, CBFβ (*CBFB*). CBFβ strengthens interactions between RUNX proteins and DNA consensus binding sequences, and is required for full activation or repression of target loci (**Figure 1.3**)[103]. The Activation domain [AD] (also referred to as the transactivation domain) contains motifs which interact with co-factors involved in trans-activation or trans-repression of target genes including MLL, p300[95]. The Inhibitory domain [ID] (also referred to as the auto-inhibitory domain) is a region of RUNX proteins which has affinity for the Runt domain and inhibits DNA-binding. Upon binding of RUNX proteins to CBFβ, the inhibitory domain is displaced and the Runt domain is able to bind to DNA[103,104]. The VWRPY motif is a region required for interaction with Groucho proteins to mediate repression of target genes. The expression of RUNX1 (and other RUNX paralogs) is driven from both distal (P1) and proximal (P2) promoters (**Figure 1.4**) which leads to the expression of three distinct canonical isoforms (**Figure 1.5**). RUNX1A lacks many of the C-terminal domains found in RUNX1B and RUNX1C, and is thought to act in a dominant-negative manner due to the lack of an activation domain. RUNX1B and RUNX1C have small differences in N-terminal peptide sequence; however the mRNAs for each differ significantly. RUNX1C mRNA is translated by 5'-cap mediated

translation, while the RUNX1B isoform driven from the P2 promoter has a 5' UTR containing an IRES sequence that is less efficient at initiating translation[105,106]. Proximal promoter usage is restricted to certain cell types and developmental stages, while the distal promoter is expressed throughout hematopoietic stem and progenitor lineages as well as the entire thymic compartment where proximal promoter usage is seen primarily in the DN2 ($CD4^-CD8^-CD44+CD25+$) compartment and $CD8^+$ mature T-cells[107] (**Figure Figure 1.6**). Interestingly, it was recently revealed that RUNX1 protein can regulate the distal *RUNX1* promoter, resulting in an auto-regulatory loop which generates greater overall levels of RUNX1 protein. These findings suggest that comprehensive analyses of RUNX1 should include all three canonical RUNX1 isoforms.

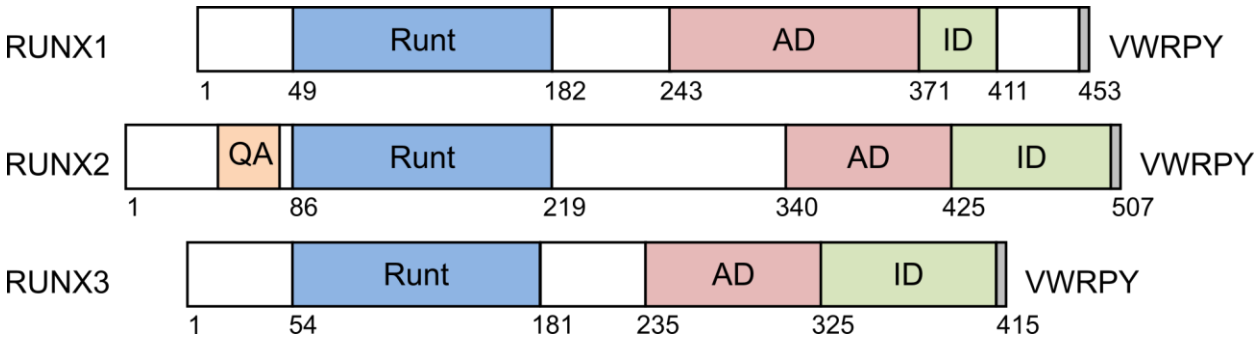

Figure 1.2 Structure of RUNX family genes.

Domains of RUNX1, RUNX3, and RUNX3 are depicted graphically including the Runt domain, Activation domain (AD), the Inhibitory domain (ID), and the VWRPY motif at the carboxy-terminus of the proteins. The QA domain refers to a unique stretch of glutamine and alanine repeats found only in the RUNX2 protein.

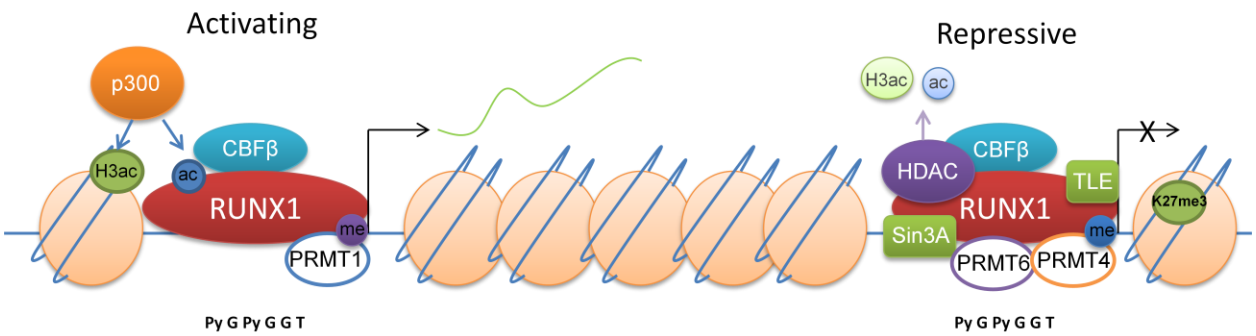

Figure 1.3 RUNX1 regulates gene expression in a context-dependent manner.

RUNX1 can act as a transcriptional activator or repressor dependent on the balance of coactivators/corepressors associated with it at a particular time. RUNX1 can recruit coactivators [for example, p300 histone acetyltransferase (p300) and protein arginine methyltransferase (PRMT1)] and epigenetic modifiers, which enhance RUNX1 activity through post-translational modification (shown as acetylation (ac) and methylation (me) of the RUNX1 protein) and impart activating modifications to chromatin [for example, histone 3 acetylation of lysine 9 and 14 (H3ac)]. RUNX1 can also recruit corepressors and epigenetic modifiers [for example, PRMT6 and PRMT4 as well as histone deacetylases (HDAC)], which inhibit RUNX1 activity through post-translational modification (removal of acetylation marks from RUNX1 and chromatin) and establish repressive chromatin modifications (for example, histone 3 lysine 27 trimethylation, 27me3). Various continuums of the two extremes that are shown no doubt exist. Figure adapted from Interplay between transcription factors and the epigenome: insight from the role of RUNX1 in leukemia *Frontiers in Immunology* (Brettingham-Moore, Taberlay and Holloway 2015), https://doi.org/10.3389/fimmu.2015.00499 © Brettingham-Moore, Taberlay and Holloway 2015, accessed December 2016. Used under creative commons attribution license.

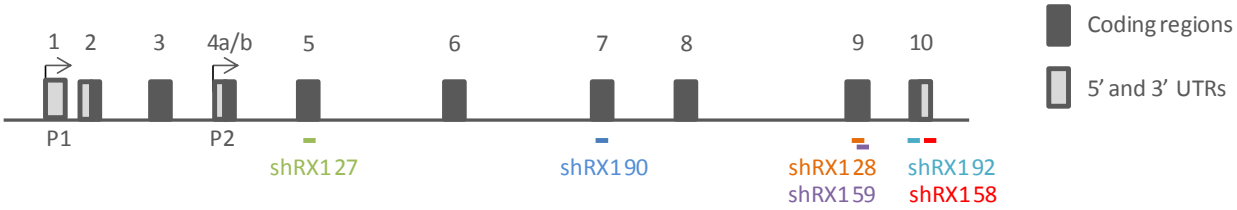

Figure 1.4 Human *RUNX1* locus.

The human *RUNX1* genomic locus, showing locations of exons targeted by shRNA clones used in this study and illustrating the two promoters (P1 and P2). Exons are represented as solid bars with exon numbers displayed above.

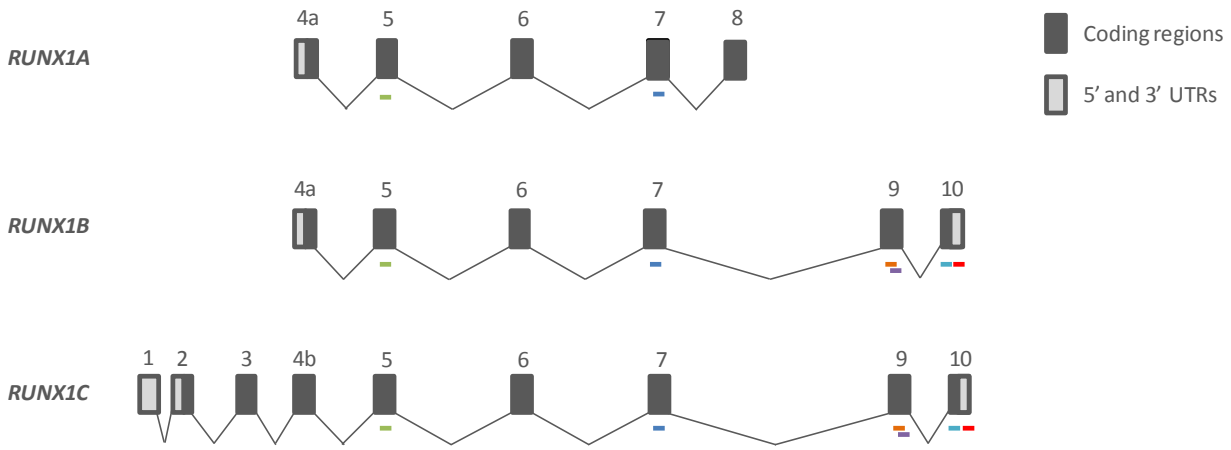

Figure 1.5 Canonical mRNA isoforms of *RUNX1.*

A graphical depiction exon usage of human *RUNX1* mRNA isoforms showing locations of exons targeted by shRNA clones. Exons are represented as solid bars with exon numbers displayed above.

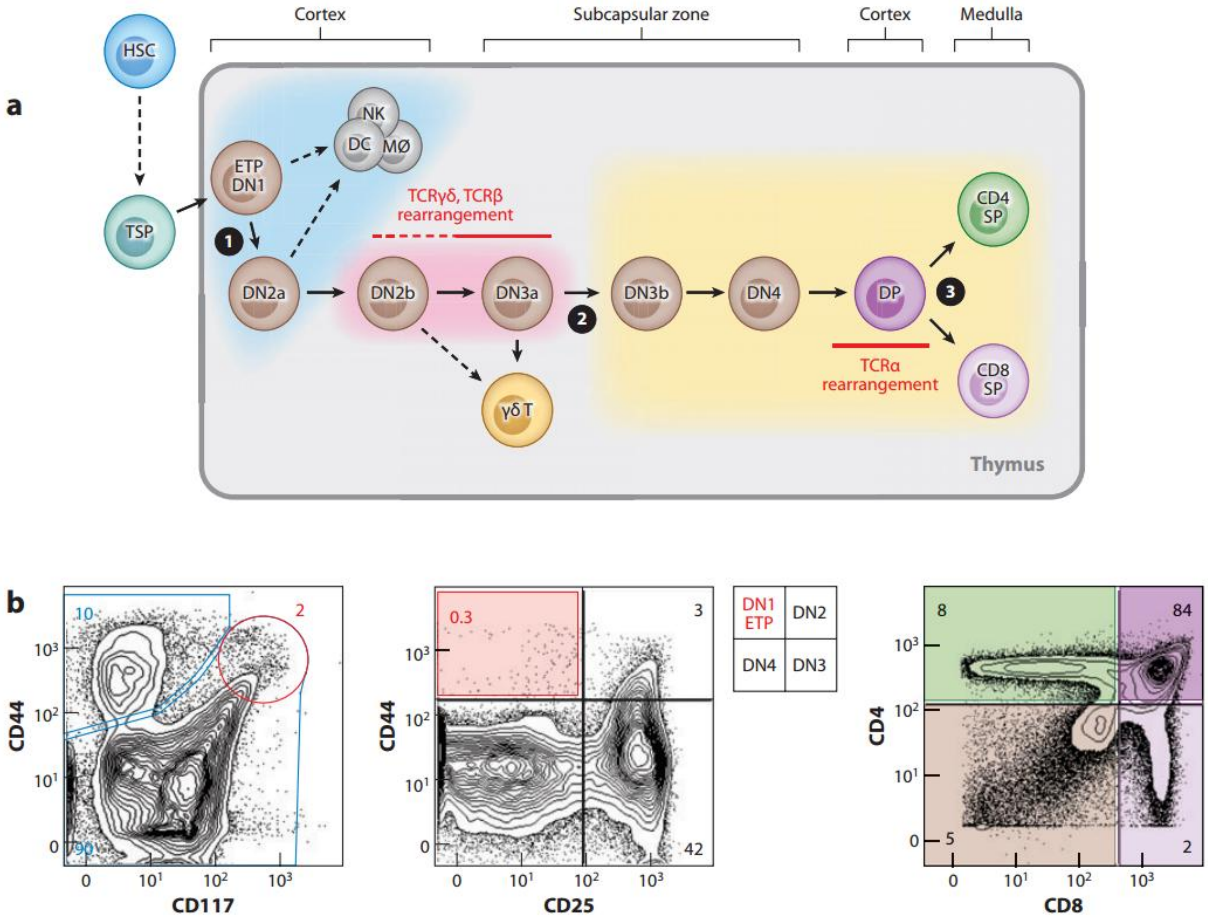

Figure 1.6 Overview of thymic T cell development

(**a**) The individual stages of T cell maturation from the earliest thymic seeding progenitor (TSP) to the fully mature CD4 and CD8 single positive (SP) cells. The expression of CD4 and CD8 surface molecules separates the CD4+CD8+ double positive (DP) and SP cells from the CD4−CD8− double negative (DN) cells. The surface expression of CD44 and CD25 characterizes the four major DN cell populations: CD44+CD25− (DN1), CD44+CD25+ (DN2), CD44−CD25+ (DN3), and DN4 (CD44−CD25−) cells. The earliest TSP is derived from a hematopoietic stem cell (HSC) in the bone marrow. HSCs undergo a gradual differentiation process and become more restricted to the lymphoid lineage. TSPs arrive at the thymus and develop to the early thymic progenitor (ETP) cell stage, a subpopulation of the heterogeneous DN1 subset that retains the potential to give rise to dendritic cells (DCs), natural killer (NK) cells, and macrophages (MØ). The DN2 and the DN3 cells can be subdivided further into two additional developmental cell stages on the basis of CD117 and CD27 cell-surface marker expression, respectively. Critical checkpoints during T cell maturation are indicated by circled numbers and are the [1] DN1 checkpoint, where Notch signaling inhibits alternative cell fate potentials; [2] the β-selection checkpoint, where the

transition from DN3a to DN3b marks the progression along the T cell receptor αβ lineage; and finally [3] the positive and negative selection checkpoint, where DP cells commit to either the CD4 SP or the CD8 SP cell fate. Cells within the thymus are grouped according to the key developmental steps: early uncommitted progenitors (*blue shading*), T cell-committed progenitors prior to separation of γδ versus αβ T cells (*pink shading*), and cells committed to the αβ T cell lineage (*yellow shading*). Dashed arrows indicate differentiation routes that have been elucidated mainly by in vitro differentiation assays. (**b**) Fluorescence-activated cell sorting (FACS) plots indicate a standard flow cytometric analysis of developing mouse thymocytes. The left panel stains for the ETP/DN population using anti-CD44 and anti-CD117 monoclonal antibodies gating on CD4−CD8− DN cells. The CD44hiCD117hi cell population defines the rare ETP cells. The middle panel defines the four major DN cell populations gating on CD4−CD8− DN cells and defines DN1, DN2, DN3 and DN4 cells using anti-CD44 and anti-CD25 monoclonal antibodies. The colors in the CD4 versus CD8 FACS profile in the right panel correlate to the four major populations described in panel a: DN1–DN4 (*brown*, lower left quadrant), DP (*dark purple*, top right quadrant), CD4SP (*green*, top left quadrant), and CD8SP (*light purple*, lower right quadrant). Figure from Mechanisms of T Cell Development and Transformation *Annual Review of Cell and Developmental Biology* (Koch and Radtke, 2011), DOI: 10.1146/annurev-cellbio-092910-154008. © Annual Reviews 2011, accessed February 2017.

1.3.3.3 Post-translational modification of RUNX1

RUNX1 has a number of names due to independent discovery in various fields and model organisms: AML1, PEBP2aB, and CBFα2. RUNX1 has been shown to interact with and be modified by a number of post-translational modification enzymes in different contexts (**Figure 1.7**). RUNX1 can interact with a number of chromatin modifiers including histone deacetylases (HDACs), methyltransferases such as MLL, acetyltransferases such as p300, as well as the polycomb repressive complex 1 (PRC1)[108-112].

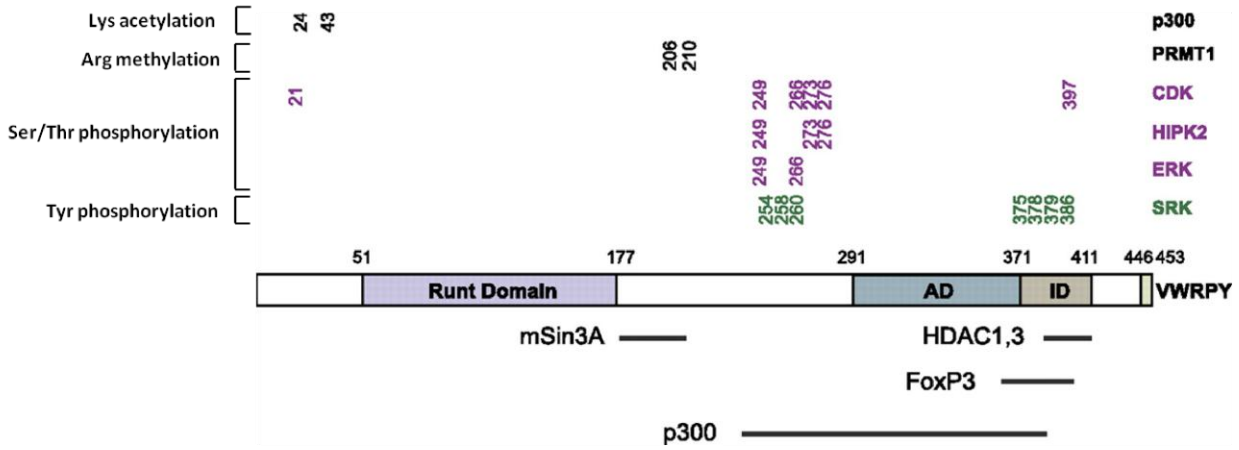

Figure 1.7 Schematic diagram of Runx1 with sites of post-translational modifications mapped.

In green text are the tyrosyl phosphorylation sites, purple shows seryl/threonyl phosphorylation sites, and black indicates the methylation (PRMT1) and acetylation (p300) sites. Runt domain is the DNA- and CBFβ-binding domain. VWRPY is the C-terminal pentapeptide required for binding TLE. Shown below are mapped interaction sites for several coregulatory proteins. Used under creative commons license from Cold Spring Harbor Laboratory Press: *Genes and Development.* **Tyrosyl phosphorylation toggles a Runx1 switch** (Neel & Speck 2012), doi: 10.1101/gad.198051.112 © Cold Spring Harbor Laboratory Press 2012, accessed December 2016.

1.3.3.4 Role of RUNX1 and RUNX3 in hematopoiesis

RUNX1 has critical roles during both embryonic and adult hematopoiesis. Deletion of *Runx1* in mice, through homozygous gene targeting, results in a loss of definitive hematopoiesis and subsequent embryonic lethality at embryonic day 12.5 (E12.5) due to hemorrhage while having little to no effect on primitive hematopoiesis[113]. It is thought that the *Runx1* null hemorrhage phenotype may be due in part to a lack of hematopoietic stem cell (HSC)-driven angiogenesis created by a lack of growth factor stimulation[114]. Fetal liver-derived cells from *Runx1* knockout mice are unable to generate colony forming units (CFU-S) as a measure of hematopoietic progenitor output and hematopoietic stem cells are absent from the dorsal aorta, gonads, and mesonephroi (AGM), while HSCs derived from the hemogenic endothelium are also dependent on *Runx1*[115,116]. In agreement with these data, similar disruption of the *Cbfb* gene, from which the obligate heterodimer of Runx1 is expressed, results in a

phenotypic copy of these Runx1-dependent effects through a lack of definitive hematopoiesis[117]. A number of research groups have generated conditional knockout models for *Runx1*, *Runx3* and *Cbfb*. There are four different targeting strategies which have attempted to ablate Runx1 function by floxing the fourth and fifth exons[118-121]. All studies utilized the *Mx1-Cre* system which allows for induction of deletion using Polyinosinic:polycytidylic acid (poly I:C), a mismatched dsRNA. Of note, one of the studies noted penetrance of thymic lymphomas upon *Runx1* deletion that were presumed to be T-ALL due to a lack of B-lineage marker expression[121]. Between these various studies, there was relatively strong concordance in phenotypes with a lack of obvious myeloid lineage abnormalities, but profound lymphoid and megakaryocyte differentiation impairment and an expansion of hematopoietic stem and progenitor (HSPC) cells. Mutations in *RUNX1* or deletion of *Runx1* in mice may be early events in creating a pre-leukemic state from an HSC, which can transform upon acquisition of secondary mutations[122-125]. Lineage negative $Sca1^{+}$ $c\text{-}Kit^{+}$ (LSK) populations enriched in hematopoietic stem and progenitor cells are expanded upon knockout of *Runx1* and appear to progress through cell cycle at a slower rate and with higher survival[118-120,126,127]. It is thought this may be due to reduced ribosome biogenesis and p53 levels, allowing for smaller cells which are better poised to handle genotoxic stress, and which may suggest why stem and progenitor cells with *RUNX1* mutations may facilitate the formation of a preleukemic clone[127,128]. Of note, there are no pronounced defects in the hematopoietic system upon *Runx3* knockout, but similarly to *Runx1* knockout, there is an expansion of hematopoietic stem and progenitor cells[129]. $Runx3^{\Delta}$ HSPCs have reduced proliferative ability as measured by colony-forming potential as well. Compound mice which have both the *Runx1* and *Runx3* alleles conditionally deleted (*Runx1; Runx3* double knockout or DKO) die from a combination of bone marrow failure and myeloproliferative disease prior to death. Knockout mice have relative expansion of HSPC and myeloid populations at the expense of erythroid and lymphoid lineages which are markedly reduced due to differentiation blocks and reduced numbers of CLP populations[130]. The authors suggested a possible role for RUNX transcription factors in DNA repair due to the phenotype's resemblance to Fanconi anemia (FA) and defective

DNA damage repair. Similarly, upon conditional knockout of *Cbfb*, mice succumb to anemia due to a lack of $CD105^+$ erythroid progenitors, along with myeloproliferative disorder with defects in dendritic cell progenitors among others[131]. The Osato lab found that conditional deletion of *Cbfb* resulted in pancytopenias due to blocks in differentiation of all myeloid and lymphoid lineages, with a profound expansion of HSPC populations including HSC[132]. Interestingly, *Cbfb* deletion appears to have a much greater effect on long-term HSC (LT-HSC) function (in addition to frequency), relative to *Runx1. Cbfb*$^{\Delta}$ LT-HSC cells are unable to repopulate transplanted mice, which suggests that Runx2 and Runx3 may play a role in supporting HSC functions in addition to Runx1[133].

1.3.3.5 Role of RUNX1 and RUNX3 in thymopoiesis

A number of studies have sought to delineate the role of RUNX transcription factors in T-cell development using various conditional knockout alleles and stage-specific Cre induction as well as overexpression. Early studies using transgenic dominant-negative Runt-domain-only mice and heterozygous knockout mice (*Runx1*$^{+/-}$) primarily focus on single positive (SP) $CD4^+$ and $CD8^+$ populations (**Figure 1.6**) and suggested an impairment at the DP to SP transition[134]. These experiments which reflect a partial reduction in Runx1 levels/functionality were expanded upon through a number of conditional knockout experiments by multiple groups. Dan Littman's group used an *Lck*-Cre system which begins to express Cre as early as the DN1 stage of T-cell development ($CD4^-CD8^-CD44^+CD25^-$) (**Figure 1.6**). They showed a profound differentiation arrest between the DN3 and DN4 stages in addition to aberrant derepression of CD4 in DN subsets and proper expression of CD8 in DP thymocytes[135-137]. Expanding upon this work, they show that Runx1 is necessary for full DN to DP transition, and by using *CD4*-Cre, they show that Runx1 also regulates maturation of mature $CD4^+$ single positive cells from DP T-cells[138]. Of note, conditional deletion of Runx3 using *CD4*-Cre in the same study, and in a similar study from another group, was also found to negatively affect the transition between DP and $CD8^+$ T-cells, and deletion of both *Runx1* and *Runx3* at the DP stage resulted in a complete block in

differentiation[139,140]. *Mx-Cre Runx1;Runx3* DKO mice display a differentiation block between the DN1 (CD44+CD25-) and DN2 (CD44+CD25+) transition resulting in an accumulation of DN T-cells[130]. Conversely, the Satake group has used *Lck*-Cre to induce exogenous overexpression of Runx1 in developing T-cells[141]. They similarly found a differentiation block between DN and DP T-cells with a drastic decrease in thymic cellularity. Recently however, the entire *Lck*-Cre system has been cast in doubt due to apparent off-target effects which show that the locus can cause massive thymic cytopenia and a block in the DN to DP transition, suggesting that studies using this system may need reinterpretation[142]. Other researchers have cultured progenitor cells on OP9-DL1, a stromal cell line expression the Notch ligand delta-like-1 (DL1), a system which recapitulates T-cell development *in vitro*[45]. One group attempted to rescue *Lck*-Cre-induced deletion of *Runx1* by reintroducing either full-length Runx1 or mutated alleles of Runx1 into fetal liver cells from a $Runx1^{lox/-}$ genetic background cultured on the OP9-DL1 system[143]. Only Runx1 alleles containing the Activation Domain (AD) were able to restore T-cell development. In this study and others, the role of the VWRPY motif was determined to play an important part in silencing of the *Cd4* locus[143,144]. Of important note however, using the *Mx*-Cre system to induce recombination of LoxP sites flanking *Runx1*, cells exhibit a differentiation block at the DN2 to DN3 transition. This suggests that there are slight differences in either the manner in which Cre recombination is induced or perhaps off-target effects mediated by each system[118]. Overexpression of Runx2 using *CD2-Runx2* transgenic mice results in an expansion of DN and immature single positive $CD8^+$ and a concomitant block in DP lineage development, similar to overexpression of Runx1[145]. Deletion of *Cbfb* using both *Vav*-Cre and *Mx*-Cre creates a differentiation arrest at the DN1 stage, leading to an accumulation of very immature thymocytes[132]. In an elegant series of experiments from Nancy Speck's lab, an allelic series of null and hypomorphic *Cbfb* alleles was used to determine the amount of protein required for proper thymopoiesis[146]. They found a dose-dependent effect on T-cell development, with 30% of wild-type levels generating fewer mature cells, but at 15% of wild-type levels there was a severe block by the DN3 stage of development with evidence of an effect as early as the ETP stage. The authors

hypothesized a possible link between Runx signaling and Notch-induced lineage commitment. Interestingly however, constitutive IL7R or Notch signaling is unable to rescue pan-Runx deletion, suggesting broader roles for the transcription factor family[147]. Of note, Runx1 appears to aid in T-cell lineage commitment in part by regulating Bcl11b expression levels, along with Notch signaling, TCF-1 and GATA3[148].

1.3.3.6 Role of RUNX1 in familial platelet disorder with predisposition to Acute Myeloid Leukemia (FPD/AML)

Germline mutations in *RUNX1* and *ANKRD26* are predisposing to aberrations in both platelet function and amount (thrombocytopenia) and those patients harbouring these coding changes often develop Acute Myeloid Leukemia as time proceeds. In those with mutations in RUNX1, the condition is termed familial platelet disorder (FPD) with propensity to Acute Myeloid Leukemia (AML) and is an autosomal dominant condition. Typically families with platelet defects present with wound healing problems or have a susceptibility to severe bleeding from relatively minor trauma and are genetically counseled to determine if there are any mutations in either of these two genes. As the name suggests, about 20-50% of patients develop acute leukemia, the vast majority of which is AML but not to the exclusion of some who develop ALL[149-151]. Of important note, lymphoid tumors from FPD/AML patients are exclusively T-cell Acute Lymphoblastic Leukemia (T-ALL)[152]. Families with *RUNX1* mutation have vastly different penetrance of myeloid malignancy and this is thought to be due in part to the nature of the mutations as some create nonsense/frameshift or missense point mutations (within the RUNT domain or the Activation domain) or the entire locus itself may also be duplicated, deleted or otherwise altered at the copy number level[150,151,153-163]. Of note, the vast majority of these mutations are believed to be deleterious to RUNX1 transcriptional activity, however certain 3' truncating mutations may enhance activity, at least as measured by a luciferase reporter[159]. Of particular note, *PRKCQ,* a transcriptional target of RUNX1 in T-ALL is also positively expressed in megakaryocytes and platelets, suggesting conservation of this particular regulatory mechanism[164,165].

1.3.3.7 Role of RUNX1 in leukemia

RUNX1 was originally described as a partner of a fusion created by a translocation of chromosomes 8 and 21 which generates the *RUNX1-ETO* fusion gene in 30% of M2 AML[166]. Of note, about 2% of B-ALL cases have focal amplifications of chromosome 21 in regions harbouring *RUNX1*[167] and have gain of 3 or more copies of *RUNX1* as measured by in-situ hybridization[168].

1.3.3.8 Role of RUNX1 in T-ALL

A body of work has generated contrasting hypotheses for the role of *RUNX1* in T-cell Acute Lymphoblastic Leukemia in recent years. A number of studies began to emerge between 2011 and 2012 that suggested *RUNX1* might function as a tumor suppressor in T-cell leukemias, due to potentially deleterious mutations in 11.5% (44/381 patients) of T-ALL discovered through next-generation sequencing efforts[4-6]. A case report described T-ALL in families with familial platelet disorders due to *RUNX1* mutations, but these new studies suggested a more frequent, widespread role for RUNX1 in this disease with mutations clustered around the RUNT domain and Activation domain (AD) (**Figure 1.2**)[152]. Of particular note, *RUNX1* mutations tend to be associated with Early T-cell Precursor acute lymphoblastic leukemia (ETP-ALL), a particularly aggressive subtype of T-ALL and are associated with inferior overall survival[5,6,169]. A limited number of functional studies have shown that TLX1 and TLX3 bind to the proximal *RUNX1* promoter, and that retroviral RUNX1 overexpression reduces the growth of ALL-SIL and HPB-ALL cell lines by MTT assay[4]. Of note, the authors suggest that TLX1 and TLX3 might repress *RUNX1* expression as a mechanism of generating a low-RUNX1 phenotype. However, changes in RUNX1 protein levels upon knockdown or overexpression of TLX1 or TLX3 were not described. *RUNX1* mutations may also cluster into domains which are required for interactions with MLL, and were suggested to create defects in epigenetic patterning of differentiation markers, leading to the creation of TCRγ-deleted ETP-ALL[170]. Of note however, these conclusions are based on correlations between *RUNX1* mutational status and immunophenotype but some work has shown that RUNX1 can repress the CD4 locus in a murine *Lmo2*-driven T-ALL

by binding to the *CD4* silencer[137,171]. Future studies should seek to determine if there is a functional role for RUNX1 in this context and if *RUNX1* mutation causes cells to reverse differentiation overtly or merely change the immunophenotype with no discernible difference in function. These roles for *RUNX1* as a tumor suppressor in T-ALL contrast with other contemporary studies which suggest RUNX1 might be a pro-growth factor, in complex with known T-ALL oncogenic transcription factors to promote a leukemogenic expression program[7-9,66]. RUNX-family consensus sites were found at regions enriched in dynamic NOTCH1/CSL binding, suggesting that RUNX1, along with other factors such as ETS family transcription factors, may regulate Notch signaling in T-ALL[9]. A follow-up by the Aster lab found that RUNX1 does indeed bind throughout the T-cell leukemia genome at regions enriched in NOTCH1 at potential enhancers enriched in H3K4me1 and H3K27Ac[8]. RUNX1 is also a key player in TAL1-transcriptional complexes along with MYB, GATA3 and other factors and creates a positive feedback loop, promoting a leukemic transcriptional programme[7]. Interestingly, somatic mutations in T-ALL cells can generate MYB binding sites which then recruit the TAL1/RUNX1 transcriptional complex, essentially generating a *de novo* enhancer region in front of the *TAL1* gene through the recruitment of CBP[66]. Very recently, *RUNX1* has been identified in T-ALL as a gene in which there has been insulated neighbourhood collapse leading to aberrant expression through super-enhancer activity[172]. Although not yet shown in T-cell leukemia, Runx1 expression is induced in normal T-cells via the calcineurin-NFAT pathway, which is a druggable pathway in T-cell Acute Lymphoblastic Leukemia through the use of calcineurin inhibitors cyclospoin A (CsA) and FK506[173,174]. In contrast to studies suggesting that mutated *Runx1* might support T-ALL transformation, *Runx1*$^{+/-}$ mice are less readily transformed than *Runx1*$^{+/+}$ mice on a p53-null background and Runx1 was found to support proliferation of T-cells[175]. These results suggest that in certain contexts, Runx1 might support oncogenesis, and cast doubt onto the view that Runx1 is a tumour suppressor.

1.4 IGF1R

1.4.1 IGF1R signaling

Insulin-like growth factor 1 receptor (IGF1R) is a receptor tyrosine kinase with sequence conservation to the Insulin receptor (InsR), which forms homodimers with itself or heterodimers with InsR to recognize its ligands, IGF-1 and IGF-2[176]. IGF signaling is important for normal growth of tissues during development[177] and has been implicated in self-renewal/pluripotency in hematopoietic and embryonic stem cell contexts[178,179]. Signaling through IGF1R is evolutionarily conserved but generally and consistently regulates cell growth[180-182]. Two α and two β subunits join through cysteine residues to form a mature tetrameric complex. Notably, the tumor-upregulated 'A' isoform of the Insulin Receptor is able to bind to IGF2 ligand and the Insulin Receptor can also form a holoreceptor with IGF1R[183,184]. Ligand binding initiates autophosphorylation of the β subunit of IGF1R, which allows binding and phosphorylation of IRS proteins (insulin receptor substrate) and Shc with subsequent activation of PI3K-AKT and RAS/RAF/MEK/ERK pathways, respectively[185-187].

1.4.2 IGF1R in Leukemia

IGF signaling also plays an important role in supporting growth/survival of cancer cells arising in many different tissue contexts[176]. Initially it was shown that IGF1R controlled the ability of SV40 large tumor antigen to transform W cells[188] and for signaling induced proliferation of Breast Cancer cell lines[189]. Subsequently, it has been suggested that serum IGF ligand levels may be associated with risk of transformation and prognosis of cancers[190]. While it has been known for quite some time that T-ALL cells express IGF1R and its ligands[191,192], it had not been appreciated to have such a critical role in leukemia-initiating cell activity until recently[2]. In this work, it was established that hypomorphic levels of IGF1R caused a severe defect in the transplantability of murine leukemias derived from active Notch signaling in secondary recipients. This suggested that high levels of IGF1R signaling mediated by transcriptional upregulation by Notch signaling is required to sustain self-renewal of T-cell leukemia clones. In addition to this study, others have shown efficacy in this context for the use of blocking antibodies and

small molecule inhibitors in disrupting proliferation of survival of T-ALL cells[193-195]. Together, this suggests that therapeutic targeting of IGF1R may have a role in reducing bulk burden of leukemia cells growth as well as in eradicating leukemia-initiating cells.

A number of studies have investigated the role of IGF1R in AML and found that it is highly expressed and that cell growth/viability is sensitive to pharmacologic IGF1R inhibition[196-199]. IGF1R is one of the most abundantly phosphorylated receptor tyrosine kinases in AML cells, particularly in cases with wild-type FLT3[200]. AML blasts secrete IGF-1/2 and thus derive growth/survival advantage through autocrine signaling. Secretion of these growth factors is increased dramatically in matched relapse samples[197,198]. Both small molecule tyrosine kinase inhibitor and blocking antibody therapies targeting IGF1R have shown activity against AML cells in pre-clinical studies[196-199]; however, there has been considerable debate as to the mechanism and specificity of these reagents, especially with regard to cross-reactivity with InsR and other related signaling molecules[201,202].

1.5 Loss-of-function methods for manipulation of gene expression

1.5.1 shRNAs

Originally described in *Caenorhabditis elegans*, yet further described in mammals, RNA interference (RNAi) is a system of gene regulation whereby double-stranded RNA (dsRNA) of short length known as small interfering RNA (siRNA) is degraded and results in silencing of gene products[203-205]. Endogenous systems (miRNAs) can be used to balance and fine-tune gene expression, but synthetic RNAi species can be generated as tools to regulate gene expression experimentally[206]. Transient silencing using commercially produced siRNA can produce a short-term knockdown of a gene product due to dilution of the siRNA species by cell division. The use of virally-driven siRNA expression via short hairpin RNAs (shRNA) can produce sustained and stable knockdown of a gene transcript through either RNA Pol II or III-driven promoters[207,208]. Choice of promoter may depend in part on the needs of the experiment, with Pol III promoters such as H1 or U6 allowing for high expression of shRNA species and Pol II constructs bringing the flexibility of tissue-specificity while maintaining capacity of

transcribing multiple shRNA/miRNA species from a single promoter[209]. Tailoring design of synthetic shRNAs using increased understanding of RNAi biochemistry has also allowed for higher levels of silencing[210].

1.5.2 Conditional Knockout Mice

The Cre recombinase enzyme from P1 coliophage mediates interaction and recombination between 34-base pair sequence motifs termed loxP sites[211]. This system was originally harnessed as a way to induce *in vivo* DNA recombination events between chromosomes[212]. Very quickly, researchers began to realize that the Cre-LoxP system could be used to induce deletion of genomic regions, including fundamentally critical exons or other functional sequences, to effectively knockout gene function similar to a full knockout, but at a temporally and spatially distinct instance chosen by the researcher[213-215].

1.6 Thesis objectives

The overall objective of this dissertation is to reveal key biological oncogenic underpinnings in leukemia initiation and maintenance in Acute Leukemias using models of Acute Myeloid Leukemia (AML) and T-cell Acute Lymphoblastic Leukemia (T-ALL). By leveraging robust, genetically-defined experimental systems involving lentiviral overexpression and knockdown in human cell lines in addition to well-defined mouse models of myeloid (MLL-AF9) and T-lymphoid (hN1ΔE) leukemia in wild-type and conditional knockout backgrounds, I aim to better understand cancer initiation and progression. Where possible, I attempt to use human patient-derived xenograft (PDX) samples and human cell lines and attempt to identify pre-clinical efficacy of certain therapeutics as a way to potentially translate my findings to the clinic.

Aim 1: Characterize the role of IGF1R signaling in supporting Acute Myeloid Leukemia pathogenesis.

Aim 2: Identify and characterize genes that collaborate with NOTCH signaling in T-cell Acute Lymphoblastic Leukemia pathogenesis.

Aim 3: Determine the contribution of RUNX1 in T-cell Acute Lymphoblastic Leukemia pathogenesis.

Chapter 2: IGF1R in Acute Myeloid Leukemia Leukemogenesis

2.1 Chapter overview

A dilemma in treatment of acute leukemias is relapsed disease following chemotherapy treatment. The concept of leukemia stem cells (LSC) or leukemia initiating cells (LIC) suggests that there is a hierarchy within the tumour responsible for the growth and promotion of the entire leukemia[216]. If currently chemotherapy is unable to target these cells effectively then remission may not be achieved or if it is, relapse may result in further treatment or lead to death. Thus, determining the molecular underpinnings which support these populations is critical in finding ways to target these populations and leading to sustained cure. The Weng lab has noted that IGF1R is critical for T-cell acute leukemia LIC activity[2]. Due to the availability of well-characterized models of LICs in Acute Myeloid Leukemia[217], I sought to determine if IGF1R was needed for LIC activity in an MLL-AF9 model of leukemia.

2.2 Introduction

2.2.1 Mll-AF9 translocations in AML

Acute myelogenous leukemia (AML) is an aggressive malignancy of immature myeloid progenitors with variable, but generally poor outcome. Characteristic chromosomal translocations that lead to the expression of novel fusion oncoproteins define and subdivide the disease into clinically relevant prognostic groups. Translocations involving the MLL locus and its various partners are among the most common and best studied[218]. A prototypic example is the t(9;11) chromosomal translocation between MLL and AF9, which leads to the expression of a novel fusion oncoprotein with transcriptional activity and drives an aberrant gene expression program. A knock-in of *Mll-Af9* controlled by the endogenous *Mll* promoter generates both AML and ALL with an extended latency, perhaps in part due to a need for collaborating mutagenic effects[219]. Enforced expression of the MLL-AF9 fusion protein in bone marrow progenitor cells leads to rapid development of a lethal AML-like disease in mice with the clonogenic activity residing in the LSK ($Lin^-Sca1^+c\text{-}kit^+$) and GMP subsets ($Lin^-c\text{-}kit^+Sca\text{-}$

$1^{-}CD34^{+}Fc\gamma RII/III^{hi}$) [217,220,221]. In contrast when human *AF9* is knocked-in to the endogenous *Mll* locus in mice, only LSK ($Lin^{-}Sca1^{+}c\text{-}kit^{+}$) cells could be transformed, suggesting dosage of the MLL-AF9 fusion protein is critical in establishing leukemia[222]. Interestingly, immunodeficient mice injected with lineage-depleted human cord blood transduced with *MLL-AF9* retrovirus have potential to develop into *de novo* B-ALL, AML, and MLL[223]. MLL-AF9 is able to recruit DOT1L, a histone methyltransferase which is able to support H3K79me2 and H3K79me3 at target genes, leading to transformation of stem and progenitor cells[224-226]. The MLL-AF9 fusion oncoprotein enacts a self-renewal program in committed myeloid progenitors in a fashion that is dependent on Wnt/β-catenin signaling and leukemic GMPs are thought to represent leukemia stem cells in this disease model[217,227].

2.2.2 Statement of hypothesis and objectives

Previous studies in the Weng lab examining the role of IGF1R signaling in T-cell acute lymphoblastic leukemia (T-ALL) observed decreased levels of IGF1R expression can compromise leukemia-initiating cell (LIC) activity in a retroviral NOTCH1 mouse bone marrow transplant model[2]. To begin to explore whether this effect was specific to T-ALL, or a more general feature common to other hematological malignancies, I performed a similar analysis to test the effect of reduced IGF1R expression on AML using the well-characterized retroviral MLL-AF9 bone marrow transplant model[217,220,221]. I hypothesized that IGF1R-low hematopoietic stem and progenitor cells are less readily transformed by MLL-AF9 and that established leukemias have impaired LIC function and/or frequency. My objectives to test this hypothesis include, 1) attempt to generate leukemias from fractionated HSPC subsets on a hypomorphic IGF1R background, 2) If successful, test clonogenic functions of these IGF1R-low tumours *in vitro* and *in vivo*, and 3) classify any cell growth phenotypes associated with reduced IGF1R levels in AML cells.

Aim 1: Characterize the role of IGF1R signaling in supporting Acute Myeloid Leukemia pathogenesis.

2.3 Materials and methods

2.3.1 Mice

The IGF1R^{neo} strain, originally generated on the 129 background[2], was backcrossed onto C57BL/6 for over 20 generations and kindly provided by M. Holzenberger. Wild-type C57BL/6 mice were used as recipients for all transplant experiments.

2.3.2 Flow Cytometry

For sorting/analysis of hematopoietic progenitor subsets, whole bone marrow cell suspensions were labeled with fluorochrome-conjugated antibodies against CD34 (RAM34), CD16/32 (93), CD117 (2B8), and Ly-6A/E (D7). Cells were also concurrently stained with a cocktail of biotinylated lineage-specific antibodies against CD3e (145-2C11), CD4 (GK1.5), CD8a (53-6.7), B220 (RA3-6B2), CD19 (eBio1D3), TER119 (TER-119), Ly-6G (RB6-8C5), and CD127 (A7R34), followed by streptavidin-conjugated PerCP/Cy5.5. For analysis of surface IGF1R expression, human cell lines were incubated with αIR3 (Calbiochem), followed by APC-conjugated secondary antibody. Lentiviral CreERT2-transduced cells were discriminated by labeling with PE-conjugated anti-NGFR antibody (Miltenyi). Flow sorting/analysis was performed on FACSAriaII, FACSCalibur, and FACSCantoII cytometers. Data was analyzed using FlowJo software (Tree Star).

2.3.3 Retroviral transduction/bone marrow transplantation

An MLL-AF9 cDNA encoding amino acids 1-1461 of MLL fused to the last 90 amino acids of AF9[217] was subcloned into the MigR1 (MSCV-IRES-GFP) retroviral vector. Replication-defective retrovirus was generated by transient transfection of PlatE packaging cells as described[2]. For primary transplant experiments, mouse hematopoietic stem/progenitor subsets were FACS sorted from bone marrow, resuspended in MLL-AF9 retroviral supernatant with supplemental cytokines (10ng/ml mIL-3, 10ng/ml mIL-6, and 20ng/ml mSCF; Peprotech) and 7μg/ml polybrene (Sigma),

and centrifuged at 400xg for one hour. Transduced GFP+ cells were then FACS sorted 42 hours later, and injected by tail vein into lethally irradiated (810 RAD) recipient mice along with $2x10^5$ whole bone marrow cells from C57BL/6 donors to rescue normal hematopoiesis. Mice were monitored daily and those developing clinical signs of disease were sacrificed immediately and tissues harvested for analysis. All animals were housed in the BC Cancer Agency Animal Resource Centre under pathogen-free conditions and in compliance with protocols approved by the University of British Columbia Committee for Animal Care.

2.3.4 Colony-forming cell (CFC) assay

Cells were plated in 20% IMDM, 20% fetal bovine serum (FBS), 20% BIT9500, and 40% methylcellulose base medium (Stem Cell Technologies) with supplemental cytokines (10ng/ml mIL-3, 10ng/ml mIL-6, 10ng/ml mGM-CSF, and 20ng/ml mSCF; Peprotech). For serial CFC assay, primary colonies from individual plates were pooled, washed in PBS, and replated under identical conditions as primary cultures.

2.3.5 Cell culture

Human AML cell lines were cultured in RPMI1640 with 10% FBS, 2mM Glutamax, 1mM sodium pyruvate, and antibiotics (Invitrogen). Primary mouse MLL-AF9 leukemia cells were cultured in the same media, but with 20% FBS, 55μM 2-mercaptoethanol, and supplemental cytokines (10ng/ml mIL-3, 10ng/ml mIL-6, 10ng/ml mGM-CSF, and 20ng/ml mSCF; Peprotech). Cell growth assays were performed by direct addition of the fluorometric indicator dye resazurin (CellTiterBlue, Promega) to cells in culture media, incubation for 30-120 minutes at 37°C, and reduced dye measured by fluorometry. Cell viability was measured by flow cytometry for propidium iodide exclusion. Cell proliferation was measured by BrdU incorporation (BrdU flow kit; BD).

2.3.6 Drugs/antibody reagents

Small molecule dual IGF1R/InsR inhibitors BMS-536924 and BMS-754807 were obtained under MTA from the manufacturer. These were resuspended in DMSO at 10 mM, and then serially diluted in Hank's Balanced Salt Solution (Invitrogen) prior to

addition to culture media. Antibodies used for western blotting were against IGF1Rα (sc-712, Santa Cruz) and ERK2 (sc-154, Santa Cruz).

2.4 Results

2.4.1 Reduced IGF1R expression impedes leukemogenic transformation of myeloid progenitors.

To study the role of IGF1R signaling in myeloid leukemogenesis, I employed a "hypomorphic" allele of IGF1R, termed $IGF1R^{neo}$, in which an integrated neo cassette in the 2nd intron results in inefficient mRNA splicing and thus reduced levels of protein expression. Full-length IGF1R protein is expressed at ~60% of wild-type levels in normal tissues of $IGF1R^{neo/neo}$ mice[228], and at ~30% of wild-type levels in T-ALL leukemias generated by transduction of $IGF1R^{neo/neo}$ bone marrow with an activated NOTCH1 retrovirus[2]. To generate AML efficiently on the $IGF1R^{neo}$ background, I transduced bone marrow-derived hematopoietic progenitors with retrovirus encoding the MLL-AF9 fusion oncogene, followed by transplantation into histocompatible recipients. This retroviral MLL-AF9 bone marrow transplantation model is well characterized and has proven useful in defining HSC-like self-renewal programs that are induced by MLL-AF9 in committed myeloid progenitors[217,220]. Accordingly, leukemic GMPs are thought to be the self-renewing leukemia-initiating cells, or LICs, in this model.

Bone marrow from age and sex-matched wild-type vs. $IGF1R^{neo/neo}$ mice was harvested and LSK and GMP subsets sorted by FACS (**Figure 2.1)**. These purified populations of cells were then transduced with MLL-AF9/GFP retrovirus, GFP^+ cells sorted by FACS, and similar numbers of transduced cells injected intravenously into lethally-irradiated C57BL/6 recipient mice along with a $2x10^5$ dose of wild-type whole bone marrow to rescue normal hematopoiesis (**Table 2.1**). Mice were subsequently monitored daily for clinical signs of leukemia (e.g. hunched position, decreased activity/grooming); animals attaining a standardized morbidity score were euthanized and tissues analyzed at necropsy.

MLL-AF9-transduced LSK cells from both wild-type and IGF1R$^{neo/neo}$ donors produced aggressive immature myeloid leukemias in recipient mice with similar penetrance and latency (**Figure 2.2A**, solid lines), and there was no significant difference in disease burden/distribution or immunophenotype (**Figure 2.3**). Importantly, reduced IGF1R expression in IGF1R^{neo} leukemias was confirmed by western blot (9 ± 3% of wild-type levels, **Figure 2.2B)**. In contrast to the situation with LSK cells, there was a significant effect of reduced IGF1R on the ability of MLL-AF9 to transform GMP cells. Whereas 36% of mice receiving MLL-AF9-transduced wild-type GMPs developed AML, none of the mice receiving MLL-AF9-transduced IGF1R^{neo} GMPs developed disease within the 180-day observation period (**Figure 2.2A**, dashed lines).

To address whether the relative resistance of IGF1R^{neo} GMPs to transformation by MLL-AF9 could be due to altered hematopoietic differentiation on the IGF1R^{neo} background, I examined bone marrow cellularity and abundance of hematopoietic stem/progenitor subsets in IGF1R$^{neo/neo}$ mice as compared to age and sex matched wild-type controls. There were no appreciable differences in either total bone marrow cellularity (**Figure 2.4A**) or relative proportions of hematopoietic stem/progenitor populations including lineage marker negative (Lin$^-$) progenitors, hematopoietic stem cell (HSC)-containing LSK (Lin$^-$ c-kit$^+$ Sca-1$^+$) cells, common myeloid progenitors (CMP; Lin$^-$ c-kit$^+$ Sca-1$^-$ CD34$^+$ FcγRII/III^{lo}), megakaryocyte-erythroid progenitors (MEP; Lin$^-$ c-kit$^+$ Sca-1$^-$ CD34$^-$ FcγRII/III$^-$), or granulocyte-macrophage progenitors (GMP; Lin$^-$ c-kit$^+$ Sca-1$^-$ CD34$^+$ FcγRII/III^{hi})[229] (**Figure 2.4B**). Additionally, analysis of peripheral blood counts revealed no significant differences between IGF1R$^{neo/neo}$ and wild-type mice (**Figure 2.5**). These data suggest that hematopoietic differentiation is not substantially distorted in IGF1R$^{neo/neo}$ mice, and support the conclusion that GMPs with reduced levels of IGF1R are qualitatively less susceptible to transformation by MLL-AF9. While I did not observe a similar defect in transformation of IGF1R^{neo} LSK cells, this cannot be concluded definitively since recipient mice were not injected with identical numbers of MLL-AF9-transduced IGF1R^{neo} vs. wild-type LSK cells as the number of transduced cells of each population was limited by the yield from the FACS sort (**Table 2.1**).

Background	Cell type	MLL-AF9+ cells injected/mouse	Normal bone marrow cells co-injected/mouse	Number of mice injected
wild-type	LSK	350	200,000	5
wild-type	GMP	5,000	200,000	11
IGF1R$^{neo/neo}$	LSK	570	200,000	6
IGF1R$^{neo/neo}$	GMP	5,000	200,000	11

Table 2.1 Cell populations used for transplant analyses.

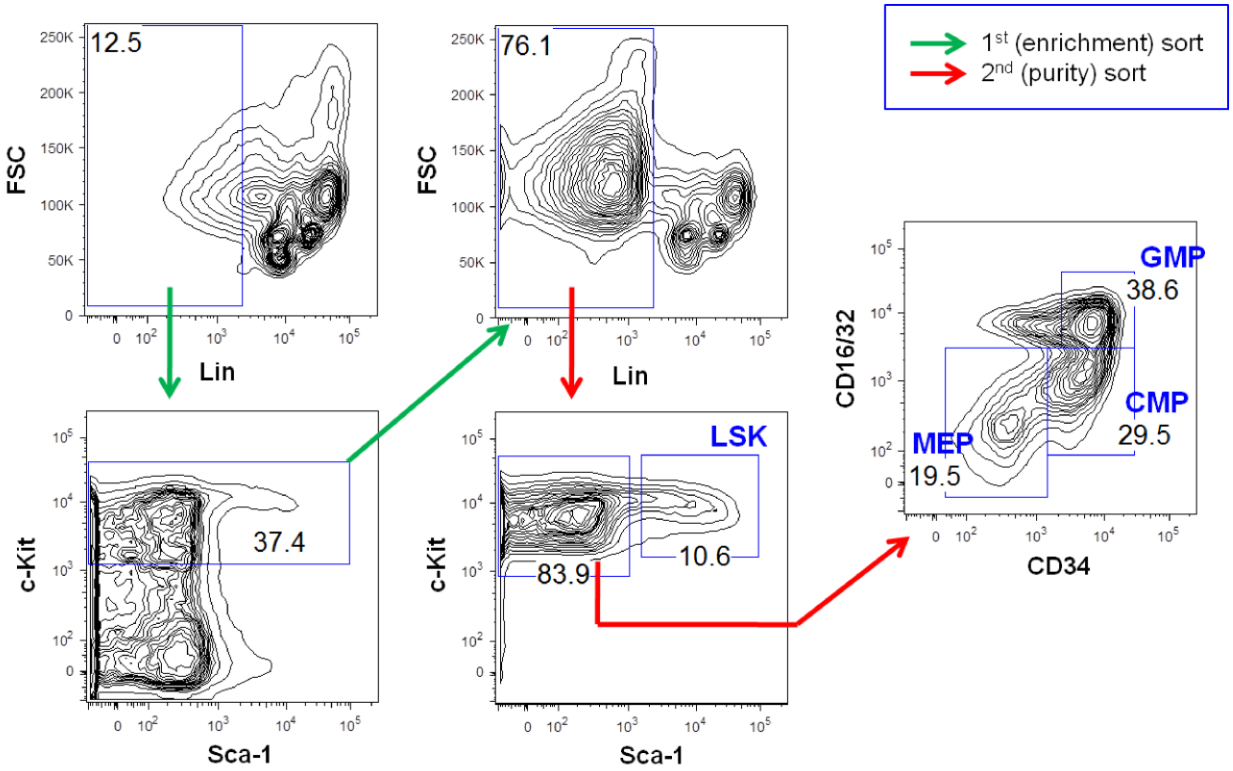

Figure 2.1 FACS sorting strategy for purification of LSK and GMP subsets.

Whole bone marrow was harvested, labeled with antibodies against lineage markers (CD3e, CD4, CD8a, B220, CD19, TER119, Ly-6G, and CD127), c-kit, Sca-1, CD34, and CD16/32 (FcγRIII/II), and sorted according to the depicted strategy. Two sequential sorts were utilized, first to enrich for the desired populations, and then repeated a second time to obtain high purity populations. *Lin, lineage; FSC, forward light scatter;*

LSK, Lin- Sca-1+ c-Kit+; GMP, granulocyte-monocyte progenitors; CMP, common myeloid progenitors; MEP, megakaryocyte-erythroid progenitors.

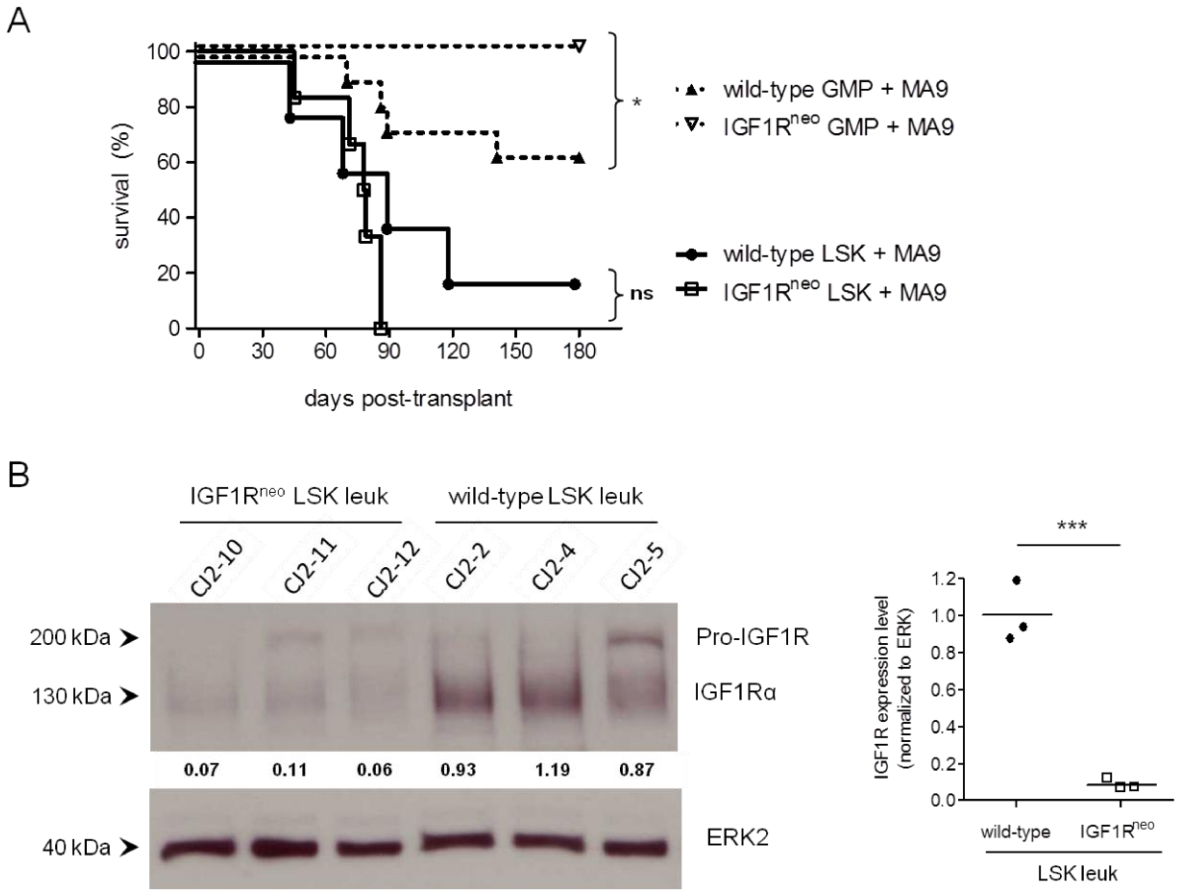

Figure 2.2 Reduced IGF1R impedes leukemogenic transformation of committed myeloid progenitors by MLL-AF9.

(A) Survival of C57BL/6 mice transplanted with MLL-AF9-transduced hematopoietic stem (LSK) or granulocyte-macrophage progenitor (GMP) cells from wild-type or IGF1R^{neo} donors. Bone marrow from age and sex matched wild-type and IGF1R$^{neo/neo}$ mice was harvested and LSK/GMP subsets were FACS sorted, transduced with MLL-AF9 retrovirus, and sorted again for successfully transduced (GFP+) cells. Similar numbers of transduced cells were then transplanted into lethally-irradiated syngeneic/congenic C57BL/6 recipients by tail vein injection along with a radioprotective "rescue" dose of whole bone marrow. Mice were monitored for clinical signs of morbidity and euthanized after attaining a predefined endpoint based on standardized scoring of clinical symptoms. Pathologic involvement by acute myeloid leukemia was confirmed at necropsy. *ns, non-significant; *, p<0.05 (Log-rank test).* **(B)** Western blot analysis of IGF1R protein expression level in primary acute myeloid leukemias derived from MLL-AF9-transduced LSK cells as in (A). Cell lysates were prepared from cell populations

containing >95% GFP+ tumor cells. Numbers below the IGF1R panel indicate relative IGF1R expression level after normalization to ERK2 loading control. Statistical analysis of the normalized IGF1R expression values is presented at the right with means indicated by horizontal bars. ****, p<0.001 (Student's t-test).*

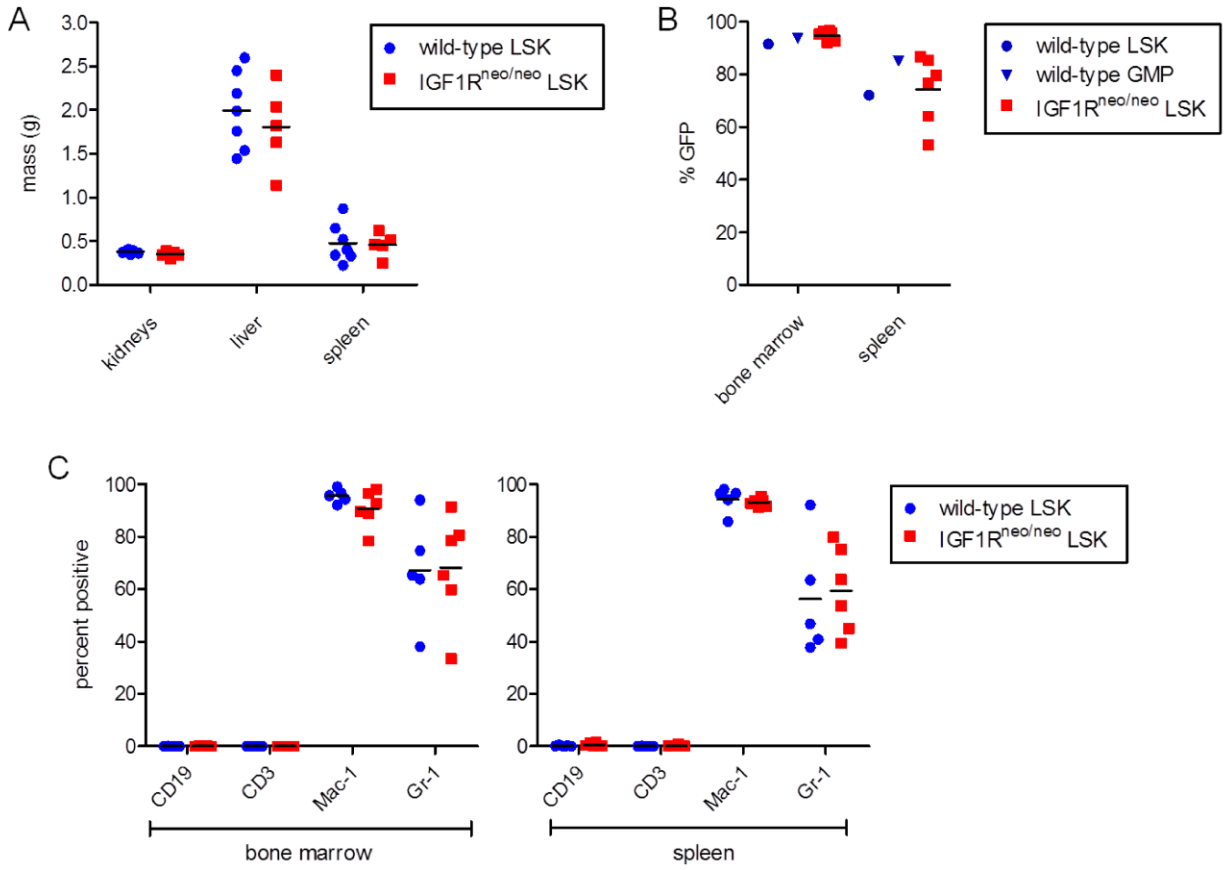

Figure 2.3 Reduced IGF1R does not affect AML disease parameters.

(A,B) Tissue involvement by MLL-AF9 leukemia cells in primary transplant recipient animals**. (A)** Organ weights at necropsy. **(B)** GFP+ fraction as assessed by flow cytometry of single cell suspensions derived from involved tissues. Each data point represents a different primary recipient animal. **(C)** Flow cytometric analysis for B-lymphoid (CD19), T-lymphoid (CD3), and myeloid (Mac-1, Gr-1) marker expression by MLL-AF9 leukemic cells from tissues of primary recipient mice. Fraction of cells positive for each marker is indicated within the GFP+ leukemia cell gate. Each data point represents a different primary recipient animal.

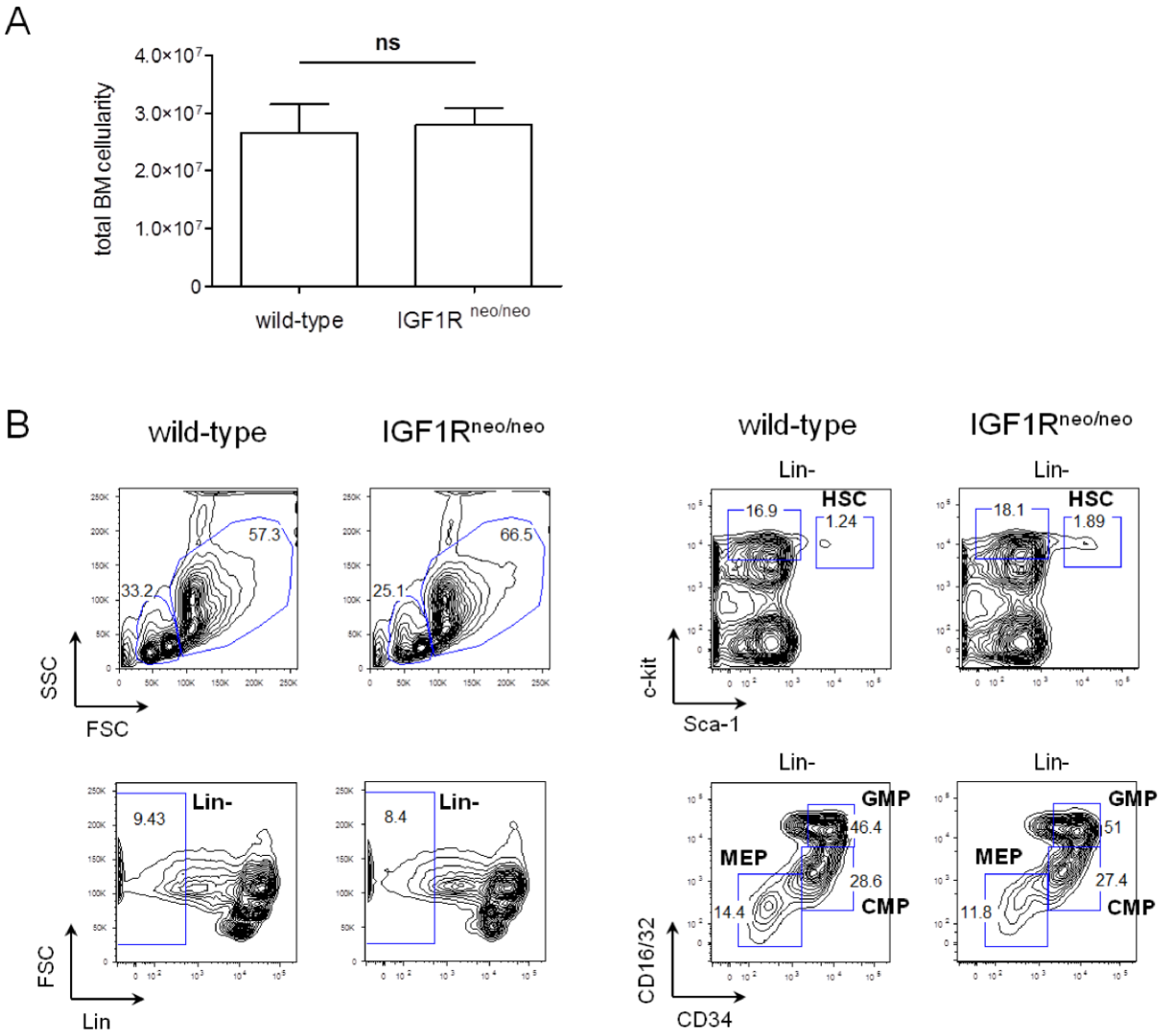

Figure 2.4 Bone marrow cellularity/composition is not perturbed in IGF1Rneo mice.

(A) Total bone marrow cellularity from wild-type vs. IGF1Rneo/neo mice. Cells were harvested from bilateral femurs and tibias, pooled, and counted manually following erythrocyte lysis. Data represent averages from 4 mice of each genotype. Error bars indicate standard deviation. *ns, non-significant (Student's t-test).* **(B)** Flow cytometric analysis of normal bone marrow cell subsets in wild-type vs. IGF1Rneo/neo mice. Cells were harvested as in (A), then stained for the indicated markers and analyzed by flow cytometry. Data depicted are representative of 3 replicates. *Lin = CD3e, CD4, CD8a, B220, CD19, Ter119, Ly-6G (Gr-1), and CD127 (IL-7Ra); HSC, hematopoietic stem cell; GMP, granulocyte-macrophage progenitor; CMP, common myeloid progenitor; MEP, megakaryocyte-erythroid progenitor; FSC, forward light scatter; SSC, side light scatter.*

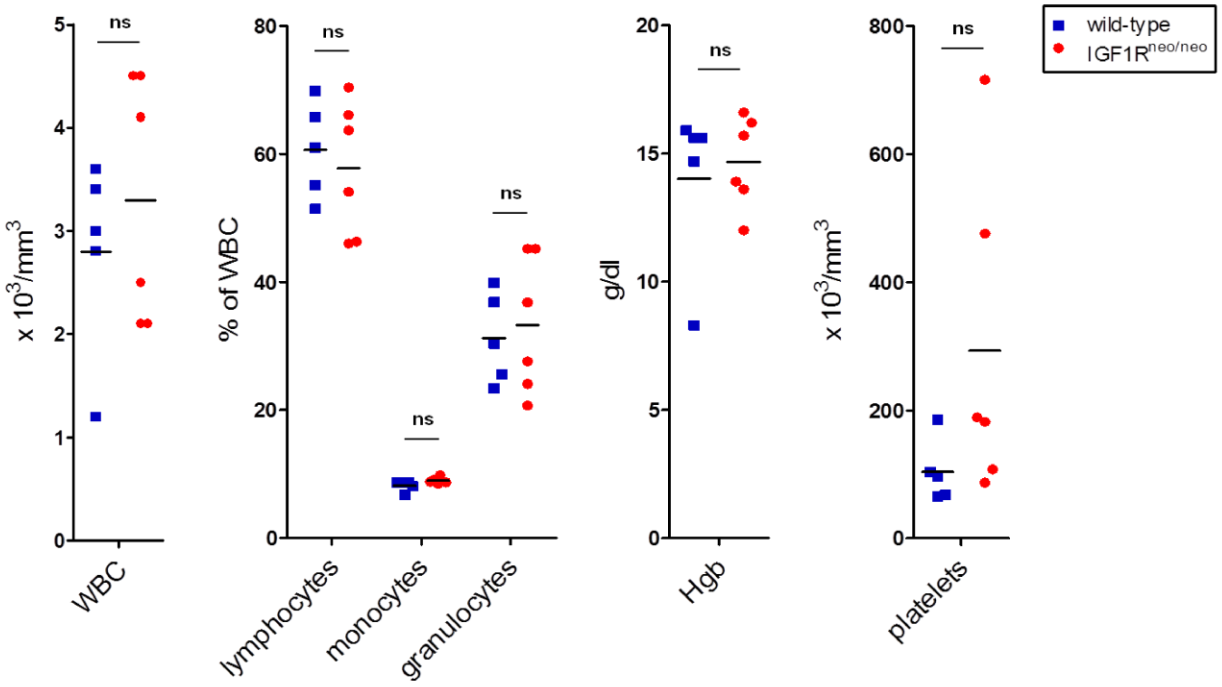

Figure 2.5 Peripheral blood counts are not perturbed in IGF1Rneo mice.

Complete blood count analysis of peripheral blood from age and sex-matched IGF1Rneo/neo and wild-type mice. Means are indicated by horizontal bars. *WBC, white blood cells; Hgb, hemoglobin; ns, non-significant (Student's t-test).*

2.4.2 Reduced levels of IGF1R do not markedly compromise leukemia-initiating cell activity.

The Weng lab had observed previously that acute T-cell leukemias generated on the IGF1R^{neo} background by transduction with activated NOTCH1 retrovirus were markedly compromised in leukemia-initiating activity as assayed by serial transplantation. In fact, the calculated LIC frequency in IGF1R^{neo} T-ALL is 1 in 14,000,000 cells (1 in 0.6-3.5 x 10^7 cells; 95% CI), or approximately 2,000-fold lower than wild-type ([2] and data not shown). To address whether this might also be the case for MLL-AF9 acute myeloid leukemias, I transplanted primary leukemias into secondary recipient mice and scored for disease propagation. In contrast to T-ALL, I observed IGF1R^{neo} MLL-AF9 AMLs to produce disease readily in secondary recipients similar to wild-type leukemias (**Figure 2.6**). These data suggest reduced IGF1R expression does not markedly compromise leukemia-initiating cell activity in MLL-AF9 AMLs as it does in NOTCH1 T-ALLs. I should

note however that these experiments were not done at limiting dilution, which makes it difficult to determine if there is a difference in the frequency of leukemia-initiating cells. Further studies will be needed to explore the basis for this difference in IGF1R dependence between T-ALL and AML leukemia-initiating cells and to determine if there is a change in LIC frequency in AML.

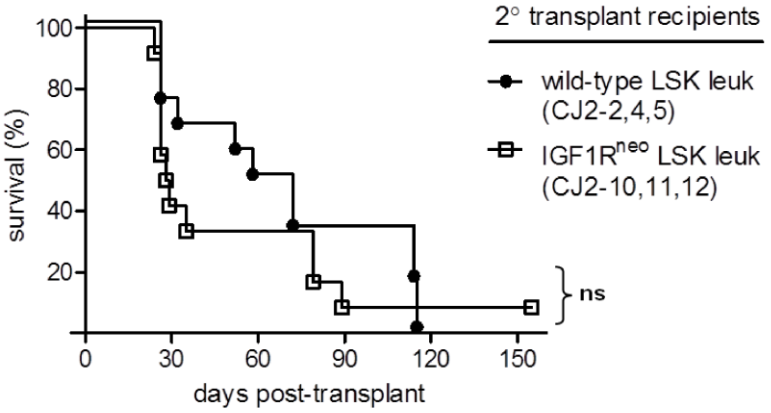

Figure 2.6 Reduced IGF1R expression does not markedly impair leukemia-initiating cell activity of MLL-AF9 AMLs.

Survival of non-irradiated, secondary transplant recipient mice injected by tail-vein with 500,000 primary MLL-AF9 leukemia cells as generated in Figure 1. Mice were monitored for clinical signs of morbidity and euthanized at the same clinical endpoints as used for evaluation of primary transplant recipients. Pathologic involvement by acute myeloid leukemia was confirmed at necropsy. Data are summarized for 3 independent primary leukemias of each genotype. ns, non-significant (Log-rank test).

2.4.3 Reduced levels of IGF1R compromise clonogenic activity of MLL-AF9 transduced GMPs.

Given that transduction of GMPs from IGF1R^{neo} mice with MLL-AF9 failed to generate AML disease, I sought to explore whether reduced IGF1R signaling might directly affect proliferation/survival in a cell autonomous fashion. To address this point, I employed colony forming cell (CFC) assays, a standard *in vitro* culture method for assessing the ability of committed myeloid progenitors to form colonies in semi-solid media. GMP cells were sorted from wild-type vs. IGF1R^{neo} bone marrow, transduced with MLL-AF9 or

empty (GFP only) retrovirus, and sorted again to separate transduced (GFP^+) from non-transduced (GFP^-) cells. Both GFP^+ and GFP^- subsets were then plated in methylcellulose-containing media under standard myeloid CFC conditions[217], and colony formation was assessed 20 days later.

Empty virus (GFP^+) and non-transduced (GFP^-) cells produced only 0-1 colonies per 1000 input cells from either background (), and no colonies formed on secondary replating. Consistent with established oncogenic MLL-AF9 function, MLL-AF9 (GFP^+) transduced cells yielded ~90 colonies per 1000 input cells, but with no significant difference between wild-type and $IGF1R^{neo}$ background (**Figure 2.8**). There was also no apparent difference in the size distribution of resulting colonies (data not shown). Upon serial replating, however, essentially every cell from primary wild-type CFCs yielded a secondary colony (~1000 colonies per 1000 input cells), whereas primary $IGF1R^{neo}$ CFCs yielded only ~50 secondary colonies per 1000 input cells. Thus, these data support that reduced levels of IGF1R negatively affect *in vitro* clonogenic activity of MLL-AF9 transduced GMPs, and suggest the inability of these cells to produce leukemia *in vivo* may be due at least in part to cell autonomous signaling defects. Further studies would be needed to address potential effects of reduced IGF1R signaling on other leukemogenic phenotypes such as self-renewal, homing/engraftment, interactions with microenvironmental niches, and immune evasion.

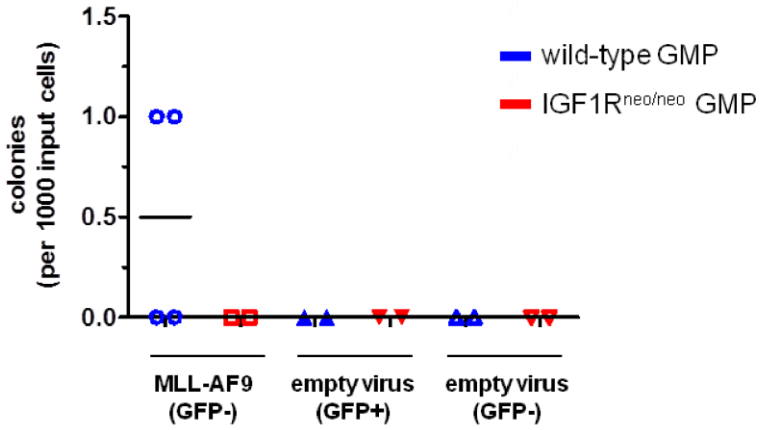

Figure 2.7 Clonogenic activity of untransduced and empty virus-transduced GMPs.

Clonogenic activity as measured by colony forming cell (CFC) assay. GMPs were FACS sorted from the bone marrow of age and sex matched wild-type and IGF1Rneo/neo donor mice and transduced with MLL-AF9 retrovirus vs. empty retrovirus control. Transduced (GFP+) and non-transduced (GFP-) cells were then FACS sorted and plated in methylcellulose-containing complete media with supplemental cytokines. Colonies were counted manually after 20 days incubation and visually confirmed for appropriate expression of GFP using an inverted fluorescent microscope. Colony yields are depicted from the first plating of non-transduced (GFP-) and empty virus-transduced (GFP+) GMP cells which served as controls. Means are indicated by horizontal bars.

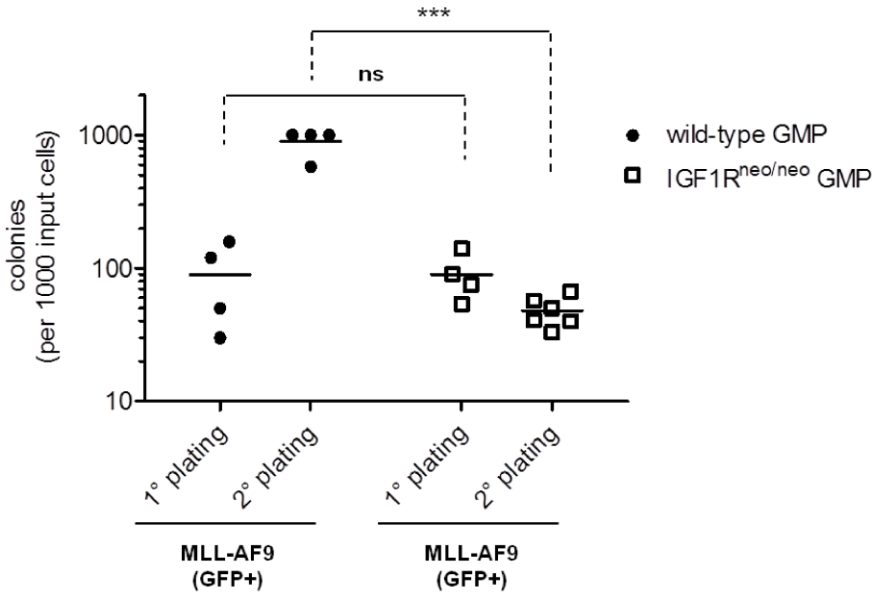

Figure 2.8 Reduced IGF1R expression impairs clonogenic activity of MLL-AF9-transduced GMPs.

Clonogenic activity as measured by colony forming cell (CFC) assay. GMPs were FACS sorted from the bone marrow of age and sex matched wild-type and IGF1Rneo/neo donor mice and transduced with MLL-AF9 retrovirus. Transduced (GFP+) cells were then FACS sorted and plated in methylcellulose-containing complete media with supplemental cytokines. Colonies were counted manually after 20 days incubation and visually confirmed for appropriate expression of GFP using an inverted fluorescent microscope. For secondary platings, colonies arising in the first plating were pooled and an equivalent number of live GFP+ cells as seeded in the first plating were re-plated into secondary cultures. Means are indicated by horizontal bars. ns, non-significant; ***, $p<0.001$ (Student's t-test).

2.4.4 Deletion of IGF1R in established leukemia cells has no effect on cell growth/viability.

Both IGF1R blocking antibodies and selective IGF1R tyrosine kinase inhibitors have been reported to antagonize growth/survival of human AML cells[196,199], but there has been ongoing debate as to the relative contributions of IGF1R and InsR signaling pathways in this context[201,202]. I thus took advantage of the defined genetics afforded by my MLL-AF9/IGF1R^{neo} mouse model to address the role of IGF1R in growth/survival of established AML cells. To this end, I cultured 3 wild-type and 3 IGF1R^{neo} MLL-AF9 LSK

leukemias *in vitro* and assayed cell growth by resazurin reduction. Despite some clone-to-clone variation, there was no evidence that reduced IGF1R expression led to a reduced net rate of cell growth (**Figure 2.9A**). This observation was corroborated by the fact IGF1R^{neo} leukemias did not show prolonged latency in secondary transplant assay as compared to wild-type leukemias (**Figure 2.6**). This finding was rather unexpected given the general importance of IGF signaling in growth regulation, and that IGF1R was expressed at 10-fold lower levels in IGF1R^{neo} leukemias as compared to wild-type controls (**Figure 2.2B**). To explore this point further, I took advantage of the fact that the IGF1R^{neo} allele, which contains flanking loxP sites around the neo cassette in intron 2 as well as around exon 3[228], can be excised by Cre-mediated recombination to ask whether genetic deletion of IGF1R would compromise AML cell growth. To this end, freshly explanted leukemia cells were transduced with lentivirus encoding tamoxifen-inducible Cre (CreERT2) and a truncated NGFR marker. Cultures were then treated with 4-hydroxytamoxifen (4-OHT) for 11 days to induce Cre-mediated deletion of IGF1R in transduced cells. Deletion of IGF1R, which was confirmed by PCR assay (**Figure 2.10**), had no demonstrable effect on cell proliferation as measured by BrdU incorporation compared to non-transduced cells in the same culture (**Figure 2.9B**). Additionally, I noted the NGFR^{+} transduced cell fraction to remain stable over extended passage of both 4-OHT treated and control cultures (data not shown). Overall, these findings support the conclusion that signaling through IGF1R is neither required for growth/survival of established AML cells, nor is there any incremental growth advantage conferred by increased levels of IGF1R expression in this context.

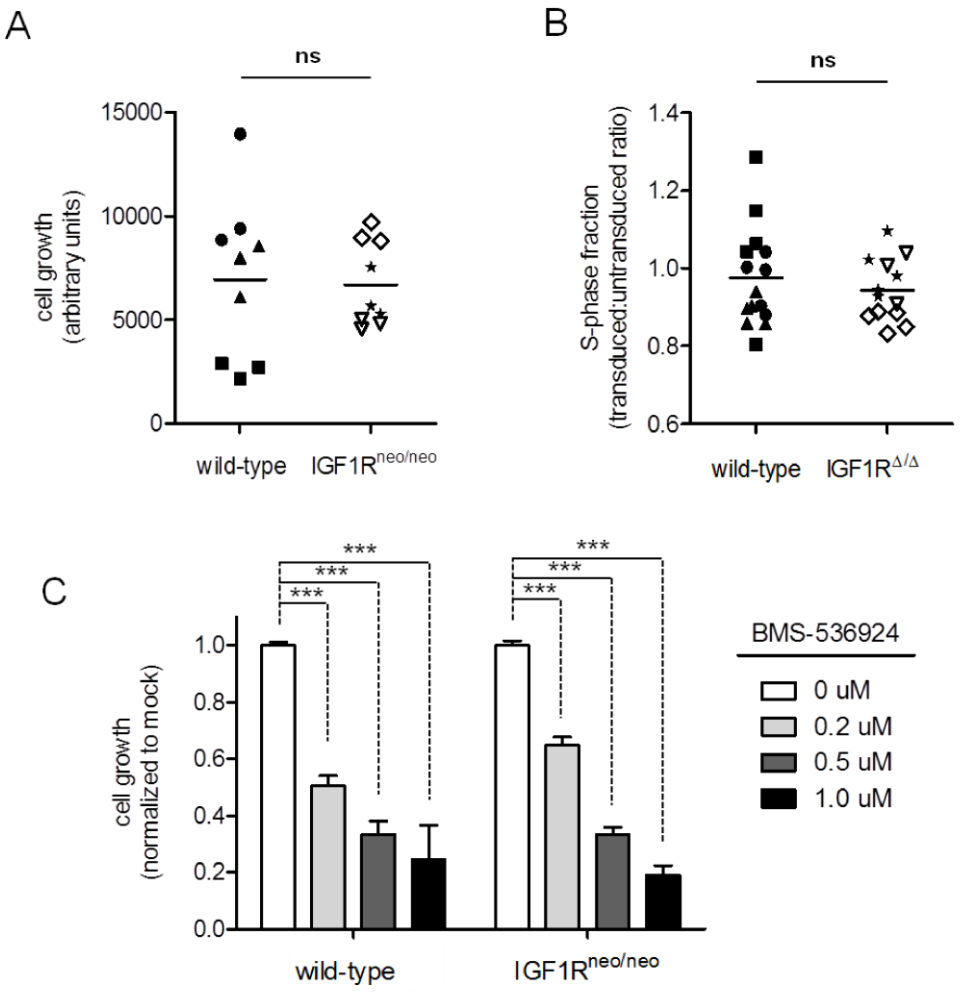

Figure 2.9 Established MLL-AF9 leukemias do not require IGF1R signaling.

(A) Growth of MLL-AF9 leukemias with reduced IGF1R expression. Freshly explanted primary MLL-AF9 (LSK) leukemias were cultured briefly on MS5 bone marrow stromal feeders, then equal numbers of cells plated on bare plastic. Cell growth was measured by resazurin reduction assay 48 hours later. Three independent leukemias (indicated by different shaped data points) of each genotype were assayed in triplicate. Means are indicated by horizontal bars. *ns, non-significant (Student's t-test).* **(B)** Proliferation of MLL-AF9 leukemias following deletion of IGF1R. Primary MLL-AF9 (LSK) leukemias were transduced with lentiviral CreERT2 (with NGFR marker), then treated with 5-10nM 4-OHT for 11 days to induce deletion of the IGF1Rneo allele. Cell proliferation was then assessed by BrdU incorporation. Transduced cells were discriminated from non-transduced cells in the same culture by labeling for NGFR. Three independent leukemias (indicated by different shaped data points) of each genotype were assayed 3-5 times each. Means are indicated by horizontal bars. *ns, non-significant (Student's t-test).* **(C)** Effect of IGF1R/InsR-selective tyrosine kinase inhibitor BMS-536924 on MLL-

AF9 leukemias. Primary MLL-AF9 leukemias were seeded at 2.5 x 10^5 cells/ml and BMS-536924 was added at the indicated doses vs. DMSO vehicle control in complete media. Cell growth was measured 48 hours later by resazurin reduction assay. One independent leukemia of each genotype was assayed in triplicate. Error bars indicate standard deviation. ***, *p<0.001 (two-way ANOVA with Bonferroni post-test analyses).*

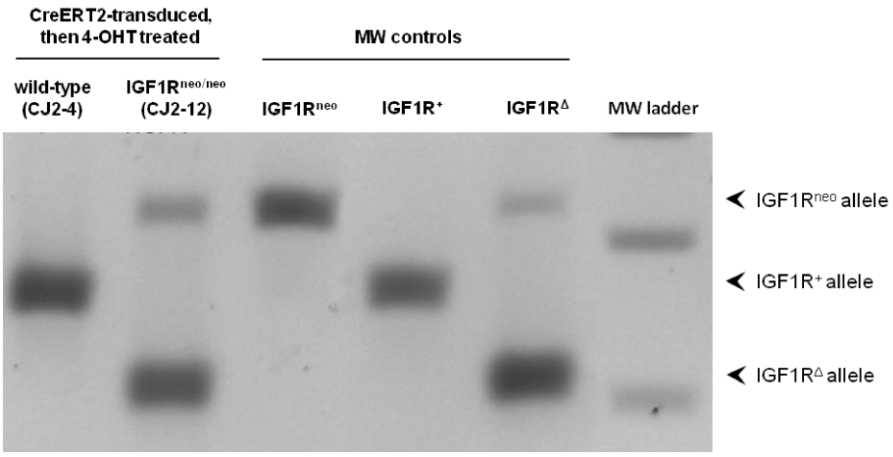

Figure 2.10 PCR confirmation of IGF1R deletion by lentiviral CreERT2.

PCR analysis for IGF1R deletion. Lentiviral CreERT2-transduced. 4-OHT-treated MLL-AF9 leukemia cells from **Figure 2.9** were FACS sorted by virtue of the lentiviral NGFR marker and genomic DNA was prepared. Multiplex PCR analysis was performed using primers to discriminate between wild-type (+), neo, and deleted (Δ) alleles of IGF1R. *MW, molecular weight.*

2.4.5 Tyrosine kinase inhibitors that preferentially target IGF1R/InsR impede AML cell growth and synergize weakly with cytotoxic chemotherapy.

In parallel with IGF1R deletion studies described above, I also explored effects of pharmacologic inhibitors on AML cell growth. As a receptor tyrosine kinase, small molecular inhibitors have been synthesized and tested over the last several years in different contexts[230]. I was interested to see if human AML cells were sensitive to IGF1R inhibition in contrast to mouse leukemia cells for which deletion had no effect on clonogenic activity. Most small molecule IGF1R inhibitors also affect insulin receptor (InsR) due to their close homology and at higher doses may be expected to cross react with more distantly related receptor tyrosine kinases. One such inhibitor, BMS-536924[231], significantly impeded growth of both wild-type and $IGF1R^{neo}$ leukemias (**Figure 2.9C**). Since genetic deletion of IGF1R had no effect on cell proliferation

(**Figure 2.9B**), I conclude that the efficacy of BMS-536924 under these assay conditions must be due to inhibition of InsR or related receptor tyrosine kinases. In support of this, BMS-536924 blocked insulin-induced signaling as measured by downstream activation of Akt (**Figure 2.11**).

I next sought to explore whether dual IGF1R/InsR inhibition was effective on human AML cells. Four human AML cell lines were selected for study and were confirmed to express high levels of surface IGF1R as measured by flow cytometry (**Figure 2.12A**). I found 2 of the 4 cell lines to be sensitive to another dual IGF1R/InsR inhibitor, BMS-754807[232], which has replaced BMS-536924 in the clinical development pipeline (**Figure 2.12B**). In parallel, cell viability was assessed by propidium iodide dye exclusion, and revealed dead cells in these cultures never to exceed 5%, suggesting that IGF1R/InsR inhibition with BMS-754807 primarily affects cell proliferation rather than survival (data not shown). These results are concordant with prior studies utilizing BMS-536924[199], but formally demonstrate efficacy of the current generation inhibitor, BMS-754807. Although I did not observe BMS-754807 to have appreciable effects on cell survival, it should be noted that the maximum dose assayed was 1 μM. In contrast, BMS-536924 was shown to induce substantial apoptosis of these same cell lines, but only at doses in the 5-10 μM range[199].

It has been suggested in the literature that IGF1R may be one of several genes whose expression correlates with chemotherapy resistance in AML[233,234]. I therefore tested whether IGF1R/InsR inhibition might enhance sensitivity to cytotoxic chemotherapy. The 2 human AML cell lines sensitive to BMS-754807 were treated with various dosing combinations of BMS-754807 and a commonly used anthracycline in AML treatment, daunorubicin, and cell growth was measured by resazurin reduction assay (**Figure 2.12C**). I observed very mild synergy between BMS-754807 and daunorubicin where the interaction accounted for 8-10% of the total variance (interaction p-value <0.0001, two-way ANOVA). Individually, BMS-754807 and daunorubicin were responsible for 25-32% and 56-61% of the total variance, respectively. These data suggest IGF1R/InsR inhibition may prove useful in combination with standard cytotoxic chemotherapy in

human AML and can be expected to show mostly additive, but perhaps slight synergistic effects. Further studies are needed for validate these observations in primary patient material and also to demonstrate efficacy *in vivo*.

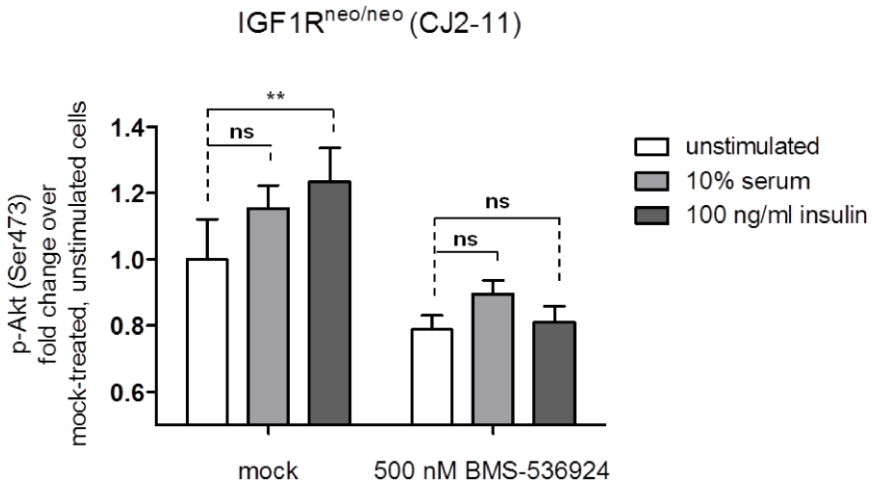

Figure 2.11 BMS-536924 blocks insulin signaling in MLL-AF9 primary leukemia cells.

Flow cytometric analysis for Akt activation by intracellular phospho-Akt (Ser473) level. Primary IGF1Rneo/neo leukemia cells from mice transplanted with MLL-AF9-transduced bone marrow LSK cells were cultured briefly *in vitro* and then serum starved overnight. Cells were then treated with BMS-536924 inhibitor for 1 hour prior to stimulation with either FBS or recombinant insulin for 10 minutes. Cells were then fixed immediately and permeabilized prior to flow cytometric analysis. All data are normalized to the mock-treated, unstimulated sample. Error bars indicate standard deviation. *ns, not significant; **, p<0.01 (two-way ANOVA with Bonferroni post-test analyses).*

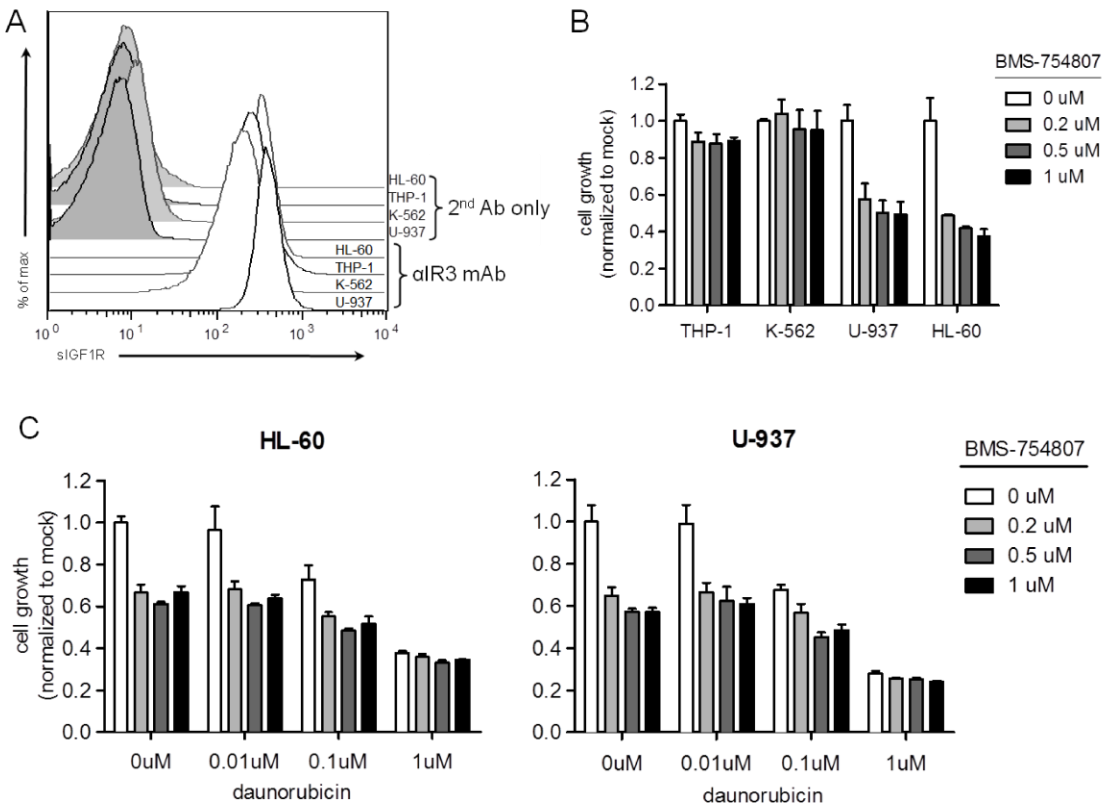

Figure 2.12 BMS-754807, an IGF1R/InsR-selective tyrosine kinase inhibitor, blocks growth of human AML cells and is weakly synergistic with daunorubicin.

(A) Flow cytometric analysis of surface IGF1R expression in human AML cell lines. Cells were labeled with primary αIR3 antibody, followed by APC-conjugated goat anti-mouse secondary antibody. **(B)** Effect of BMS-754807 on cell growth. Cells were plated at 2.5 x 10^5 cells/ml and BMS-754807 was added at the indicated doses vs. DMSO vehicle control in complete media. Cell growth was measured 48 hours later by resazurin reduction assay. All assays were performed in triplicate. Error bars indicate standard deviation. **(C)** Effects of BMS-754807 and daunorubicin on cell growth. Cells were plated at 5x10^5 cells/ml and BMS-754807 and/or daunorubicin were added at the indicated doses vs. DMSO/water vehicle controls, respectively, in complete media. Cell growth measured 24 hours later by resazurin reduction assay. All assays were performed in triplicate. Error bars indicate standard deviation.

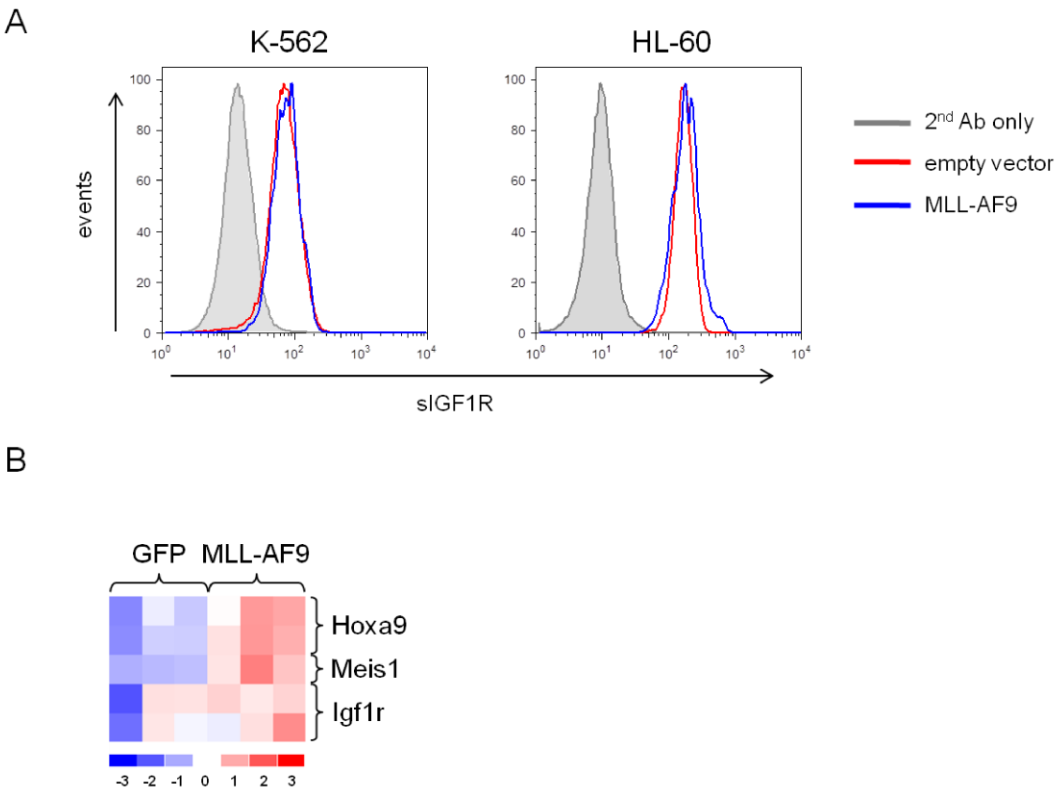

Figure 2.13 MLL-AF9 does not regulate IGF1R expression level.

(A) Flow cytometric analysis of surface IGF1R expression in human AML cell lines K-562 and HL-60 transduced with MLL-AF9 retrovirus or empty vector control. *sIGF1R, surface IGF1R.* **(B)** Microarray expression profile analysis of mRNA levels from triplicate samples of mouse GMP cells transduced with MLL-AF9 retrovirus or empty GFP vector control. Normalized data were downloaded from Gene Expression Omnibus (accession #GSE3721) and analyzed with dChip software. All available probesets for Igf1r and known MLL-AF9 targets Hoxa9 and Meis1 are depicted. Scale is expression level normalized across all samples with mean=0 and standard deviation=1 for each probeset.

2.5 Discussion

Using genetically engineered mice that express decreased levels of IGF1R, I have demonstrated that IGF1R signaling contributes to oncogenic transformation of GMP cells by the MLL-AF9 fusion oncoprotein. As prior work supports the idea that MLL-AF9 is capable of re-engaging a self-renewal program in committed GMPs[217], my data suggest that IGF signaling may collaborate with MLL-AF9-induced genes to support the

leukemic self-renewal program. Of note, IGF signaling has been shown to play an important role in self-renewal of embryonic stem (ES) cells[178], and IGF1R is expressed at higher levels in hematopoietic stem cells (HSCs) as compared to more differentiated progenitor subsets[179]. Additionally, IGF1R is differentially overexpressed in $CD34^{+}CD38^{-}$ AML stem cells as compared to their $CD34^{+}CD38^{+}$ differentiated progeny[235]. Interestingly, it was recently found that IGF1R is associated with CML blasts and BCR-ABL+ clonogenic activity, suggesting these findings might be broadly applicable to both chronic and acute myeloid neoplasia[236]. Further studies will be needed to determine which signaling pathways downstream of IGF1R are most relevant for leukemia initiation/self-renewal, and to what extent dependence on these signals vary with cell/developmental context.

It is interesting to note that the transforming potential of MLL-AF9 is also dependent on its level of expression and the level of DOT1L recruitment[225]. Whereas retroviral transduction drives high-level expression of MLL-AF9 in bone marrow progenitors and is relatively efficient at generating AML disease, “knock-in” of AF9 into the endogenous MLL locus achieves much lower levels of expression and is comparatively impotent in generating disease[222]. Furthermore, in striking similarity to my observations with reduced IGF1R, MLL-AF9 expression at lower, “knock-in” levels efficiently transformed LSK cells, but GMPs were resistant to transformation under these conditions. Given this similarity, I considered the possibility that MLL-AF9 might induce expression of IGF1R. Of note, in B-cell acute lymphoblastic leukemia (B-ALL) cells HOXA9, a key mediator of MLL-induced gene programs, positively regulates IGF1R expression[237] and a related MLL fusion protein, MLL-AF4, binds to the IGF1R locus[238]. I was unable, however, to detect changes in IGF1R expression in human AML cells following transduction with MLL-AF9 retrovirus (**Figure 2.13 A**), and published expression profile data from mouse GMPs transduced with MLL-AF9 retrovirus showed consistent upregulation of known targets Meis1 and Hoxa9[217], but not Igf1r (**Figure 2.13 B**).

It is interesting to note the differences between my results and those seen in T-cell leukemias[2]. Recent work in T-cell leukemias has shown that dendritic cells may secrete

IGF ligands, suggesting that the microenvironment may play a role. If stem and progenitor cells occupy regions of relative abundance or austerity in terms of ligand, it could also have effects on relative difference between these subsets[239]. Additional studies will be needed to determine if the dosage-dependent effects of MLL-AF9 and IGF1R on transformation of GMPs are mechanistically related.

It remains unclear what underlying mechanism is responsible for the difference in transformation susceptibility between GMPs and LSKs as revealed either at physiologic MLL-AF9 dosage in the Kersey lab's knock-in study[222], or via reduced IGF1R expression in the current study. One possibility could be that the threshold for transformation may be higher in GMPs where the self-renewal program presumably must be re-initiated as opposed to HSCs where it needs only to be maintained. This difference may hold clinical significance in that self-renewal activity of leukemia stem cells which originated by transformation of committed progenitors may be dependent on high levels of MLL-AF9 expression and/or IGF1R signaling whereas those arising by transformation of HSCs may not. Accordingly, novel therapies targeting these pathways may potentially be more effective against "progenitor-derived" than "stem cell-derived" leukemias.

Despite my observation that genetic deletion of IGF1R had no apparent effects on growth of established murine MLL-AF9 leukemias, it is notable that these mouse cells were nonetheless sensitive to dual IGF1R/InsR inhibition. This suggests that there may be significant functional redundancy between IGF1R and InsR in AML cells, which implies that the relative "non-specificity" of small molecule kinase inhibitors may actually be an advantage over IGF1R-specific neutralizing antibodies. Going one step further, my data also raise the possibility that the observed efficacy of anti-IGF1R antibodies against AML cells *in vitro*[196] may not in fact be acting solely by blocking IGF1R signaling, but perhaps also through direct/indirect cytotoxic effects such as may potentially result from high density antibody binding to the surface of the cell. IGF1R inhibitors may also find use in combination with other inhibitors such as RAS inhibitors, and have been shown recently to be synergistic[240]. Additional strategies targeting the

SUMOylation of IGF1R could also be relevant going forward, but may act through other targets[241]. Regardless of the actual mechanism, the efficacy of any IGF1R inhibitor strategy will have to be validated in human patients and balanced with associated side effects[201,202].

Chapter 3: RUNX1 in T-cell Acute Lymphoblastic Leukemia

Leukemogenesis

3.1 Chapter overview

Retroviral insertional mutagenesis is a powerful, widely used tool to uncover collaborating oncogenes and pathways necessary to establish a tumour. Previously, alleles of *NOTCH1* have been used which have selected for further sustained Notch signaling[3]. Thus, I wanted to discover genes which are outside of the Notch signaling pathway, but work in parallel with it to support clonal establishment. Once discovered, I wanted to confirm collaboration *in vivo* using bone marrow transplantation of a weakened allele of Notch which would not generate leukemias in isolation. Using a multicistronic system, I hoped to determine if any of these genes could generate a tumour in concert with NOTCH1.

3.2 Introduction

3.2.1 Retroviral insertional mutagenesis

Originally, transforming retroviruses were understood to promote oncogenesis or leukemogenesis by hijacking a neighbouring proto-oncogene as in the case of viruses such as Rous sarcoma virus (RSV) and the *v-Src* gene[242,243]. Studies of viral-induced tumours in the 1980s suggested however that proto-oncogenes were capable of exploiting the promoter or enhancer activity of the viral LTR of retroviruses which had integrated nearby as observed for *Myc* and the virus(**Figure 3.1**)[244]. Researchers have since leveraged slow transforming, and acute transforming, retroviruses (and later transposable elements) to perform *in vivo* screens to discover genes that collaborate with each other in the establishment of a clonal tumour. These screens began with Southern blot and genomic library screening, but have since moved to PCR-based methods and eventually high-throughput screens involving next-generation sequencing[245,246]. These insertional mutagenesis screens can be performed on a transgenic background or using a retrovirus carrying a transgene, using either replication-defective or replication-competent viral particles. Typically, the retrovirus or

transposon can interrupt gene regulation in one of a number of ways (**Figure 3.2**). Genes can become directly interrupted by the integration of an element (intragenic), altering the reading frame or generating alternately spliced dominant-negative, hypomorphic or neomorphic, alleles leading to loss of normal gene functioning. Alternatively, and more commonly found as being selected for during tumourigenesis, are intergenic mutations where the integrated genetic element may lead to aberrantly high expression levels of a gene which may not typically be active in the tissue or developmental stage and thus generate leukemia. This can be accomplished either by inverse-oriented enhancer elements within the virus/transposon or through the promoters in the viral LTRs which are not under the same controls that the endogenous gene is beholden to. In determining how to prioritize which genes the researcher may wish to pursue in functional validation, typically they are prioritized based on frequency of mutation. Common insertion (or integration) sites (CIS) are “hot-spot” regions of the genome where recurrent integration is noted in multiple tumours, suggesting that the mutation was under selection and did not occur just by chance. Typically, any insertion more than 1 is considered a CIS, however in large-scale screens which have interrogated hundreds of tumours it is advantageous to use more rigorous statistical analyses to categorize what a CIS is. The use of kernel convolution (using Gaussian distributions), Monte Carlo analysis, and Poisson distributions have all been proposed recently to estimate regions of recurrent mutation in order to guard against the potential of random integrations throughout the genome[247-250]. Once, a common insertion site has been identified, it is typically validated by attempting to overexpress the gene of interest (the CIS locus) along with the gene or genes previously used in the original screen. This can be accomplished by retroviral/lentiviral overexpression of a transgene or by crossing transgenic mice strains. An example of this paradigm is the example of Runx2 and Myc, whereby an inducible version of Myc is able to collaborate with Runx2 to generate fully penetrant T-cell leukemia with a mean latency of 36 days[251]. In a sobering reminder of the caveats of early human gene therapy trials, T-ALLs arose during attempts to treat Severe Combined Immunodeficiency (SCID-X1) where patients were found to have recurrent integrations of a lentivirus (carrying the common γ-chain) near

the gene *LMO2*[252]. The same year, researchers described that integrations which create dominant-negative isoforms of *Ikzf1* (Ikaros) are selected for using the Moloney Murine Leukemia Virus (MoMLV) on an *lck*-N^{IC} (Intracellular NOTCH1 aka ICN) transgenic mouse background in 40% of mice[3,253]. It was subsequently revealed that the transgenic line lacked regions of the *NOTCH1* transactivation domain, creating a hypomorphic allele of intracellular NOTCH1[254]. The loss of Ikaros function was later shown to result in an enhancement of Notch signaling, suggesting that these mutations act to potentiate Notch signaling on a weakly leukemogenic background[255]. This is important to note in that one might therefore infer that a "stronger" allele of NOTCH1, such as the ΔE allele of NOTCH1, would be expected to generate polyclonal tumours if it was the only mutation required for generating leukemias. Importantly however, the leukemias which derive from these constructs on a wild-type syngeneic background are clonal[43,256]. This would suggest then that other collaborating mutations or disruptions are required to collaborate with ΔE to aid in the establishment of a clone of cells.

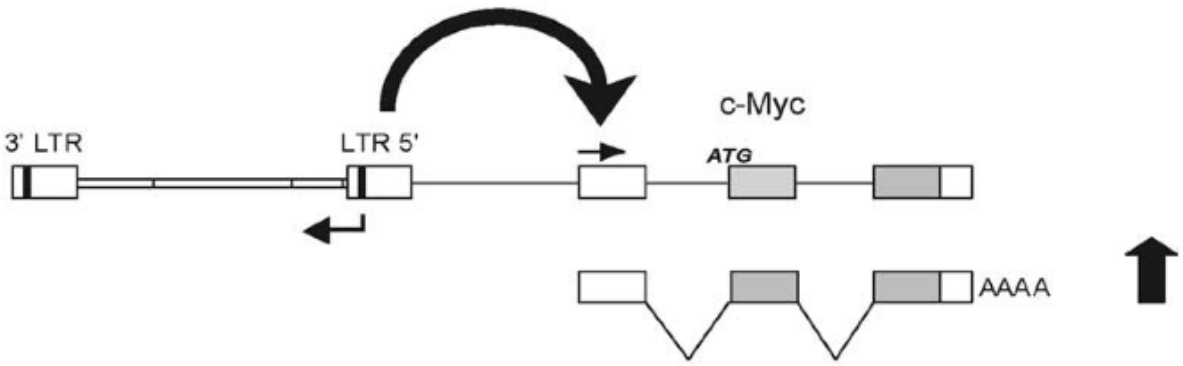

Figure 3.1 Induction of c-Myc expression by proviral enhancer.

The enhancer in the 5' LTR of the provirus, which is integrated upstream of the c-Myc gene enhances c-Myc expression. The provirus is inserted such that the transcriptional direction of the provirus is opposite to transcription of the cellular gene. Exons are drawn as boxes (coding sequences depicted in grey). The transcriptional and translational start site of the c-Myc gene is indicated (horizontal arrow and ATG, respectively). Reprinted by permission from Macmillan Publishers Ltd: *Oncogene*. Figure from Retroviral insertional mutagenesis: past, present and future (Uren, Kool, Berns, van Lohuizen, 2005), doi:10.1038/sj.onc.1209043. © Nature Publishing group 2005, accessed December 2016.

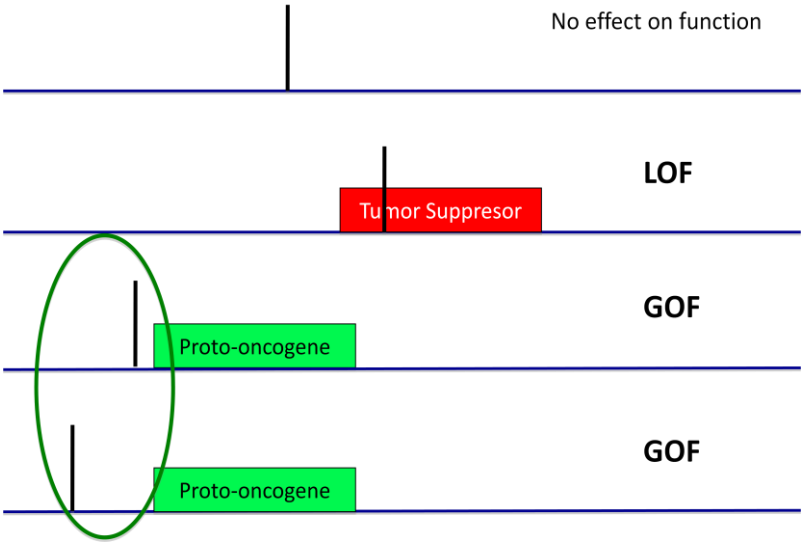

Figure 3.2 Effects of viral integration on genes near protein-coding elements.

Viral integrations throughout the genome may have no net effect on function or the function may not be obvious. Some integrations may interrupt the coding sequence of a gene or interrupt enhancer functions resulting in a loss of expression or expression of dominant-negative isoforms. Additionally, integrations may integrate upstream of a proto-oncogene resulting in overexpressing or loss of developmental stage specific control by viral promoter/enhancer usage. The occurrence of more than one integration near the same gene in multiple tumours is called a common integration site.

3.2.2 Selection of insertional mutagenesis strategy

Early insertional mutagenesis studies involved the use of probing genomic libraries from tumours using retroviral long-terminal repeat (LTR) sequences but have since progressed to a number of PCR-based methods which include but are not limited to: splinkerette PCR, panhandle PCR, capture PCR, inverse PCR, *Alu* PCR, vectorette PCR and boomerang PCR[257-261]. Splinkerette PCR is an advancement of the vectorette design, which contained a mismatched region, suitable for PCR walking and amplification of regions of known sequence with a restriction enzyme site of the experimenter's choosing (**Figure 3.4**)[259]. Some of the key concerns which splinkerette PCR specifically addresses are end-repair priming, whereby the overhangs of vectorettes are filled in during the first round of amplification, and allow exponential amplification of vectorette oligonucleotides at the expense of amplifying correctly-adapted viral DNA-gDNA complexes[261]. Instead of a mismatched region, the

splinkerette contains a mismatched hairpin loop which reduces end-repair priming and non-specific priming (on one strand) during annealing and elongation steps of the PCR. However, it should be noted that the method does have caveats that are associated with all PCR-based methods such as amplification bias which may over-represent certain amplicons and under-represent others. Once splinkerette PCR reactions have been amplified, it is necessary to de-multiplex them as they contain a heterogeneous mix of genomic regions. For the relatively low number of leukemias studied, I chose to use the TOPO-TA kit to shotgun clone the integrants followed by capillary read sequencing (Sanger sequencing).

3.2.3 Multicistronic 2A peptide lentivectors

In attempting to deliver multiple gene products to cells, there are limited options, each with a number of caveats. It is possible to cross multiple strains of transgenic mice, however there are issues associated with random integration of the transgene and copy number of the transgene among others[262]. Internal ribosome entry sites (IRES) are elements which allow for translation of two polypeptides from the same promoter (bicistronic expression), but unfortunately this limits the researcher to two open reading frames which are often translated at unequivalent amounts and the cassette is rather large which limits cDNA size. It is also possible to transduce cells with multiple lentiviruses or retroviruses in order to deliver the number of cDNAs desired. However, the delivery of multiple viruses results in multiple integration events, which may have unpredictable outcomes on the biology of the cell of interest that may be unrelated to the cDNAs carried within. 2A peptide sequences are advantageous because they allow multiple cDNAs to be transcribed from one promoter and for stoichiometric translation of these sequences.

The 2A peptide sequences were originally characterized in the Picornavirus foot-and-mouth disease virus (FMDV)[263]. Cleavage takes place using *cis*-acting hydrolase elements (CHYSELs) at the C-terminal region of the 2A sequence between two coding regions by what is termed a ribosome “skip”, whereby there is a pause at a specific Gly-Pro bond which is more accurately described as a halt in translation and re-initiation of

translation[264-266]. Several of these 18-22 amino acid sequences are available for building multi-cistronic lentivectors from multiple picornaviruses including F2A (FMDV), T2A (*Thosea asigna* virus), E2A (equine rhinitis A virus) and P2A (porcine teschovirus-1)[267-269]. The system has shown promise in restoring T-cell developmental blocks in CD3-deficient mice by concurrently expressing CD3ε, CD3γ, CD3δ and CD3ζ [270]. A key caveat to multi-cistronic 2A cassettes is that fusion proteins may be created due to incomplete cleavage, which may be a result of tissue-specific expression and/or the presence of N-terminal signal sequences[271-273].

3.2.4 Statement of hypothesis and objectives

Previous studies attempting to identify mutations which collaborate with Notch signaling have been unsuccessful at discovering other mutations which do not act to sustain higher levels of Notch signaling. I sought to use leukemias generated using an allele of *NOTCH1* (ΔE) which generates relatively high levels of Notch signaling in order to find genes which are considered removed from the canonical Notch signaling pathway[274]. I hypothesized that higher levels of leukemogenic active Notch signaling will select for Notch-independent mutations and that those lesions would collaborate with Notch signaling to enhance leukemogenesis. I also hypothesized that these mutations would collaborate with a weak allele of NOTCH1 to shorten latency and increase penetrance of leukemia initation. The objectives to address this hypothesis include 1) Clone out and map retroviral integration/insertion sites to the mouse genome, 2) Clone multi-cistronic vectors carrying a subset of those genes found to potentially collaborate with NOTCH1 and measure their potential to enhance leukemogenesis by bone marrow transplantation and subsequent leukemia-related mortality.

Aim 2: Identify and characterize genes that collaborate with NOTCH signaling in T-cell Acute Lymphoblastic Leukemia pathogenesis.

3.3 Materials and methods

3.3.1 Retroviral insertional mutagenesis

This study utilized banked frozen bone marrow from leukemic hNOTCH1ΔE mice which had been generated using 5-FU bone marrow transplantation as described previously[2]. In batches of 4, genomic DNA was isolated from 88 mouse T-ALLs using the PureLink® Genomic DNA Mini Kit. To clone out integration sites I modified a previously published protocol [246]. While the original protocol was designed for use with the Murine Leukemia Virus (MuLV), the sequences used were adapted to the MSCV-IRES-GFP and MSCV-IRES-NGFR retroviruses, which are derived from MuLV. The original protocol suggested digestion of gDNA with Sau3AI followed by ligation and EcoRV digestions. Due to differences in viral sequence, I instead digested the leukemia gDNA with MspI followed by EcoRV or Sau3AI followed by NheI. Due to the last change, another splinkerette adaptor was made which matched the sticky-end genomic overhangs created by MspI (**Table 3.1**). PCR-amplified integrations were cloned using the TOPO TA Cloning® Kit for Sequencing with One Shot® TOP10 Electrocomp™ E. coli (Invitrogen, Cat. No. K4580-01) according to the instructions in the protocol.

Oligonucleotide name	Oligonucleotide sequence	Notes
Long-strand adaptor	CGAAGAGTAACCGTTGCTAGGAGAGACCGTGGCTGAATGAGACTGGTGTCGACACTAGTGG	
Short-strand adaptor (Sau3AI)	GATCCCACTAGTGTCGACACCAGTCTCTAATTTTTTTTTTTCAAAAAAA	Contain hairpin and Sau3AI 5' overhang
Short-strand adaptor (MspI)	CGCCACTAGTGTCGACACCAGTCTCTAATTTTTTTTTTCAAAAAA	Contain hairpin and MspI 5' overhang
Splink1	CGAAGAGTAACCGTTGCTAGGAGAGACC	1st round PCR primer on splinkerette adaptor
U3 LTR#5	GCGTTACTTAAGCTAGCTTGCCAAACCTAC	1ST round PCR primer on MSCV-based retroviral LTR
Splink2	GTGGCTGAATGAGACTGGTGTCGAC	2nd round PCR primer on splinkerette adaptor
U3 LTR#1	CCAAACCTACAGGTGGGGTCTTTC	2ND round PCR primer on Mig dE viral LTR
U3 LTR#Sau	CTAGCTTGCCAAACCTAC	variant on U3 LTR #5 for the 1st round of PCR on Mig dE viral LTR for Sau3AI digested gDNA

Table 3.1 Oligonucleotides used in Retroviral Insertional Mutagenesis Splinkerette protocol.

3.3.2 Data analysis

Sequences derived from Sanger sequencing were mapped to the mouse genome using the *iMapper* website (http://www.sanger.ac.uk/cgi-bin/teams/team113/imapper.cgi). Briefly, the web-based interface allows import of FASTA sequences and uses the sequence from the retrovirus to map viral integrations to the mouse genome in Ensembl[275]. Only "good" sequences which contain regions of the genome with adjacent viral sequence are considered integration sites for my study.

3.3.3 Cloning ΔE/ΔEΔL 2A-lentivectors

Lentivectors containing multi-cistronic cassettes containing an allele of human NOTCH1 (ΔE or ΔEΔL), with or without a RUNX allele, and GFP as a selectable marker were cloned using nested PCR. Primers containing required restriction enzyme sites, as well as portions of 2A site were used for a first round of PCR (**Figure 3.3**). Reactions were purified using a PureLink^{TM} Quick PCR Purification Kit (Invitrogen, Cat. No. K310002) and a second round of PCR using more of the 2A sequence and a restriction enzyme consensus site was used to generate a complete 2A-Gene-of-interest cassette. The different cassettes were ligated into intermediate vectors, followed by transfer of the NOTCH-RUNX-GFP cassette into a pRRL-based self-inactivating lentivector.

3.3.4 Bone marrow transplants

Primary mouse leukemias were generated from bone marrow cells collected from 5-fluorouracil treated donor mice from wild-type C57BL/6J backgrounds. Bone marrow was transduced with lentiviruses as indicated by spinoculation[2] followed by injection of indicated numbers of GFP+ cells into the tail vein of lethally irradiated (810 RAD) congenic recipient mice 3 days later. Mice were monitored for clinical symptoms of leukemia and euthanized using standard protocols with leukemia-infiltrated tissues banked for further analyses. All animals were housed in the BC Cancer Agency Animal Resource Centre under pathogen-free conditions and in compliance with protocols approved by the University of British Columbia Committee for Animal Care

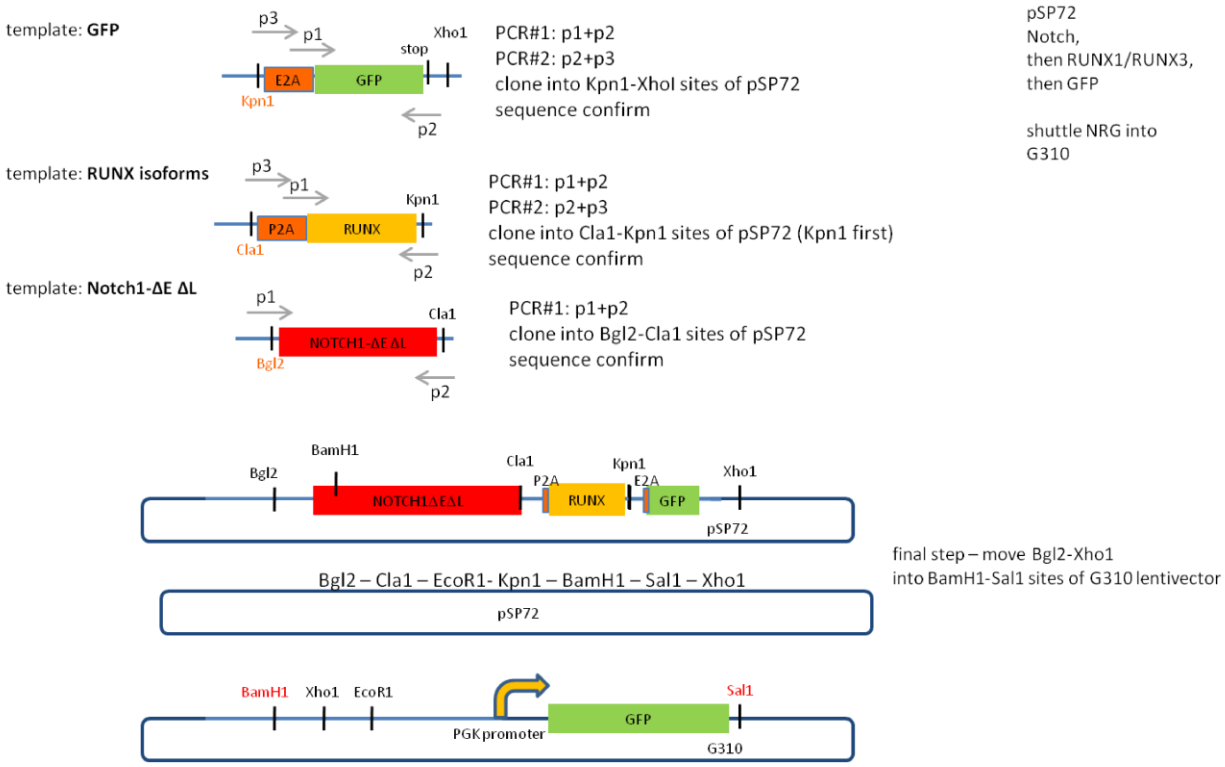

Figure 3.3 Cloning strategy for 2A lentiviral constructs.

Laddered PCR reactions were carried out using primers encoding restriction enzyme sites and sequences of P2A and E2A sequences.

3.3.5 Western blotting

Antibodies used were anti-Cleaved Notch1 (Val1744) [(clone D3B8) Rabbit mAb #4147, Cell Signaling Technology], anti-Hemagglutinin (anti-HA) [(clone HA-7) mouse mAb #H9658, Sigma-Aldrich], and anti-RUNX3 [(clone 527327) mouse mAb #MAB3765, R&D Systems], β-actin (Sigma Aldrich; AC-15).

3.4 Results

3.4.1 Retroviral insertional mutagenesis study design

Utilizing a bank of murine leukemias that our lab already possessed, I isolated genomic DNA (gDNA) from 88 NOTCH1ΔE (ΔE) leukemias. I used a well-established splinkerette ligation system which had a readily available protocol which I adapted to our specific retrovirus[246]. Samples were digested with restriction enzymes with 4-bp

recognition sequences to produce fragments ranging from 400-1700bp, followed by ligation to splinkerette adaptors and PCR amplification of viral LTR-genomic DNA fragments (**Figure 3.4**). Amplified integrants were then TOPO-TA cloned and transformed followed by isolation of plasmid DNA and subsequent capillary read end sequencing (**Figure 3.5**). Sequences were aligned to the mouse genome using *iMapper* (Ensembl) and each output integrant was confirmed by visual confirmation to have viral LTR sequence directly adjacent to mouse genomic DNA sequence.

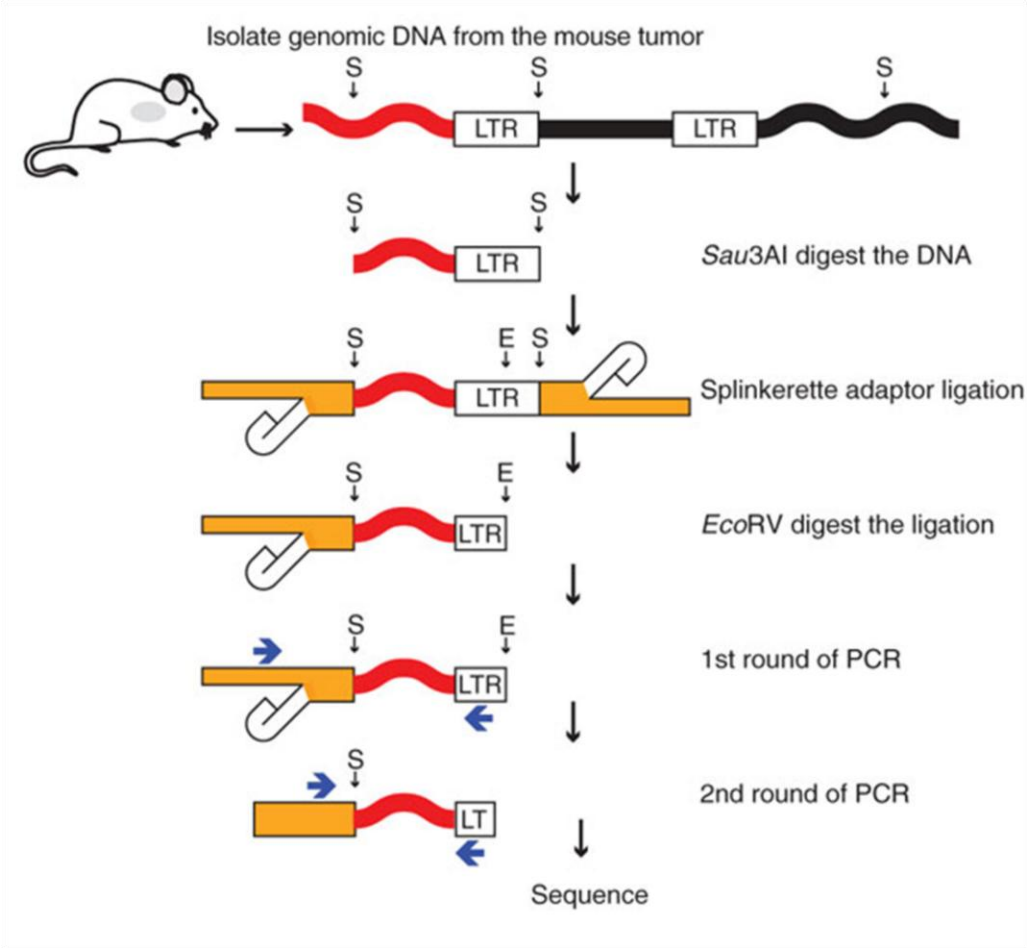

Figure 3.4 Overview of the splinkerette-PCR protocol.

The steps performed to generate splinkerette-PCR products for sequencing. E and S refer to EcoRV and Sau3AI, respectively. Reprinted by permission from Macmillan Publishers Ltd: Nature Protocols. Figure based on **A high-throughput splinkerette-PCR method for the isolation and sequencing of retroviral insertion sites** (Uren et

al. 2009), doi:10.1038/nprot.2009.64 © Nature Publishing Group 2009, accessed February 2017. http://www.nature.com/nprot/index.html

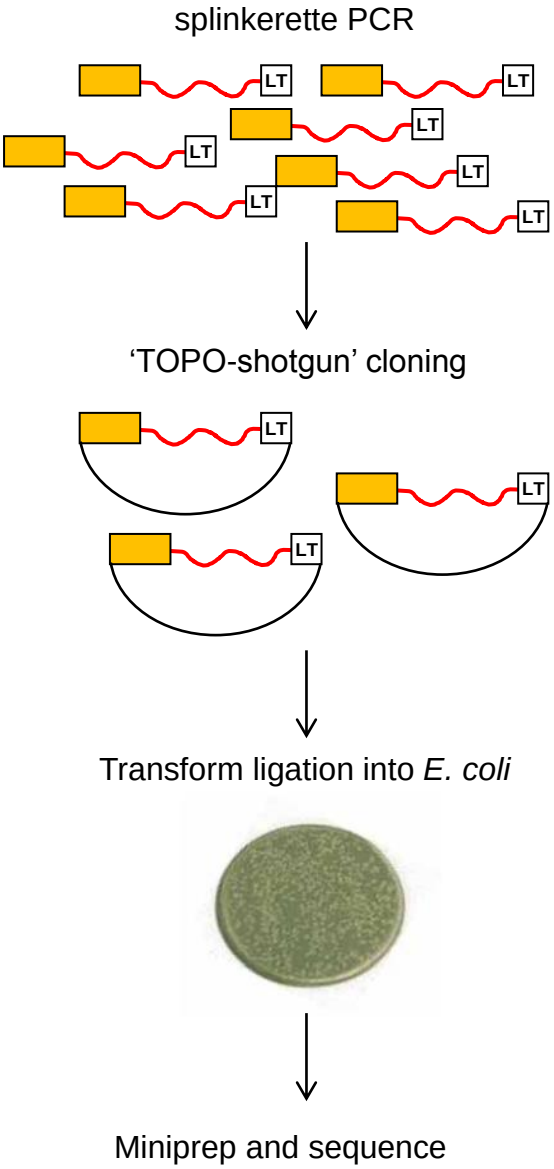

1. Digest Leukemic gDNA
2. Ligate adaptors
3. PCR amplify integrants
4. TOPO-TA clone integrants
5. Transform into *E. coli*
6. Pick colonies
7. Sequence
8. Map to Mouse genome

Figure 3.5 High throughput splinkerette PCR.

Reprinted by permission from Macmillan Publishers Ltd: Nature Protocols. Figure based on **A high-throughput splinkerette-PCR method for the isolation and sequencing of retroviral insertion sites** (Uren et al. 2009), doi:10.1038/nprot.2009.64 © Nature Publishing Group 2009, accessed December 2016. http://www.nature.com/nprot/index.html

3.4.2 Retroviral insertional mutagenesis study analysis

From the 88 ΔE leukemias, I was able to recover a total of 143 loci which had integration events (**Appendix A**). Independent integration events were defined as those in which there was at least one base pair difference between the end of the viral sequence and the start of genomic sequence. Of these, there were 130 loci which had single integration events where the ΔE retrovirus had no other independent integrations. 13 loci had more than 1 integration event, suggesting that multiple leukemias contained integrations at or near the same gene (**Table 3.2**). For the case of this study I will refer to these as common insertion sites (CIS). There were two integrations into loci near the genes *Chi3l1/Mybph/Adora1*, *F11r/Slamf7/Slamf1*, *Pten*, *Il12rb1*, *Gga1/AL592169.14/Sh3bp1*, *Rhoa/Gpx1/Usp4*, *Smad6*, *Irfbp2*, *Lfng / Ttyh3*, *Sos2/Arf6, Dpp10/Snora17*. Finally, there were three independent integrations near the genes *Ikzf1*, *Nup214/Fam78a/Abl1*, and *Runx3*. Of note, there are a number of other insertional mutagenesis studies in which T-cell leukemias/lymphomas were interrogated for integration site location. Many of these have been deposited in the Retroviral Tagged Cancer Gene Database (RTCGD), a public repository of data from past retroviral and transposon-based studies relating to tumourigenesis[276]. Upon cross-reference with this database, a number of my single integration site loci became CIS if I expand to include these other studies. Some of the genes found to become CIS include *Runx1* (**Table 3.3**). Additionally, some of the CIS from my study were further strengthened by a number of these other studies including *Runx3* and *Lfng*.

Gene	Number of Independent Integrations	Number of Total integrations recovered
Ikzf1	3	45
Nup214/Abl1	3	6
RUNX3	3	4
Slamf1	2	4
PTEN	2	3
IL12RB1	2	5
GGA1	2	3
RHOA	2	3
SMAD6	2	3
IRFBP2	2	10
LFNG	2	4
ADORA1	2	8
SOS2/ARF6	2	3

Table 3.2 Common insertion sites in hN1ΔE retroviral insertional mutagenesis study using Splinkerette-PCR.

The closest genes to the integrations are noted in addition to both the number of independent integrations recovered and the total number of integrations recovered.

Gene
RUNX1
MID1
PTMA
PECAM1
IKZF3 (Aiolos)
LMO2
BACH2
JAKMIP1

Table 3.3 Loci containing integrations in independent studies.

These genes are found as single insertion sites in hN1ΔE retroviral insertional mutagenesis screen using Splinkerette-PCR but are found in other screens found in the Mouse Retrovirus Tagged Cancer Gene database in other mouse models of T-ALL.

3.4.3 Collaboration of *RUNX1/RUNX3* and *NOTCH1*

I sought to functionally validate the RUNX transcription factors in the context of activated Notch signaling to test for formal collaboration *in vivo*. The rationale for this being that *Runx3*, *Ikzf1* and *Nup214/Abl1* were all the most frequently integrated CIS, and that *Runx3* was a gene which had not yet had thorough functional characterization in the context of T-ALL[3,277]. The orientation of the integrations near *Runx3* in my ΔE insertional mutagenesis study with the virus oriented inversely to the gene (**Figure 3.6**) was suggestive of an enhancer function as had been shown previously in other studies such as in the case of upregulation of *Myc* (**Figure 3.1**)[257,278,279]. *Runx1* was also in the same family of transcription factors as *Runx3* and could be considered a CIS when combined with other studies (**Table 3.4**). Finally, coinciding with the results of my integration studies, a number of groups were beginning to report that human T-ALL patients harboured recurrent loss-of-function mutations in *RUNX1*[4-6]. Based on this line of thinking I sought to determine if NOTCH1 formally collaborated with alleles of RUNX1

and RUNX3 in T-ALL leukemogenesis. I hypothesized that some or all alleles of RUNX1 and RUNX3 would increase penetrance and shorten latency of a "weakened" allele of NOTCH1, ΔEΔL. The ΔEΔL allele of NOTCH1 has both the EGF-like repeats (E) and Lin12/Notch repeats (L) deleted. While able to induce ectopic $CD4^+CD8^+$ DP T-cell development, it could not generate leukemogenic levels of Notch signaling and mice did not succumb to any hematologic disease[274]. This is in contrast to the stronger ΔE allele of NOTCH1, which sustains supraphysiologic Notch signaling levels and can induce short latency, 100% penetrant T-ALL[43]. Thus, perhaps genes which collaborate with Notch signaling might be able to overcome any controls exerted on normally developing cells and lead to a leukemic clone which would be seen by enhanced penetrance of hematologic disease. To accomplish this, I first performed limiting dilution of ΔE and ΔEΔL in order to determine an input dose at which ΔE created 100% penetrant disease and ΔEΔL created 0% penetrant disease. Multi-cistronic 2A lentiviruses were cloned which contained an allele of NOTCH1 followed by GFP as a selectable marker (**Figure 3.7**). I generated lentiviral particles of each construct and transduced 5-FU Bone Marrow followed by injection into lethally irradiated (810 RAD) recipient mice which were rescued with 2.5 $x10^5$ normal BM cells. Mice were injected with $1x10^2$, $1x10^3$ and $1x10^4$ GFP+ cells from each of these two constructs and monitored for clinical signs of leukemia according to a standard set of clinical criteria. Mice injected with the highest two doses of ΔE all succumbed to disease, while only 50% (2/4) of mice at the lowest dose of $1x10^2$ were moribund (**Figure 3.8**). In contrast, none of the mice from the three ΔEΔL cohorts fell sick from any clinical signs of leukemia. This suggested that using the highest dose which generated fully penetrant disease in the ΔE cohort ($1x10^4$), which did not cause sickness in the ΔEΔL mice, would be ideal to test for collaboration with RUNX1 and RUNX3. cDNAs of *RUNX3* and HA-tagged *RUNX1A*, *RUNX1B*, and *RUNX1C* were subcloned into lentivectors with NOTCH1 ΔEΔL (**Figure 3.7**) as described in the methods section. In order to determine if I was achieving proper 2A peptide cleavage, and not generating fusion proteins, western blot analysis of 293T cells transduced with the lentivectors was done (**Figure 3.7**). Of note, all constructs produced species consistent with active Notch signaling as noted by S3-cleaved

NOTCH1 signal (hNOTCH1 Val1744). Additionally, bands corresponding with the sizes of RUNX1A (27 kDa), RUNX1B (48 kDa), and RUNX1C (51kDa) were all observed at their expected molecular weight when probed for with the Hemagglutinin antigen and RUNX3 was also at its expected molecular weight of between 43-48 kDa. I then completed bone marrow transplants for each construct with 8 recipients per construct at $1x10^4$ GFP+ cells per recipient mouse. At 88 and 174 days post-injection, two ΔEΔL-RUNX3 mice had clinical signs of leukemia including splenomegaly (**Figure 3.9**) and were euthanized (**Figure 3.8**). Of note, the former mouse had clear infiltration of cells in the bone marrow, spleen and thymus which were $GFP^+Gr\text{-}1^-CD11b^-CD19^-$ $Thy1^+CD3e^+CD8a^+CD4^+$ (**Figure 3.10**), however in the latter mouse there was no clear GFP+ fraction, despite the presence of a $CD4^+CD8^+$ population of cells in the bone marrow. A ΔEΔL-RUNX1B mouse developed leukemia at 99 days post-injection, however none of the cells in the bone marrow were GFP^+, despite splenomegaly and kidney infiltration, two commonly involved sites of T-ALL in mice. At 185 days post-injection a ΔEΔL-RUNX1A mouse became ill and was found to have a relatively small spleen, but had a rather large thymic lymphoma and was found to have ~3% $GFP^+CD4^+CD8^+$ DP T cells in the bone marrow. As they exhibited signs of clinical leukemia displaying markers of immature T-cell development, I have classified all of these tumours as T-ALL. The remainder of the RUNX1A/RUNX1B and RUNX1C/RUNX3 cohorts of mice displayed no signs of leukemia and were followed to 265 days and 280 days, respectively. At this point, they were euthanized and their spleens were analyzed by flow cytometry for any evidence of GFP expression (**Figure 3.11**). None of the mice had more than 2% GFP+ cells in their spleens, suggesting perhaps there were some aberrant cells but not enough to say the mice had leukemia.

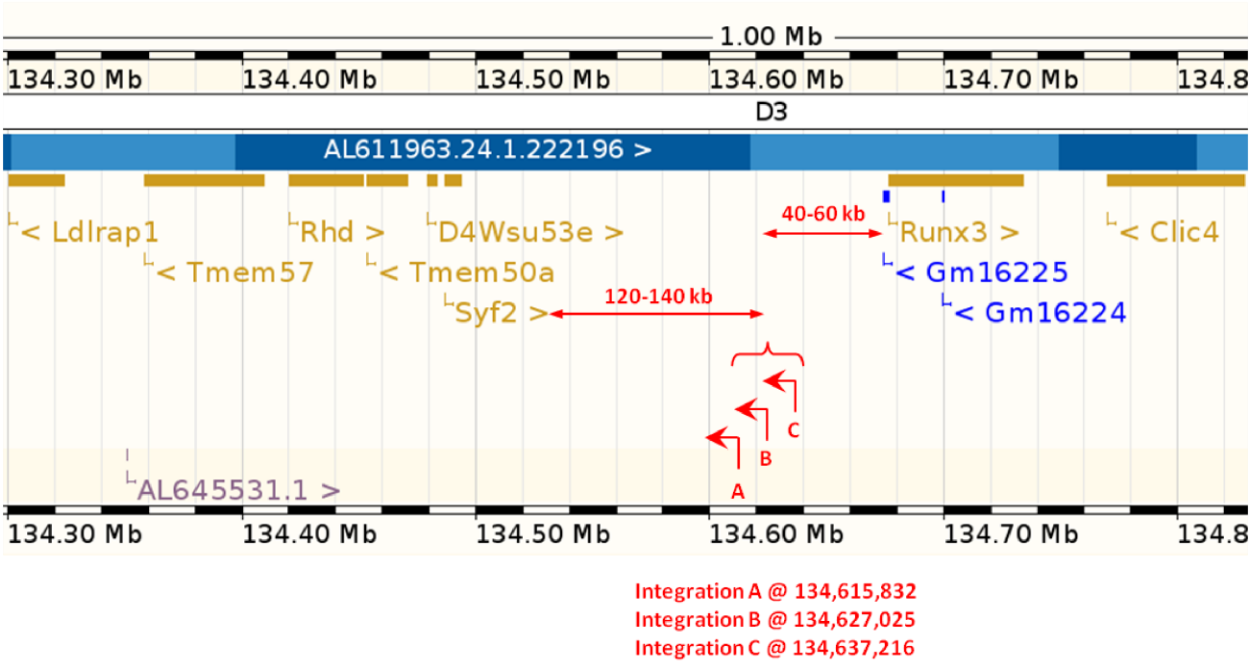

Figure 3.6 *Runx3* common insertion site.

A graphical depiction of the three integrations at mRunx3 on the UCSC genome browser.

Gene	Genetic Background	Mutagen	Integration Recovery Method	Number of Integrations	Distance from gene	Orientation	Study
Runx1	**C57Bl6**	**∆*E***	**splinkerette**	**1**	**421.148kb**	**5' - inverse**	**present**
Runx1	*p27Kip*$^{-/-}$ (C57Bl6/129)	M-MuLV	splinkerette	1	59.784kb	5' - inverse	Hwang et al. PNAS, 2002
Runx1	*Eed*$^{1989/1989}$ (101/R1 x C3Hf/R1)	M-MuLV	Inverse PCR	1	46.697kb	5' - inverse	Sauvageau et al. Blood, 2008
Runx3	**C57Bl6**	**∆*E***	**splinkerette**	**3**	**39.351 kb** **49.542 kb** **60.735 kb**	**5' - inverse**	**present**
Runx3	*p27Kip*$^{-/-}$ (C57Bl6/129)	M-MuLV	splinkerette	1	50.122kb	5' - same	Hwang et al. PNAS, 2002
Runx3	NIH/Swiss	SL3-3	Inverse PCR	1	39.061kb	5' - inverse	Kim et al. J Virol, 2003
Runx3	AKR/J	SL3-3	Inverse PCR	1	1.823kb	3' - same	Kim et al. J Virol, 2003

Table 3.4 Summary of retroviral insertional mutagenesis studies with *Runx1* or *Runx3.*

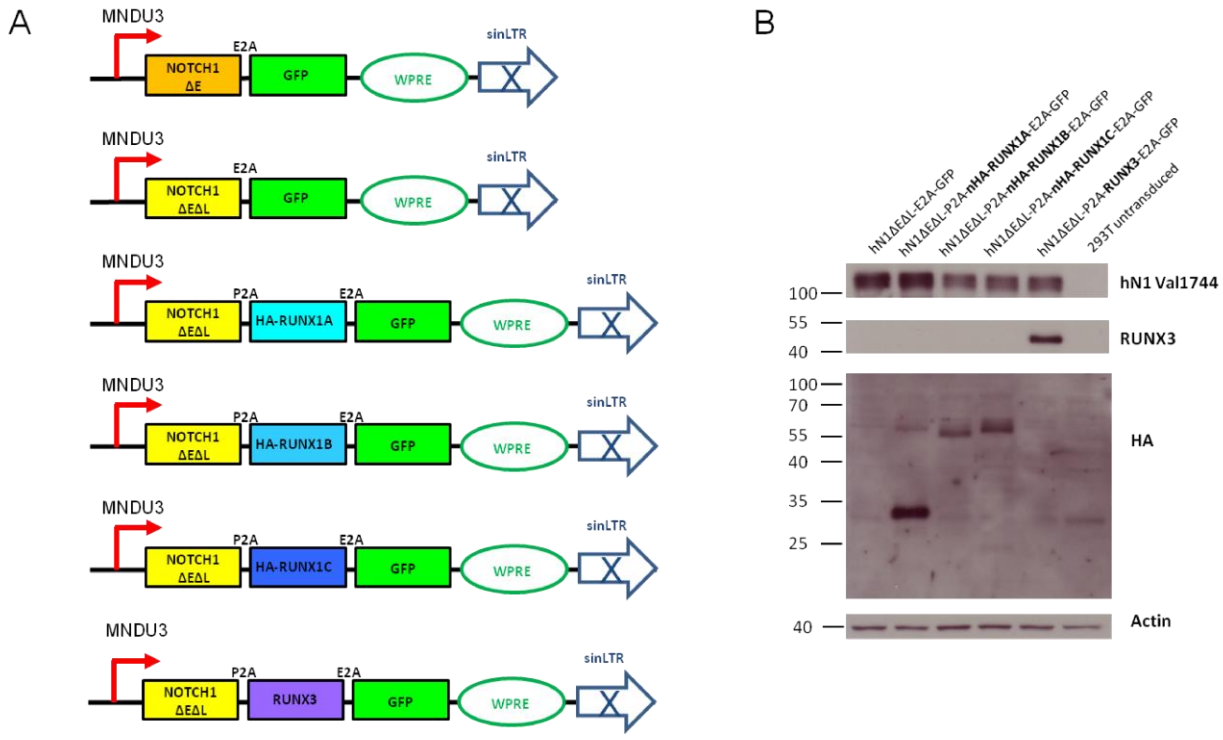

Figure 3.7 Multicistronic 2A lentivectors for expression of multiple genes.

(**A**) Graphical depiction of multicistronic lentiviruses used for bone marrow transplants. (**B**) Western blots of the lentivectors depicted transduced in 293T cells for NOTCH1 Val1744 (Cell Signaling Technology), RUNX3 (R&D Systems), Hemagglutinin [HA] (Sigma-Aldrich) and Actin (Sigma Aldrich).

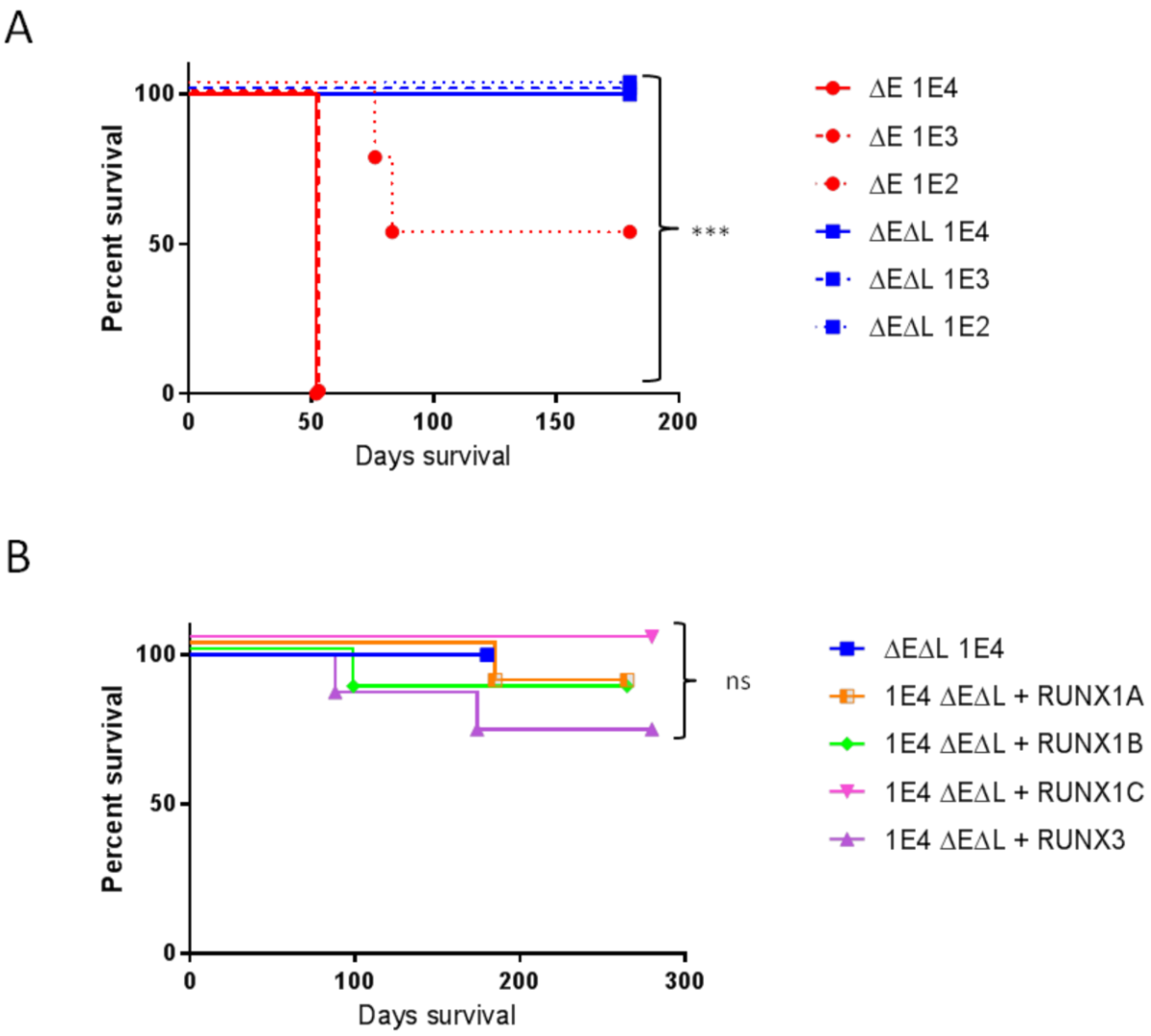

Figure 3.8 Kaplan-Meier curve of ΔE and ΔEΔL 5-FU bone marrow transplants.

(**A**) Survival of C57BL/6 mice transplanted with $1x10^2$, $1x10^3$, or $1x10^4$ ΔE, ΔEΔL-transduced 5-FU stem and progenitor enriched cells from wild-type donors. (**B**) Survival of C57BL/6 mice transplanted with ΔEΔL-RUNX1A, ΔEΔL-RUNX1B, ΔEΔL-RUNX1C or ΔEΔL-RUNX3-transduced 5-FU stem and progenitor enriched cells from wild-type donors. Bone marrow from age and sex matched wild-type and transduced with ΔE-E2A-GFP, ΔEΔL-E2A-GFP, ΔEΔL-P2A-RUNX1A-E2A-GFP, ΔEΔL-P2A-RUNX1B-E2A-GFP, ΔEΔL-P2A-RUNX1C-E2A-GFP, or ΔEΔL-P2A-RUNX3-E2A-GFP lentivirus. Similar numbers of transduced cells were then transplanted into lethally-irradiated syngeneic/congenic C57BL/6 recipients by tail vein injection along with a radioprotective "rescue" dose of whole bone marrow. Mice were monitored for clinical signs of morbidity and euthanized after attaining a predefined endpoint based on standardized scoring of

clinical symptoms. Pathologic involvement by T-ALL was confirmed at necropsy. *ns, non-significant; ***, p<0.001 (Log-rank test).*

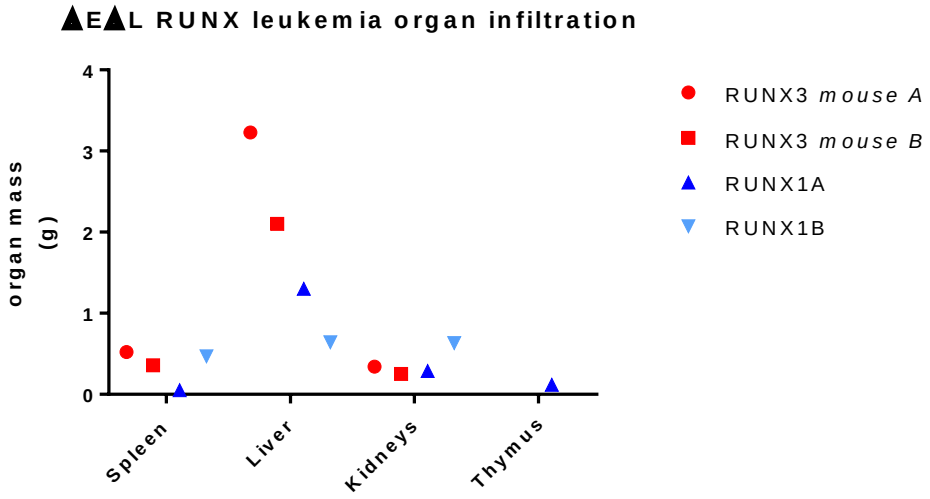

Figure 3.9 ΔEΔL collaboration leukemia organ weights and disease latency.

Mass of organs from mice that were euthanized due to clinical signs of leukemia. One mouse with involvement of the thymus is noted (ΔEΔL-P2A-RUNX1A-E2A-GFP).

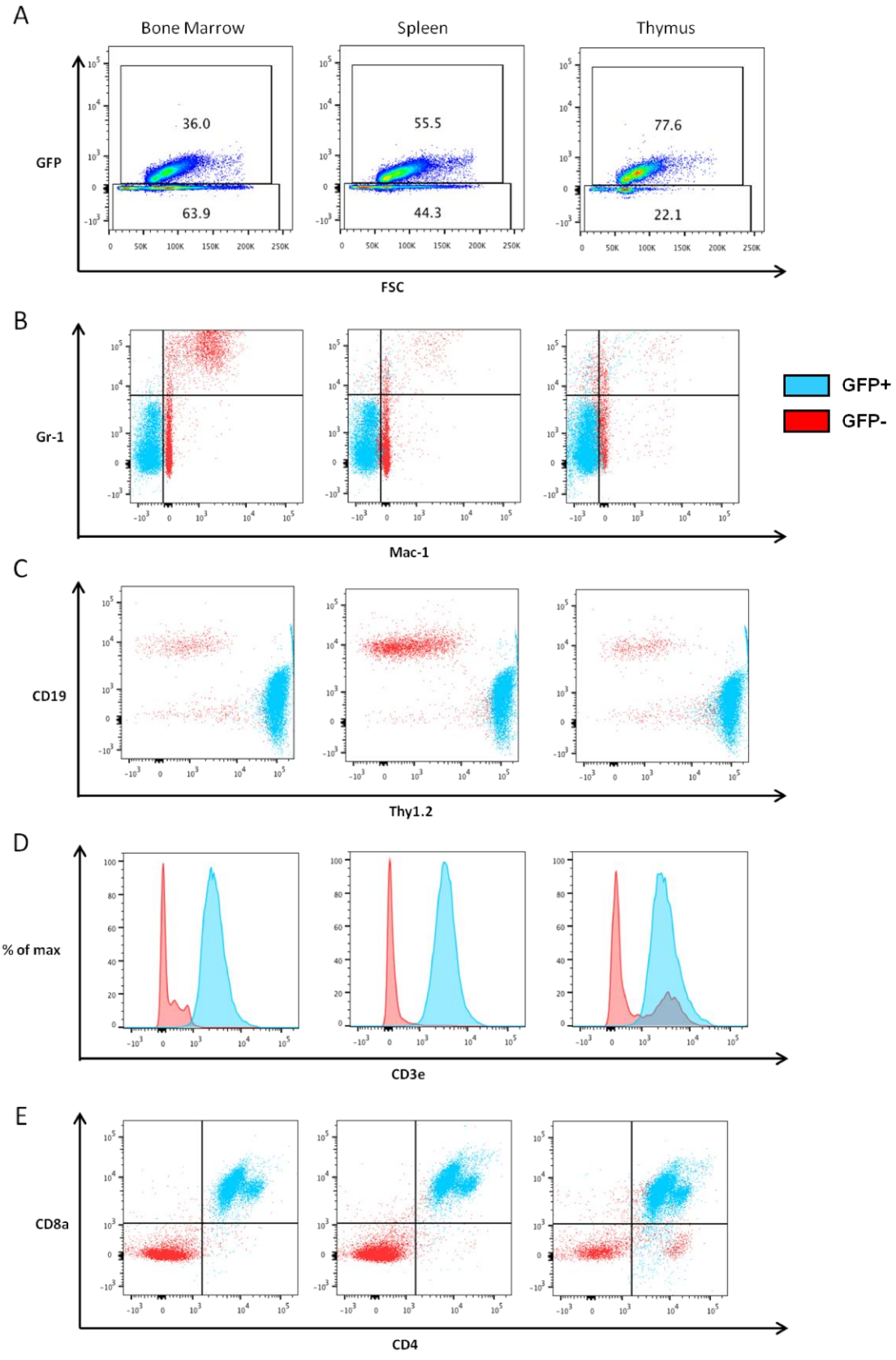
A
Bone Marrow
Spleen
Thymus
GFP
36.0
63.9
55.5
44.3
77.6
22.1
FSC
B
Gr-1
Mac-1
GFP+
GFP-
C
CD19
Thy1.2
D
% of max
CD3e
E
CD8a
CD4

Figure 3.10 Presentation of ΔEΔL-P2A-RUNX3-E2A-GFP moribund mouse (88 day latency).

(A) Flow cytometry plot of GFP expression for bone marrow, spleen and thymus. **(B)** Flow cytometry plot of Gr-1, Mac-1 for bone marrow, spleen and thymus. **(C)** Flow cytometry plot of CD19, Thy1 for bone marrow, spleen and thymus. **(D)** Flow cytometry histogram plot of CD3e for bone marrow, spleen and thymus. **(E)** Flow cytometry plot of CD4, CD8 for bone marrow, spleen and thymus.

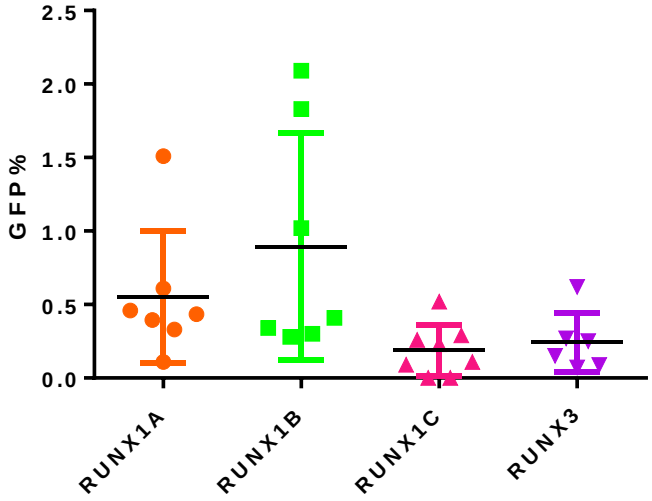

Figure 3.11 GFP expression in Spleen of ΔEΔL-RUNX mice at experimental endpoint.

All remaining experimental mice were euthanized at 280 days. Flow cytometric analysis of homogenized spleen following red blood cell lysis was performed. Events are gated on viable events by Propidium Iodide exclusion for GFP expression.

3.5 Discussion

3.5.1 Retroviral insertion sites cloned from ΔE leukemias

It is notable that *Runx3* was selected for in my insertional mutagenesis screen as Runx transcription factors have been well-described as common insertion sites in T-cell leukemias in a number of contexts. Using transgenic CD2-*Myc* mice, James Neil and Ewan Cameron's groups found that all three murine Runx genes (*Runx1*, *Runx2* and *Runx3*) were common insertion sites for the Moloney murine leukemia virus and suggested these genes could enhance leukemogenesis[280-282]. The mutations originally

described upstream of the P1 promoter of *Runx2* show the virus oriented in an inverse direction relative to the locus, and were found to create *de novo* enhancer activity which drove expression of the gene[280]. Of note, similar mechanisms of aberrant overexpression of Runx1 have been found in which inverse-oriented integrations upstream of the P1 and P2 promoters or within the 5' UTR seem to generate both B-cell and T-cell leukemia in mice[281,283-285]. Similar mutations which lead to overexpression of full length Runx3 have also been discovered in a number of other insertional mutagenesis screens[282,286-288]. These results suggest that the orientation of location of integration of the MSCV-ΔE retrovirus is likely operating in a similar manner. The Neil and Cameron groups suggested that the similarity in activation and overexpression of collaborating Runx genes might hint at functional redundancy at some level as a collaborating oncogene in murine leukemia/lymphomas[289]. Despite this evidence, there existed the possibility that non-canonical, shorter isoforms similar to Runx1a (**Figure 1.5**) were being aberrantly transcribed due to viral integration; however studies interrogating this have suggested that these tumours express full-length, wild-type Runx1 isoforms[251,290].

The *Sleeping Beauty* system utilizes a DNA element (the transposon) and an enzyme (the transposase) that allows the donor DNA containing cloned viral LTRs to be integrated into genomic regions containing a TA dinucleotide[291]. Thus, transposition of the *Sleeping* Beauty element can alter gene expression in a similar manner to retroviral integration. Work from Neil Copeland & Nancy Jenkins popularized the use of the *Sleeping Beauty* transposon in insertional mutagenesis. They discovered that two of the leukemias generated in the screen had mutations in both *Runx2* and *Notch1*, suggestive of potential collaboration[292]. One of the most interesting studies in the context of both Runx and Notch collaboration in T-cell leukemogenesis is one in which the Sleeping Beauty transposable element was in control of different T-cell developmental stage-specific promoters[293]. Using, *Vav*, *Lck*, and *CD4* promoters, researchers were able to induce transposition-based mutagenesis in HSC, DN T-cells and DP T-cells, respectively. Interestingly, many of the *Vav*-derived tumours which had *Notch1* mutations were found to have concurrent *Runx1* mutations, suggesting that

these two genes may collaborate in initiating leukemia at this specific stage of development. Mutations into *Ikzf1* were found in this model as well, which served as a positive control relative to other studies[3]. Additionally, *Runx1* has been also shown to be an insertion site in other T-cell leukemia models created from an *Eed* hypomorph background and a *Cdkn1b*$^{-/-}$ background[294,295].

3.5.2 Collaboration between RUNX1/RUNX3 and NOTCH1

It should be noted that this study confirms the lack of leukemogenic activity produced by the ΔEΔL allele of NOTCH1 as I was unable to generate leukemia at a high dose of cells and suggests that the Lin12/Notch repeats are indeed necessary for complete leukemia initiation[274]. An alternative to using the ΔEΔL allele would have been to use the ΔE allele at the lower dose of $1x10^2$ cells, or perhaps an even lower dose, in order to perhaps show enhanced penetrance or shorten the latency of the leukemia; however the leukemia initiating cell frequency would not have changed using this approach. The ΔEΔL allele however provides sufficient Notch signaling activity to generate aberrant T-cell development in the bone marrow, without providing sufficient oncogenic signaling to select for collaborating mutations and develop clonal malignancy. It is interesting to note in that regard, that the addition of alleles of RUNX1 and RUNX3 was sufficient to allow for malignant disease in some of the recipients. It should be noted that the mice which displayed clinical symptoms requiring euthanasia had expanded immature populations resembling T-ALL. Although it remains possible that these leukemias may represent clonal outgrowths containing stochastic mutations which allowed for T-ALL to develop by chance alone. However it is more plausible that GFP expression was somehow downregulated perhaps due to inefficient cleavage of the 2A vector or some other unknown method of silencing, as none of the control ΔEΔL-only mice became sick despite having cohorts of the same size, and some of the mice displayed heterogeneous GFP expression. As such, it is likely that there was formal collaboration between RUNX1/RUNX3 and NOTCH1 in initiating clonal disease.

Chapter 4: RUNX1 in T-cell Acute Lymphoblastic Leukemia Maintenance

4.1 Chapter overview

4.2 Introduction

Recent studies have reported mutations in the *RUNX1* gene in T-cell neoplasms at the same time as research showing that this genes also functions in oncogenic transcription factor complexes to support growth. These dichotomous findings suggest that RUNX1 could be serving multiple roles which have yet to be fully defined. As such, I wanted to explore the phenotypes associated with RUNX1 in established T-ALL cells, and by doing so, further explore my findings in Chapter 3. My goals were to use a number of methods to deplete and augment the amount of RUNX1 in T-ALL cells and to determine how that impacted the cellular and molecular phenotypes in both human and mouse leukemias.

4.2.1 RUNX1 as a tumour suppressor in T-ALL

The *RUNX1* gene, a member of the RUNT-related transcription factor family also known as *AML1*, is deregulated in many subtypes of hematologic malignancy. Initially, *RUNX1* was characterized as a locus frequently interrupted by translocations in Myeloid (RUNX1-ETO[166]) and B-lymphoid (TEL-RUNX1[296]) malignancies. These mutations generate fusion proteins which alter the range of interacting proteins from primarily co-activators to mostly co-repressors[289]. In addition to these gross chromosomal lesions, point mutations and small insertions and deletions in *RUNX1* have been described in Acute Myeloid Leukemia (AML) and Myelodysplastic Syndromes (MDS)[297-299] and are believed to result in amorphic, hypomorphic or antimorphic versions of the wild-type protein.

This paradigm is consistent with recently described heterozygous point mutations and small indels found in *RUNX1* by several groups using next-generation sequencing of T-ALL[4-6,169]. Mutations in T-ALL were recently discovered through large-scale sequencing

efforts in the *RUNX1* coding sequence in patterns closely mimicking those found in myeloid neoplasms. The majority of these are found in the RUNT domain, which controls DNA-binding and interactions with an obligate heterodimer, CBFβ. Other mutations are C-terminal to these disruptions and may create truncated proteins lacking the activation domain, required for interactions with a milieu of co-activators and co-repressors. Similar to examples found in other hematopoietic cancers, the pattern of these mutations suggests there is selection for phenotypic changes brought on by a loss of RUNX1 function. Since a subset of *RUNX1* mutations appear unable to transactivate the CSF promoter in 293T cells[4], these mutations have been suggested to be evidence of a tumor suppressor function in T-ALL. The monoallelic nature of the mutations suggests loss-of-function RUNX1-gene expression patterns that are generated through dominant-negative interactions and/or haploinsufficiency and may be responsible for the establishment or maintenance of a leukemic clone. Supporting this hypothesis, it is of note that a presumed loss-of-function LacZ insertional mutation in the *Runx1* locus in mice predisposes to T-ALL development[300]. It remains unclear how these mutations function to promote T-ALL, however a higher rate of mutation in the aggressive ETP-ALL subtype suggest that these mutations may play a role in this group of patients specifically[5,6]. It is of note that the ETP-ALL subtype displays aberrant myeloid marker expression and shares many similar expression hallmarks with AML. Furthermore, ETP-ALL contains a mutational spectrum that resembles myeloid malignancy, which may suggest that *RUNX1* mutations in this subtype may be functioning to alter differentiation, similar to type II mutations found in AML[301].

4.2.2 RUNX1 as an oncogene in T-ALL

This data suggesting the *RUNX1* gene functions as a tumor suppressor contrasts with evidence suggesting that RUNX1 provides growth supportive signals required to sustain T-cell leukemia. NOTCH1 transcription factor (TF) ChIP-seq data has revealed that RUNX1 consensus sites are frequently found to be co-localized in regions of the T-ALL genome enriched in NOTCH1/CSL binding and H3K4me1 sites[9]. Follow-up studies have shown that RUNX1 is physically located near many of these regions that we now

understand to be superenhancers[8], which are wide tracts of active chromatin that are supportive of gene transcription. This model builds upon data from the Brand lab, which showed that RUNX1 is not only a target of the oncoprotein TAL1, but is required for TAL1 binding in Jurkat cells, where over half of all TAL1 binding sites have RUNX consensus sequences[302]. Additionally, experiments from Sanda *et al.* demonstrate that RUNX1 functions in a feed-forward loop with TAL1 and GATA3, regulating MYB and a number of other genes which function to promote growth of T-ALL cells[7].

4.2.3 Statement of hypothesis and objectives

Due to the occurrence of *Runx3* as a common integration site and as a gene which collaborates with Notch to initiate leukemia (in Chapter 3; page 52), I hypothesized that RUNX3 supports growth of T-cell leukemia cells. I also found the occurrence of *Runx1* integrations in my study and showed that some alleles are able to collaborate with NOTCH1, thus suggesting that RUNX1 might also support growth. However, there are conflicting data regarding the nature of *RUNX1* as providing both supportive and detrimental signals in regulating cell growth. Given this and the small number of cell lines and samples assayed in prior work, as well as the recent description of *RUNX1* mutations in T-ALL, I undertook a large functional study to determine the role of *RUNX1* in established T-ALL cells. I hypothesized that while it remains possible that *RUNX1* is a tumour suppressor in leukemia initiation/pre-leukemia, that once a leukemic clone is established, T-ALL cells would be dependent on RUNX1 for their proliferation and survival. In order to address this hypothesis, my objectives included: 1) Determine the expression and growth phenotypes associated with RUNX family members; 2) delineate the phenotypes associated with loss-of-function by knockdown and/or knockout or overexpression of RUNX family members; 3) determine the downstream mediators of RUNX1; and 4) identify mechanisms whereby RUNX family members and Notch signaling may collaborate in regulating growth.

Aim 3: Determine the contribution of RUNX1 in T-cell Acute Lymphoblastic Leukemia pathogenesis.

4.3 Materials and methods

4.3.1 Viruses/Tat-Cre

High titer lentivirus was generated by transient co-transfection of 293T cells with packaging/envelope vectors as described previously[164]. The pLKO.1 Puro^R expression vector containing the scrambled non-silencing control in pLKO.1puro vector was obtained from Addgene (#1864)[303] and shRNAs against *RUNX1* (shRUNX1-58, TRCN0000013658; shRUNX1-59, TRCN0000013659; shRUNX1-60, TRCN0000013660; shRUNX1-90, TRCN0000338490; shRUNX1-92, TRCN0000338492; shRUNX1-27, TRCN0000338427; shRUNX1-74, TRCN0000235674; shRUNX1-75, TRCN0000235675; shRUNX1-76, TRCN0000235676) were obtained and cloned as described previously[303]. A PGK-GFP cassette was subcloned into sites containing the PGK-Puro^R cassette to generate pLKO.1 GFP versions of the above constructs. Human RUNX3 and Hemagglutinin (HA)-tagged RUNX1A, RUNX1B and RUNX1C were cloned into a pRRL-containing self-inactivating lentivirus (**Figure 4.1**). As described previously[304], the CreERT2 (Cre recombinase-mutated estrogen receptor ligand-binding domain fusion protein) cassette was subcloned into a pRRL-containing lentiviral vector using GFP as a selectable marker from pCAG-CreERT2 (Addgene #14979). The Cre Reporter construct was acquired from Addgene (#62732) and has been previously described[305]. All constructs were verified by Sanger sequencing. For transduction, T-ALL cells were left overnight with viral supernatant in the presences of 4µg/ml polybrene, followed by washout with PBS or complete media. For experiments using the Tat-Cre recombinase (Millipore, SCR508), the enzyme solution was diluted with appropriate media at a concentration of 100 units/ml [1 unit = 0.948µg] and sterile-filtered using a 0.2µm surfactant free cellulose acetate syringe filter (NALGENE®, #190-9920) and incubated with cells in culture for durations indicated.

Figure 4.1 Layout of pRRL-based lentivector used to overexpress various gene(s)-of-interest.

4.3.2 Bone marrow transplants

Primary mouse leukemias were generated from bone marrow cells collected from 5-fluorouracil treated donor mice from the *Runx1*$^{lox/lox}$ (formal name: B6;129-*Runx1*$^{tm3.1Spe}$/J^{119}), *Cbfb*$^{lox/lox}$ (formal name: B6.129P2-*Cbfb*^{tm1Itan}/J^{139}), or wild-type C57BL/6J backgrounds. Bone marrow was transduced with MSCV-IRES-tNGFR hN1ΔE retrovirus by spinoculation[2] followed by injection of 1x10^4 – 4x10^4 NGFR+ cells into the tail vein of lethally irradiated (810 RAD) congenic recipient mice 3 days later. Mice were monitored for clinical symptoms of leukemia and euthanized using standard protocols with leukemia-infiltrated tissues banked for further analyses. All animals were housed in the BC Cancer Agency Animal Resource Centre under pathogen-free conditions and in compliance with protocols approved by the University of British Columbia Committee for Animal Care.

4.3.3 Cell culture

Human patient-derived xenograft (PDX) samples used in this study were described previously[164,256]. Cells were expanded *in vivo* using NOD/Scid/*Il2rg*–/– (NSG) for up to 2 passages before experimental analysis or protein lysis. Cells were cultured in WIT-L media as previously described for *in vitro* cell proliferation experiments[306]. Established T-ALL cell lines were cultured in RPMI 1640 medium containing 10% FBS, 2mM L-glutamine, 1Mm sodium pyruvate, and Penicillin/Streptomycin. T-ALL cell lines used in this study are listed in **Table 4.1**, mutation status of PI3K/AKT and MAPK pathways for a subset of lines is listed in **Table 4.2**, and PTEN protein expression and IL7Rα mutation status for a subset of lines is listed in **Table 4.3**. As described previously[307],

cell line identities were verified by STR profiling (externally by Genetica) and were obtained from the research groups of Drs. Adolfo Ferrando (Columbia University, New York), Jon Aster (Brigham & Women's Hospital, Boston), and Thomas Look (DFCI, Boston). Explanted T-ALL cells from the spleen or bone marrow of moribund mice were grown in the same complete media above but with 20% FBS, and supplemented with 10ng/ml IL-2 and IL-7 (Peprotech). Pharmacologic inhibition of Notch signaling *in vitro* was done using 1 μM γ-secretase inhibitor XXI (compound E; ALX-270-415, Alexis).

Designation	Clinical Details	Cytogenetic Info	*NOTCH1* HD mutation	*NOTCH1* PEST mutation	Year Established	Reference
ALL-SIL	17yo male, PB at relapse	t(10;14)(q24;q11) Hox11-TCRD ; *NUP214-ABL1*	L1594P	2475 AHP*STOP	1979	Drexler, Guide to Leukemia-Lymphoma Cell Lines, Second Edition, 2010
CCRF-CEM	3yo female, PB at relapse	submicroscopic del(1)(p32) SIL-SCL	1595 INS PRLPHNSS FHFL	2413 P/S	1964	Foley et al., Cancer 18:522-529 (1965)
DND-41	13yo male, PB	t(5;14)/Hox11L2	L1594P, D1610V	2444 CCSHWAPAAWR CTLFCPRRAPPC PRRCHPRWSHP*	1977	Drexler et al., Leuk. Res. 9:209-229 (1985)
HPB-ALL	14yo male, PB at diagnosis	t(5;14)(q35;q32.2)/ Hox11L2	L1575P	2443 EGRGRCSHWAP AAWRCTLFCPRR APPCPRRCHPR WSHP*STOP	1973	Morikawa et al., Int. J. Cancer 21:166-10 (1978)
CCRF-HSB2	11yo male, PB at relapse	t(1;7)(p34;q34) LCK-TCRB, submicroscopic del(1)(p32) SIL-SCL	-	-	1966	Adams et al., Cancer Res. 28:1121-1125 (1968), Adams et al., Exp. Cell Res. 62:5-10 (1970)
Jurkat	14yo male, PB at 1st relapse		-	-	1976	Schneider et al., Int. J. Cancer 19:621-626 (1977)
Karpas 45	2yo male, BM at diagnosis	t(X;11)(q13;q23) MLL-AFX	-	2460 *STOP	1972	Karpas et al., Leukemia Res. 1:35-49 (1977); Borkhard et al., Oncogene 14:195-202 (1977)
KE-37	27yo male	t(8;14)(q24;q11) MYC-TCRA	-	2460 *STOP	1979	Drexler et al., Leukemia Res. 9:209-229 (1985)
KOPT-K1	6yo male	t(11;14)(p13;q11) TTG2-TCRD, TTG2 = LMO2	L1601P	2515 RVP*STOP	-	Dong et al., Leukemia 9:1812-1817 (1995).
Loucy	38yo female, PB at relapse	t(16;20), gdTCR	-	-	1987	Ben-Bassat et al., Cancer Genet. Cytogenet. 49:241-248 (1990)
MOLT 13	2yo female, BM at relapse	-	ND	ND	1983	Drexler et al., Hematol. Oncol. 7:115-125 (1989)
MOLT 3	19yo male, PB at relapse	-	1601 L/P	2515 RVP*STOP	1971	Minowada et al., J. Natl. Cancer Inst. 49:891-895 (1972)
MOLT4	19yo male, PB at relapse	-	1601 L/P	2515 RVP*STOP	1971	Minowada et al., J. Natl. Cancer Inst. 49:891-895 (1972)

Designation	Clinical Details	Cytogenetic Info	*NOTCH1* HD mutation	*NOTCH1* PEST mutation	Year Established	Reference
P12 Ichikawa	7yo male, PB	-	-	-	1978	Kitahara et al., Acta Hematol. Jpn. 41:140 (1978); Watanabe et al., Cancer Res.38:3494-3498 (1978)
Peer	4yo female, PB at 2nd relapse	gdTCR	L1601P	-	1977	Ravid et al., Int. J. Cancer 25:705-710 (1980); Heyman et al., Leukemia 8:425-434 (1994)
PF-382	6yo female, pleural effusion at 2nd relapse	-	1575 L/P	2494ASCILWTTP PATSYRCLSTPS SPRPLSPLTSGP ARPRIPTSPTGPR ASPA LPPACSPRSPAF RRPSSKRRAPRD PGFLSQAFGRLC ALCGCQ GRPEEPF*STOP	1983	Pegoraro et al., J. Natl. Cancer Inst. 75:285-290 (1985)
REX	-	-	-	2467 T/M	-	Breitmeyer et al., J Immunol. 138:726-31 (1987)
RPMI 8402	16yo female, PB	t(11;14)(p15;q11) TTG1-TCRD, submicroscopic del(1)(p32) SIL-SCL	1584 INS PVELMPPE	-	1972	Moore et al., In Vitro 8:434 (1973); Huang et al., J. Natl. Cancer Inst. 53:655-660 (1974)
SUP-T11	74yo male, BM at diagnosis		-	-	1989	Smith et al., Blood 73:2182-2187 (1989)
SUP-T13	2yo female	*P16INK4A* deletion	-	-	1987	Smith et al., Blood 73:2182-2187 (1989)
TALL-1	28yo male, BM	-	-	-	1976	Miyoshi et al., Nature 267:843-844 (1977)
THP-6	-	-	ND	ND	-	Minegishi et al., Tohoku J. Exp. Medicine 151:283-292 (1987); Minegishi et al., Leuk Res 12:227-232 (1988)

Table 4.1 Summary of T-ALL cell lines used in this dissertation

The age of the patient at diagnosis or relapse is noted, notable genetic lesions, *NOTCH1* mutational status, year of establishment as well as any relevant references. PB, peripheral blood; ND, not determined; yo, years old.

	RAF1	BRAF	RAC1	NF1	NF2	NRAS	HRAS	KRAS	MAP2K1	MAP2K2	MAP2K4	MAP3K1	MAP3K13	AKT1	PIK3CA	MTOR	TSC1	TSC2
ALLSIL[1]																		
CCRF-CEM[1]				p.R711H				p.G12D										
DND41[1]						p.Q61H			p.K84K		p.A279T							p.Q1525R p.V1372M
HPBALL[2]				p.Y80H p.I634T														
Jurkat[1]	p.A237T	p.A728V	p.C18Y		p.L582L									p.R200H			p.R1093*	p.Q1686* p.I61T
Karpas 45[1]	p.V128A		p.G54G	p.Q1841K	p.L549L				p.R47Q	p.A176T	p.S144I	p.S312G	p.T70M		p.G122S			p.C1609C
KE-37[1]						p.G12D												
Loucy[1]																		
MOLT 4[1]				p.G1502G	p.T352M	p.G12C			p.D67N	p.D156N			p.T203M			p.A1134T	p.D541Y p.P1142P p.A808V p.P1142H p.E1162K p.E788K	p.N1707S
MOLT 13[1]						p.G12D												p.R1245Q
P12 Ichikawa[1]						p.G12D												
Peer[2]												p.T949del						p.W164*
PF-382[1]						p.G12S			p.F129L									p.K250E
RPMI 8402[1]							p.A134S											p.A614T
SUP-T11[2]												p.T949del						
TALL-1[1]						p.G12D												

Table 4.2 Cell line mutations in PI3K/AKT and MAPK pathways as documented in COSMIC[1] and CCLE[2] databases.

Coding sequence mutations were filtered by the following criteria: Inclusion in the Cancer Gene Census list (http://cancer.sanger.ac.uk/census); predicted to be pathogenic by the FATHMM-MLK algorithm (http://fathmm.biocompute.org.uk/); and involvement in PI3K/AKT and/or MAPK signaling pathways. 1. http://cancer.sanger.ac.uk/cosmic. 2. http://www.broadinstitute.org/ccle. Table adapted from IGF1R Derived PI3K/AKT Signaling Maintains Growth in a Subset of Human T-Cell Acute Lymphoblastic Leukemias. *PLOS One* (Gusscott S. et al., 2016), doi:10.1371/journal.pone.0161158.s019 © Gusscott et al. 2016, accessed April 2017. Used under creative commons attribution license.

Cell Line	PTEN expression	PTEN reference	IL7R mutation status[308]
ALL-SIL	+	Zuurbier[309]	WT
HPB-ALL	+	Zuurbier[309]	WT
TALL-1	+	Zuurbier[309]	WT
CCRF-HSB2	+	Zuurbier[309]	WT
KOPT-K1	+	You[310]	WT
RPMI 8402	-	Zuurbier[309]	WT
MOLT 4	-	Zuurbier[309]	WT
SUP-T13	-	This report	WT
CUTLL1	+	You[310]	ND
THP-6	-	This report	ND
PF-382	-	Zuurbier[309]	WT
MOLT 13	-	This report	ND
Karpas 45	-	Zuurbier[309]	ND
Jurkat	-	You[310]	WT
DND-41	+	Zuurbier[309]	mutated
Loucy	-	Zuurbier[309]	WT
KE-37	-	Zuurbier[309]	WT
REX	ND		ND
Peer	+	Zuurbier[309]	WT
P12 Ichikawa	-	Zuurbier[309]	WT
CCRF-CEM	-	Zuurbier[309]	WT
SUP-T11	+	This report	WT

Table 4.3 PTEN protein expression and IL7Rα mutational status in human T-ALL cell lines.

ND, not determined. Table adapted from IGF1R Derived PI3K/AKT Signaling Maintains Growth in a Subset of Human T-Cell Acute Lymphoblastic Leukemias. *PLOS One* (Gusscott S. et al., 2016), doi:10.1371/journal.pone.0161158.s019 © Gusscott et al. 2016, accessed April 2017. Used under creative commons attribution license.

4.3.4 Proliferation/Apoptosis assays

Cells were fixed and labeled with anti-BrdU antibody following a pulse of 10 μM BrdU for 1 hr at 37°C, according to manufacturer instructions (FITC or APC BrdU Flow kit; BD) and analyzed by flow cytometry. Cells were gated for viable cells by PI exclusion. Apoptotic cells were identified by staining with Annexin V-FITC/Propidium Iodide. Cell viability was assessed by propidium iodide (PI) or 4',6-Diamidino-2-Phenylindole (DAPI) exclusion and analysis by flow cytometry.

4.3.5 Flow cytometry/western blot and antibodies

Intracellular Phospho-flow cytometry. Cells were serum-starved overnight (16 hr) and then stimulated for 10 minutes using FBS (Sigma Aldrich) or recombinant IGF1 or IL7 (both from Peprotech). Cells were then fixed for 10 minutes using 1.5% paraformaldehyde, followed by permeabilization using 100% methanol. Cells were then labeled with Phospho-AKT (S473) Rabbit mAb Alexa Fluor® 647 (Cell Signaling) or the equivalent isotype control using equivalent amounts of antibody, or alternatively Phospho-STAT5 (Y694) Mouse mAb Alexa Fluor® 647 (BD Phosflow). Mean fluorescence intensity values were normalized to the isotype control and subsequently to the unstimulated control cells. IGF1R/IL7R surface expression. IGF1R was labeled using the αIR3 anti-human antibody (Calbiochem), followed by allophycocyanin-conjugated secondary antibody. IL7R was labeled using the anti-human CD127/IL7R (clone eBioRDR5) antibody directly conjugated to allophycocyanin (eBioscience). Western Blot. Antibodies used for western blotting were against RUNX1 (Active Motif; no clone number, raised against a synthetic peptide of residues 231-245 of RUNX1), RUNX3(R&D Systems; 527327), β-actin (Sigma Aldrich; AC-15), PTEN (Abcam; Y184), p21 (BD Pharmingen; 70/Cip1/WAF1), p27 (BD Pharmingen; 57/Kip1/p27), Bcl-xL (Cell Signal, 54H6), Bcl-2 (Cell Signal, 50E3), Mcl-1 (Cell Signal, D35A5), ERK2 (Santa Cruz, sc-154), MYB (Millipore; 1-1) and MYC (Santa Cruz; N-262).

4.3.6 Growth assays

In vitro competition assays. T-ALL cell lines were transduced with virus and cultured for 3 days to allow for the expression of GFP in order to mitigate effects of pseudo-transduction. Starting on day 3 cells were analyzed for GFP expression on a BD FACSCalibur or BD LSRFortessa flow cytometer with propidium iodide (PI) used to gate on viable cells. Percentage of GFP+ cells was normalized to the initial day of the experiment (day 3) and then normalized to the non-silencing control cells. Absolute cell count experiments. T-ALL cell lines were transduced with virus and cultured for 3 days to allow for the expression of the Puromycin^{R} cassette. Cells were then cultured in the presence of 1µg/ml of Puromycin for 3 days before being plated at a density of 5x10^{5}cells/ml. Every two days, cells were counted using the Vi-CELL® automated cell viability analyzer using Trypan Blue exclusion and replated at the initial seed density of 5x10^{5}cells/ml. Cumulative fold expansion was calculated based on these absolute cell counts. Cell Proliferation Dye. Primary human T-ALL cells were transduced with lentivirus and 3 days later, loaded with Cell Proliferation Dye eFluor450 (eBioscience). Cells were then incubated for a week with media changes before analysis using the violet laser of the BD LSRFortessa cell analyzer. Resazurin reduction. Cell growth was measured by CellTiter-Blue assay (Promega) and resazurin reduction was normalized to media-only control. Inducible Cell Lines. In order to generate doxycycline-inducible cell lines, cDNAs of RUNX1A, RUNX1B, RUNX1C, and GFP were subcloned into pLVX-Tight-Puro. Following transduction of cells with pLVX-Tet-On Advanced (Clontech, altered as described previously[164]) and selection with G418, I transduced cells with their respective pLVX-Tight-Puro lentivector constructs and selected for stable cell lines using puromycin.

4.3.7 Droplet digital PCR (ddPCR)

Cells were processed into genomic DNA using a Genomic DNA Mini Kit (K182002, Invitrogen) and DNA yield was quantified using a nanodrop with 150ng of input gDNA per reaction. Primers were designed that flank the LoxP sites of the *Runx1^{lox}*, *Cbfb^{lox}*, or Cre reporter (Addgene #62732), with one primer between the LoxP sites as indicated in

(**Figure 4.2**). Droplet digital PCR reactions were then run using the QX200™ ddPCR™ EvaGreen Supermix (Bio-Rad, #1864033) with NcoI and EcoR1 included in the *Cbfb* and *Runx1* reactions respectively (5 units of enzyme per reaction) followed by quantification on the QX200™ Droplet Digital™ PCR System (Bio-Rad, #1864001). The amount of deletion was enumerated by measuring the fractional abundance of positive deleted droplets (a) relative to the sum of positive deleted droplets (a) and positive floxed droplets (b), as described by a/a+b.

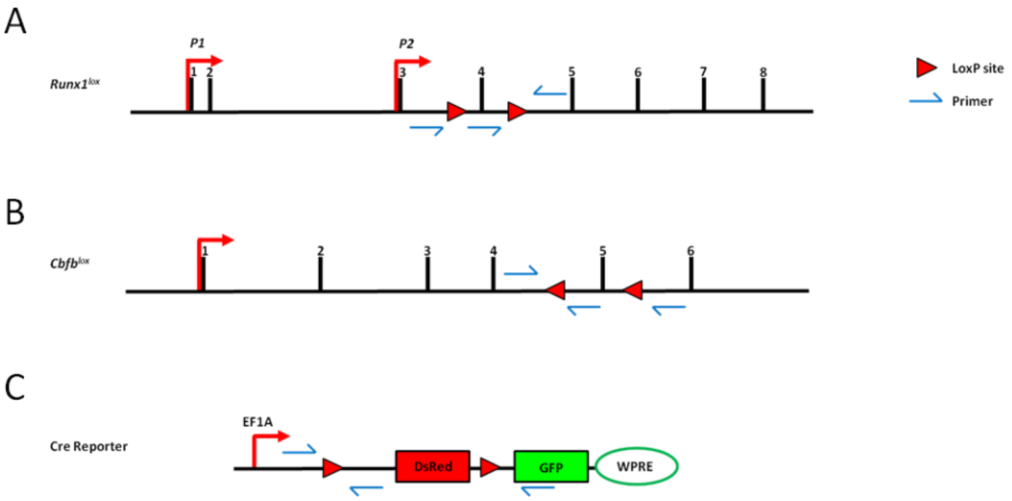

Figure 4.2 Graphical depiction of *Runx1*$^{lox/lox}$, *Cbfb*$^{lox/lox}$ loci and Cre reporter vector.

(**A**) *Runx1*$^{lox/lox}$ locus depicted showing location of primers used in ddPCR assay relative to floxed exon 4. (**B**) *Cbfb*$^{lox/lox}$ locus depicted showing location of primers used in ddPCR assay relative to floxed exon 5. (**C**) Cre reporter vector depicted showing primers used in ddPCR assay relative to floxed DsRed.

4.3.8 RNA-seq analysis pipeline

Paired-end sequence reads from RNA-seq were aligned to a reference transcriptome through BWA 0.5.7, based on the reference genome including annotated exon-exon junctions[311]. JAGuaR v 2.0.3 was used to create a custom reference transcriptome[312]. Reads were aligned to this reference transcriptome (NCBI GRCh37-lite reference with Ensembl v75 annotations) followed by 'repositioning' to genomic coordinates. This

allows reads which span exon-exon junctions to be transformed into large gapped alignments.

Using an inhouse analysis pipeline and RNA-seq quality control (QC), profiles were generated and QC metrics were used to assess the quality of RNA-seq libraries. This included intergenic reads fraction, 3′-5′ bias, strand specificity, intron–exon ratio, intergenic reads fraction, GC bias and reads per kilobase of transcript per million reads mapped (RPKM) discovery rate. Exon-specific usage and gene expression was quantified by calculating modified RPKM metrics as described[313]. The normalization factor used in the RPKM calculations excluded reads from mitochondrial sequence, reads falling into top 0.5% expressed exons considering as a source of potential outliers and ribosomal genes and as such it represented the total number of reads aligned to coding exons. Gene-specific RPKM was calculated by the total number of reads aligned to all exons normalized by total length of exons. Pairwise comparisons between different samples was performed to identify differentially expressed genes using a custom DEfine matlab tool (FDR cutoff=0.05, Minimum number of aligned reads = 10).

4.3.9 ChIP-seq analysis pipeline

Isolated cells were flash frozen and provided to the Hirst Lab where ChIP-seq libraries were generated according to standard protocols. Briefly, cells were lysed followed by MNase digestion. Antibodies against the marks H3K36me3, H3K4me3, H3K4me1, H3K9me3, H3K27Ac, and H3K27me3 were used for immunoprecipitation[314]. Histones were removed from DNA followed by Adenine addition to 3’ ends, ligation of sequencing adaptors and PCR amplification. Libraries were sequenced on either Illumina HiSeq 2000 or 2500 following the manufacturer’s protocols with paired-end 75nt or 100nt sequencing chemistry using custom index adapters during library construction. For the generation of the heatmap showing the distribution of H3K27Ac and H3K27me3; the signal +/-2kb from the transcription start site was normalized by the library depth multiplied by a factor of 10^8. The heatmap was constructed using deepTools[315] was used for matrix calculation and ComplexHeatmap[316] package in R for plotting.

Sequencing reads were aligned to hg19 and for gene annotation Ensembl version hg19v75 was used.

4.3.10 Microarray expression profiling

Viable cells were selected for using a Miltenyi Dead cell removal kit (130-090-101). Total RNA was isolated by TRIzol (Invitrogen) extraction/PureLink™ RNA Mini Kit (ambion) and submitted to the McGill University/Génome Québec Innovation Centre for expression profiling using Affymetrix GeneChip® PrimeView™ Human Gene Expression Array. Data were analyzed using the Partek® Flow® suite with the Microarray toolkit. CEL files were uploaded and intensity values were converted to aligned reads using STAR[317]. Reads were quantified using an annotation model (Partek E/M) to hg38 Ensembl Transcripts release 86. Samples were normalized by total count. Differential gene expression was determined using Partek "gene specific analysis" from the Partek® Flow® suite[318-322]. Data were then filtered by False Discovery Rate (FDR) and/or fold change followed by hierarchical clustering on both samples and genes using average linkage cluster distance metric and Euclidean point distance metric.

4.4 Results

4.4.1 Survey of RUNX1 and RUNX3 in T-cell Leukemia

In a set of experiments to determine the relative importance of RUNX family members in T-ALL cell growth, I transduced human and mouse T-ALL cells with a dominant-negative version of RUNX transcription factors which should bind to RUNX consensus sequences and interfere with normal functions. More specifically, I used the RUNT domain fused to a nuclear localization signal (NLS), based on a construct described previously, and which had GFP as a selectable marker[323]. In an approach I used throughout this study, I measured the frequency of the transduced population (GFP^+) of viable cells (PI^-) in the culture over the course of 1.5-3 weeks (**Figure 4.3**). This construct appeared to result in a growth defect that was due in part to reduced proliferation and enhanced cell death as measured by BrdU incorporation (representing S phase) and PI staining (representing DNA content, in this case enhanced sub-G_1

fraction), respectively. In trying to ascertain the redundancy of the paralogous family members, I undertook a search of existing gene expression data and found that while RUNX1 and RUNX3 appear to be widely expressed across many subtypes of T-ALL (**Figure** 4.4), RUNX2 appears to be relatively lowly expressed. Because of this, I focused my first functional experiments on RUNX1 and RUNX3 using a lentiviral knockdown approach (**Table 4.4**). Using a pool of pLKO.1 shRNAs targeting both RUNX1 and RUNX3 (**Figure 4.5 A**, **Table 4.5**) to create a pan-RUNX knockdown, I found that the vast majority of human T-ALL cell lines tested were dependent on one or both of these genes for growth (**Figure 4.6**). Interestingly, proliferation was abrogated upon knockdown of RUNX1, RUNX3 or RUNX1 and RUNX3 using pooled shRNAs (**Figure 4.7**). RUNX1 knockdown produced the greatest relative reduction in BrdU incorporation. Using a cell proliferation dye, very similar to CFSE typically used in immunology, I found that a patient-derived xenograft (PDX), M18-1-5, transduced with a pool of shRNAs targeting RUNX1 and RUNX3 divided less *in vitro* in contrast to untransduced internal control cells in the same culture (**Figure 4.8**). Of note, I found that almost all T-ALL cells appeared to express RUNX1 and RUNX3, albeit at heterogeneous levels. It appeared as though patient-derived xenografts express, on average less RUNX1, relative to cell lines. Cell lines tended to group into RUNX3-high and RUNX3-low lines (**Figure 4.9 A**), while there was no obvious correlation between mutation status of *RUNX1* and protein expression (**Figure 4.9 C**), with several cell lines containing *RUNX1* mutations (**Table 4.6**) appearing to have high expression relative to wild-type lines and I was unable to detect polypeptides of smaller molecular weight which might have been consistent with a truncated protein species. In attempting to segregate the roles of RUNX1 and RUNX3 in supporting the growth of T-ALL cells, I found that the cells were relatively more sensitive to RUNX1 depletion, in comparison to RUNX3 depletion (**Figure 4.9 D**) despite sufficient knockdown of RUNX3 (**Figure 4.5 B**). Based on these early experiments and the frequency of *RUNX1* mutation, I focused the rest of my studies on RUNX1.

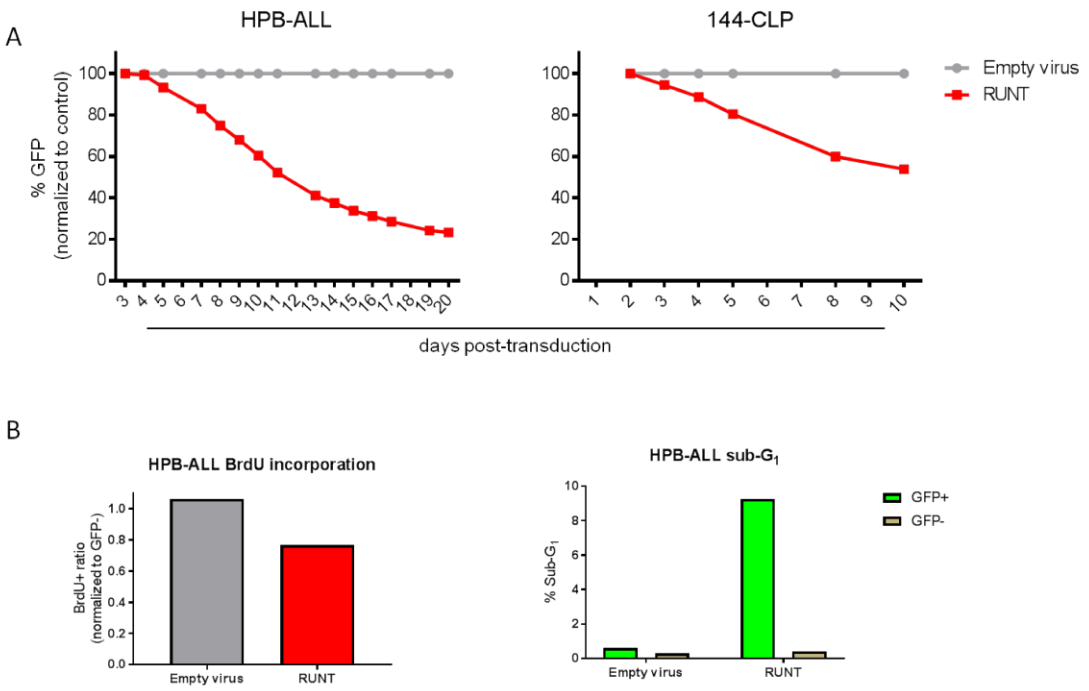

Figure 4.3 Pan-RUNX interference results in growth defects.

(A) HPB-ALL cells and 144-CLP cells were transduced as indicated with pseudotyped retrovirus containing empty vector (MSCV-IRES-GFP) or a dominant-negative version of RUNX1 termed “RUNT”. Heterogeneous cultures of transduced (GFP+) and untransduced (GFP-) cells were analyzed for GFP expression every few days by flow cytometry for the durations indicated. **(B)** HPB-ALL cells transduced with empty vector or RUNT were incubated with BrdU according to the manufacturer’s protocol. Cells were fixed and permeabilized and labeled with anti-BrdU AlexaFluor 647 antibody. Cells were then analyzed using a FACScalibur cytometer and gated on the fractions indicated.

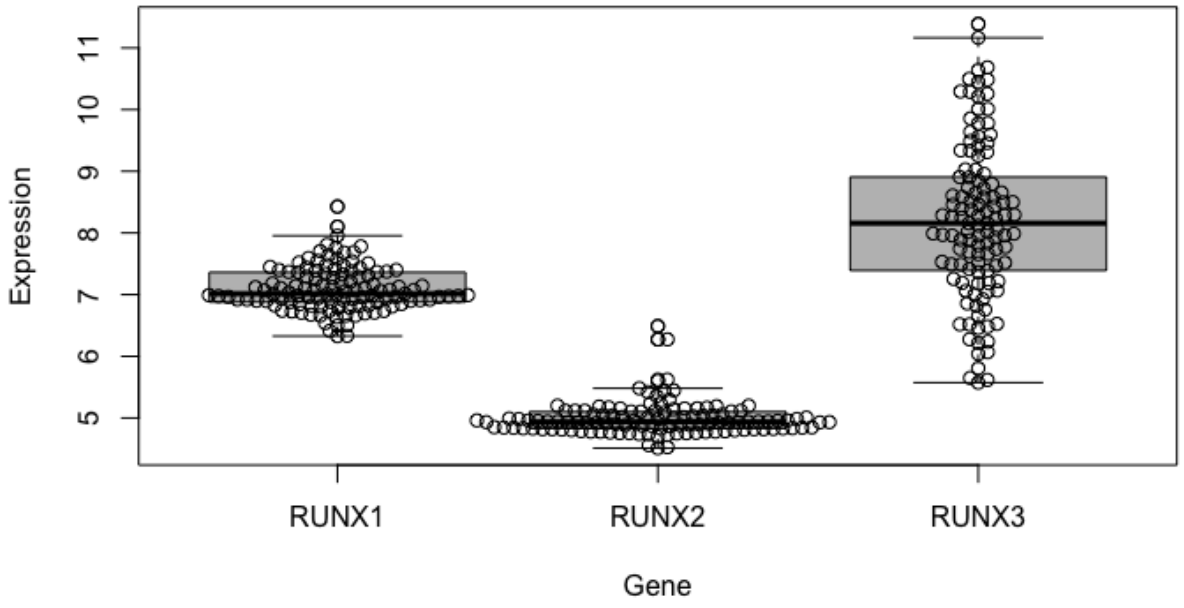

Figure 4.4 Expression of RUNX family members in T-ALL.

Gene expression profile data of human T-ALL samples for RUNX1, RUNX2, and RUNX3 taken from previously published data[65]. Data are shown as a box and whisker plot with the median depicted as a bold line, the box bounds the 3rd (top line) and 1st (bottom line) quartiles and the whiskers represent the 3rd or 1st quartiles plus 1.5 times the interquartile range. The GEO accession number is GSE26713.

Shortened Clone name	Clone name	Gene(s) Targeted	Region Targeted	Isoforms Targeted
shRUNX1-58	TRCN0000013658	*RUNX1*	3' UTR	AML1B AML1C
shRUNX1-59	TRCN0000013659	*RUNX1*	Exon 9	AML1B AML1C
shRUNX1-60	TRCN0000013660	*RUNX1*	Exon 6-7 junction	AML1A AML1B AML1C
shRUNX1-90	TRCN0000338490	*RUNX1*	Exon 7	AML1A AML1B AML1C
shRUNX1-92	TRCN0000338492	*RUNX1*	3' UTR	AML1B AML1C
shRUNX1-27	TRCN0000338427	*RUNX1*	Exon 5	AML1A AML1B AML1C
shRUNX1-28	TRCN0000338428	*RUNX1*	Exon 9	AML1B AML1C
shRUNX3-74	TRCN0000235674	*RUNX3*	3' UTR	RUNX3 isoform 1 RUNX3 isoform 2
shRUNX3-75	TRCN0000235675	*RUNX3*	Exon 6	RUNX3 isoform 1 RUNX3 isoform 2
shRUNX3-76	TRCN0000235676	*RUNX3*	Exon 3	RUNX3 isoform 1 RUNX3 isoform 2

Table 4.4 shRNA clones against RUNX1 and RUNX3.

The shortened clone names are those used throughout this study, while the clone name refers to the name designated by the BROAD institute's RNAi consortium.

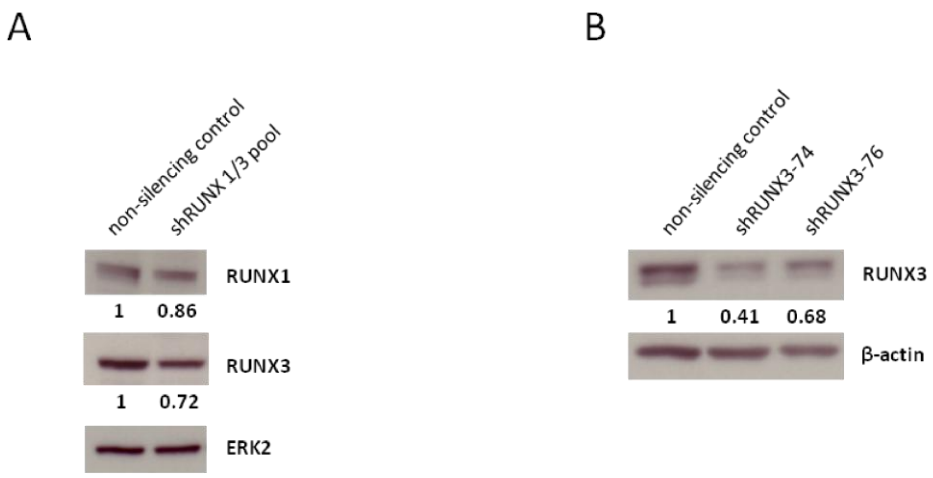

Figure 4.5 Knockdown of RUNX1 and RUNX3 protein using an shRNA pool or individual clones against RUNX3.

(A) HPB-ALL was transduced with the indicated shRNA clones targeting RUNX3, or **(B)** an equimolar pool of shRNAs targeting RUNX1 and RUNX3. **(A, B)** 3 days post-transduction, homogeneous cultures were selected by incubation with puromycin for 3 days before lysis for immunoblot and probed for RUNX1 and/or RUNX3 protein expression.

Pool name	**Gene Targeted**	**Clones used (all at equimolarity)**
shRUNX1 pool	*RUNX1*	TRCN0000013659
		TRCN0000013660
shRUNX3 pool	*RUNX3*	TRCN0000235674
		TRCN0000235675
		TRCN0000235676
shRUNX1/3 pool	*RUNX1* and *RUNX3*	TRCN0000013659
		TRCN0000013660
		TRCN0000235674
		TRCN0000235675
		TRCN0000235676

Table 4.5 shRNA clones used in pool against RUNX1, RUNX3 or RUNX1 and RUNX3.

Those experiments noted to have a pool of shRNAs as described use an equimolar pool of lentiviral constructs in order to knockdown expression of RUNX1, RUNX3 or RUNX1 and RUNX3.

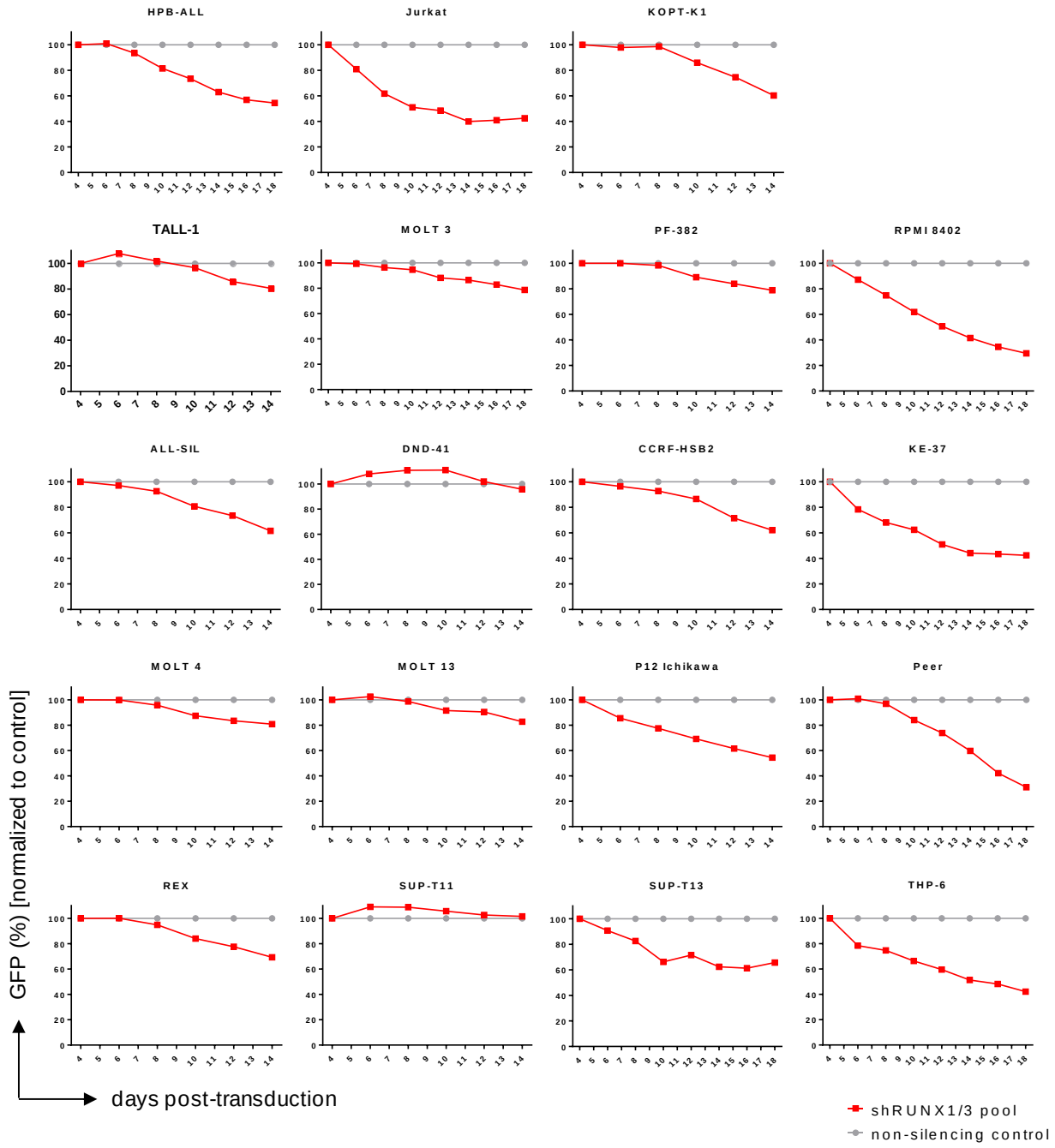

Figure 4.6 *In vitro* competition assay of pan-RUNX1/3 knockdown.

Human T-ALL cell lines were transduced as indicated with pLKO.1 GFP lentiviruses encoding scrambled non-silencing control or a pool of equivalent titre shRNA clones (**Table 4.5**) directed against *RUNX1* and *RUNX3* gene products. Heterogeneous cultures of transduced (GFP+) and untransduced (GFP-) cells were analyzed for GFP expression every few days by flow cytometry for the durations indicated. GFP expression is normalized to the non-silencing control.

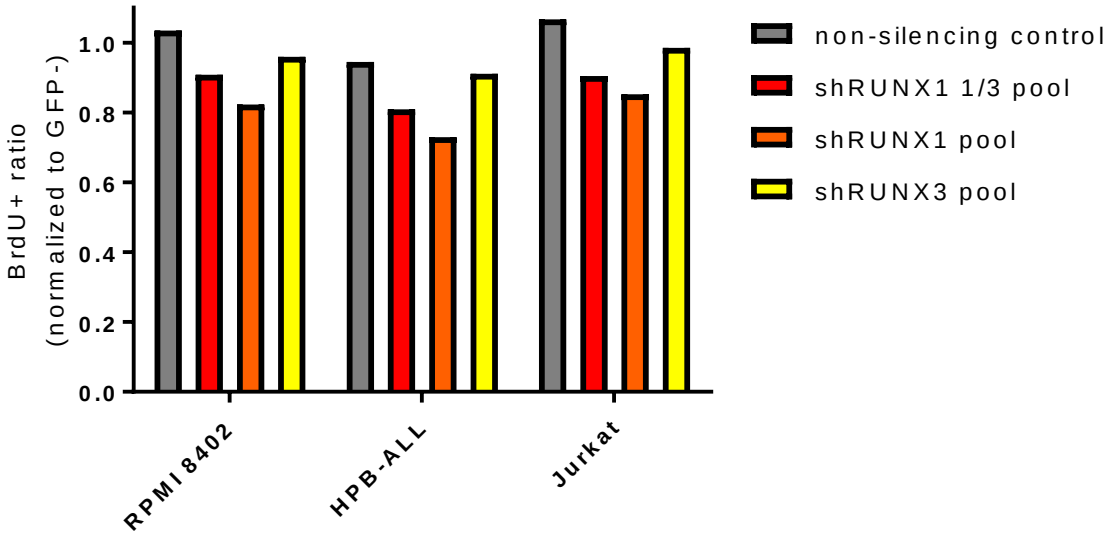

Figure 4.7 BrdU incorporation in RUNX-depleted T-ALL cells.

The T-ALL cell lines RPMI 8402, HPB-ALL, and Jurkat were transduced with either a non-targeting control or pools of shRNAs as indicated (**Table 4.5**). 9 days post-transduction, cells were incubated with BrdU according to the manufacturer's protocol. Cells were fixed and permeabilized and labeled with anti-BrdU AlexaFluor 647 antibody. Cells were then analyzed using a FACScalibur cytometer and gated on the GFP+ (transduced) and GFP- (untransduced) fractions. The ratio of GFP+ to GFP- subsets is displayed.

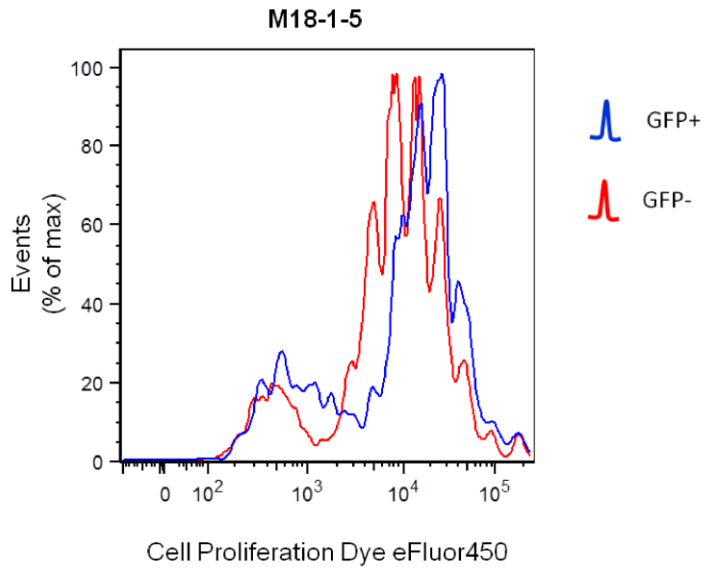

Figure 4.8 Patient-derived xenograft M18-1-5 cell proliferation upon RUNX1/3 depletion.

The PDX M18-1-5 was transduced with a pool of shRNAs against RUNX1 and RUNX3 as indicated (**Table 4.5**) and cultured on MS5-DL1 feeders in WIT-L media. 72 hours following transduction, cells were loaded with the Cell Proliferation Dye eFluor450 (eBioscience, #65-0842) and replated on feeders with fresh media. One week post-loading, T-ALL cells were isolated and analyzed on a BD LSRFortessa flow cytometer. As cells divide, their mean fluorescence is halved, with proliferative cell fractions moving to the left side of the plot over time and non-proliferative fractions remaining on the right hand side of the plot. The transduced (GFP+) and untransduced (GFP-) populations are plotted.

A

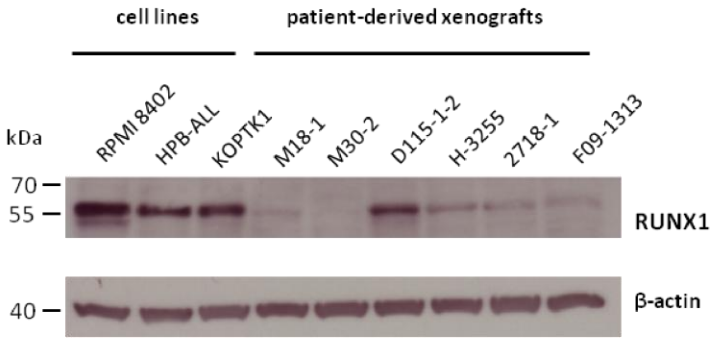
cell lines
patient-derived xenografts
kDa
RPMI 8402
HPB-ALL
KOPTK1
M18-1
M30-2
D115-1-2
H-3255
2718-1
F09-1313
70
55
RUNX1
40
β-actin

B

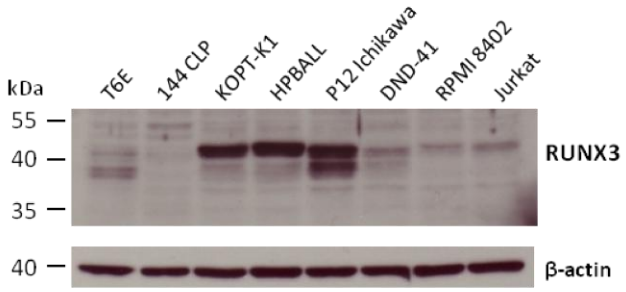
kDa
T6E
144 CLP
KOPT-K1
HPBALL
P12 Ichikawa
DND-41
RPMI 8402
Jurkat
55
40
35
RUNX3
40
β-actin

C

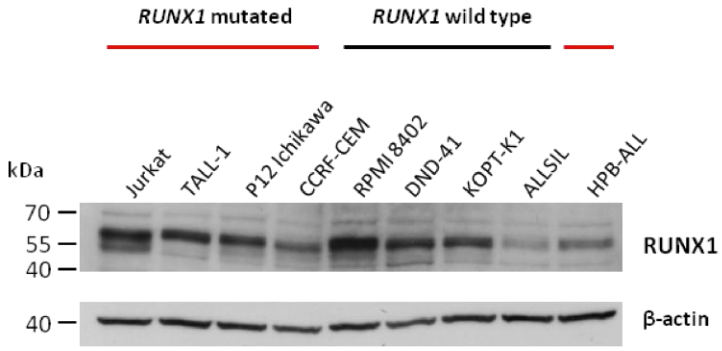
RUNX1 mutated
RUNX1 wild type
kDa
Jurkat
TALL-1
P12 Ichikawa
CCRF-CEM
RPMI 8402
DND-41
KOPT-K1
ALLSIL
HPB-ALL
70
55
40
RUNX1
40
β-actin

D

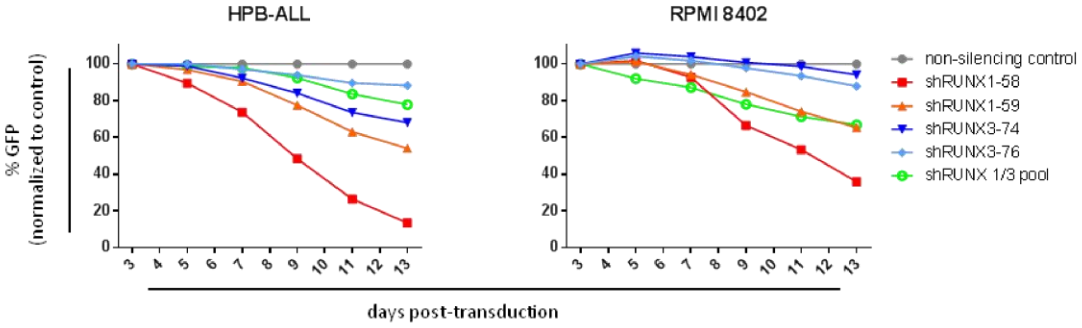
HPB-ALL
RPMI 8402
% GFP
(normalized to control)
100
80
60
40
20
0
3
4
5
6
7
8
9
10
11
12
13
days post-transduction
non-silencing control
shRUNX1-58
shRUNX1-59
shRUNX3-74
shRUNX3-76
shRUNX 1/3 pool

Figure 4.9 Expression and survey of RUNX1 and RUNX3 in human T-cell leukemia.

(A) Western blot of a panel of T-ALL patient-derived xenograft samples using an antibody against RUNX1 (Active Motif, polyclonal: aa 231-245) and β-actin as a loading control. A subset of human T-ALL cell lines are provided as reference. **(B)** Western blot of several human T-ALL cell lines using an antibody against RUNX3 (R&D Systems, monoclonal: aa 186-415) and β-actin as a loading control. **(C)** Western blot of several human T-ALL cell lines using an antibody against RUNX1 (Active Motif, polyclonal: aa 231-245) and β-actin as a loading control. RUNX1 mutation status is listed above the samples. **(D)** In vitro competition assay. Cell lines were transduced as indicated with pLKO.1 GFP lentiviruses encoding non-silencing control or shRNA lentivirus targeting RUNX1, RUNX3 or a pool of clones targeting both gene products (**Table 4.5**). Heterogeneous cultures of transduced (GFP+) and untransduced (GFP-) cell lines were analyzed for GFP expression every few days by flow cytometry for the durations indicated. GFP expression is normalized to the non-silencing control.

4.4.2 RUNX1 is required for the growth of established human T-ALL cells

In trying to better understand the functional contribution of *RUNX1* in T-cell neoplasms, I knocked down RUNX1 expression using individual clones of pLKO.1 shRNA lentivectors (**Figure 4.10**). Several of the clones were able to consistently achieve between 30-80% knockdown depending on the cell line transduced (**Figure 4.11**). Using an *in vitro* growth competition experiment, I found that shRUNX1-transduced cells tend to compete poorly with untransduced control cells in the same dish (i.e. the % GFP+ decreases over time), with a mild correlation between level of knockdown and severity of phenotype, suggesting future work should confirm if there is a dose-dependent effect (**Figure 4.12 A**, **Figure 4.11**). Notably, there was no correlation between *RUNX1* mutation status and growth phenotypes, as several of the cell lines used have *RUNX1* mutations of a similar nature found in patients (**Table 4.6**). In an expanded screen, I found a consistently strong growth impairment phenotype using additional lentiviral clones (**Figure 4.13 A**). In order to confirm these results, I also measured growth by performing cell counts on purified populations of transduced cells. To this end, I next used drug selection to generate homogenous populations of non-silencing control or RUNX1 knockdown T-ALL cell lines and measured their growth using by automated cell counting (**Figure 4.12B**, **Figure 4.13 B**). I found as much as a 5-fold difference between the growth of control cells and RUNX1-depleted cells. In order to better understand how

the amount of RUNX1 might affect cell growth, I attempted the corollary experiment in which I used an inducible system to enforce the expression of the three canonical RUNX1 isoforms: RUNX1A, RUNX1B, RUNX1C (and GFP as a control in HPB-ALL) (**Figure 4.14**). All three constructs were able to generate strong, dose-dependent induction of gene expression (**Figure 4.14**). Strikingly, there was consistent growth impairment upon induction of exogenous RUNX1 in Jurkat, RPMI 8402 and HPB-ALL cells (**Figure 4.12 C**). This was suggestive to me that perhaps T-ALL cells have reached an equilibrium-point at which their RUNX1 expression is finely balanced. To test this, I took these inducible cell lines and transduced them with an shRNA that targets the 3' UTR (shRUNX1-58) which is lacking in the cDNAs of our inducible system (**Figure 4.12 D**). As such, attempting to knockdown RUNX1 in cells which have dox-induced expression will only knockdown the endogenous RUNX1. I found strikingly that there was relative selection for cells in which the endogenous RUNX1 had been depleted upon exogenous RUNX1 induction (**Figure 4.12 E**). This suggested that reducing the expression of RUNX1 from the high levels achieved during dox-induction helps to partially rescue the growth impairment, in support of my hypothesis of an equilibrium-point for RUNX1 levels. It should be noted that these phenotypes could be cell-type specific, and these findings should be extended to a broader sample size.

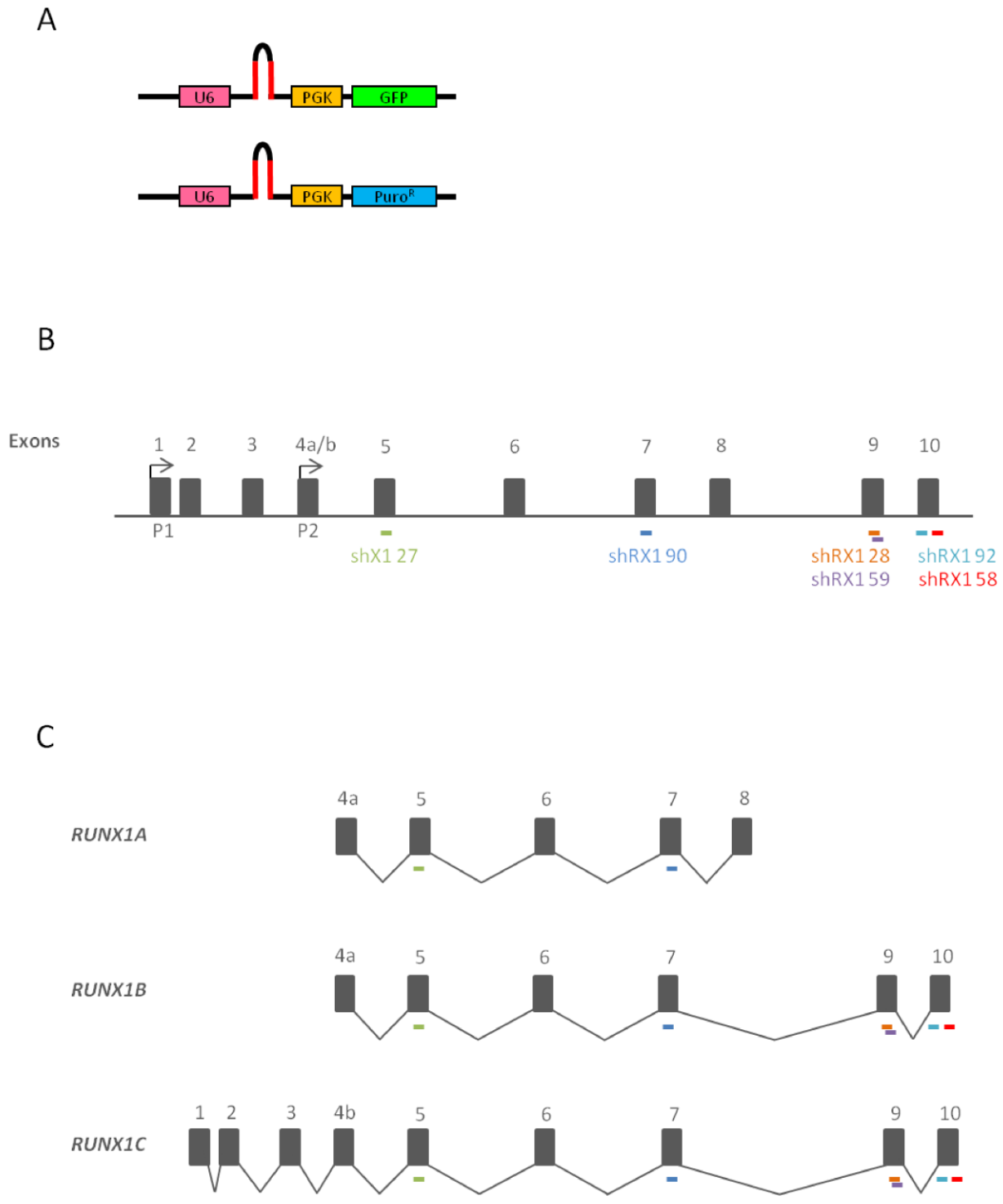

Figure 4.10 shRNAs used to knockdown RUNX1.

(A) The structure of the pLKO.1 GFP and pLKO.1 Puro^R lentivectors used in this study. The expression of the shRNA hairpin is driven by the U6 promoter, while the selectable

markers GFP and Puromycin^{R} are driven by the PGK promoter. **(B)** A graphical depiction of the human *RUNX1* genomic locus, depicting the two promoters (P1 and P2) as well as the regions targeted by the shRNA clones used in this study. **(C)** A graphical depiction of human *RUNX1* mRNA isoforms as well as the regions targeted by the shRNA clones used in this study.

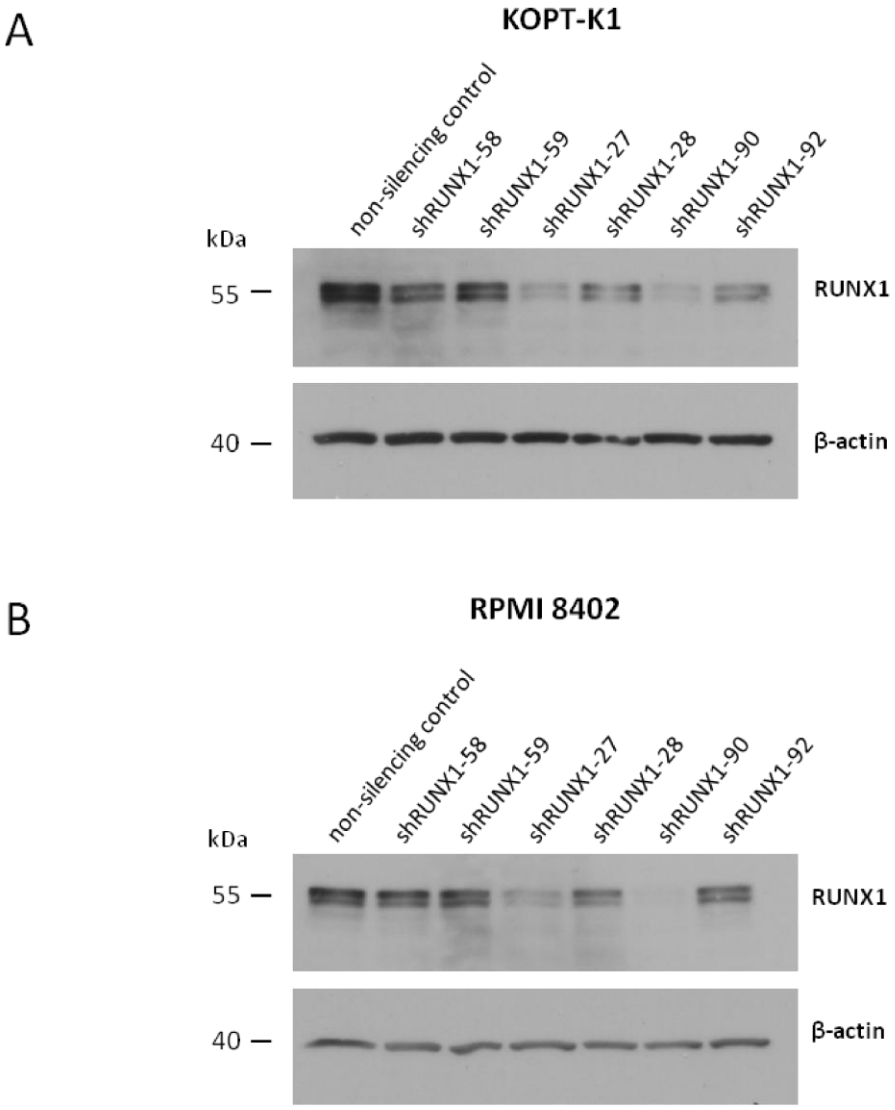

Figure 4.11 Knockdown of RUNX1 and RUNX3 protein in T-ALL cell lines.

The cell lines **(A)** KOPT-K1 and **(B)** RPMI 8402 were transduced with pLKO.1 PuroR vectors containing the indicated shRNA clones against RUNX1. 3 days post-transduction, homogeneous cultures were selected by incubation with puromycin for 3 days before lysis for immunoblot and probed for RUNX1 and/or RUNX3 protein expression.

Cell Line	RUNX1 mutation	Predicted protein†
TALL-1	413_414insG	R139fs*47 STOP (186 amino acids)
JURKAT	365 G>A	122 A>T
P12-ICHIKAWA	173 C>A	58 H>N
CCRF-CEM	1027 G>A	343 A>T (29 L>S)
MOLT 16	?	29 L>S, 197 R>W, 343 A>T
HPB-ALL	?	29 L>S

† annotation based on AML1B isoform

Table 4.6 Human T-ALL cell lines with *RUNX1* mutations.

Data is taken from the COSMIC database or described in publication[170].

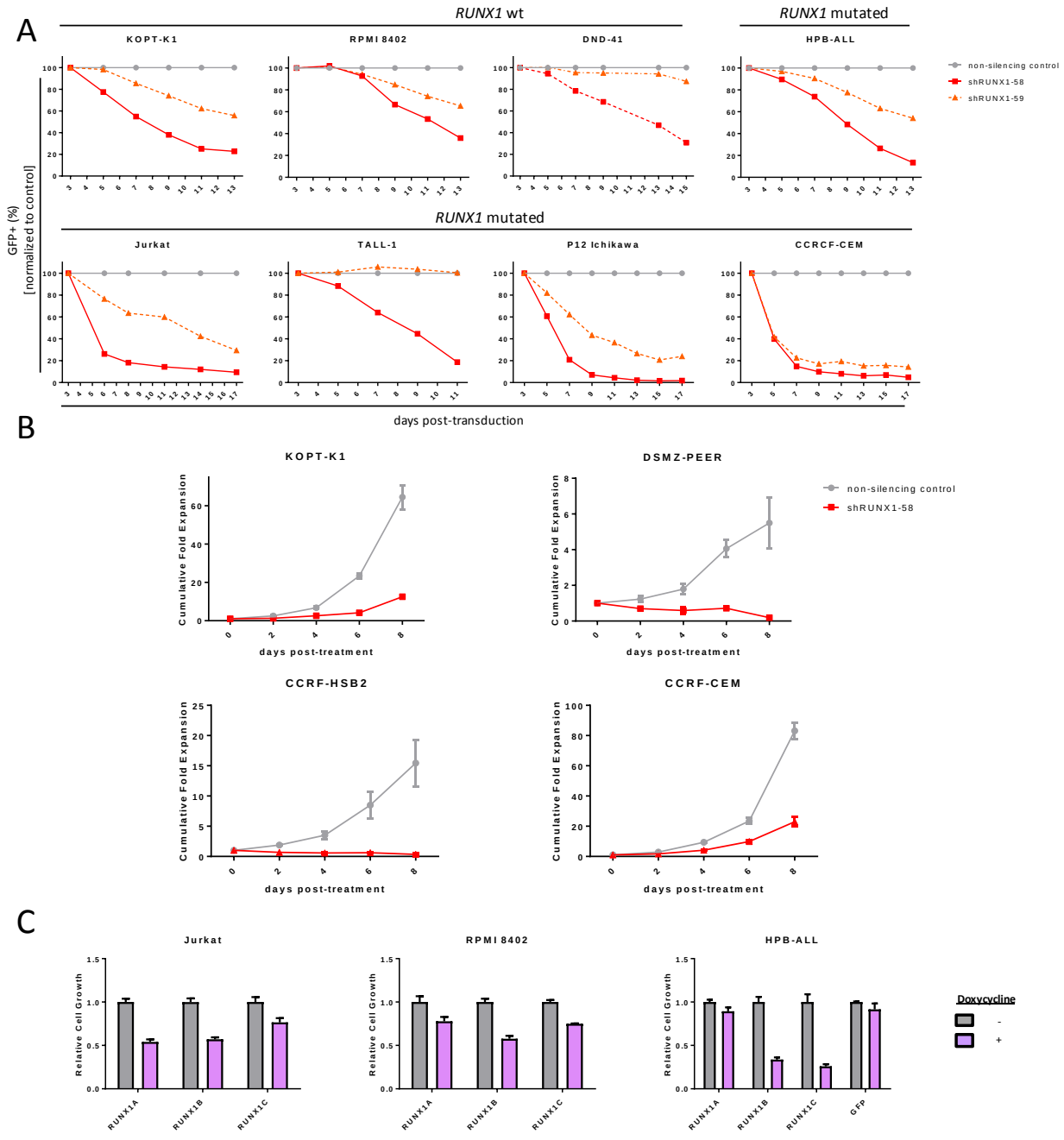
A
RUNX1 wt
RUNX1 mutated
KOPT-K1
RPMI 8402
DND-41
HPB-ALL
non-silencing control
shRUNX1-58
shRUNX1-59
GFP+ (%)
[normalized to control]
RUNX1 mutated
Jurkat
TALL-1
P12 Ichikawa
CCRCF-CEM
days post-transduction
B
KOPT-K1
DSMZ-PEER
CCRF-HSB2
CCRF-CEM
Cumulative Fold Expansion
days post-treatment
non-silencing control
shRUNX1-58
C
Jurkat
RPMI 8402
HPB-ALL
Relative Cell Growth
RUNX1A
RUNX1B
RUNX1C
GFP
Doxycycline
-
+

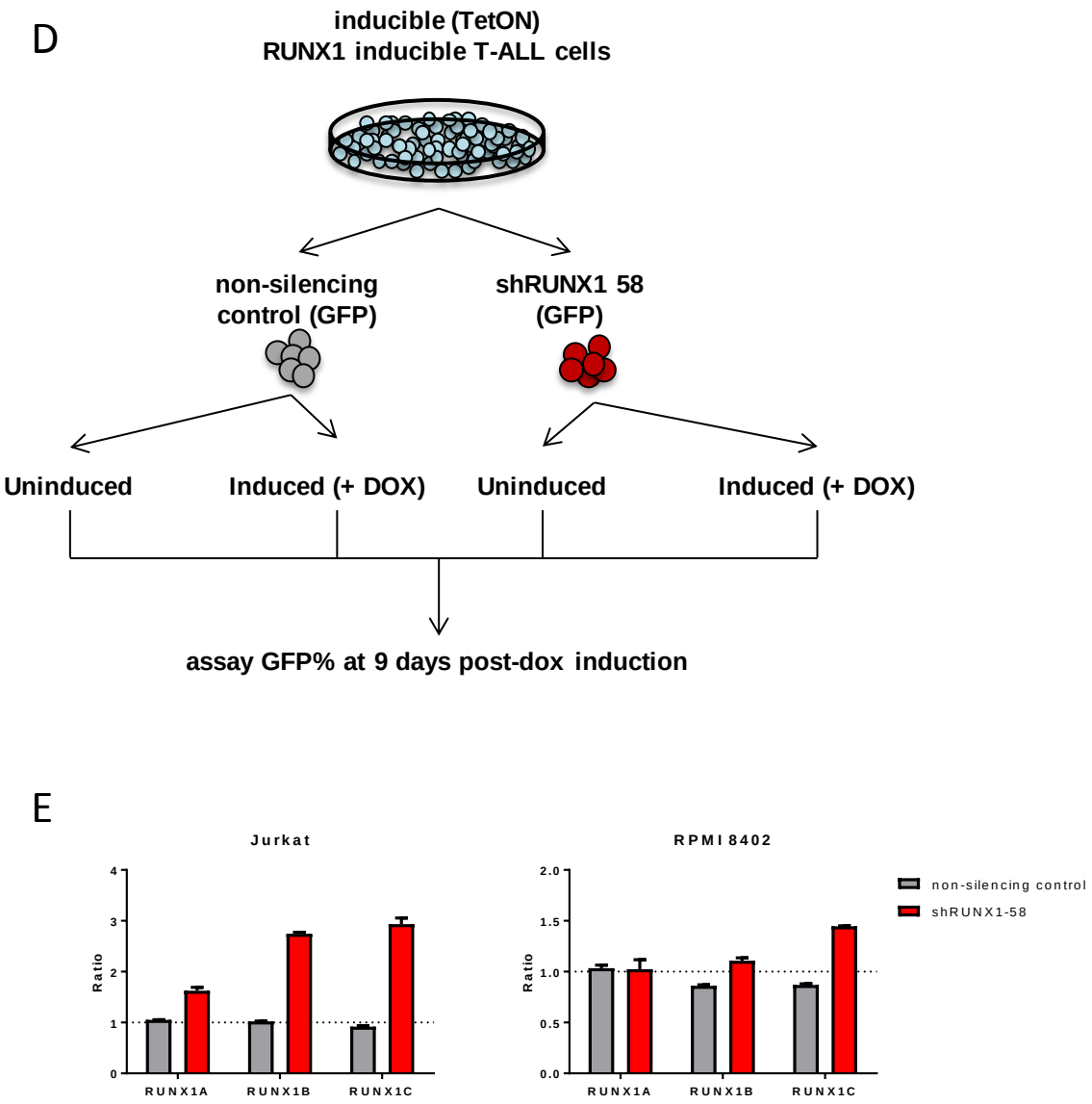

Figure 4.12 Endogenous RUNX1 protein is required for growth of human T-ALL cells.

(A) In vitro competition assay. Cell lines were transduced as indicated with pLKO.1 GFP lentiviruses encoding non-silencing control or shRNA clones targeting RUNX1. Heterogeneous cultures of transduced (GFP+) and untransduced (GFP-) cell lines were analyzed for GFP expression every few days by flow cytometry for the durations indicated. GFP expression is normalized to the non-silencing control. RUNX1 mutation status is listed above the cell lines. **(B)** Growth curves. The cell lines indicated were transduced with pLKO.1 PuroR lentiviruses encoding non-silencing control or shRUNX1-58. 72 hours post-transduction, cells were treated with 1µg/ml of Puromycin. Following 72 hours of selection for transduced cells, cells were plated at a density of

$5x10^5$ cells/ml. Every two days, cells were counted using the Vi-CELL® automated cell viability analyzer using Trypan Blue exclusion. Cells were then replated at the original density and cumulative fold expansion was calculated for an 8 day period. **(C)** Inducible RUNX1 expression. Stable cell lines were generated and selected containing inducible expression systems for the genes indicated. Cells were plated in triplicate at low density, gene expression induced or not induced with 1µg/ml doxycycline, and resazurin reduction was measured 3 days later using a plate reader. Mean cell growth is normalized to an uninduced control with error bars representing standard deviation. **(D, E)** Growth rescue experiment. **(D)** Experimental schema. Inducible cell lines were transduced with either pLKO.1 GFP non-silencing control or pLKO.1 shRUNX1-58. 48h post-transduction, exogenous gene expression was either induced or not induced and GFP expression was measured 9 days later. **(E)** The ratio of GFP expression between induced and not induced conditions is depicted for each cell culture indicated.

A

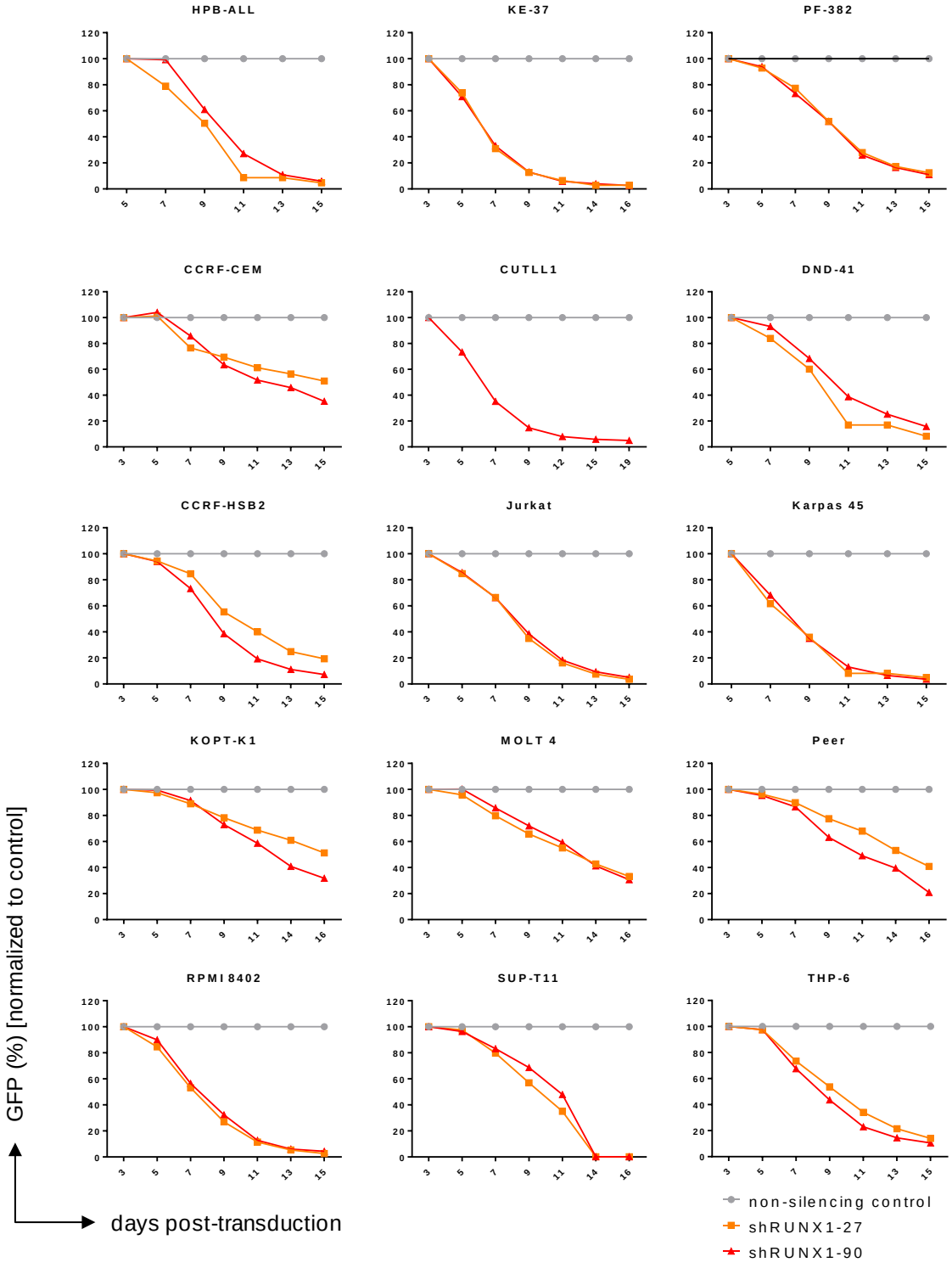
HPB-ALL
KE-37
PF-382
CCRF-CEM
CUTLL1
DND-41
CCRF-HSB2
Jurkat
Karpas 45
KOPT-K1
MOLT 4
Peer
RPMI 8402
SUP-T11
THP-6
GFP (%) [normalized to control]
days post-transduction
non-silencing control
shRUNX1-27
shRUNX1-90

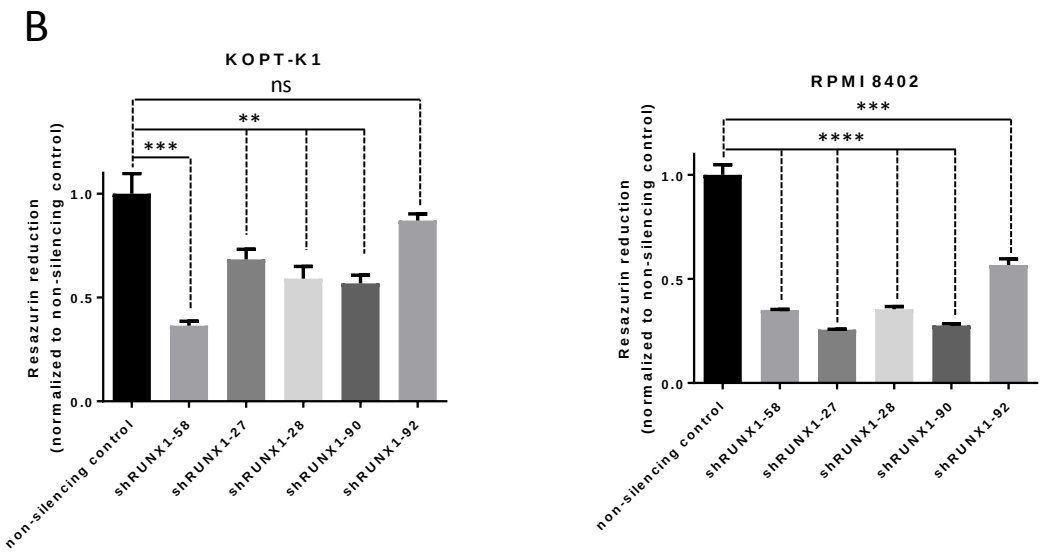

Figure 4.13 A survey of RUNX1-dependent growth.

(A) In vitro competition assay. Cell lines were transduced as indicated with pLKO.1 GFP lentiviruses encoding non-silencing control or shRNA clones targeting RUNX1 (shRUNX1-90 or shRUNX1-27). Heterogeneous cultures of transduced (GFP+) and untransduced (GFP-) cell lines were analyzed for GFP expression every few days by flow cytometry for the durations indicated. GFP expression is normalized to the non-silencing control. **(B)** The cell lines indicated were transduced with pLKO.1 PuroR lentiviruses encoding non-silencing control or shRNAs against RUNX1 as shown. 72 hours post-transduction, cells were treated with 1µg/ml of Puromycin. Following 72 hours of selection for transduced cells, cells were plated in triplicate at low density and resazurin reduction was measured 2 days later using a plate reader. Mean relative fluorescent units are depicted and error bars represent standard deviation.

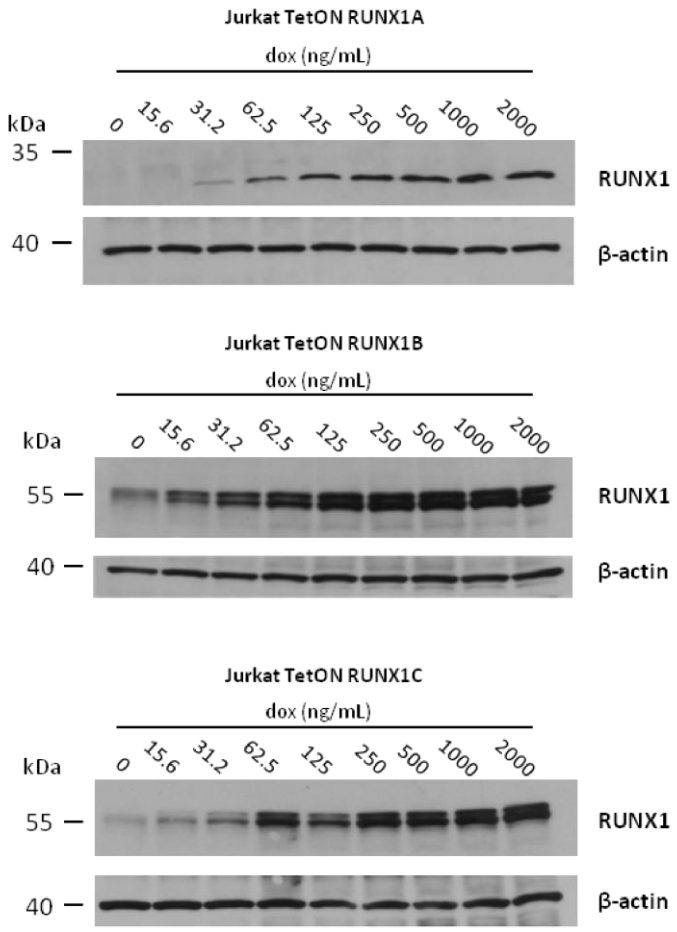

Figure 4.14 Inducible expression of RUNX1.

Stable cell lines were generated and selected containing inducible expression systems for the isoforms of RUNX1 indicated. Exogenous gene expression was induced with doxycycline at the doses indicated and 48h later cell lysates from each condition were made and probed via immunoblotting using an antibody against RUNX1, with β-actin serving as a loading control.

4.4.3 Runx1 is required for the growth of established mouse NOTCH1-driven T-ALL cells

In order to test if these RUNX1-dependent phenotypes were conserved or a result of cell line/PDX heterogeneity, I sought to use a murine conditional knockout approach to deplete cells of RUNX signaling. As such, I generated NOTCH1-ΔE leukemias[43] using *Cbfb*$^{lox/lox}$, *Runx1*$^{lox/lox}$ and wild-type C57 BL/6J bone marrow donors (**Figure 4.15**). Due to the nature of Cbfb as an obligate partner for all Runx family members, and mediator

of protection from ubiquitin-mediated degradation, the ablation of this important protein should function as a pan-Runx knockout[324]. Using a version of the Cre recombinase fused to the Human Immunodeficiency Virus (HIV) protein Tat, known as Tat-Cre[325], I induced deletion of *Cbfb* and found a concomitant growth defect as measured by tracking the dynamics of the $Cbfb^{\Delta}$ population over time (**Figure 4.16 A**). Using a complementary method, I transduced two other clones of $Cbfb^{lox}$ leukemia with lentivirus containing CreERT2 and induced deletion using 4-hydroxytamoxifen (4OHT). Yet again, I noted a reduction in the frequency of the $Cbfb^{\Delta}$ in an *in vitro* competition with $Cbfb^{lox}$ cells (**Figure 4.16 B**). Due to a role for Runx1 loss-of-function in murine T-ALL leukemogenesis[326], it was unclear if loss of Runx1 would cause a growth impairment, or a growth advantage. Upon treatment of two $Runx1^{lox}$ leukemias with Tat-Cre, I noted a similar diminution of *in vitro* growth in $Runx1^{\Delta}$ leukemic cells as that seen in $Cbfb^{\Delta}$ cells (**Figure 4.16 C**). This phenotype was again further supported in three other clones using CreERT2 to induce deletion, with the $Runx1^{\Delta}$ population failing to compete relative to $Runx1^{lox}$ cells (**Figure 4.16 D**). The use of Cre recombinase in LoxP-mediated deletion has caveats, one of which is the theoretical concern of Cre toxicity. Of important note then, through the use of a reporter of LoxP recombination which was lentivirally transduced into wild-type cells, I found there was no obvious genotoxic stress mediated by treatment with Cre recombinase in my hands (**Figure 4.16 E**). These results suggest that murine T-cell Acute Lymphoblastic Leukemias are dependent on Runx1, and that it's possible at least some of its growth-supportive functions may be conserved between mouse and human.

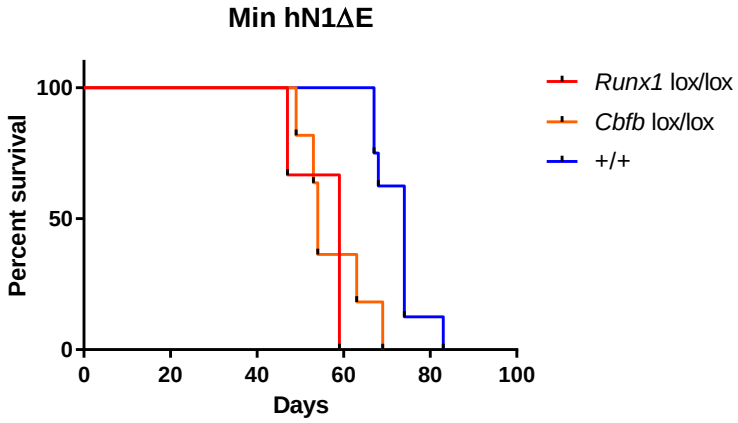

Figure 4.15 Leukemias generated on *Runx1*$^{lox/lox}$ and *Cbfb*$^{lox/lox}$ backgrounds.

Survival of C57BL/6 mice transplanted with hN1ΔE-transduced 5-FU bone marrow from wild-type, *Runx1*$^{lox/lox}$ or *Cbfb*$^{lox/lox}$ donors. Age and sex matched wild-type and *Runx1*$^{lox/lox}$ or *Cbfb*$^{lox/lox}$ mice were injected with 5-FU, 4 days later bone marrow was harvested and transduced with hN1ΔE retrovirus. Similar numbers of transduced cells were then transplanted into lethally-irradiated syngeneic/congenic C57BL/6 recipients by tail vein injection along with a radioprotective “rescue” dose of whole bone marrow. Mice were monitored for clinical signs of morbidity and euthanized after attaining a predefined endpoint based on standardized scoring of clinical symptoms. Pathologic involvement by T-cell acute lymphoblastic leukemia was confirmed at necropsy.

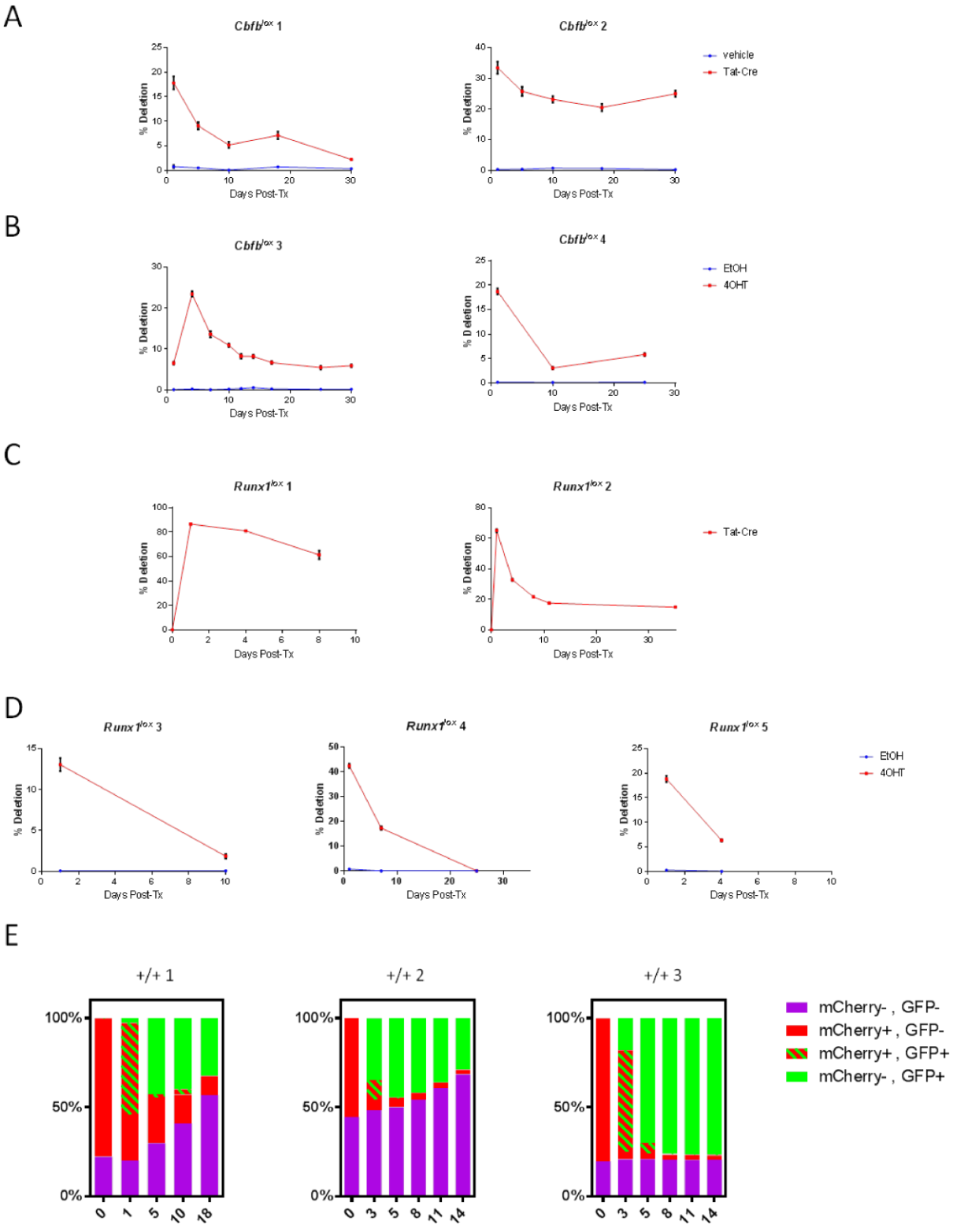

Figure 4.16 Murine NOTCH1-driven leukemias are dependent on *Runx1* and *Cbfb.*

(A, B) *Cbfb*^{lox} leukemia or **(C, D)** *Runx1*^{lox} leukemia *in vitro* deletion experiments. **(A, C)** Leukemic cells were treated with 100 units of Tat-Cre recombinase or vehicle for 24 hours before washout. Cells were harvested at the times indicated and the level of deletion plotted. **(B, D)** Cells were transduced with CreERT2-GFP lentivirus and sorted for GFP+ cells. Cells were then treated with 4OHT to induce deletion (or EtOH as a control) for 24h before washout. Cells were harvested at the times indicated and the level of deletion plotted. **(E)** Wild-type leukemias were transduced with a Cre reporter lentivirus, and 5 days post-transduction, followed by treatment with 100 units of Tat-Cre recombinase 24 hours before washout. Expression of GFP and mCherry was measured on a BD LSRFortessa flow cytometer and gated on viable cells. Transduced cells are dsRed+ and the excision of dsRed by Cre-mediated recombination at LoxP sites induces GFP expression. Excised cells begin to express GFP while dsRed degrades until they only express GFP.

4.4.4 RUNX1 promotes cell proliferation, viability and cell size

In order to determine if the effect of RUNX1 knockdown was via cell cycle arrest or loss of cell viability, I next pulsed HPB-ALL, RPMI 8402 and KOPT-K1 cells in which RUNX1 had been knocked down with BrdU to determine their relative proliferation compared to a non-silencing control (**Figure 4.17**). I found that not only did RUNX1 knockdown cells incorporate less BrdU, but they also had a greater sub-G_1 fraction (**Figure 4.18 A**). To further explore the presence of the sub-G_1 fraction found in cell cycle analysis, I next looked at apoptosis using Annexin V/PI (**Figure 4.18 B**). In both HPB-ALL and KOPT-K1 cells, I found that knockdown of RUNX1 caused an increase in both early and late apoptosis, as well as bona fide dead cells. The reduced proliferative phenotype of RUNX1 knockdown was confirmed in patient-derived xenograft (PDX) samples using a cell proliferation dye similar to CFSE (**Figure 4.18 C**). I found that despite lower endogenous levels of RUNX1 compared to cell lines (**Figure 4.9 A**), PDX samples remained dependent on RUNX1 for their proliferation. These results suggest that RUNX1 is required for the full growth potential of established human T-ALL cells by regulating cell cycle and survival. I noted anecdotally during my *in vitro* competition experiments (**Figure 4.13**) that the GFP+ fraction appeared somewhat smaller as measured by forward light scatter. I retrospectively analyzed these data further and noted that RUNX1 depletion appeared to result in reduced cell size in many of the cell lines (**Figure 4.19**).

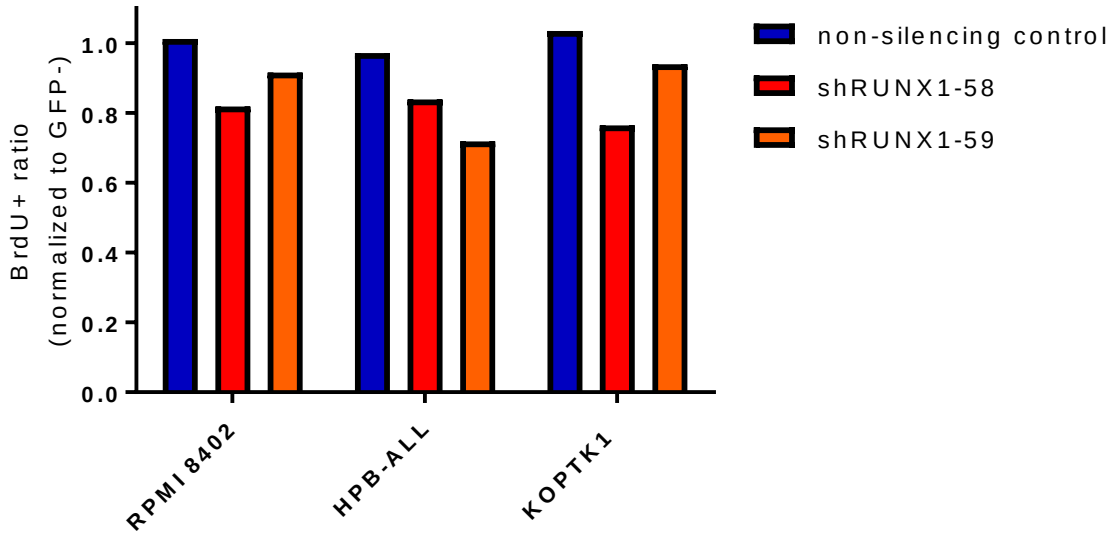

Figure 4.17 RUNX1 contributes to the proliferation of T-ALL cells – BrdU incorporation assay.

The cell line HPB-ALL was transduced with either pLKO.1 non-silencing control GFP, pLKO.1 shRUNX1-58 GFP, or pLKO.1 shRUNX1-59 lentivirus. 4 days following transduction, cells were incubated with BrdU according to the manufacturer's protocol. Cells were fixed and permeabilized and labeled with anti-BrdU AlexaFluor 647 antibody. Cells were then analyzed using a FACScalibur cytometer and gated on the GFP+ (transduced) and GFP- (untransduced) fractions. The ratio of GFP+ to GFP- subsets is displayed.

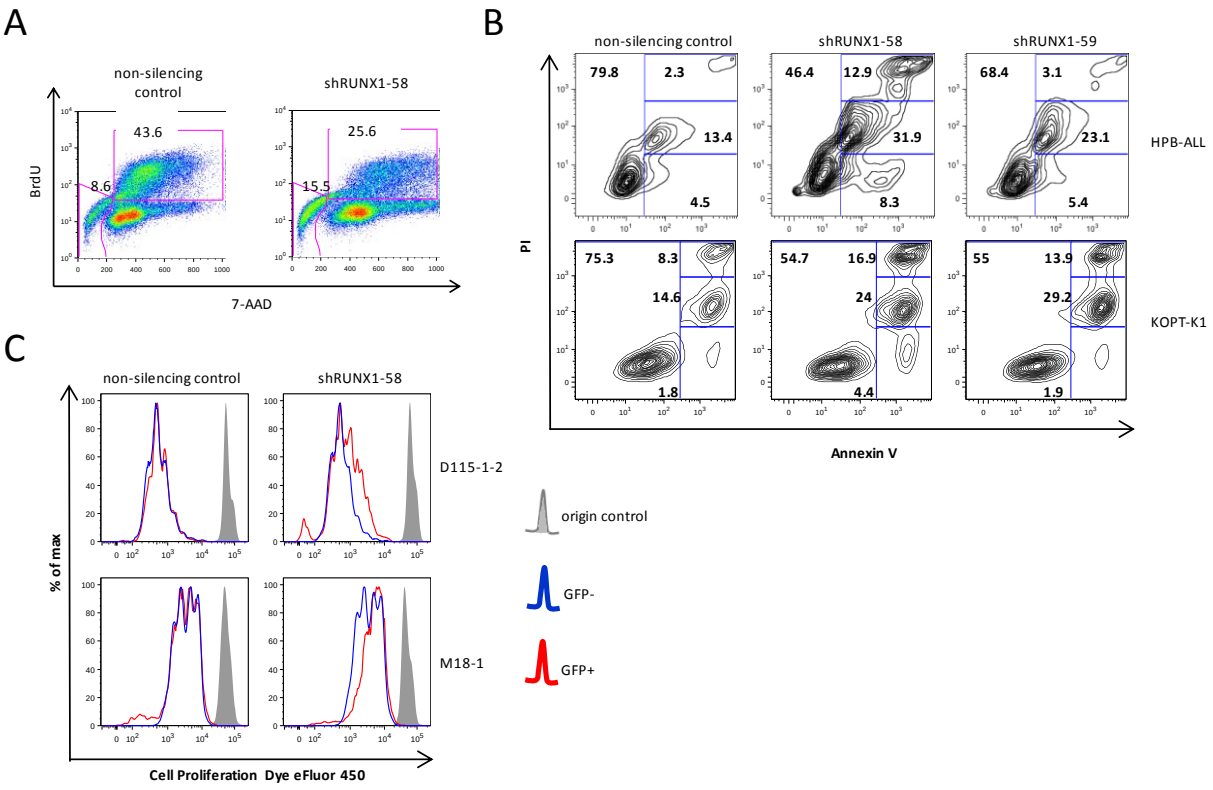

Figure 4.18 RUNX1 contributes to growth through both proliferation and survival.

(A) BrdU incorporation assay. The cell line HPB-ALL was transduced with either pLKO.1 non-silencing control GFP or pLKO.1 shRUNX1 58-GFP lentivirus. 4 days following transduction, cells were incubated with BrdU according to the manufacturer's protocol. Cells were fixed and permeabilized and labeled with anti-BrdU AlexaFluor 647 antibody. Cells were then analyzed using a FACScalibur cytometer and gated on the transduced GFP+ fraction. The gates in the figure indicate the sub-G_1 and S-phase fractions. **(B)** Cell Viability assay. Cells were transduced with pLKO.1 Puro^R lentiviruses encoding non-silencing control, shRUNX1-58 or shRUNX1-59. 72 hours post-transduction, cells were treated with 1µg/ml of Puromycin. Following 96 hours of selection for transduced cells, cells were labeled with antibody against Annexin V, stained with Propidium Iodide (PI) and analyzed on a BDFACSCalibur. **(C)** Cell Proliferation Dye assay – patient-derived xenograft (PDX) samples. Samples were transduced with shRNAs against RUNX1 as indicated and cultured on MS5-DL1 feeders in WIT-L media[306]. 72 hours following transduction, cells were loaded with the Cell Proliferation Dye eFluor450 (eBioscience, #65-0842) and replated on feeders with fresh media. One week post-loading, T-ALL cells were isolated and analyzed on a BD LSRFortessa flow cytometer. As cells divide, their mean fluorescence is halved, with proliferative cell fractions moving to the left side of the plot over time and non-proliferative fractions remaining on the right hand side of the plot.

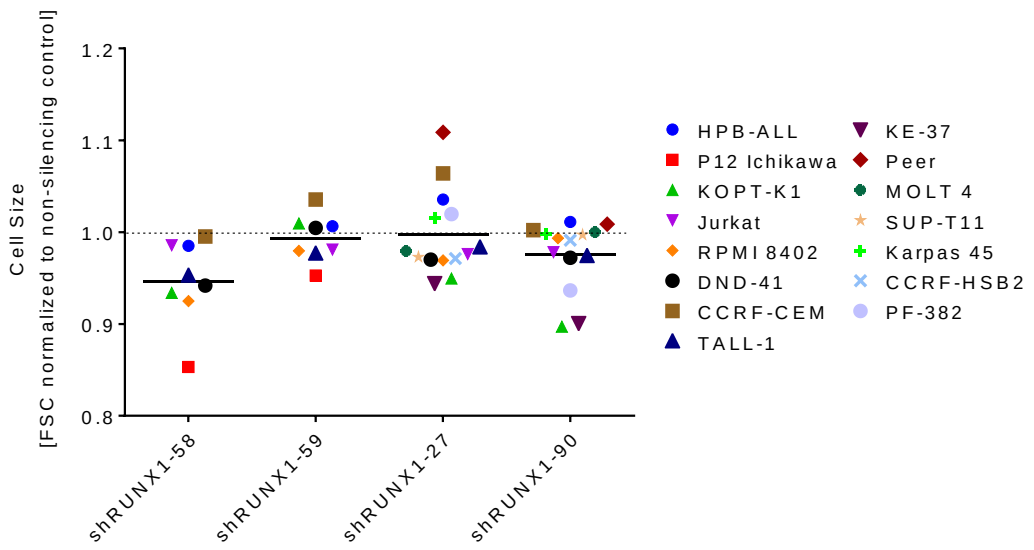

Figure 4.19 RUNX1 knockdown effects on cell size

Cell size measurement by forward light scatter (FSC). Cells lines transduced with GFP-tagged shRUNX1 lentiviruses were assayed by flow cytometry at 5-7 days post-transduction. FSC values among gated GFP+ cells were normalized to non-silencing controls. Mean and standard deviation values are plotted for the entire shRNA knockdown group.

4.4.5 Phenotypes associated with RUNX1 and RUNX3 overexpression

In order to gain a clearer understanding of the underlying contributions of RUNX1 to cell growth, I overexpressed cDNAs of all three canonical isoforms (**Figure 4.20 A**). In competition with untransduced cells, enforced expression of RUNX1A, RUNX1B, and RUNX1C was selected against over the course of two weeks in culture (**Figure 4.20 B**). This selection was due in part to reduced proliferation of the transduced RUNX1-expressing cells, as these cells incorporate less BrdU relative to untransduced cells (**Figure 4.20 C**). I was additionally interested to see if enforced RUNX3 expression would have similar effects as RUNX1 overexpression. Interestingly, RUNX3 appears to induce proliferation, causing cells to cycle faster than they normally would as they appear to incorporate more BrdU (**Figure 4.21**). Finally, the T-ALL cell line DND-41, which is γ-secretase inhibitor sensitive (cell cycle arrest upon Notch inhibition), is able to escape complete arrest through enforced RUNX3 expression. Cells transduced with retroviral RUNX3 at low transduction efficiency normally remain at a low GFP%,

however this population of cells is selected for under conditions in which Notch signaling is inhibited (**Figure 4.22**).

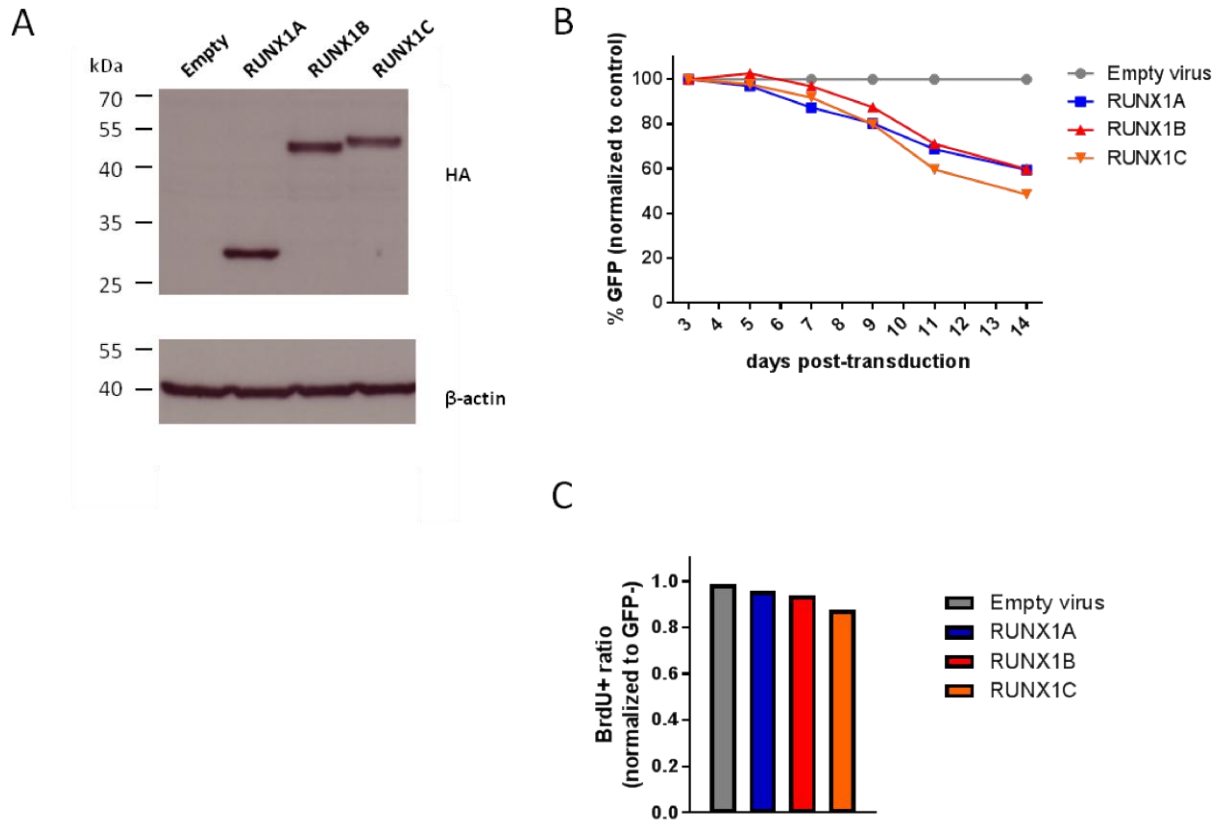

Figure 4.20 RUNX1 overexpression results in reduced growth and proliferation.

KOPT-K1 cells were transduced with pRRL-based lentivectors containing HA-RUNX1A, HA-RUNX1B, and HA-RUNX1C. **(A)** Western blot. 4 days following transduction, cells were lysed to confirm expression of RUNX1 alleles by western blot. Cells were incubated with either antibodies against anti-HA (Sigma Aldrich) and β-actin (Sigma Aldrich) was used as a loading control. **(B)** In vitro competition assay. Transduced with the constructs as indicated, heterogeneous cultures of transduced (GFP+) and untransduced (GFP-) KOPT-K1 cells were analyzed for GFP expression every few days by flow cytometry for the durations indicated. GFP expression is normalized to the empty vector control. **(C)** BrdU incorporation assay. 4 days following transduction, cells were incubated with BrdU according to the manufacturer's protocol. Cells were fixed and permeabilized and labeled with anti-BrdU AlexaFluor 647 antibody. Cells were then analyzed using a FACScalibur cytometer and gated on the GFP+ (transduced) and GFP- (untransduced) fractions. The ratio of GFP+ to GFP- subsets is displayed.

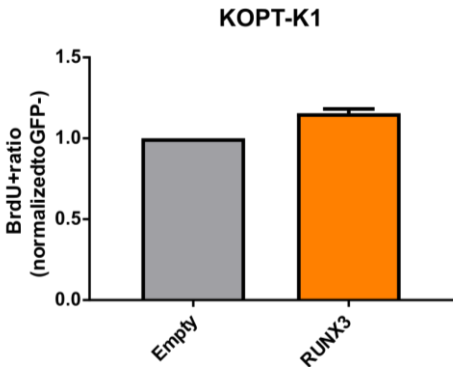

Figure 4.21 Enforced RUNX3 expression induces cells to incorporate more BrdU.

KOPT-K1 cells were transduced in duplicate with a pRRL-based lentivector containing RUNX3 or empty vector. 4 days following transduction, cells were incubated with BrdU according to the manufacturer's protocol. Cells were fixed and permeabilized and labeled with anti-BrdU AlexaFluor 647 antibody. Cells were then analyzed using a FACScalibur cytometer and gated on the GFP+ (transduced) and GFP- (untransduced) fractions. The ratio of GFP+ to GFP- subsets is displayed and normalized to the empty virus control.

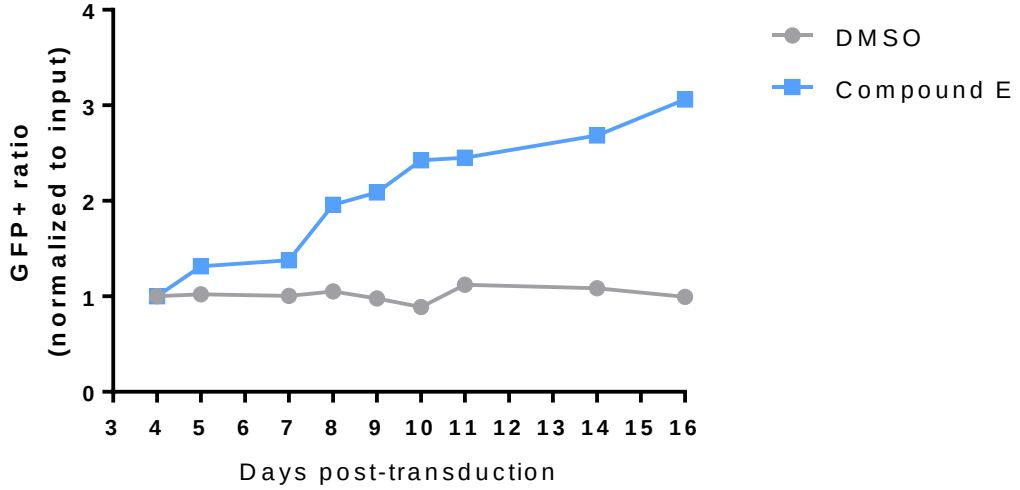

Figure 4.22 RUNX3 can partially rescue Notch inhibition in DND-41 cells.

The T-ALL cell line DND-41 was transduced with pseudotyped retrovirus containing RUNX3 and split into two cultures: one with vehicle (DMSO) and one with a γ-secretase inhibitor (Compound E). Heterogeneous cultures of transduced (GFP+) and untransduced (GFP-) cells were analyzed for GFP expression every few days by flow

cytometry for the durations indicated. GFP% is normalized to input GFP expression to generate a ratio.

4.4.6 RUNX1 regulates the expression of important oncogenes and tumor suppressors in human T-ALL

In exploring potential mediators of the growth phenotypes observed when RUNX1 levels are depleted, I sought to explore if regulatory relationships existed between well-established oncogenes and tumor suppressors, some of which are known to be dynamic Notch signaling targets enriched in NOTCH1 and RUNX1 binding[8,9]. Due to the canonical function of RUNX1 as a transcription factor, I explored mRNA expression levels from RNA-seq data generated in collaboration with the Hirst Lab. I found that while there were trends, RUNX1 did not appear to have a consistent role in regulating the mRNA levels of several important target genes such as *MYC*, *IGF1R*, *IL7R*, and the tumor suppressor *CDKN1B* (**Figure 4.23 A**, **B**). While, this data show trends, the nature of unicate data makes it difficult to interpret individual experiments (**Figure 4.23 A**). However, as an example of this variation, IGF1R appears to be positively regulated by RUNX1 across three cell lines (**Figure 4.23 B**). I first explored the protein expression of IGF1R and IL7R, two receptor tyrosine kinases which have established roles in regulating growth and survival of T-ALL cells and which has been shown to be bound by RUNX1 by local ChIP qRT-PCR[2,9,327]. Upon transduction with GFP-containing shRNA lentivectors targeting RUNX1, I found there to be a correlation between the level of surface IGF1R and the level of RUNX1, proportional to the relative strength of the shRNA at achieving knockdown (**Figure 4.24 A, B**). Additionally, although many T-ALL cell lines do not express detectable amounts of surface IL7R, I used the line HPB-ALL, which expresses IL7R on its surface, to test if RUNX1 could regulate IL7R protein expression in this context (**Figure 4.24 C**). Of note, I found there to be a relatively strong effect on IL7R expression upon RUNX1 knockdown using either of two shRNAs. Consistent with my results, conditional knockout of *Runx1* in mice has been found to result in reduced levels of Il7r in immature DN and mature CD4+ T cells, suggesting this regulation by RUNX1 may be conserved across species[138]. In the case of receptor tyrosine kinases, such as IL7R and IGF1R, changes in expression are not necessarily

reflective of activation status. For this reason, I chose to measure the net output of the pathways downstream of these enzymes by measuring the amount of phosphorylated target proteins. I serum-starved cells overnight and then pulsed them with the appropriate stimuli/ligand followed by analysis by flow cytometry. One of the key pathways downstream of IGF1R in T-ALL is PI3K-AKT signaling, the net output of which we can measure using phospho-AKT levels via flow cytometry. Control and RUNX1 knockdown HPB-ALL cells were serum starved and then pulsed with either one of two doses of serum or IGF1 ligand. RUNX1 knockdown was capable of significantly reducing the activation of AKT (**Figure 4.24 D**). This was seen most robustly in the shRUNX1-58 knockdown cells, in which there was a roughly 2-fold reduction in activation. IL7R is also known to signal through the PI3K-AKT pathway, and although stimulation with IL7 did not produce high levels of activation, RUNX1 knockdown was capable of blunting the small amount of activation provided by the cytokine (data not shown). Pulsing with IL7 however did lead to high levels of activation of STAT5 which is an important downstream mediator of IL7R signaling via phosphorylation by JAK1/JAK3 (**Figure 4.24 E**). This activation was more dramatically reduced upon RUNX1 knockdown than that seen for AKT. These results suggest that RUNX1 is necessary for full activation of the PI3K-AKT and JAK-STAT pathways downstream of IGF1R and IL7R in T-ALL cells. I attempted to rescue RUNX1 knockdown by culturing cells depleted of RUNX1 with supraphysiologic amounts of IGF-1 and IL-7 in order to see if lowered amounts of receptor could be compensated by stimulating the remaining amount on the surface (**Figure 4.25**). Interestingly, excess cytokine could not overcome RUNX1 depletion, suggesting that either the amount of IGF1R and IL7R is still not enough to support PI3K-AKT and JAK-STAT signaling or that these receptor tyrosine kinases are only a subset of RUNX1 effectors.

It has been previously shown that RUNX1 represses the expression of the cyclin-dependent kinase inhibitor (CKI) proteins p21 and p27 in hair follicle stem cells[328]. I analyzed the expression of p27 (*CDKN1B*) in puromycin-selected RUNX1 knockdown cells and found that depletion of RUNX1 resulted in up to 4.5 fold derepression of p27 protein, suggesting that RUNX1 represses p27 expression (**Figure 4.26**). However,

when I examined the expression of p21 (*CDKN1A*) I found that RUNX1 knockdown had no significant effect on its expression. These results suggest that RUNX1 may potentiate cell cycle/proliferation at least in part through repression of the CKI p27. Due to the high frequency of mutation, repression or deletion of the *PTEN* locus in T-ALL, it remained possible that potential differences I noticed in PI3K-AKT signaling (**Figure 4.26**) were due to RUNX1 regulation of PTEN protein expression[55]. However, it appears as though RUNX1 does not regulate the protein expression in four PTEN-expressing cell lines: RPMI 8402, HPB-ALL, KOPT-K1 and TALL-1 (**Figure 4.26**). Due to the evidence suggesting that RUNX1 might mediate growth through a feed-forward loop involving MYB in Jurkat cells, I sought to determine if this was a more general phenomenon in T-ALL[7]. Interestingly, I did not see any expression of MYB protein in KOPT-K1 and there was no change in MYB protein levels in HPB-ALL cells upon RUNX1 knockdown (**Figure 4.27**). I became interested in analyzing any effects RUNX1 may have on regulators of apoptosis in T-ALL due to viability defects observed upon RUNX1 knockdown. Additionally, RUNX1 has been shown to regulate Bcl-2 levels in Acute Myeloid Leukemia[329], and thus I looked at the expression of the family members Bcl-2, Mcl-1, and Bcl-xL (**Figure 4.28**). Of note, RUNX1 did not seem to consistently affect the levels of any of the anti-apoptotic family members, however there was a decrease of the pro-apoptotic, small Mcl-1 isoform.

Data from Tom Look's lab suggests that TAL1 negatively regulates FBXW7 expression through mIR-223[330]. Since RUNX1 participates in a transactivation complex with TAL1 I hypothesized that RUNX1 has the potential to regulate *MYC* due to its high frequency of overexpression as a target of the Notch pathway/FBXW7. I found RUNX1 to positively regulate MYC protein expression in 4/5 cell lines examined (**Figure 4.24 E, Figure 4.26**). The cell line HPB-ALL was an outlier from this pattern, suggesting that RUNX1 may be decoupled from MYC expression or even repress its expression in certain contexts/genetic backgrounds. Future studies should confirm the mechanism by which RUNX1 directly regulates MYC expression or acts through regulation of mIR-223/FBXW7.

A

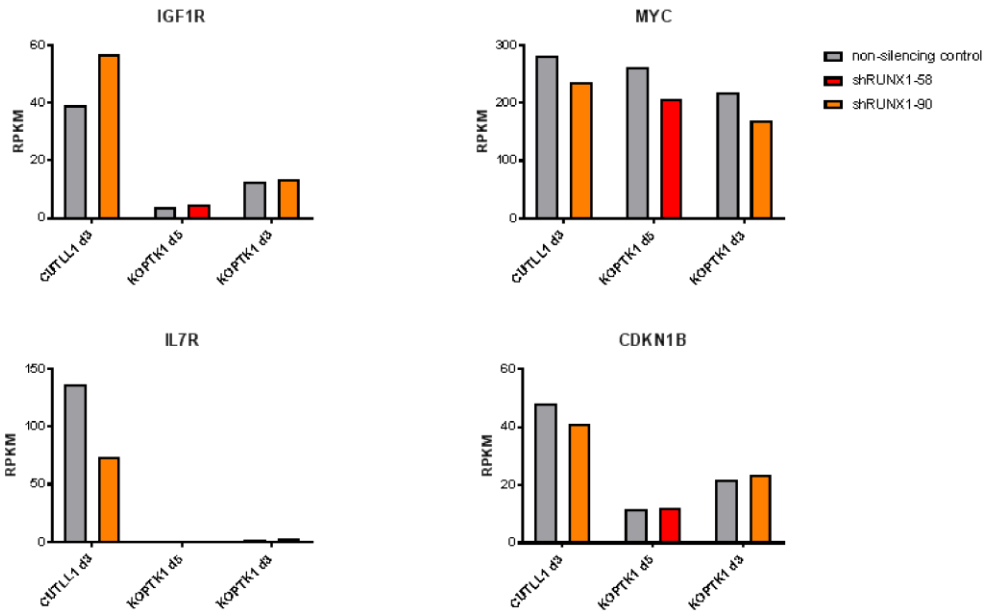

B

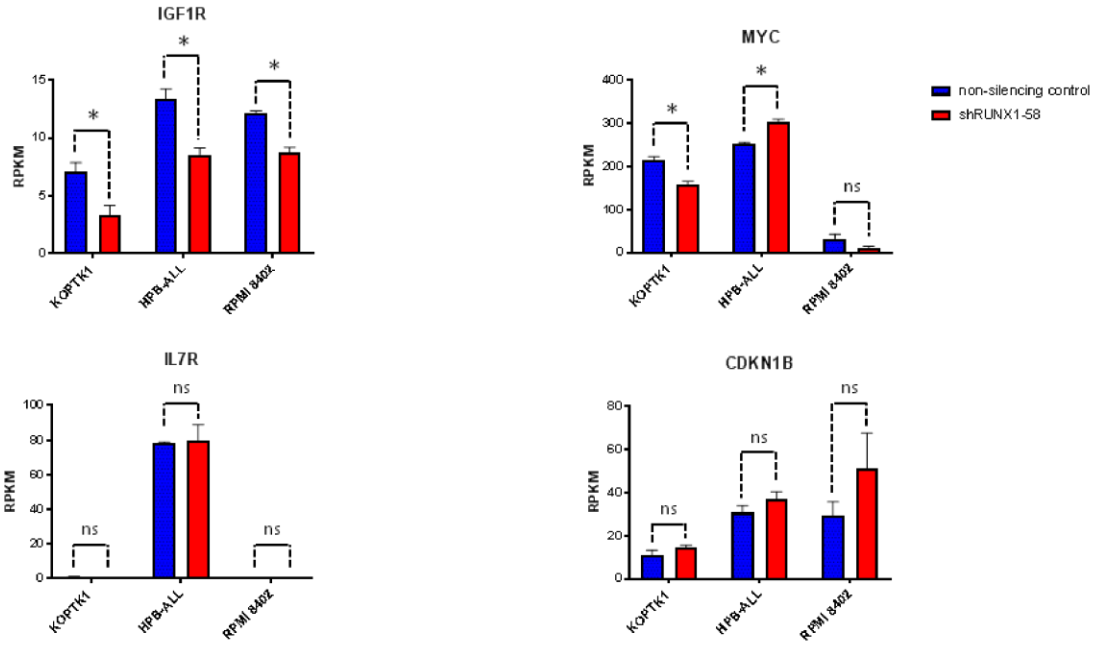

Figure 4.23 shRUNX1 effects on mRNA expression of key T-ALL oncogenes and tumour suppressors.

(A, B) Normalized RPKM reads for **(A)** unicate HiSeq data and **(B)** duplicate MiSeq data are plotted for the cell lines (and number of days post-transduction of the indicated viruses) and conditions indicated for the genes: *IGF1R*, *MYC*, *IL7R* and *CDKN1B*. **, p<0.05 (Student's t-test).*

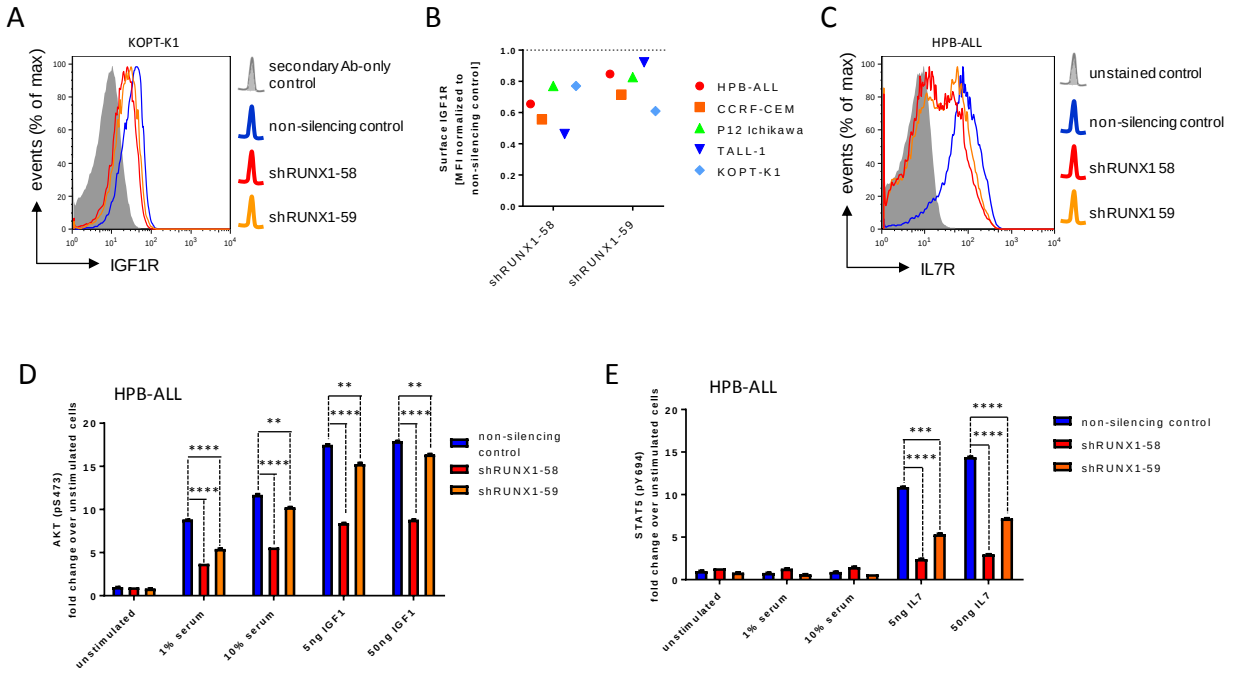

Figure 4.24 RUNX1 regulates IGF1R and IL7R, potentiating downstream signaling.

(A,B) IGF1R protein expression by flow cytometry. Cell lines were transduced with GFP-tagged shRUNX1 lentiviruses or non-silencing control. Cell surface IGF1R expression was assayed by flow cytometry at 7 days post-transduction. Mean fluorescence intensity (MFI) of gated GFP+ cells is plotted after normalization to non-silencing controls. **(C)** IL7R protein expression by flow cytometry. HPB-ALL cells were transduced with with GFP-tagged shRUNX1 lentiviruses or non-silencing control. Cell surface IL7R expression was assayed by flow cytometry at 7 days post-transduction. Mean fluorescence intensity (MFI) of gated GFP+ cells is plotted after normalization to non-silencing control. Data depicted are representative of multiple replicates. **(D)** AKT and **(E)** STAT5 activation assay. HPB-ALL cells were transduced with shRUNX1 lentiviruses carrying a puromycin resistance marker and selected for 4 days beginning at 3 days post-transduction. Cells were then serum-starved for 16 hours, pulsed for 10 minutes with either serum or recombinant ligand, and fixed immediately thereafter. Cells were stained for intracellular phosphorylated AKT (pS473) or STAT5 (pY694) and assayed by flow cytometry. MFI are plotted after normalization to mock stimulated controls. Mean and standard deviation for assays performed in duplicate are plotted.

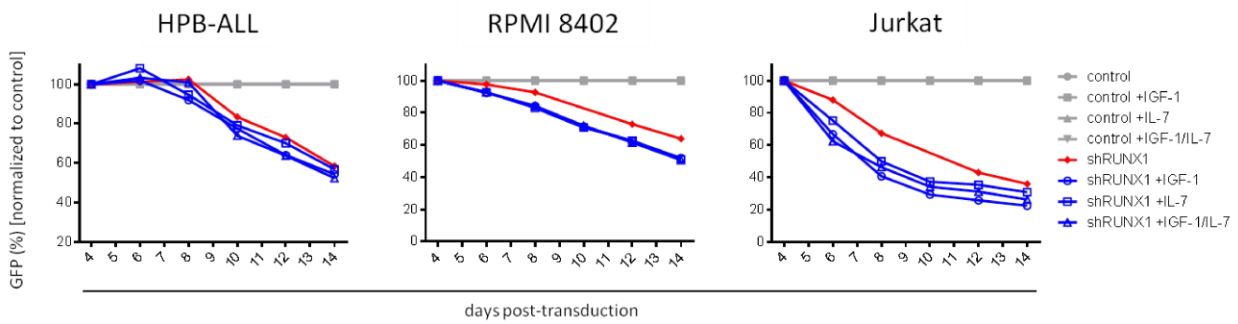

Figure 4.25 Exogenous IGF-1 or IL-7 cannot compensate for RUNX depletion.

The human T-ALL cell lines HPB-ALL, RPMI 8402, and Jurkat were transduced as indicated with pLKO.1 GFP lentiviruses encoding scrambled non-silencing control or a pool (**Table 4.5**) of equivalent titre shRNA clones directed against RUNX1. Cells were cultured in standard media (RPMI 1640 + Pyruvate) or with supplemental recombinant IL-7 (50ng/ml), IGF-1 (50ng/ml) or both cytokines in the culture media for the duration of the experiment. Heterogeneous cultures of transduced (GFP+) and untransduced (GFP-) cells were analyzed for GFP expression every few days by flow cytometry for the durations indicated. GFP expression is normalized to the non-silencing control.

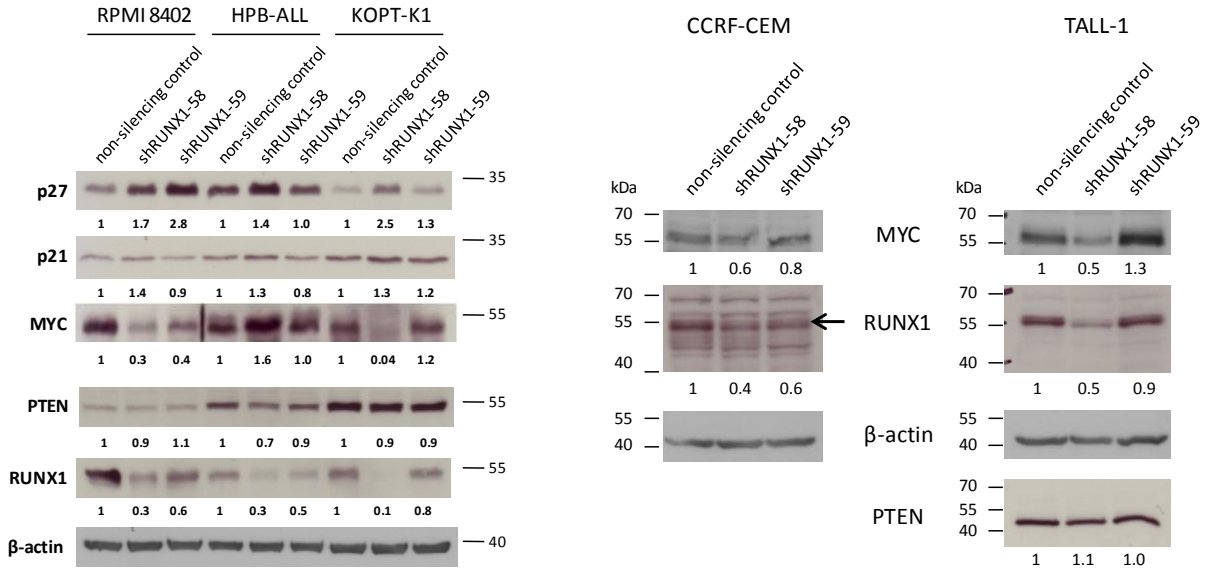

Figure 4.26 p27^{Kip1}/p21^{Waf1}/MYC/PTEN protein expression after RUNX1 knockdown.

Cell lines were transduced with shRUNX1 lentiviruses carrying a puromycin resistance marker and selected for 3 days beginning at 3 days post-transduction. Whole cell lysates were prepared and used for western blotting with antibodies as indicated.

Numbers below each panel indicate band intensities after normalization to the β-actin loading control and are expressed relative to the respective non-silencing control.

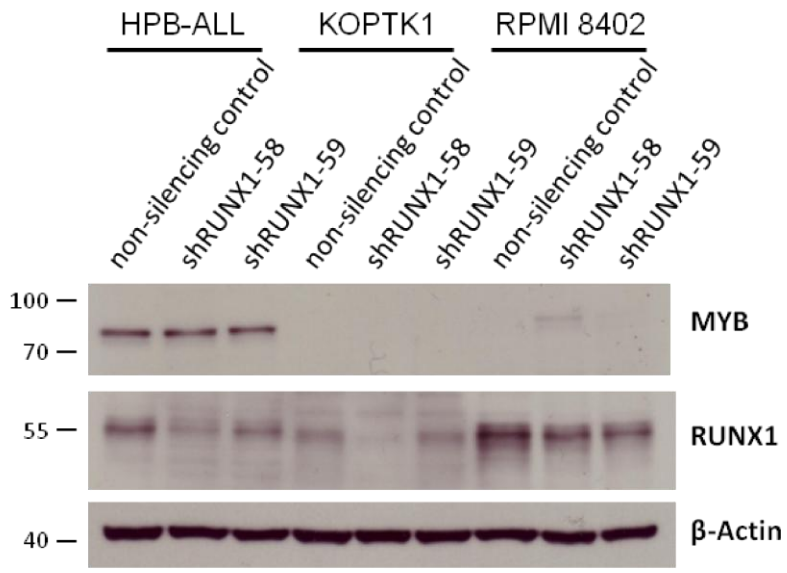

Figure 4.27 RUNX1 does not appear to regulate MYB expression in a subset of T-ALL cell lines.

MYB expression upon RUNX1 knockdown. RPMI 8402, HPB-ALL, and KOPT-K1 cells were transduced with pLKO.1 Puro^{R} lentiviruses encoding non-silencing control, shRUNX1-58 or shRUNX1-59. 72 hours post-transduction, cells were treated with 1µg/ml of Puromycin. Following 72 hours of selection, cell lysates were generated and then immunoblotted for MYB (Millipore) and Actin (Sigma Aldrich).

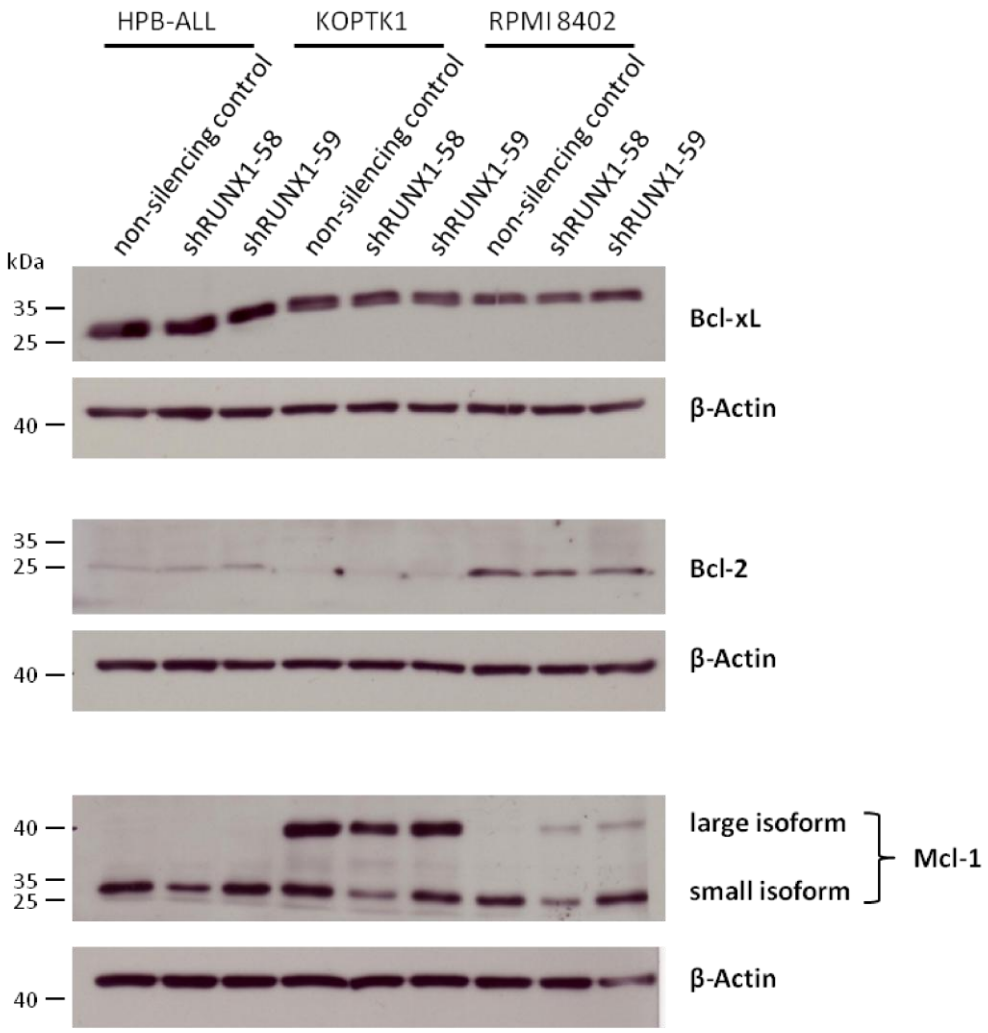

Figure 4.28 RUNX1 does not show consistent regulation of anti-apoptotic Bcl-2 family members.

Bcl-xL, Bcl-2, and Mcl-1 expression upon RUNX1 knockdown. RPMI 8402, HPB-ALL, and KOPT-K1 cells were transduced with pLKO.1 Puro^{R} lentiviruses encoding non-silencing control, shRUNX1-58 or shRUNX1-59. 72 hours post-transduction, cells were treated with 1µg/ml of Puromycin. Following 72 hours of selection, cell lysates were generated and then immunoblotted for Bcl-xL (Cell Signal), Bcl-2 (Cell Signal), Mcl-1 (Cell Signal), and Actin (Sigma Aldrich).

4.4.7 Regulation of gene expression and the epigenome by RUNX1.

I noted that an ortholog of RUNX1 in *Drosophila* called Lozenge (Lz) was necessary for Notch to bind and activate enhancers in haemocytes, a blood cell in this species[331]. Thus, I was interested in determining how RUNX1 and NOTCH1 contributed to the regulation of H3K27 modification, as NOTCH1 and RUNX1 binding is enriched near regions of H3K27Ac signal and this histone modification is correlated with gene transcription[8]. I transduced CUTLL1 cells with pLKO.1 GFP non-silencing control or pLKO.1 GFP shRUNX1-90 lentivirus and sorted for GFP+ viable cells at 3 days post-transduction. Additionally, I transduced KOPT-K1 cells with pLKO.1 GFP non-silencing control or pLKO.1 GFP shRUNX1-58 lentivirus and sorted for GFP+ viable cells at 5 days post-transduction. In generating samples in which Notch signaling had been inhibited, I sorted viable cells which had been treated with the γ-secretase inhibitor Compound E for 3 days (CUTLL1) or 5 days (KOPT-K1). I flash froze the sorted cells which were then prepared for ChIP-seq of the marks described in **Figure 4.29** (H3K27Ac and H3K27me3) by the Hirst lab. By comparing the difference in these marks between the control and the lentivirus or drug, we are able to note the dynamic nature of these marks in both Notch inhibition (**Figure 4.29 A, C**) and RUNX1 knockdown (**Figure 4.29 B, D**). Notably, while there was no obvious difference between the H3K27me3 changes in most conditions, there appeared to be a larger change in KOPT-K1 cells with Notch inhibition (**Figure 4.29C**). Notably, there was an interesting difference in H3K27Ac. When Notch signaling is inhibited while there is a change for KOPT-K1 cells (**Figure 4.29C**), there is a more pronounced effect in both KOPT-K1 cells (**Figure 4.29D)** and CUTLL1 cells (**Figure 4.29B**) upon RUNX1 knockdown. Here there is a striking difference in this mark upon knockdown of RUNX1, where there is a dramatically lower amount of this mark across the majority of TSS sites. While this difference could be attributable to differences in rank order between the RUNX1 non-silencing and DMSO H3K27Ac intensities, Spearman rank correlation shows that the levels at each gene are well correlated with R values in both cell lines at 0.95 (**Figure 4.30**).Interestingly, RUNX1 knockdown appears to reduce H3K27Ac signal at promoters and enhancers of some target genes identified in this dissertation (**Appendix B** Most

notably there is clear loss of signal for the Notch target genes *MYC* (**Appendix B.1**), *IGF1R* (**Appendix B.2**) and *DTX1* (**Appendix B.4**). Additionally, the well annotated enhancers E3 and E5 for *IL7R* appear to have depletion of H3K27Ac as well (**Appendix B.3**)[8].

In order to determine which genes might be regulated by RUNX1 in a more unbiased manner, I sought to use global gene expression profiling to find RUNX1 transcriptional target genes. As such, I used Affymetrix GeneChip® PrimeView™ Human Gene Expression Arrays which were chosen because they offer comprehensive coverage of the human genome with 9-11 probes per gene set. I transduced HPB-ALL, KOPT-K1 and RPMI 8402 cells with pLKO.1 Puro non-silencing control or pLKO.1 Puro shRUNX1-58 lentivectors in duplicate. Three days later, cells were selected using 1µg/ml of Puromycin for 3 days, after which cells were enriched for viable cells using a Miltenyi Dead cell removal kit and total RNA was isolated and assayed on the Microarray chips at the McGill University and Génome Québec Innovation Centre. In analyzing the data, I first looked at how the samples clustered using hierarchical clustering (**Appendix C.1**) and found them to group well by cell line. Indeed, this is confirmed by analysis of the principal components (**Appendix C.2**). In an unfiltered analysis, the cell lines separated well from each other and duplicates of each lentiviral condition appeared to cluster together. However, when I filter the gene list using a false discovery rate (FDR) of 0.01, the genes hierarchically cluster by cell line as well as by condition showing the difference between non-silencing control cells and shRUNX1-58 (**Figure 4.31**). With these criteria as a filter, there are 156 common down-regulated genes (**Appendix C.3**) and 32 upregulated genes (**Appendix C.4**). If I look at individual cell lines using the more stringent criteria of an FDR of 0.01 and at least a 1.5 fold change, I see differences between each cell line in the number of genes which seem to change their expression (**Appendices C.5, C.8, C.11**). KOPT-K1 seems to have the lowest number of genes which change their expression with only 11 genes downregulated (**Appendix C.6**) and 11 genes upregulated (**Appendix C.7**) upon RUNX1 knockdown. HPB-ALL cells have 97 downregulated genes (**Appendix C.9**) and 21 upregulated genes (**Appendix C.10**) by the same criteria. The cell line which had the

greatest number of differentially expressed genes using these same criteria was RPMI 8402 with 208 downregulated genes (**Appendix C.12**) and 82 upregulated genes (**Appendix C.13**). In totally there were 8 genes shared between KOPT-K1, RPMI 8402 and HPB-ALL (**Figure 4.32**). Notable genes include *CD3G* and *PGK1*, among others (**Figure 4.33**).

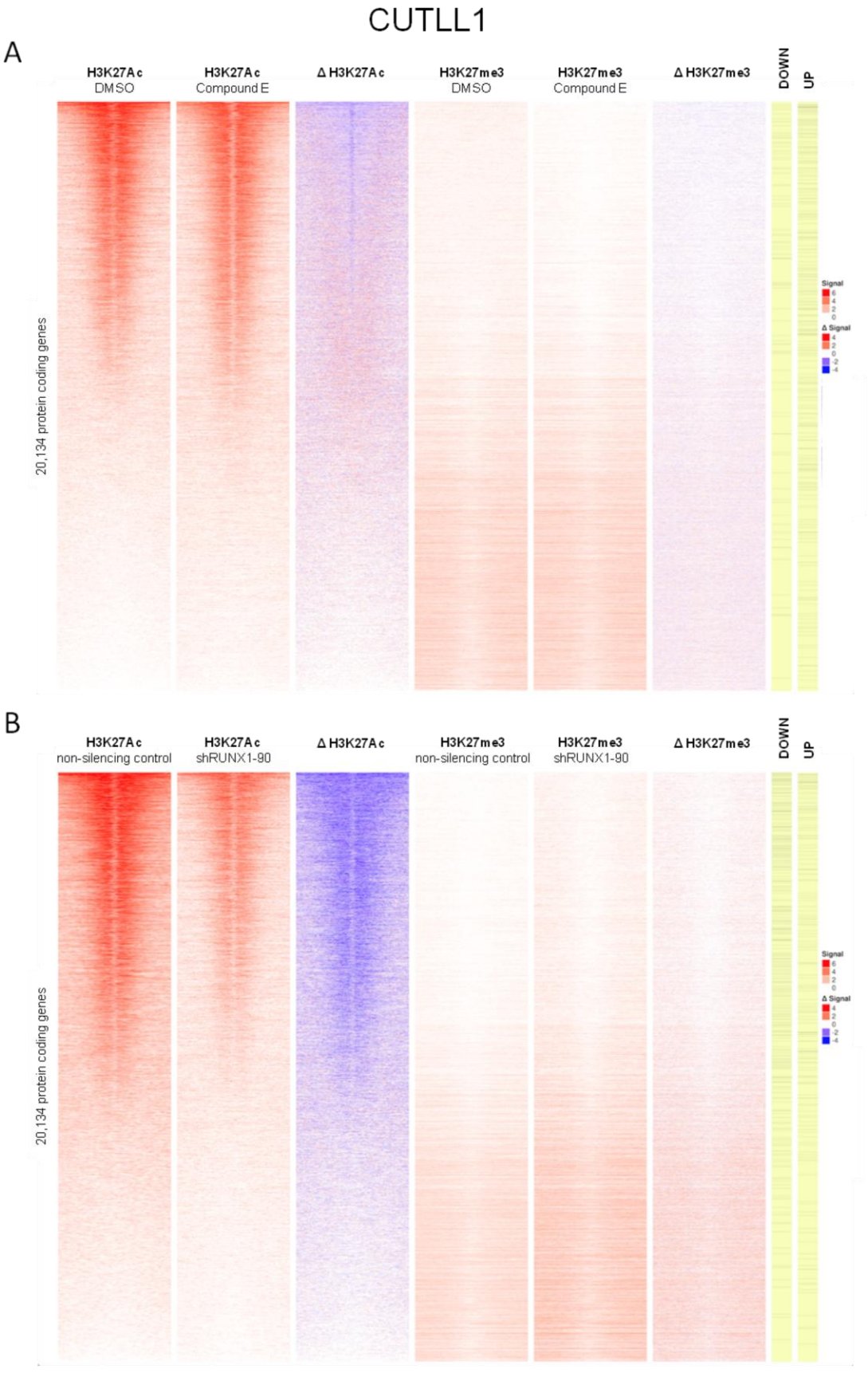
CUTLL1
A
H3K27Ac
DMSO
H3K27Ac
Compound E
Δ H3K27Ac
H3K27me3
DMSO
H3K27me3
Compound E
Δ H3K27me3
DOWN
UP
20,134 protein coding genes
Signal
Δ Signal
B
H3K27Ac
non-silencing control
H3K27Ac
shRUNX1-90
Δ H3K27Ac
H3K27me3
non-silencing control
H3K27me3
shRUNX1-90
Δ H3K27me3
DOWN
UP
20,134 protein coding genes
Signal
Δ Signal

KOPT-K1

C

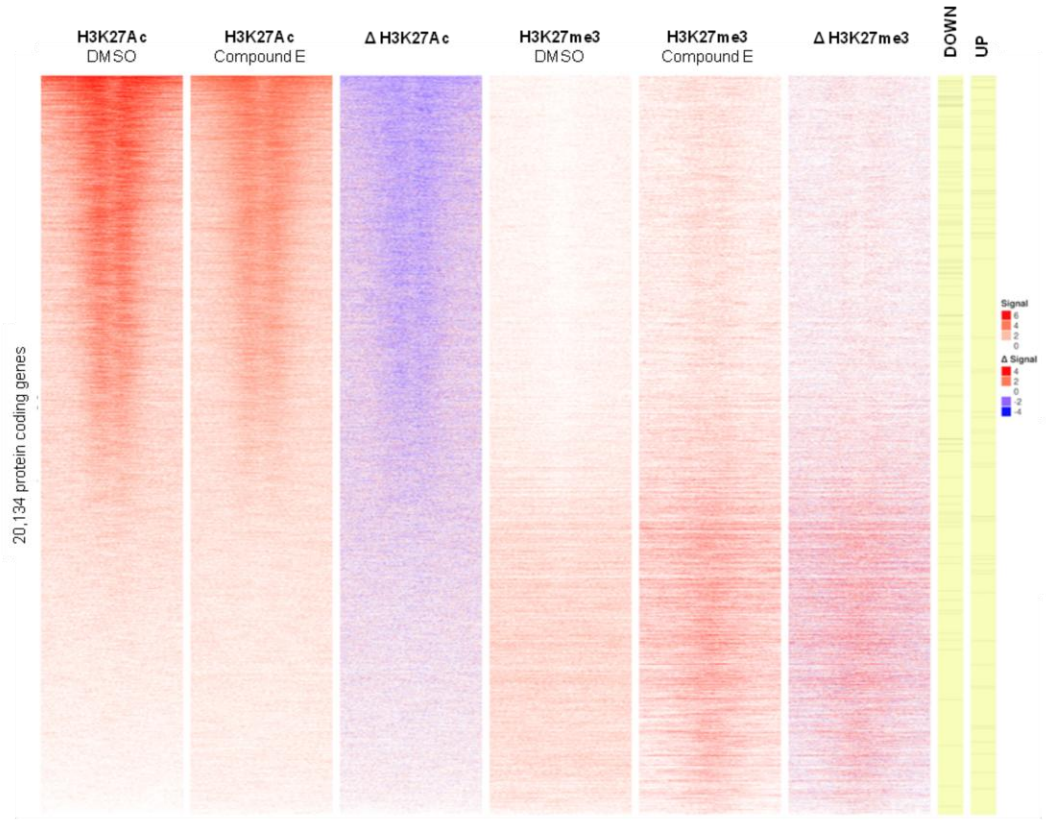
H3K27Ac
DMSO
H3K27Ac
Compound E
Δ H3K27Ac
H3K27me3
DMSO
H3K27me3
Compound E
Δ H3K27me3
DOWN
UP
20,134 protein coding genes
Signal
Δ Signal

D

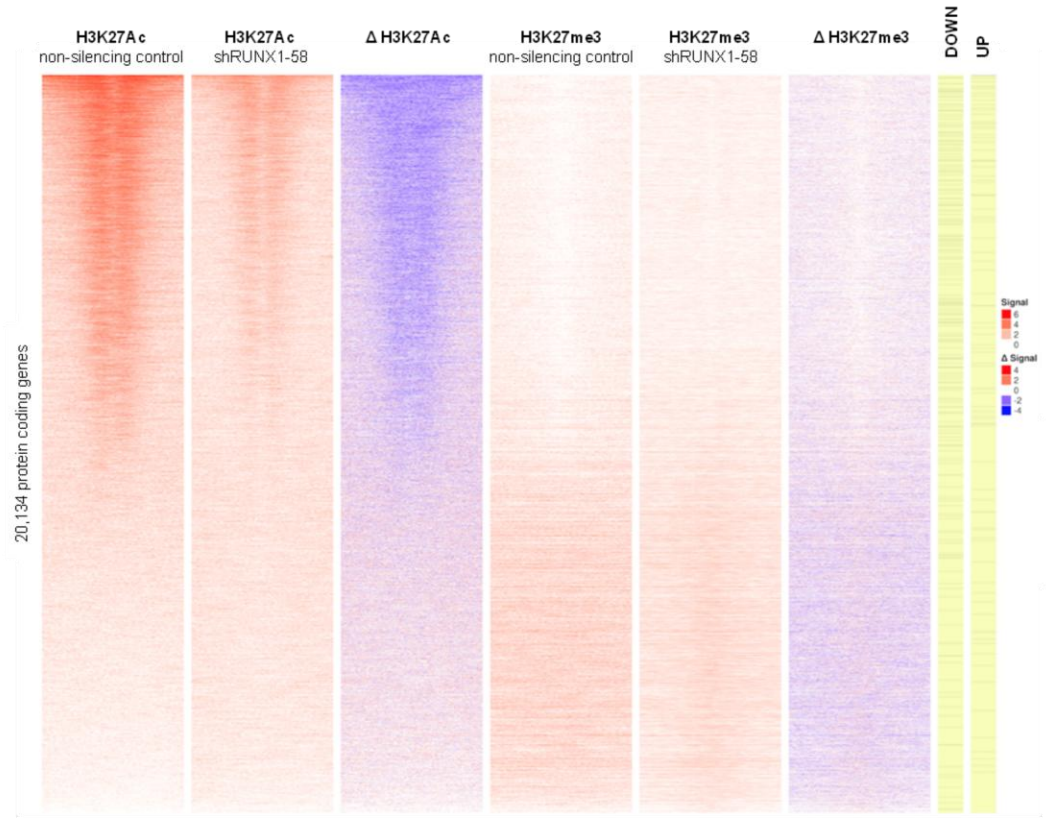
H3K27Ac
non-silencing control
H3K27Ac
shRUNX1-58
Δ H3K27Ac
H3K27me3
non-silencing control
H3K27me3
shRUNX1-58
Δ H3K27me3
DOWN
UP
20,134 protein coding genes
Signal
Δ Signal

Figure 4.29 H3K27Ac and H3K27me3 upon RUNX1 depletion or Notch inhibition.

(A) CUTLL1 cells treated with vehicle (DMSO) or the γ-secretase inhibitor Compound E for 3 days or **(B)** CUTLL1 cells were transduced with either pLKO.1 GFP non-silencing control or pLKO.1 GFP shRUNX1-90. **(C)** KOPT-K1 cells treated with vehicle (DMSO) or the γ-secretase inhibitor Compound E for 5 days or **(D)** KOPT-K1 cells were transduced with either pLKO.1 GFP non-silencing control or pLKO.1 GFP shRUNX1-58. **(A, C)** Cells were sorted for viable events and flash frozen. The heatmap shows the distribution of H3K27ac and H3K27me3 at annotated promoters (+-2kb) of protein coding genes. Each row represents the normalized signal centering transcription start (TSS) site for each of the 20,134 genes' promoters. The genes are ordered in reference to the "H3K27Ac DMSO" lane from highest H3K27Ac signal to lowest. The three leftmost lanes represent H3K27Ac signal and the three rightmost lanes represent H3K27me3 signal. "Δ" lanes refer to the net signal difference between Compound E and DMSO. Genes that are differentially expressed between DMSO and Compound E by RNA-seq (FDR cutoff 0.05) are represented by bars on the right hand side of the plot. **(B, D)** 3 days post-transduction (for CUTTL1) or 5 days post-transduction (for KOPT-K1), cells were sorted for GFP+, viable events and flash frozen. The heatmap shows the distribution of H3K27ac and H3K27me3 at annotated promoters (+-2kb of the TSS) of protein coding genes. Each row represents the normalized signal centering transcription start (TSS) site for each of the 20,134 genes' promoters. The genes are ordered in reference to the "H3K27Ac non-silencing control" lane from highest H3K27Ac signal to lowest. The three leftmost lanes represent H3K27Ac signal and the three rightmost lanes represent H3K27me3 signal. "Δ" lanes refer to the net signal difference between shRUNX1-90 and non-silencing control. Genes that are differentially expressed between non-silencing control and shRUNX1-90 or shRUNX1-58 by RNA-seq (FDR cutoff 0.05) are represented by bars on the right hand side of the plot.

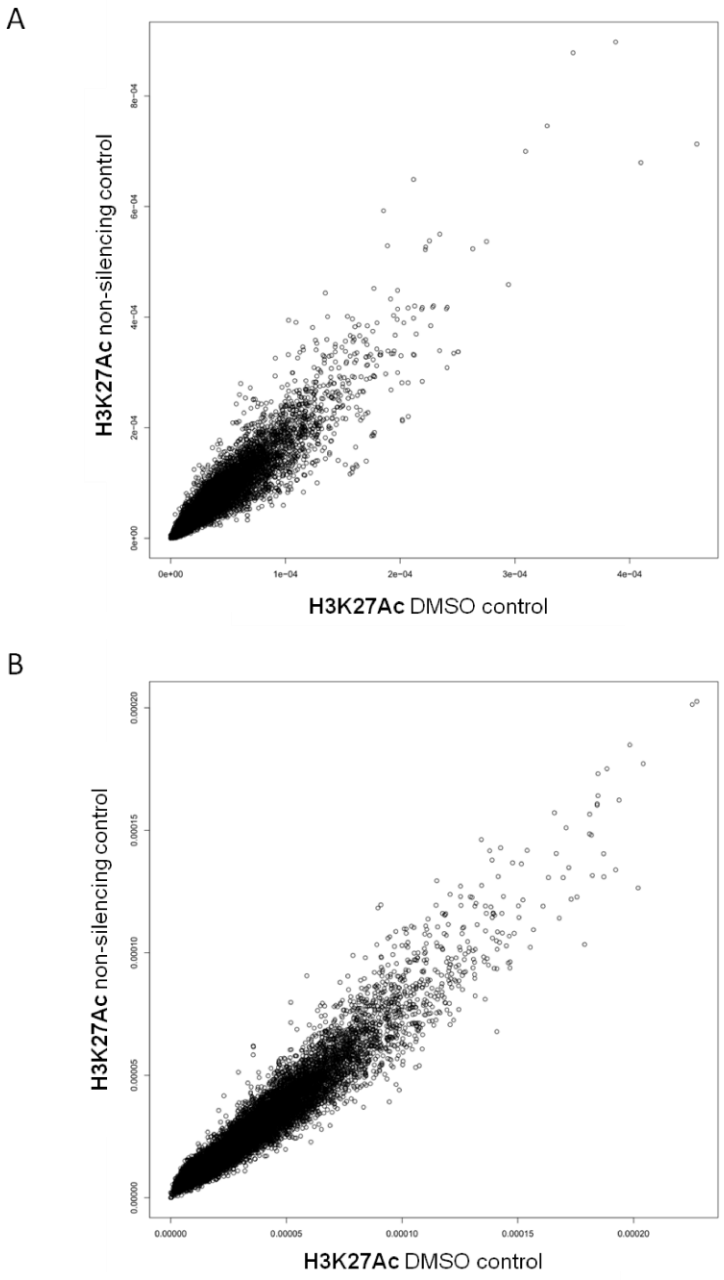

Figure 4.30 Spearman correlation between order of genes in control samples.

The Spearman rank correlation between the order of genes in the samples “H3K27Ac DMSO” and “H3K27Ac non-silencing control” in **(A)** CUTLL1 cells and **(B)** KOPT-K1 cells. The R value for CUTLL1 is 0.9529026 and the R value for KOPT-K1 is 0.9558209.

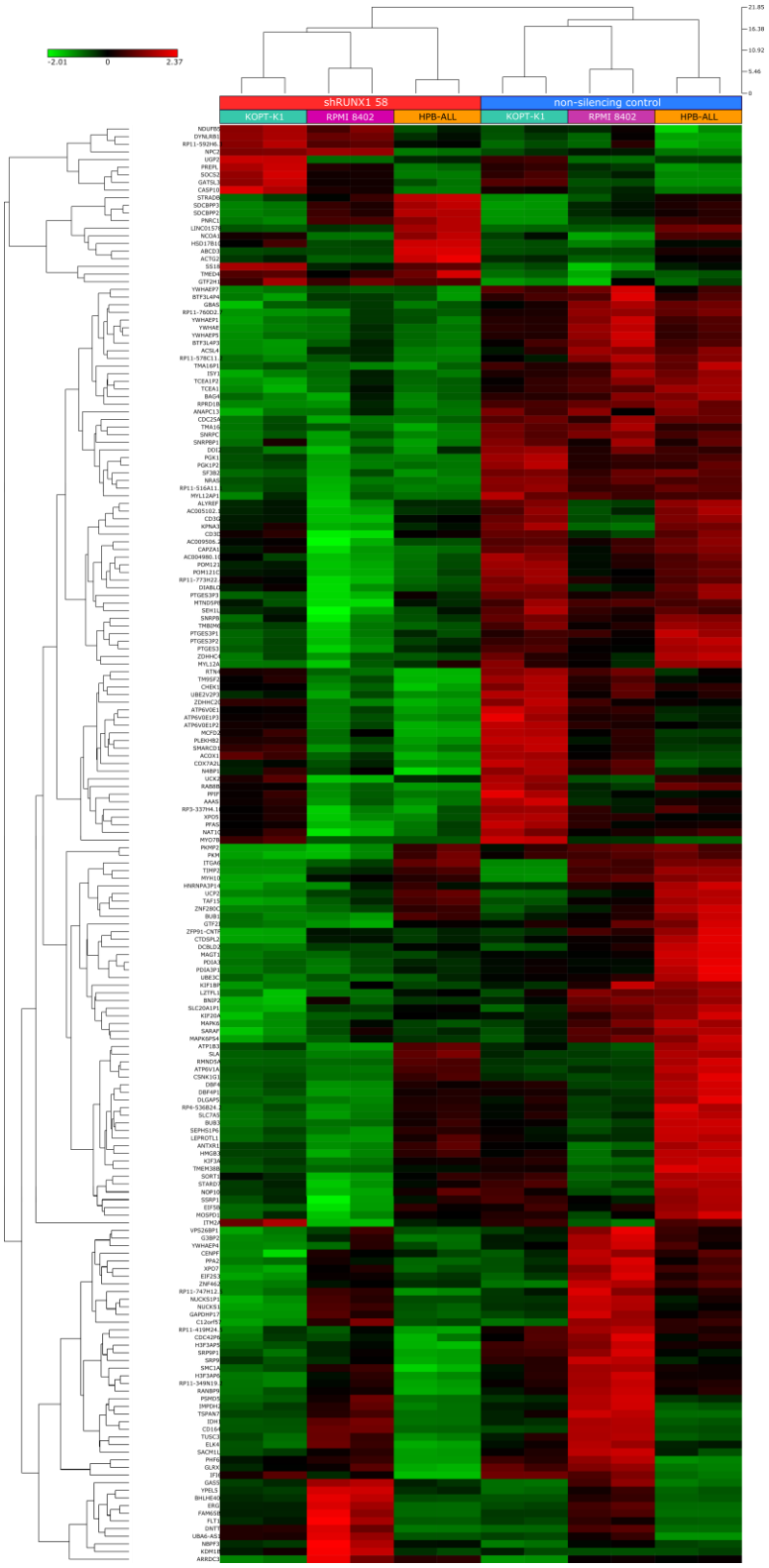

Figure 4.31 Hierarchical clustering of all samples filtered by a FDR of 0.01 (non-silencing control vs. shRUNX1-58)

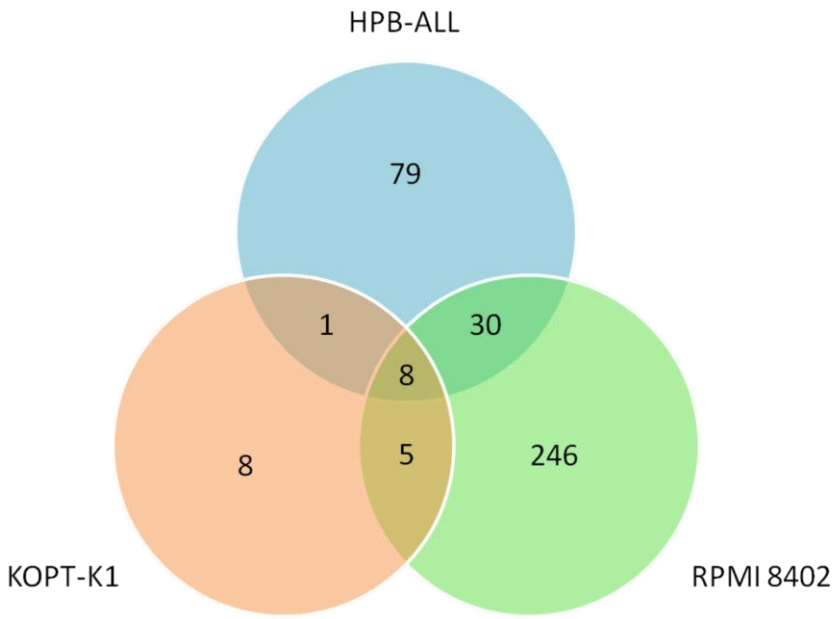

Figure 4.32 Venn diagram of common differentially expressed genes between each cell line

The number of differentially expressed genes in **Appendices C.6, C.7, C.9, C.10, C.12, C.13** are depicted in a Venn diagram. Differentially expressed genes do not have batch correction in this analysis. Criteria for filtering are a 1.5 fold change or more and an FDR of 0.01.

HPB-ALL/KOPT-K1/RPMI 8402	HPB-ALL/KOPT-K1	HPB-ALL/RPMI 8402		KOPT-K1/RPMI 8402
BTF3L4P3	CTDSPL2	AC005102.1	PPA2	CASP10
CD3G		ACSL4	PTGES3P2	MYO7B
COX7A2L		ATP6V0E1	RANBP9	NPC2
H3F3AP6		ATP6V0E1P2	RP11-516A11.1	PKM
PGK1		ATP6V0E1P3	RP11-578C11.2	SS18
PGK1P2		CDC25A	RP11-760D2.7	
RP11-349N19.2		CTNND1	SF3B2	
YWHAE		DBF4P1	SNRPC	
		DCBLD2	SRP9	
		G3BP2	SRP9P1	
		H3F3AP5	TCEA1P2	
		NRAS	TM9SF2	
		PDIA3	TMBIM6	
		POM121	YWHAEP5	
		POM121C	ZNF462	

Figure 4.33 Common differentially expressed genes between cell lines

Shared gene lists from **Figure 4.32.** Differentially expressed genes do not have batch correction in this analysis. Criteria for filtering are a 1.5 fold change or more and an FDR of 0.01.

4.4.8 CDK7 inhibitor THZ1-mediated phenotypes and RUNX1

Previously, Nathanael Gray's lab had shown that the CDK7 inhibitor THZ1 produced a dramatic decrease in RUNX1 levels in Jurkat cells, and induced similar expression patterns to those found in RUNX1-depleted cells[69]. I sought to determine if this was a more generalizable phenomenon in T-cell leukemia. Interestingly, short-term THZ1 treatment was able to dramatically reduce the amount of RUNX1 protein in Jurkat, KOPT-K1, CCRF-CEM, DND-41 and P12 Ichikawa (**Figure 4.34 A**). In order to determine if this is an indirect effect of THZ1, I overexpressed RUNX1B or RUNX1C isoforms using a pRRL-based lentivector which uses GFP as a selectable marker and treated these cells with THZ1. I found that cells which have enforced RUNX1 expression are selected for upon treatment with THZ1, however they still eventually show viability defects (**Figure 4.34 B**). This suggests that exogenous RUNX1 may partially rescue THZ1-mediated growth defects, and suggests that THZ1 does indeed act by inhibiting RUNX1 expression indirectly through CDK7 inhibition. Due to a paucity of inhibitors directly targeting the transcription factor RUNX1, it's possible that THZ1 may represent a practical, indirect way of reducing RUNX1 levels and impairing bulk tumour growth. THZ1 also appears to have efficacy against patient-derived xenografts *in vitro*, as these T-ALL cells are unable to expand even at a relatively low concentration of 100nM (**Figure 4.35**). The fact that we don't see clear dose-dependent inhibition of growth however suggests that either I used too high of a concentration of THZ1 or that CDK7 inhibition does not linearly correlate with phenotype. This should be further explored in future work with this drug within a T-ALL context and further genetic studies should attempt to confirm the link between CDK7 and RUNX1.

A

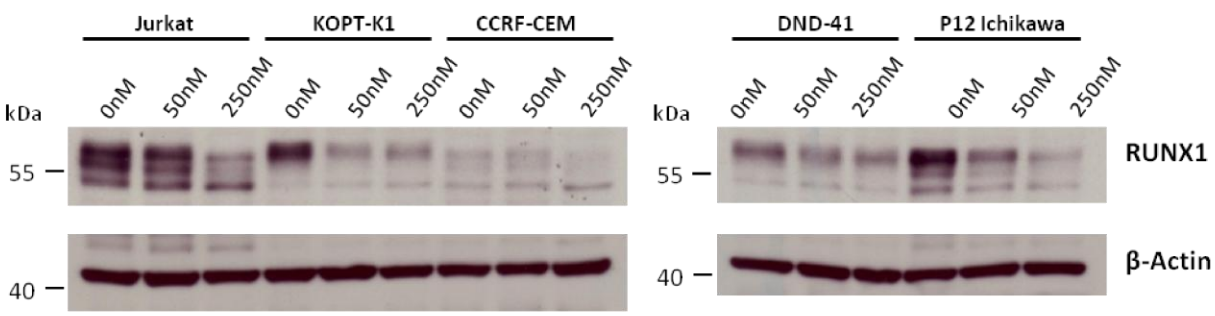
Jurkat
KOPT-K1
CCRF-CEM
DND-41
P12 Ichikawa
0nM
50nM
250nM
kDa
55
40
RUNX1
β-Actin

B

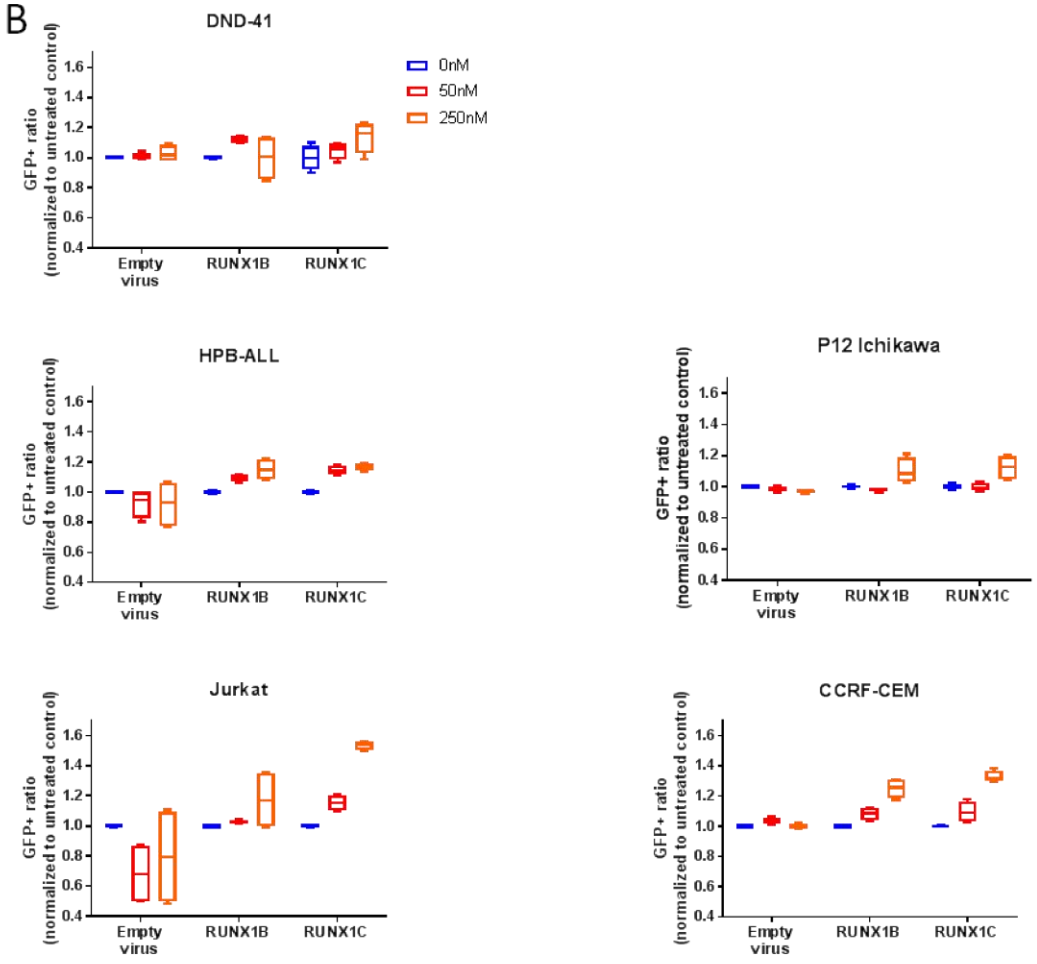
DND-41
HPB-ALL
P12 Ichikawa
Jurkat
CCRF-CEM
0nM
50nM
250nM
GFP+ ratio
(normalized to untreated control)
Empty virus
RUNX1B
RUNX1C

Figure 4.34 Exogenous RUNX1 can partially compensate for THZ1-mediated RUNX1 depletion.

(A) T-ALL cell lines were treated with the indicated amount of the CDK7 inhibitor THZ1 for 24 hours and cell lysates were probed by western blot for RUNX1 with β-actin used as a loading control. **(B)** The human T-ALL cell lines indicated were transduced with lentiviruses containing cDNAs of *RUNX1B*, *RUNX1C* or an empty vector. 72h post-transduction, cells were treated for 24h with THZ1 at the concentrations indicated in triplicate, followed by flow cytometry for viability and GFP expression. GFP expression in viable cells was normalized to the untreated control.

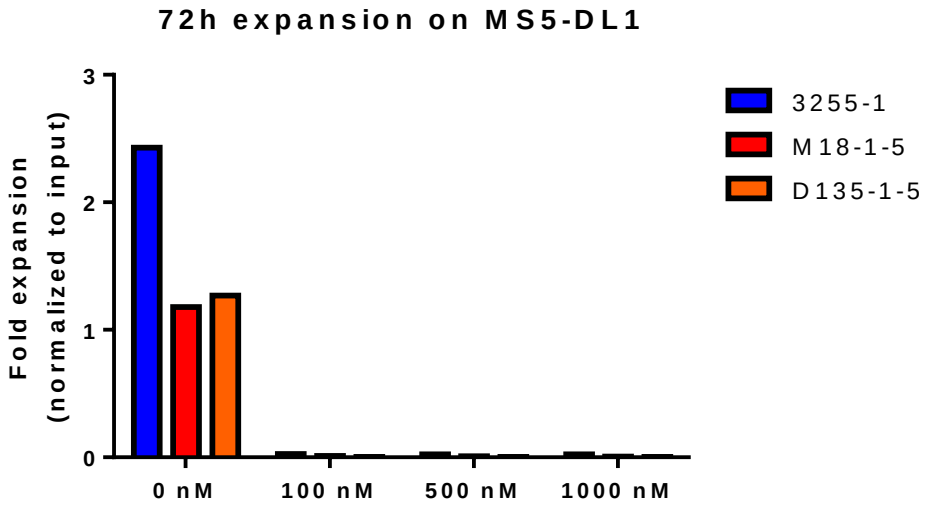

Figure 4.35 THZ1 inhibits growth of human patient-derived xenografts *in vitro.*

Patient-derived xenografts (patient IDs 3255-1, M18-1-5 and D135-1-5; n = 3) were treated with THZ1 for 3 h followed by compound washout. An aliquot of input cells was then counted by flow cytometry using a known quantity of flow cytometry calibration beads (data not shown; Molecular Probes). The remaining cells were plated onto MS5-DL1 feeder cells in the presence of serum-free media (supplemented with 0.75 μM SR1, 10 ng ml−1 interleukin (IL)-7, 10 ng ml−1 IL-2). Seventy-two hours later, cultures were harvested by vigorous pipetting with Trypsin, filtered through nylon mesh to deplete feeders, and counted by flow cytometry using a known quantity of flow cytometry calibration beads and with gating to discriminate between T-ALL cells and carryover feeders. The final cell number was normalized to the input cell number to calculate fold expansion. This experiment was performed once per patient-derived sample. N.B., published in Kwiatkowski N, Zhang T, Rahl PB, Abraham BJ, Reddy J, Ficarro SB, Dastur A, Amzallag A, Ramaswamy S, Tesar B, [Jenkins CE], Hannett NM, McMillin D, Sanda T, Sim T, Kim ND, Look T, Mitsiades CS, Weng AP, Brown JR, Benes CH, Marto JA, Young RA, Gray NS. Targeting transcription regulation in cancer with a covalent CDK7 inhibitor. Nature. 2014 Jul 31;511(7511):616-20. doi: 10.1038/nature13393.

4.4.9 Notch regulates PKCθ through RUNX1 and RUNX3

Vincenzo Giambra in our group had noted a number of important phenotypes associated with PKCθ in T-ALL. In particular, he found that PKCθ regulated intracellular reactive oxygen species (ROS), and that low levels of PKCθ and ROS were associated with higher leukemia initiating cell (LIC) frequency. We found that RUNX1 levels were correlated with PKCθ expression levels in a cohort of 264 primary patient samples and identified RUNX1-binding sites in the *PRKCQ* proximal promoter and intronic enhancers[65,164,332-334]. Additionally, I find RUNX1 to be highly correlated with PKCθ in RNAseq data from patient-derived xenograft samples, several of which were used throughout my dissertation (**Figure 4.36**). As such, I hypothesized that RUNX1 might regulate PKCθ expression in T-cell leukemia. Consistent with this idea, I found that knockdown of RUNX1 using two different shRNA clones led to reduced PKCθ protein levels (**Figure 4.37 A**). Interestingly, we found that NOTCH1/CSL appear to bind to a region upstream of the RUNX3 P1 promoter associated with enhancer marks (H3K4me1), which suggested that Notch might regulate RUNX3 [164,335,336]. Since RUNX family members can cross-regulate each other[337], and are able to mediate both repression and activation of target genes, I hypothesized that NOTCH1 promotes RUNX3 expression, RUNX3 represses RUNX1, and RUNX1 upregulates PKCθ[338] (**Figure 4.37 D**). Of note, overexpression or knockdown of RUNX3 results in reciprocal RUNX1 expression changes. Additionally, I found that Notch inhibition using γ-secretase inhibitor (GSI) leads to a pronounced decrease of RUNX3, and higher amounts of RUNX1 and PKCθ (**Figure 4.37 B, C**). In an expanded panel of T-ALL cell lines, I find this pattern to hold true, suggesting this may be a generalized phenomenon (**Figure 4.38 A, B, C**). Work from others in the Weng lab was able to show that dominant negative Mastermind-like-1 (DN-MAML)[339] recapitulated GSI effects on RUNX3, and as this is considered by the field to be a more proximal way to inhibit the NOTCH1 activation complex, confirms that these effects are specific to Notch signaling[164]. It is also important to note that in both CUTLL1 and KOPT-K1 cells, depletion of RUNX1 causes a reduction of H3K27Ac, H4K4me3 and H3K36me3 (KOPT-K1 only) marks, suggesting that RUNX1 depletion at promoter/enhancer regions

facilitates gene expression in part through remodeling of local chromatin in this context (**Figure 4.39**).

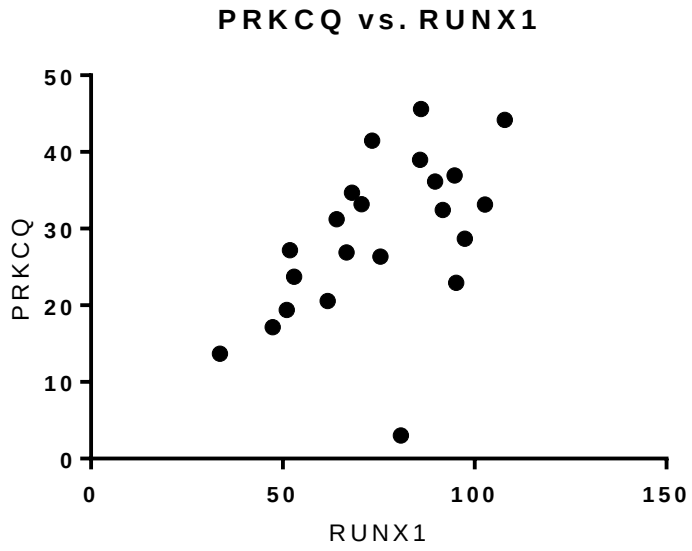

Figure 4.36 Pearson correlation between RUNX1 and PKCθ.

Pearson correlation of RNAseq expression data from 22 patient-derived xenografts[340]. R=0.5318, 95% CI=0.1421 to 0.7788; R squared = 0.2828. P=0.0108.

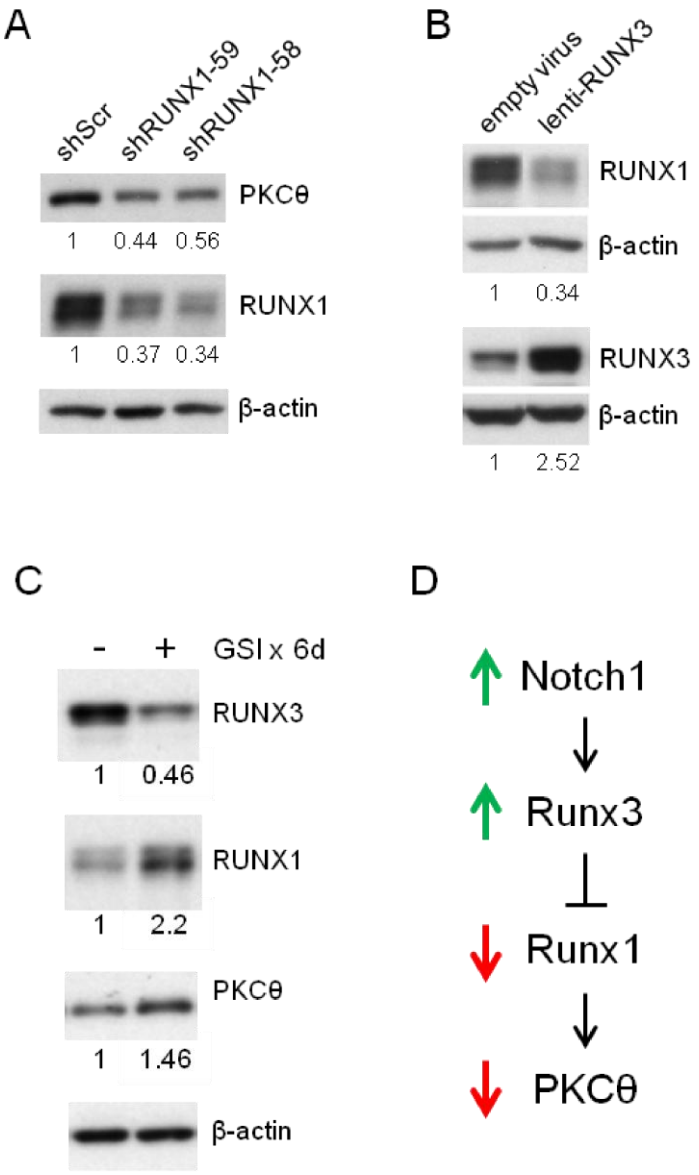

Figure 4.37 Notch signaling regulates PKCθ & RUNX protein expression.

Western blot analyses of PKCθ, RUNX1, and RUNX3 protein levels in CUTLL1 cells following (**A**) shRNA-mediated knock-down of RUNX1, (**B**) lentiviral overexpression of RUNX3, and (**C**) Notch inhibition with γ-secretase inhibitor (GSI, 1 μM compound E). Numbers below each panel indicate fold change after normalization to β-actin loading control. (**D**) Schematic of transcriptional circuit involving NOTCH1, RUNX3, RUNX1, and PKCθ.

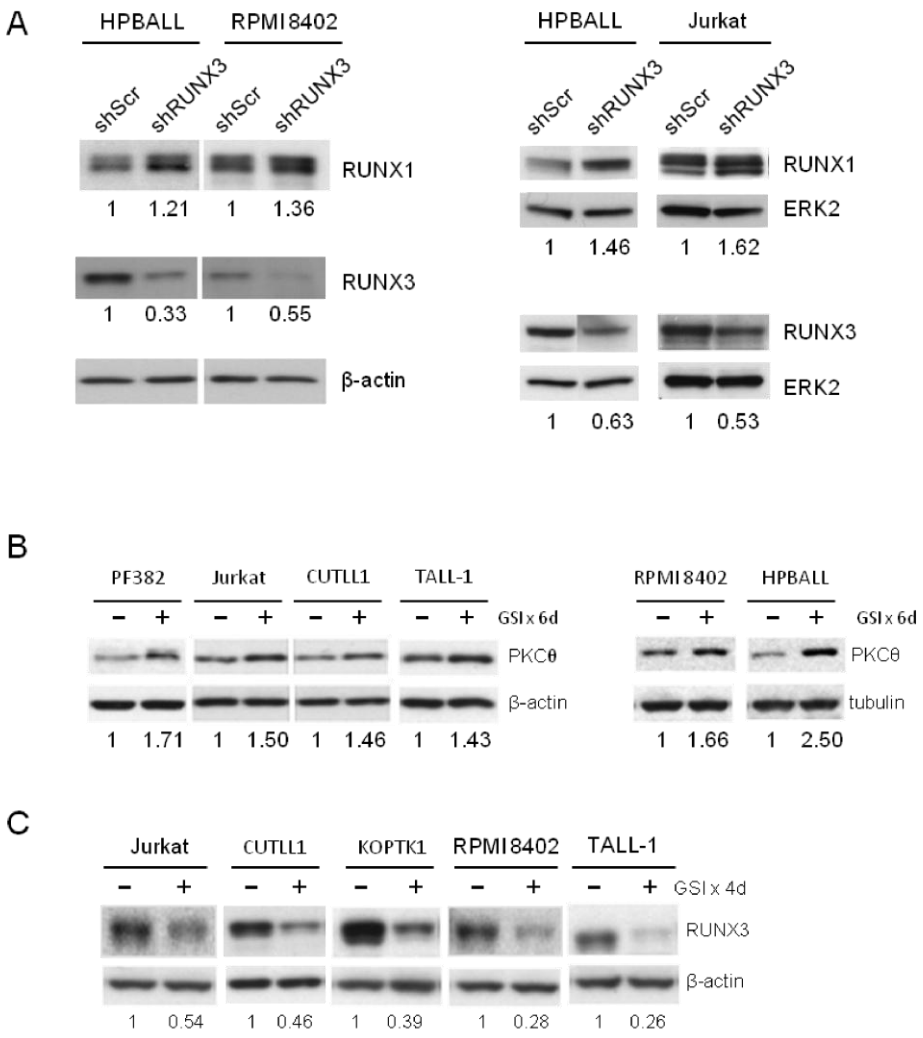

Figure 4.38 Knockdown of RUNX proteins modulates PKCθ.

(A) Knock-down of RUNX3 induces RUNX1 in T-ALL cells. Western blot analysis of RUNX1 and RUNX3 protein levels in human T-ALL cell lines transduced with lentiviral shRNAs against RUNX3 (shRUNX3) vs. scrambled negative control (non-silencing control). Numbers below each panel indicate fold change over control cells after normalization to β-actin or ERK2 loading control. Western blot analysis of **(B)** RUNX3 and **(C)** PKCθ protein levels in human T-ALL cells treated in vitro with γ-secretase inhibitor (GSI) to block Notch signaling vs. DMSO vehicle control. Numbers below each panel indicate fold change over control cells after normalization to β-actin or tubulin loading control. Data depicted are representative of multiple replicates.

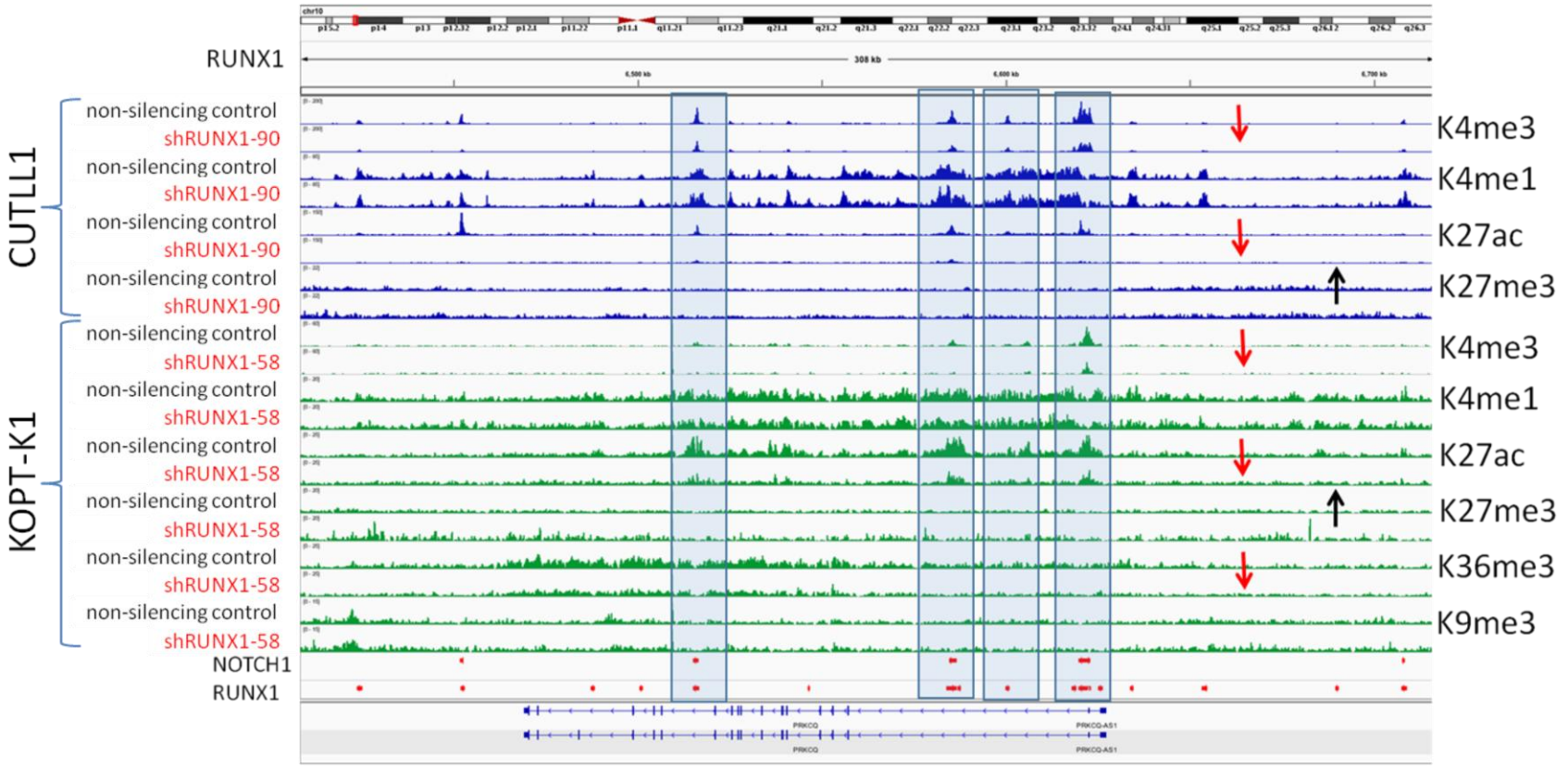
RUNX1
CUTLL1
non-silencing control
shRUNX1-90
non-silencing control
shRUNX1-90
non-silencing control
shRUNX1-90
non-silencing control
shRUNX1-90
KOPT-K1
non-silencing control
shRUNX1-58
non-silencing control
shRUNX1-58
non-silencing control
shRUNX1-58
non-silencing control
shRUNX1-58
non-silencing control
shRUNX1-58
non-silencing control
shRUNX1-58
NOTCH1
RUNX1
K4me3
K4me1
K27ac
K27me3
K4me3
K4me1
K27ac
K27me3
K36me3
K9me3

Figure 4.39 RUNX1 depletion at PKCθ locus depletes activatory histone marks and induces inhibitory histone marks.

RUNX1 and NOTCH1 Transcription Factor ChIP-seq binding is depicted as red bars from publically available data[8,9] (GEO accessions: GSE51800, GSE29600). H3K27Ac ChIP-seq is depicted above for the tracks with labels. Arrows depict general trends for each set of tracks in each cell line. Histone marks H3K4me4, H3K4me1, H3K27Ac, H3K27me3, H3K36me3, and H3K9me3 are depicted as noted.

4.4.10 Notch and RUNX1 regulate growth additively

In exploring the role of RUNX1 in immature T-cell leukemias, I became aware of work by Hongfang Wang in Jon Aster's lab, who had identified RUNX consensus sequences and RUNX1 binding near dynamically regulated Notch target genes bound by NOTCH1 and/or CSL[8,9]. I hypothesized that RUNX1 could mediate Notch signaling or act parallel to Notch signaling, and thus sustain growth signals in collaboration with Notch. In order to explore this idea, I attempted to see if there were additive effects of RUNX1 depletion and Notch inhibition. I found that inhibiting Notch or knocking down RUNX1 had similar effects on cell growth in the GSI-sensitive cell line KOPT-K1, both resulting in a 5-fold reduction in growth (**Figure 4.40 A**). The combination treatment, resulted in a significant reduction in growth and accounted for 18.4% of the total variation (Two-way ANOVA Interaction P value=0.0008) with cells expanding less than 3 fold over 8 days, as opposed to over 60-fold in the control. It is interesting to note however, that the GSI-resistant cell line CCRF-CEM is sensitive to RUNX1 knockdown, and actually appears to sensitize cells to Compound E (Two-way ANOVA Interaction P value=0.0028), resulting in a stronger additive effect (**Figure 4.40 B**). However, this effect was only 3.4% of the total variation. This additive growth effect of RUNX1 and Notch signaling may be a result of dose-dependent effects on gene regulation. Using IGF1R and IL7R (from section 4.4.6), as a paradigm for RUNX1-regulated target genes, I see that the surface expression of IGF1R and IL7R are reduced upon Notch inhibition and RUNX1 knockdown in KOPT-K1, HPB-ALL and RPMI 8402 (**Figure 4.41**). Most notably however, is the additive effect of RUNX1 and Notch interference, causing a further reduction in cell surface levels of these two important T-ALL signaling receptors. Importantly, these findings are confirmed in a patient-derived xenograft sample, D135-1-

5, which has a pronounced reduction in proliferation as measured by a cell proliferation dye (**Figure 4.42**). Finally, IGF1R surface levels are markedly reduced upon pan-RUNX knockdown in the same PDX, showing additive regulation along with Notch signaling (**Figure 4.43**).

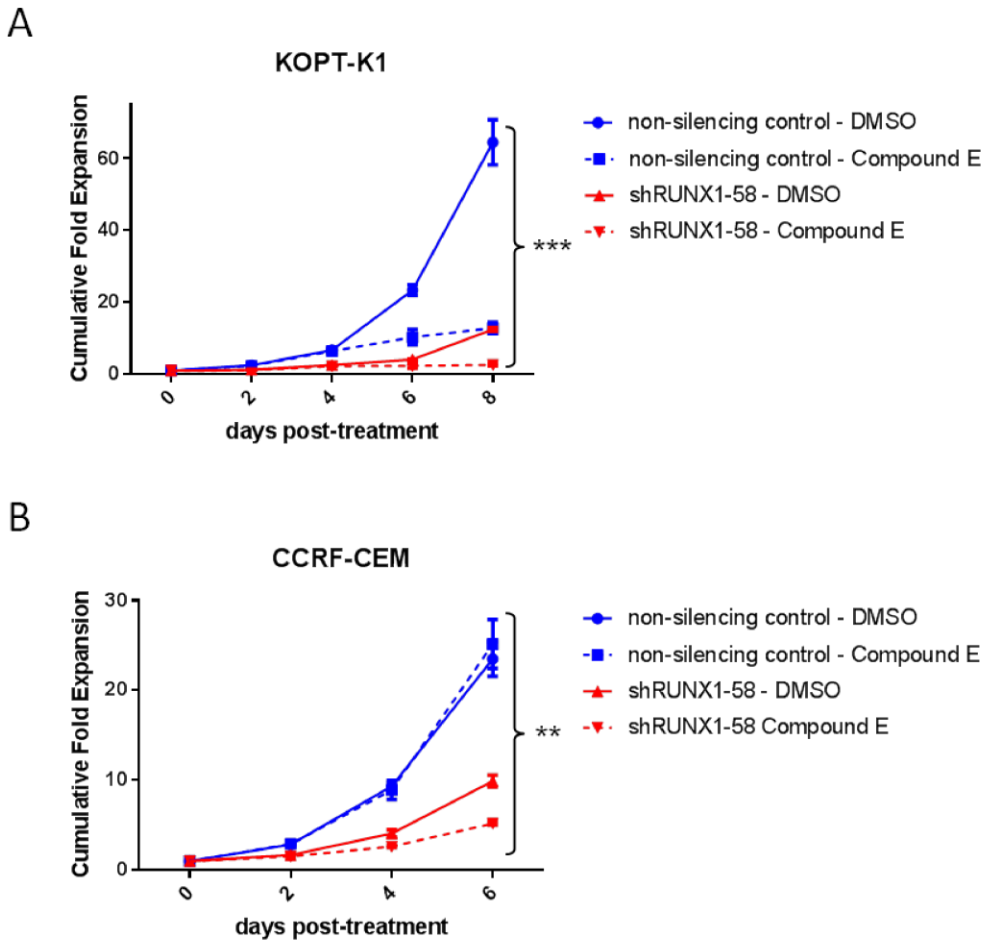

Figure 4.40 Depletion of RUNX1 and Notch inhibition in T-ALL cells results in additive disruption of growth.

The T-ALL cell lines **(A)** KOPT-K1 and **(B)** CCRF-CEM were either transduced with pLKO.1 Puro non-silencing control or pLKO.1 Puro shRUNX1-58 and selected for 3 days before being cultured in the presence of vehicle (DMSO) or γ-secretase inhibitor (Compound E) [day 0]. Each sample was done in duplicate with mean fold expansion plotted with error bars representing standard deviation. Cells were counted by ViCell® and replated at the same density every 2 days. ****, p<0.01; ***, p<0.001 (Two-way ANOVA).*

A

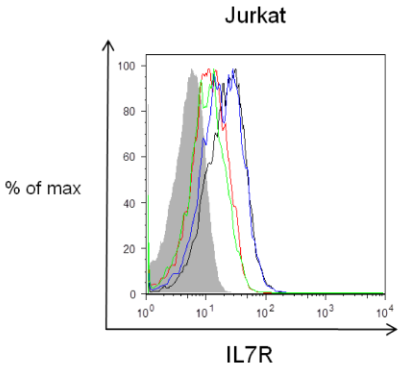

	IL7R (MFI)	IL7R (normalized)
non-silencing control + DMSO	20.5	1
non-silencing control + Compound E	10.8	0.40
shRUNX1 pool + DMSO	17.9	0.84
shRUNX1 pool + Compound E	9.9	0.34
unstained control	4.4	0

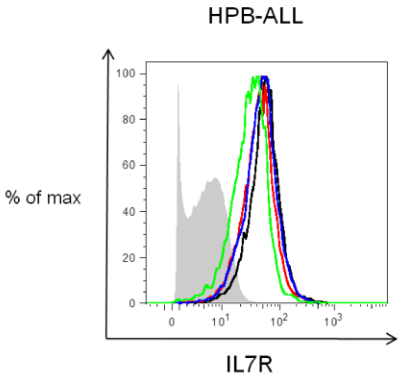

	IL7R (MFI)	IL7R (normalized)
non-silencing control + DMSO	51	1
non-silencing control + Compound E	39	0.85
shRUNX1 pool + DMSO	43	0.93
shRUNX1 pool + Compound E	28	0.61
unstained control	5	0

B

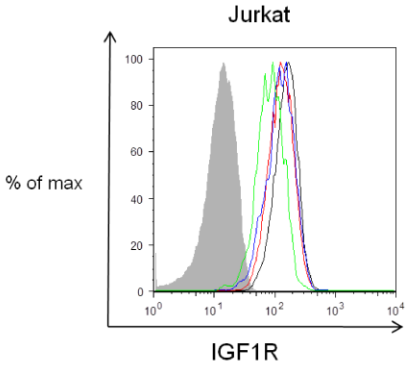

	IGF1R (MFI)	IGF1R (normalized)
non-silencing control + DMSO	155	1
non-silencing control + Compound E	128	0.81
shRUNX1 pool + DMSO	123	0.78
shRUNX1 pool + Compound E	84	0.50
secondary-only only	12	0

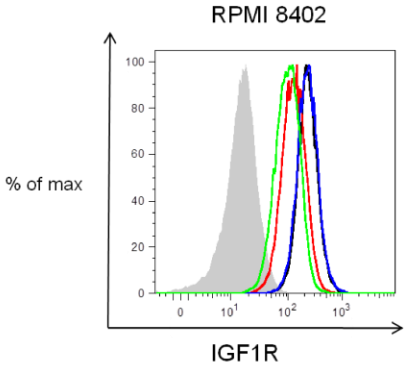

	IGF1R (MFI)	IGF1R (normalized)
non-silencing control + DMSO	226	1
non-silencing control + Compound E	124	0.52
shRUNX1 pool + DMSO	225	0.99
shRUNX1 pool + Compound E	95	0.38
secondary-only only	15	0

Figure 4.41 RUNX1 and Notch signaling additively regulate IL7R and IGF1R.

T-ALL cell lines were transduced with pLKO.1 GFP non-silencing control or a pool of pLKO.1 GFP lentiviruses targeting RUNX1 (**Table 4.5**). Three days post-transduction, cells were incubated with either DMSO or the γ-secretase inhibitor Compound E. Four days later they were analyzed by flow cytometry. **(A)** IL7R cell surface expression in Jurkat and HPB-ALL cells. Cells were labeled with APC-conjugated primary antibodies against IL7R (clone eBioRDR5, eBioscience) and analyzed by flow cytometry. **(B)** IGF1R cell surface expression in Jurkat and RPMI 8402 cells. Cells were labeled with primary antibodies against IGF1R (clone αIR3) followed by secondary labeling with eFluor660-conjugated Goat F(ab')2 anti-Mouse IgG and analyzed by flow cytometry.

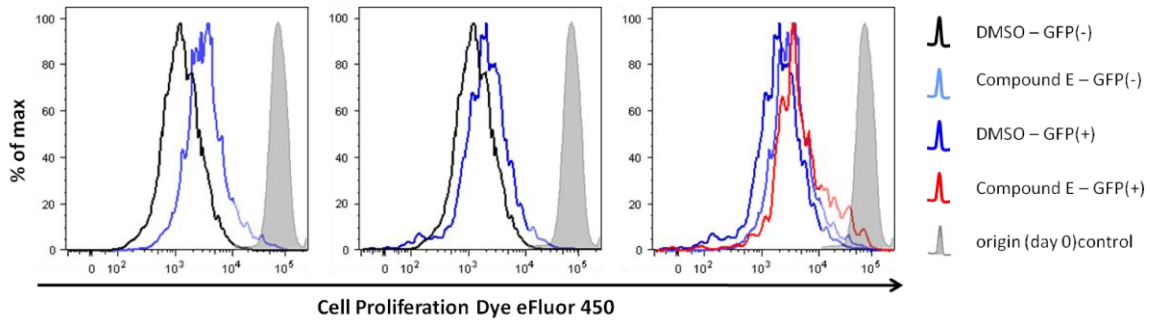

Figure 4.42 RUNX1 and Notch signaling support growth of a T-ALL patient-derived xenograft.

A T-ALL patient-derived xenograft, D135-1-5, was transduced with a pool of shRNAs targeting RUNX1 and RUNX3 (**Table 4.5**). Three days later, cells were loaded with Cell Proliferation Dye eFluor 450 and cultured for 10 more days in the presence of either vehicle (DMSO) or the γ-secretase inhibitor Compound E. At this point, cells were analyzed by flow cytometry. The transduced (GFP+) and untransduced (GFP-) fractions are noted.

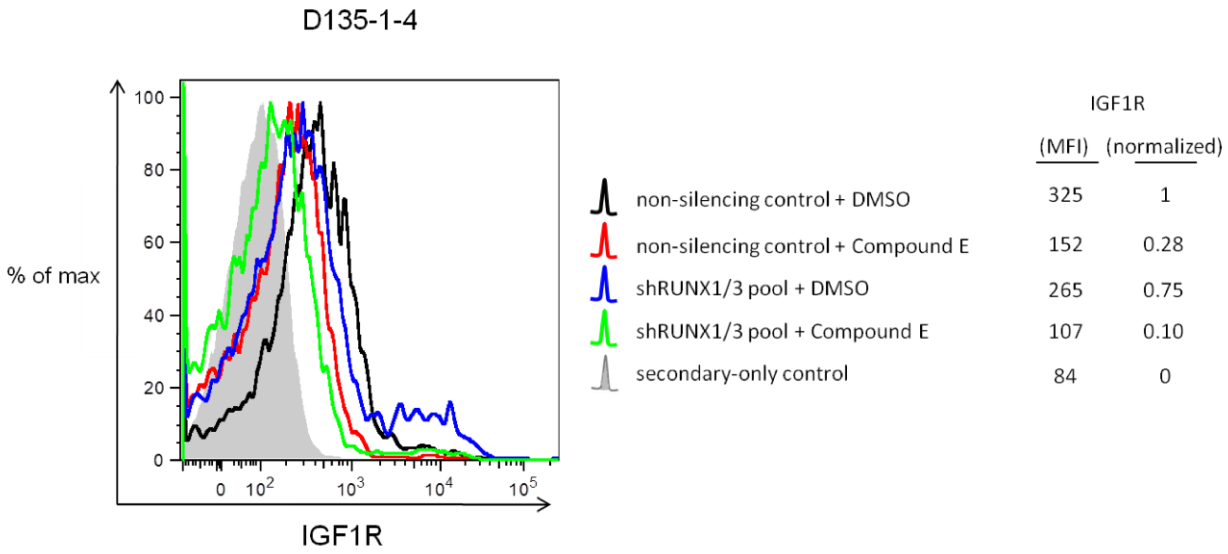

Figure 4.43 Notch signaling and RUNX1 support the expression of IGF1R

A T-ALL patient-derived xenograft, D135-1-5, was transduced with either pLKO.1 GFP non-silencing control or a pool of pLKO.1 GFP lentiviruses targeting RUNX1 and RUNX3 (**Table 4.5**). Three days later, cells were cultured in the presence of either vehicle (DMSO) or the γ-secretase inhibitor Compound E. Six days later they were analyzed for IGF1R cell surface expression by flow cytometry. Cells were labeled with primary antibodies against IGF1R (clone αIR3) followed by secondary labeling with eFluor660-conjugated Goat F(ab')2 anti-Mouse IgG and analyzed by flow cytometry.

4.5 Discussion

4.5.1 Survey of RUNX1 and RUNX3 in T-cell Leukemia

In beginning to explore the functional effects of interference with RUNX family member functions, we utilized a dominant-negative version of RUNX family members which consists of the RUNT domain fused to a nuclear localization signal. The RUNT domain is highly conserved across all RUNX paralogs and between mouse and human orthologs and as such it represents a powerful tool as a pan-RUNX inhibitor. It is interesting to note then that interference in both mouse and human cells results in growth defects, attributable in theory to any and all RUNX family members. The Aster lab has utilized a similar construct in CUTLL1 cells and shown it to interfere with growth on par with DN-MAML, a dominant-negative version of Mastermind-like protein 1 (MAML1), which is a potent Notch pathway inhibitor[130,339]. They referred to it primarily

as interfering with RUNX1; however this effect could also be a result of interference with paralogous genes. As RUNX2 doesn't seem to be expressed in human primary patient samples, it suggested to me that interference through RUNT acts predominantly through RUNX1 and RUNX3. However, it should be noted that dominant-negative elements may not only result in a loss-of-function phenotype but may acquire neomorphic and hypermorphic phenotypes[341]. Thus, it remains possible that the phenotypes attributed to the RUNT construct are a result of unknown effects of an artificial construct perhaps due to multimerization, alteration of targeting to different loci, or a result of changing the complement of interacting proteins and other molecules.

I chose to use RNAi as a method by which to abrogate RUNX1/3 functions in a more specific manner. In order to confirm my RUNT results, I used a pan-RUNX1/3 shRNA pool which was at a 1:1:1:1:1 ratio to knockdown RUNX1 and RUNX3. I note in a very broad panel of T-ALL cell lines that interference with RUNX1 and RUNX3 has very similar effects to RUNT on growth of cells in an *in vitro* competition, a finding that was verified in a PDX sample. Additionally, it seems as though the vast majority of the effect on cell proliferation is provided through RUNX1, as knockdown of RUNX1 vs. RUNX3 produced a greater effect on BrdU incorporation in the former relative to the latter. This suggested to me that RUNX1 might be the more important player in growth of established T-ALL cells, especially when the frequency of *RUNX1* mutations is taken into account.

4.5.2 T-ALL cells require both RUNX1 and RUNX3

I found RUNX1 and RUNX3 to be expressed in T-ALL patients at the mRNA level using interrogation of published expression profiling data. However, mRNA is processed or translated inconsistently, and as such it is well described that mRNA and protein levels do not correlate perfectly with each other[342,343]. Using a western blot assay, I was able to confirm that RUNX1 and RUNX3 protein was expressed in all T-ALL cell lines and patient samples, albeit to variable degrees, with some cell lines or patients being categorized into relatively high, or low RUNX1 or RUNX3 expressing lines.

In comparing the growth dynamics between cells which have been depleted of RUNX factors, it is important to recognize that my pool of shRNAs had an unequal number of shRNAs targeting each paralog, and that different shRNA clones have different efficiencies in producing efficient knockdown. This could result in bias in this set of experiments. Therefore, I chose to knockdown RUNX1 and RUNX3 using individual shRNAs, in part to determine the relative contribution of RUNX1 and RUNX3, but also to identify if there were correlations between RUNX1 amount and growth. I found that RUNX3 knockdown did not appear to necessarily result in as dramatic a growth defect as RUNX1 depletion, an effect that was substantiated in both a RUNX1-high/RUNX3-low cell line (RPMI 8402) and a RUNX1-low/RUNX3-high cell line (HPB-ALL), which suggested that there was little correlation between RUNX1/RUNX3 expression level and RUNX-depletion phenotypes. Based on these results, I focused the majority of the following experiments on further interrogating RUNX1 primarily.

4.5.3 T-ALL cells with *RUNX1* mutations remain dependent on RUNX1

As very little is known about how heterozygous *RUNX1* mutations affect stability and expression of RUNX1 protein, it was interesting to note that I saw no correlation between mutation status and protein expression. I was unable to detect a protein at a size consistent with a degradation product or truncated protein either. This suggests that either the mutated allele is silenced and the wild-type allele is upregulated in compensation or that *RUNX1* mutations do not affect protein stability. Also important to note, I did not detect a protein species consistent with the RUNX1A isoform, despite my antibody having recognized overexpressed RUNX1A in other sets of experiments. Mutation status did not appear to have any effect on dependence on RUNX1. Cell lines with *RUNX1* mutations are still sensitive, and in some cases more sensitive to RUNX1 depletion. This could lend support to the possibility that established T-ALL cells have become more dependent on the remaining wild-type allele as the deleterious mutated allele is silenced. If the wild-type allele is the only allele expressed, the remaining mRNA would be especially precious to the cell. It is important to note that RUNX1 depletion appears to be dose dependent, with severity of growth phenotype correlated

with level of knockdown, and this effect remains consistent across a broad panel of cell lines. Should RUNX1 have critical functions in T-ALL cells which are not described by canonical transcription factor function and instead rely on other possibilities such as protein scaffolding, then the mutations may have no effect on RUNX1 protein function or acquire a neomorphic function. However the data from alternative models (MDS/AML) do not currently support this model. A lack of uniform mRNA changes upon knockdown of RUNX1 knockdown in my hands is consistent with this model.

4.5.4 Deletion of *Runx1* and *Cbfb* in murine T-ALL

Cell lines and patient-derived xenografts represent genetically heterogeneous experimental systems, while data from humans is perhaps more relevant to the biology of T-cell leukemia, mouse models represent tractable, more genetically defined systems. In trying to better understand phenomena associated with RUNX transcription factors, I generated leukemias on conditional knockout backgrounds in which the *Runx1* and *Cbfb* alleles had been targeted for deletion. I generated leukemias using the very well-characterized hNOTCH1ΔE allele, an active form of NOTCH1, which generates leukemia at short latency with high penetrance[43]. With the advent of more quantitative and accurate forms of PCR, namely digital PCR, and the knowledge that incomplete deletion of a floxed allele might interfere with the proper interpretation of data that followed, I was interested in using droplet digital PCR to better quantify the level of deletion upon recombination with Cre recombinase. Droplet digital PCR (ddPCR) allows the PCR reaction to be fractionated into upwards of 20,000 droplets within which there is an individual amplification reaction. These droplets are then enumerated in a manner very similar to flow cytometry, allowing for quantitation of positive and negative events. The EvaGreen reagent is a dsDNA-binding dye which is optimized for ddPCR. The assay I generated was able to discriminate between floxed and deleted alleles of *Runx1* and *Cbfb*, thus I was able to quantify the amount of deleted vs. floxed allele within a preparation of gDNA. It is important to note that in experiments very similar to shRNA knockdown *in* vitro completion assays, I saw a consistent selection against *Runx1* or *Cbfb* deletion, where the deleted population of cells is selected against. This is

contrasted with wild-type leukemias which were transduced with a Cre reporter. These cells had strong “pseudo-deletion” (acquisition of GFP expression and loss of dsRed expression), but there was no notable selection against the pseudo-deleted fraction relative to the floxed fraction. In two of the leukemias, the vector itself was selected against, but change had no association with Cre recombinase activity. Of important note, the highest relative deletion I was able to achieve was ~85%, but rarely did I achieve higher than 40-50%. This could suggest that either technical challenges imposed by the delivery/induction of the enzyme’s activity or relative accessibility of the floxed locus could be limiting, or that past deletion experiments using endpoint PCR as a readout to quantify deletion have overestimated deletion efficiency. The level of deletion I achieved limited the extent to which I was able to characterize the phenotypes associated with deletion, and the heterogeneity in the system would have made it difficult to interpret *in vivo* experiments. From these mouse experiments, I conclude that *Runx1* and *Cbfb* appear to be necessary for *in vitro* growth and propagation of Notch-driven T-ALL. Interestingly, previously it has been shown that deletion of *Runx1* might actually induce T-cell leukemogenesis, supporting the idea that Runx1 might be a tumour suppressor[121]. As such, Runx1 levels must be tightly tuned to generate and maintain leukemia growth and propagation.

4.5.5 RUNX1 contributes to the proliferation and survival of T-ALL cells

Net cell growth represents a combination of cell proliferation/division and survival/cell death. As such, a culture which is contracting in growth may predominantly consist of cells under cell cycle arrest, undergoing apoptosis, or some combination of these two. Inhibition of Notch signaling is known to only affect cell proliferation, generally leading to cell cycle arrest of T-ALL cells without affecting survival. In fact, reversal of Notch inhibition by GSI-washout allows cells to re-enter the cell cycle and begin to proliferate again[8]. However it appears that RUNX1 supports both proliferation and survival of T-ALL cells, including patient-derived xenografts. The kinetics of *in vitro* competition experiments in certain cell lines was consistent with this, as some cell lines have a precipitous drop in the transduced population that is faster than would be explained by a

lack of population doublings alone. Additionally, it was interesting that RUNX1 knockdown also reduces cell size consistently across a broad panel of T-ALL cell lines relative to a non-silencing control suggesting that regulation of pathways that regulate cell size such as mTOR might be something to look at in the future[344].

4.5.6 Phenotypes associated with enforced expression of RUNX1 and RUNX3 in T-cell leukemia

In further exploring phenotypes associated with RUNX transcription factors in T-ALL, I sought to overexpress/forcibly express alleles of RUNX1 and RUNX3. It was interesting to note that work from Adolfo Ferrando's group found that enforced expression of RUNX1B reduced cell growth as measured by MTT assay[4]. Therefore I overexpressed all three alleles of RUNX1, as I was unsure if there might be different phenotypes associated with each allele. The three canonical RUNX1 alleles have been shown to carry different phenotypes, with RUNX1A believed to act predominantly as a dominant-negative allele, while RUNX1B and RUNX1B are predominantly similar in protein sequence, barring differences in their N-termini. Interestingly, all three alleles were selected against in an *in vitro* competition over the course of two weeks. This could be due to antagonism of RUNX1B and RUNX1C by dominant-negative effects of RUNX1A. In the case of RUNX1B and RUNX1C, it's possible that overexpression results in neomorphic, or off-target effects of spurious RUNX1 activity. I should note that I did not properly test the long-term growth of these cells, and it remains possible that they only receive a short-term growth burst from RUNX3 and not long-term sustained growth. Changing the balance of RUNX1-target genes also represents a likely outcome from RUNX1 overexpression that could result in proliferation defects. It is important to note that increased copy-number of RUNX1 is not selected for, but point mutations are. This could lend support to the idea that RUNX1 is a tumour suppressor in leukemogenesis. This does not preclude the possibility however that RUNX1 shares aspects of being a tumour suppressor. In fact an argument could be made that this lends evidence to the idea that RUNX1 expression must be tightly regulated. If RUNX1 levels fall or rise, it causes dramatic changes for the cell. Overexpression of any gene however is fraught

with potential caveats. These include the possibility of spurious integrations, causing interruptions in other coding regions; however for this to occur within a large culture of cells with thousands of integrations seems unlikely. Very high levels of overexpression may also result in overloading of the cell's ribosomes and molecular chaperones, and could result in altered protein conformation and change the milieu of binding partners. Additionally, the "hit-and-run" mechanism that is typically thought to produce short temporal bursts of transcription may be altered in the event of overexpression, leading perhaps to longer states of DNA-bound RUNX1[345]. In overexpressing RUNX1, I must note that the amount of its obligate heterodimer, CBFβ has not changed. As such, it is possible that the molecular stoichiometry of RUNX1: CBFβ has been pushed off balance. If we consider that CBFβ might be limiting, there is likely to be unbound RUNX1 in the cytoplasm and/or nucleus and unbound RUNX1 may be targeted for degradation[324]. Alternatively, it might be able to bind to some of its partner genes and create a dominant-negative effect by acting as a sponge for limiting pro-growth co-factors. Another tempting possibility is that the stoichiometry found at RUNX consensus sites throughout the genome may also be off balance, if normally only a fraction of these are bound or activated in T-ALL cells. Genes not normally bound in T-ALL cells may now suddenly be bound by RUNX1/ CBFβ, which could alter gene expression and interrupt normal growth.

In stark contrast to the phenotypes associated with RUNX1 overexpression enforced expression results of RUNX3 in KOPT-K1 cells results in cells proliferating faster that they might normally. This is interesting because it suggests that perhaps RUNX3 might induce a proliferation-derived transcriptional programme and points to a mechanism by which *Runx3* was selected for as a common insertion site in Chapter 3. Many of the same caveats associated with overexpression as described above could also explain this phenotype, however with an opposite pro-growth phenotype it is also possible that RUNX3 was limiting from these cells and this enforced expression provides an oncogenic pro-growth gene expression programme. Interpreting this data however, requires integration of RUNX3 effects on RUNX1 expression. As seen towards the end of the chapter, I show that RUNX3 can repress RUNX1, and so this RUNX3-dependent

proliferation may be due in part to reduced RUNX1 protein. However, due to the large amount of data suggesting that RUNX1-depletion results in growth defects, it suggests that this RUNX3-induced proliferation is due to RUNX1-independent functions of RUNX3. It is also important to note then that RUNX3 is able to overcome Notch inhibition in a GSI-sensitive cell line, DND-41. As shown previously with MYC in the same cell line, this points to a possibly important role for RUNX3 that should be explored further in an expanded panel of cell lines[77].

4.5.7 RUNX1 regulates IGF1R and IL7R cell surface protein

In originally selecting genes to explore for functional validation as RUNX1 target genes in T-ALL, I first looked to well-characterized NOTCH1 target genes due to strong support for RUNX1 and NOTCH1 co-localization at Notch pathway dynamic sites[8,9]. Therefore I used lentiviral knockdown of RUNX1 (and in some cases RUNX3 as well) to examine IGF1R, IL7R, MYC, PTEN, p21 and p27 expression. In interpreting the RNA-seq data for IGF1R, IL7R, MYC and p27, it should be noted that some of the samples were done at different time points, with different shRNA clones. Thus it is difficult to make a clear distinction in whether or not they are transcriptional targets. I would note then, in contrast to the RNA-seq data in unicate, that the duplicate data is likely the most consistent: it is likely the best controlled experiment and should most likely be given the greatest weight in interpretation. I would suggest then, that despite these genes not showing consistent regulation, that protein expression is more important in functional outcomes for these genes. In contrast to the IL7R mRNA data, but consistent with the IGF1R mRNA data, I saw reliable regulation of cell surface IL7R and IGF1R protein across multiple cell types, including patient-derived xenograft samples. As the regulation of mRNA and protein is not exactly consistent, future efforts should attempt to better determine how RUNX1 effects protein expression as there may be post-transcriptional regulatory mechanisms which are involved. This may also be a result of secondary changes that are independent of RUNX1's role in regulating H3K27Ac. Regardless, this reduction in IGF1R and IL7R had direct effects on signaling through these receptors as PI3K-AKT and JAK-STAT pathways were less sensitive to

stimulation with IGF1 and IL7 ligand, respectively. As these two cell surface receptors have strong links to T-ALL cell growth, proliferation, and in the case of IGF1R, LIC-activity, these represent two important novel RUNX1 target genes in T-ALL[2,346-350].

4.5.8 MYC protein expression is regulated by RUNX1

Links between MYC and Runx family members have a storied history, with *Runx2* described as a common insertion site in 30% of CD2-*Myc* T-ALL accelerated by MoMLV[280,351]. Subsequent to these earlier studies, the same groups also showed that *Runx1* and *Runx3* can also collaborate with *Myc* to induce leukemia[352]. Additionally, there is strong selection to maintain *Runx1* floxed alleles in an Eμ-Myc model of B-cell lymphoma when conditional deletion is induced, leading to p53-null leukemias[353]. It is important to note that Janice Telfer's lab found that a mutated version of *Runx1*, which has a C-terminal deletion (Runx1.d190), induces expression of both *MYC* mRNA and protein in Jurkat cells[354]. Interestingly, they found that endogenous RUNX1 is shown to bind to the *MYC* locus in both mouse and human cells, suggesting this regulation is through direct transcriptional regulation by RUNX1. Prior experiments have shown that this mutant lacks domains required to interact with co-factors to properly mediate target gene activation. Thus, this construct exhibits enhanced DNA-binding relative to wild-type RUNX1, and this mutant blocks CD4-silencing activity normally caused by domains which support repression[355,356]. My data do not directly agree with the data from the Telfer lab and this could be to a number of differences in our studies. While they had used only the Jurkat cell line, my study found changes in a broader panel of T-ALL cell lines, showing that RUNX1 positively regulates MYC protein levels in 4/5 cell lines tested. It should be noted that one of the cell lines tested, HPB-ALL showed derepression of MYC upon RUNX1 knockdown, suggesting in this line that it was indeed repressing the gene. It is possible that there is some variation in regulation of MYC by RUNX1, perhaps due to a different milieu of cofactors in each different genetic background, or a different set of collaborating mutations. Another possible explanation is the difference in our experimental methodologies. While I used an shRNA approach to deplete endogenous RUNX1 levels, the Telfer lab used an artificial domain-deletion

construct that had been overexpressed. As such, this allele of RUNX1 may have neomorphic functions independent from canonically understood dominant-negative functions, as described elsewhere in this discussion. Based on the results of my research, I would conclude that in most circumstances, RUNX1 positively regulates MYC in human T-ALL cells. However further work should be done on a larger cohort of samples, preferably on patient-derived material.

4.5.9 RUNX1 does not induce PTEN expression

PTEN is mutated or silenced in up to 20% of T-ALL and has also been shown to be a target of Notch signaling in certain contexts[357-359]. While there is some disagreement on whether *PTEN* mutations confer GSI-resistance, it remains an important tumour suppressor gene in T-cell leukemias[256,358,360]. Of note, *Runx1* deletion did not induce any expression changes in Pten in hematopoietic stem cell-enriched populations[127]. It was interesting to note then that PTEN was not apparently regulated in 4 cell lines tested at the protein level, however in HPB-ALL cells there was some reduction in PTEN levels upon RUNX1 knockdown. So in this context, reduction in RUNX1 levels by downregulation or mutation could represent a way to reduce PTEN protein levels, however more functional studies on this link should be performed to definitively call it a target of RUNX1.

4.5.10 RUNX1 may regulate growth in part through $p27^{Kip1}$

$p27^{Kip1}$ and $p21^{Cip1}$ are also important Notch targets that we analyzed for regulation by RUNX1. Notch was shown to upregulate SKP2, a ubiquitin ligase complex, which in turn degrades $p27^{Kip1}$ and $p21^{Cip1}$, which are important Cyclin-dependent kinase inhibitors (CKI) which regulates G_1-S phase transition[361-364]. It was interesting to see then that RUNX1 depletion resulted in derepression of $p27^{Kip1}$, but not $p21^{Cip1}$. This suggests that RUNX1 may be regulating these proteins through a mechanism that is independent of SKP2. Regardless, RUNX1 repressing $p27^{Kip1}$ represents an important regulatory mechanism by which it may support cell cycle progression. Interestingly, RUNX1 appears to repress $p21^{Cip1}$ and $p27^{Kip1}$ in hair follicle stem cells, and binds to the *CDKN1A* locus specifically, so this mechanism may be conserved in T-ALL cells[328].

Future work should address whether RUNX1 regulation of $p27^{Kip1}$ is through SKP2, direct binding and repression or other means.

4.5.11 Effects of RUNX1 knockdown on MYB and Bcl-2 family member expression

I was interested in extending the findings made by Takaomi Sanda during his time in Tom Look's lab where they found RUNX1 regulation of MYB. They showed data supporting a feed-forward loop between RUNX1/GATA3/TAL1 and MYB in Jurkat cells and I wanted to see how this applied to a broader panel of T-ALL cell lines including RPMI 8402 which carries the SIL-TAL1 translocation[7]. It was interesting to see that RUNX1 knockdown appeared to induce expression of MYB in RPMI 8402, suggesting that it was being repressed. This suggests that the RUNX1/GATA3/TAL1 complex inducing MYB may be limited to certain contexts or molecular subtypes of T-ALL, and although I used the same antibody that was used in Sanda et al., my data lacks the cell line used in their study, Jurkat, which makes complete interpretation difficult.

In trying to determine how RUNX1 might support cell survival phenotypes, I performed western blots for anti-apoptotic Bcl2-family members Bcl-2, Bcl-xL and Mcl-1. Previously it was shown that RUNX1 overexpression can induce Bcl-2 expression in a T-cell hybridoma cell line upon treatment with anti-CD3 and that RUNX1 can regulate Bcl-2 in AML cells as well[329,365]. I did not see any regulation of Bcl-2 or Bcl-xL, however it appears that RUNX1 represses the expression of the larger, anti-apoptotic isoform, and supports expression of the pro-apoptotic isoform of Mcl-1. This could suggest that other mechanisms which regulate cell survival may be important in the case of RUNX1. Interestingly, work from Nancy Speck's lab suggests that Runx1-low HSPCs may have lower levels of p53 which may result in pro-survival signals[128]. Future work should look at RUNX1-mediated p53 expression as well as the expression of other mediators of p53-dependent apoptosis such as Puma, Noxa and Bax.

4.5.12 Phenotypes associated with the CDK7 inhibitor THZ1

In collaboration with Nathanael Gray's lab, it was shown that the drug THZ1 covalently-inhibits CDK7, a Cyclin-dependent kinase which regulates transcription initiation by

phosphorylating the larger subunit, RPB1, of RNA polymerase II[69,366]. However, it should be noted that at high concentrations, THZ1 has cross-reactivity on CDK12 and CDK13, however the effects on RNA polymerase II appear to be specific to CDK7 as enforced expression of CDK7 C312S restores phosphorylation levels of the C-terminal domain. This finding allowed the generation of specific inhibitors against CDK12/13 using THZ1 as a starting scaffold[367]. Most interestingly though, cells treated with THZ1 appeared to have dramatically less RUNX1 protein, suggesting it was uniquely affected through this mechanism of transcriptional attenuation. In fact, there was significant enrichment between RUNX1 expression targets and THZ1 expression targets In Jurkat cells using gene set enrichment analysis (GSEA), suggesting many of the effects mediated by THZ1 may be through RUNX1. RUNX1 protein levels were confirmed to be lower in THZ1-treated Jurkat cells, however I used an expanded panel and found consistently lower RUNX1 levels across 5 cell lines in a dose-dependent manner. Of note, induced expression of RUNX1B or RUNX1C, especially, was able to partially rescue THZ1 mediated growth abrogation. Eventually the cells still apoptosed, however the selection for RUNX1 suggests it was indeed partially responsible for the phenotypes described in Kwiatkowski et al.[69]. Therefore, THZ1 represents an exciting way to potentially indirectly inhibit RUNX1, as it has proven difficult to target transcription factors using traditional therapeutics, with some exception[368]. In terms of therapeutic potential of this drug, the sensitivity of T-ALL PDX samples suggests a promising therapeutic window, even at low concentrations of the drug, and supports further pre-clinical and clinical studies. It is important to understand though that while THZ1 might have effects through CDK7, and possibly also CDK12/13 and has potential off-target effects, it acts in part through repression RUNX1.

4.5.13 Notch and RUNX signaling have roles in parallel and in series

These results thus reveal a novel mechanism connecting NOTCH1 to LIC activity though negative regulation of PKCθ via RUNX1 and RUNX3, and are consistent with prior studies showing that Notch signaling promotes LIC activity[369,370]. Variation among individual cell lines suggests other factors likely impinge upon components of the

NOTCH1-RUNX3-RUNX1-PKCθ transcriptional circuit; however, the overall consistent effects support the relevance of these results. In this regard, my results suggest that RUNX transcription factors act downstream of Notch signaling. However, as RUNX consensus sites and RUNX1 binding are near Notch consensus sequences, there could be some level of cross-regulation at play that should be further researched. I found that Notch could directly regulate the expression of RUNX3 in several T-ALL cell lines and this increase in RUNX3 levels was linked to repression of RUNX1 protein levels. RUNX1 was found to bind directly to the *PRKCQ* locus, mediating direct transcriptional activation of PKCΘ. Through the repression of reactive oxygen species (ROS), low levels of PKCΘ maintained through the RUNX family were found to enhance leukemia initiating cell (LIC) activity of T-ALL cells. In this respect, RUNX1 acted as a LIC-suppressor, whereby low levels of RUNX1 were necessary to maintain low levels of ROS.

Knockdown of RUNX1 and blocking Notch with γ-secretase inhibitors (GSI) has a profound additive effect on cell growth in both GSI-sensitive (exhibit a cell cycle defect upon inhibition) and GSI-resistant (do not exhibit a cell cycle defect upon inhibition) T-ALL cell lines. This is interesting as it suggests that RUNX1 is perhaps supporting growth in ways independent of Notch1, in addition to those ways in which it can also modulate Notch targets. Additionally, as this additive effect was described at the level of protein modulation of key Notch and RUNX1 target genes, it suggests that the additive growth phenotypes may also be a result of the cumulative actions of NOTCH1 and RUNX1 at target loci like IGF1R and IL7R.

These phenotypes are of greater interest in the light of genome-wide molecular analyses using Microarrays and ChIP-seq to interrogate mRNA expression changes and epigenomic changes. Further experiments should determine if the gene expression targets identified in my gene expression profiling experiments are true RUNX1 target genes in T-ALL. However, a difficulty in interpreting these results comes from the use of duplicates instead of triplicates. Thus, it remains difficult to determine if there are any outlier samples if there are only two replicates for each condition. These results may

gain increased confidence if future work seeks to repeat these results using the same cell lines under similar conditions. Nevertheless, I identified 188 common target genes between the three T-ALL cell lines. Relative confidence in this data is buoyed by evidence of this regulation across multiple lines in that regard. Additionally, it may not be wise to assume that there would necessarily be large expression changes due to RUNX1 depletion. Especially in the light of my epigenomic data showing that RUNX1 seems to regulate H3K27Ac levels, it remains possible that RUNX1's primary role is to recruit histone acetyltransferases (HAT) or block the activity of histone deacetylases (HDAC). Future work should focus on identifying if RUNX1 interacts with any HATs or HDACs. Additionally, it would be of interest to determine if RUNX1 creates an environment that is favorable for NOTCH1 binding to dynamic Notch sites.

4.5.14 RUNX1 as tumour suppressor or oncogene

Data suggesting that *RUNX1* gene functions as a tumor suppressor[4-6] stands in contrast to recent evidence proposing that RUNX1 provides growth supportive signals required to sustain T-cell leukemia. ChIP-seq data from the Aster lab has shown that RUNX1 is frequently found to be colocalized near regions of the T-ALL genome enriched in NOTCH1/CSL binding and H3K4me1 sites[8,9]. Additionally, work from the Look group demonstrated that RUNX1 functions in a feed-forward loop with TAL1 and GATA3 regulating MYB as well as a number of other genes which function to promote growth[7]. It is important to note that RUNX1 has been shown in Acute Myeloid Leukemias to provide growth supportive signals as well. This is in contrast to the paradigm that *RUNX1* is a tumour suppressor in myeloid lineages because of the generation of dominant-negative alleles such as RUNX1-ETO, and because of the presence of mutations that are similar to those found in T-ALL. James Mulloy's group was able to show that RUNX1, whether wild-type of mutated, was able to reduce the growth in AML1-ETO and MLL-AF9 Acute Myeloid Leukemia when overexpressed[329]. Similar to my experiments, they also knocked down RUNX1 and found similar results, suggesting again that there is a required middle-ground in RUNX1 expression necessary in AML, despite selection for mutated alleles that reduce RUNX1 activity. They do suggest

however that RUNX1 overexpression in cord blood leads to myeloid differentiation. Additionally, ETP-ALL has mutations that are similar in patterning to those found in myeloid disease, and so *RUNX1* mutations may be leading to a myeloid-biased expression pattern. An alternate possibility is that loss of RUNX1 may delay progression of T-cell through intrathymic maturation and thus may result in an increased pool of T-cell progenitors susceptible to accumulating additional genetic hits and subsequent transformation. My experiments did not address differentiation however future experiments should focus on this idea in T-cell leukemogenesis. It is difficult to determine how T-ALL cells might be able to differentiate, as they are an aberrant cell population entirely. Some have suggested that changes in cell surface markers are a sign of bona fide differentiation[170]. However, the loss or acquisition of markers on an aberrant cell may not be true differentiation of the clone but may represent superficial change. The differentiation functions of RUNX1 on normal populations of cells may be more revealing in future work. Interestingly, Goyama et al. point out that the loss of Runx1 in bone marrow accelerates leukemogenesis in an MLL-ENL model of leukemia[371]. The authors of this study suggest that this leads to compensation by other Runx family members and that deletion of both *Runx1* and *Cbfb* are required to disrupt leukemogenesis. Based on this data, they suggest that higher levels of RUNX1 are tumor suppressive, but that lower levels are growth promoting, and complete ablation is disastrous to cell propagation. The model that the authors suggest is quite striking, however I would alter it slightly. I would distinguish the difference between leukemogenesis and leukemia maintenance. Interestingly, all lymphoblastic leukemias which arise from Familial Platelet Disorder pedigrees are T-cell ALLs, suggesting that mutated RUNX1 is associated with T-cell leukemogenesis specifically in the lymphoid lineage. In line with these concepts, a model (**Figure 4.44**) I would like to put forward is that RUNX1 acts as a tumour suppressor in leukemia initiation, where high levels of RUNX1 are detrimental to the establishment of a neoplasm; however when expressed at lower levels it functions as a prosurvival factor in leukemia maintenance, and can contribute to enhancing LIC frequency by keeping PKCθ levels low. In this model, I would suggest that RUNX1 mutations are selected for as an early event, perhaps as

Nancy Speck's group suggests, as a preleukemic event[128]. Interestingly, mice with reduced levels of Cbfb protein have developmental blocks which are determined in part to the degree to which the protein level is reduced[146,147]. However, there are other reports suggesting that loss of Runx1 reduces the efficiency of leukemogenesis, so these concepts are still not clear[175]. This suggests that dosage dependent effects are a key factor in the Runx family's actions in a T-cell developmental context.

In integrating our current knowledge of both RUNX1 and RUNX3, I will raise a final possibility relating to the interplay of these two paralogous genes in T-ALL. My data suggests that RUNX1 is tightly regulated, with both overexpression and knockdown causing proliferation defects, while high RUNX3 appears to induce proliferation in T-ALL cells. Several years ago now, authors linking the relationship of the Wnt/β-catenin pathway members TCF-1 and LEF-1 described an idea relating to competition of these proteins for TCF-1/LEF-1 consensus sequences[372,373]. It was suggested apropos T-cell malignant transformation, that TCF-1 acts primarily to repress LEF-1 expression, which was described to be oncogenic. Consistent with this, they note that TCF-1 tends to have lower expression in human T-ALL. Using these findings as a paradigm, one could imagine the possibility that RUNX1 acts similarly to restrict access of RUNX3 to RUNX consensus sequences. Thus, mutations in RUNX1 could function to potentiate the access of RUNX3 to drive a pro-growth oncogenic transcription programme.

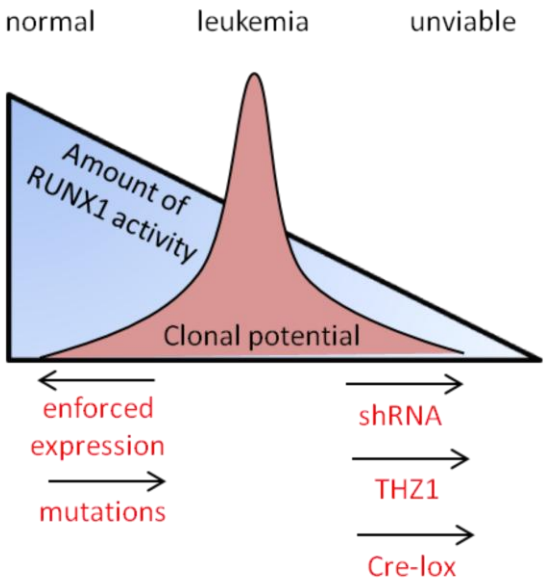

Figure 4.44 A model of RUNX1 activity in T-ALL leukemia

I propose a model whereby moderate levels of RUNX1 support T-ALL. Various means, either by *de novo* mutation or by experimental manipulation which alter the amounts of RUNX1 compromises leukemia growth.

Chapter 5: General Conclusions

5.1 Summary of findings

Despite clear advances in survival outcome for patients with Acute Leukemias of all ages in recent decades from changes in chemotherapy regimens, long-term side effects in children with T-ALL and treatment-associated toxicity in older adults are clear problems necessitating other treatment options. As such, my dissertation focused on identifying and clarifying roles for genes previously described as altered in other hematologic malignancies, with clear roles in hematopoietic stem and progenitor cells and T-cell development. The availability of targeted therapies against these gene products and the prognostic relevance of recently described mutations in *RUNX1* suggested that I should focus my attention on understanding the phenotypic patterns and downstream effectors that might be supporting leukemia biology. My studies focused on the role of IGF1R and RUNX1 in leukemia initiation and maintenance of Acute Myeloid Leukemia and T-cell Acute Lymphoblastic Leukemia, respectively. IGF1R is an important oncogenic signaling protein in T-cell leukemias which is responsible for supporting leukemia initiating cell (LIC) activity as well as growth of bulk cells[2]. I sought to determine if IGF1R can contribute to myeloid neoplasia by reducing IGF1R protein levels genetically and by interfering with IGF1R using small molecule inhibitors. I describe here that decreased IGF1R expression significantly impairs malignant transformation of committed granulocyte-monocyte progenitors (GMPs) with an associated cell-autonomous decrease in clonogenic activity. In contrast to T-cell lymphoid leukemias, myeloid leukemias with decreased IGF1R are readily transplantable into secondary recipients, and unexpectedly, genetic deletion of IGF1R had no effect on bulk cell proliferation. Nonetheless, pharmacologic inhibition of IGF1R using small molecule tyrosine kinase inhibitors was sufficient to inhibit growth of both murine and human AML cells *in vitro.* To my knowledge, these data represent the first assessment of IGF1R signaling in AML using a genetically defined system, and suggest the efficacy of IGF1R inhibitors in clinical development may be due in part to activity against related tyrosine kinases such as InsR.

T-cell leukemias which derive from strong Notch signaling remain clonal, suggesting that other mutations are required to collaborate with Notch signaling. Therefore, I used a highly penetrant, short latency leukemia-inducing allele of NOTCH1 (ΔE) and screened leukemias our lab had banked in order to find collaborating mutations. I found a large number of mutations which were potential common integration sites. I recovered *Ikzf1* and *Abl*, two previously known Notch-collaborating genes which suggested my strategy to recover integrations worked as expected. Additionally, I found a common integration site into *Runx3* and a single integration into a family member, *Runx1*. Based on these results and recently described mutations in the *RUNX1* gene in human T-ALL patient samples, I focused my attention on confirming collaboration with these genes. Using a 2A lentiviral system, I co-expressed alleles of RUNX1 and RUNX3 with a weaker allele of NOTCH1, ΔEΔL, in a multicistronic vector necessitating just one integration. I found that all alleles except for RUNX1C were able to cause a difference in penetrance of leukemia suggesting that they collaborated with Notch signaling to transform cells. I found that depletion of RUNX1 and RUNX3 in a broad panel of cell lines antagonized growth. Interestingly, overexpression of RUNX3 induced proliferation but RUNX1 reduced the proliferation of T-ALL cells, suggesting that RUNX1 expression must be balanced. Of note, using another approach to deplete cells of Runx proteins, I found that deletion of Runx1 and Cbfb using Cre recombinase-mediated recombination resulted in a similar growth defect, confirming the reliance of T-ALL cells on RUNX1 and CBFB. RUNX1 appears to regulate proliferation, survival and size of T-ALL cells and this is likely due in part through regulation of MYC, IGF1R, IL7R, and $p27^{Kip1}$. In attempting to determine how RUNX1 regulates survival I looked at the expression of anti-apoptotic Bcl-2 family members, but did not see any regulation at the protein level. As RUNX1 appears to support growth in established tumour cells, interference with it may be therapeutically attractive. I noted that the CDK7 inhibitor THZ1 may be an attractive indirect inhibitor of RUNX1, however as RUNX1 appears to directly regulate PKCθ and thus LIC activity, one could expect this might help in eradicating bulk tumour growth but might enhance LIC frequency and increase rate of relapse. Therefore, care should be taken when exploring ways to interfere with RUNX1 clinically. Finally, I found

that depletion of RUNX1 causes a genome-wide depletion of H3K27Ac, a change which does not occur when Notch signaling is blocked. Interestingly, this epigenomic change does not seem to have wide-ranging effects on RNA expression levels but this could be due to the time point used. RUNX1 and Notch signaling appear to additively support cell growth, suggesting that RUNX1 may generate a state permissive to Notch signaling.

5.2 Conclusions relating to hypotheses

The overarching goals of thesis dissertation were to better understand how aberrant signaling proteins and transcription factors contribute to leukemia in a context-dependent manner. *In chapter 2, my aim was to characterize the role of IGF1R signaling in supporting MLL-AF9 leukemogenesis.* I hypothesized that stem and progenitor-enriched populations with hypomorphic amounts of IGF1R would exhibit MLL-AF9-associated transformation defects relative to wild-type cells and that established leukemias might have impaired LIC function and/or frequency. I was able to show that IGF1R$^{neo/neo}$ GMP were unable to be transformed in part due to clonogenic defects as measured by colony forming potential, however IGF1R$^{neo/neo}$ LSK-derived MLL-AF9 leukemias exhibited no LIC defects relative to controls. Of note, I also found established human AML cell lines to be sensitive to IGF1R/InsR dual inhibitors, but experiments on IGF1R$^{neo/neo}$ tumours suggest that this is due in part to cross-reactivity on the Insulin Receptor.

In chapter 3, my aim was to Identify and characterize putative common integration sites in murine T-cell leukemogenesis in collaboration with NOTCH signaling. Based on previous screens involving weak alleles of NOTCH1 selecting for more Notch signaling, I hypothesized that stronger alleles of NOTCH1 would collaborate with genes in other pathways, providing other supportive signals in leukemic clone initiation. In this regard, it should be noted that while I still recovered integrations into the *Ikzf1* gene, they represented a lower proportion of the total integrations. I was able to later functionally characterize two of the integration sites on a broader functional level: RUNX1 and RUNX3. I also hypothesized that genes harbouring integrations would collaborate

genetically to enhance leukemia initiation. I was able to show that certain alleles of RUNX1 and RUNX3 were able to enhance penetration of the hNOTCH1ΔEΔL allele.

In chapter 4, my aim was to determine the contribution of RUNX1 (and RUNX3) to leukemia maintenance in T-cell Acute Lymphoblastic Leukemia and identify a potential mechanism by which it supports the disease. I hypothesized that RUNX3 and RUNX1 supported the growth of established T-ALL cells, despite evidence that *RUNX1* appeared to be a tumour suppressor based on the distribution of mutations in the RUNT and Activation Domains. Based on a number of experimental approaches, including shRNA knockdown and Cre-lox mediated deletion, I found that RUNX1 and RUNX3 were necessary for growth of T-ALL cells through the regulation of a number of downstream target genes. Interestingly, T-ALL cells have acquired an optimal amount of RUNX1 expression for growth as both increasing and decreasing expression levels results in reduced proliferation and viability. RUNX3 however appears to be tolerated at high levels and actually induces cells to grow faster. I also found a role for RUNX1 in regulating the epigenome through modulating H3K27Ac, as well as a number of downstream target genes, many of which are important oncogenes such as IGF1R, IL7R, $p27^{Kip1}$ and MYC. Finally, I show that RUNX1 could be abrogated using CDK7 inhibitor and that Notch signaling and RUNX1 contribute to growth in an additive manner which may be a result of target gene expression. These results point to an important role for RUNX1 in T-cell Acute Lymphoblastic Leukemia biology.

5.3 Strengths and Limitations of this research

My research contained a number of strengths based on the models and techniques I employed to perform my research. The vast majority of my research utilized relatively specific genetic approaches to alter the expression of particular gene products. Where possible, conditional knockout approaches were used on syngeneic inbred mouse strains which minimized effects which may represent variation in the genetic background of the individual. I also used shRNA knockdown, an approach widely validated and which has been shown to be quite specific in mediating knockdown of

gene products by RNA interference. In order to mitigate the possibility of off-target effects, I used multiple shRNAs targeting different exons of the RUNX1 gene. Through the use of multicistronic 2A lentivectors, I was able to transduce cells with only one integration event, as opposed to co-transduction of two separate viruses which may have caused greater variation in phenotypes due to integration artifacts. These vectors also allow for relatively 1:1 stoichiometric expression of gene products. However, I was unable to see GFP expression in my leukemias suggesting that cleavage may have been altered or that the virus was not involved with the generation of the leukemias, which is somewhat unlikely as my control viruses generated leukemias. By sorting specific stem and progenitor populations in my MLL-AF9 IGF1R experiments, I was able to uncover phenotypes which may have been skewed as I only enriched for hematopoietic stem and progenitor cells using other means (Lineage depletion or 5-FU enrichment). The use of droplet digital PCR in quantifying the deletion of the *Runx1* and *Cbfb* alleles was a key strength of this analysis, allowing for accurate quantification of the relative amount of deletion in the population of cells. It should be noted that this process is still dependent on PCR amplification, and there may be biases associated with this process. A key strength of these experiments is that in the case of my functional studies in T-cell leukemia, that I was able to use patient-derived xenograft samples, which allowed me to confirm some of the key findings from cell lines using relatively rare samples. Additionally, the gene expression profiling experiments were able to sample the expression of all known genes in an unbiased manner, as opposed to biased “cherry-picking”, although it should be noted that I did use this approach early on in the functional validation of some of the most important genes I found to be regulated by RUNX1. Through the use of small molecule inhibitors, I was also able to highlight possible therapeutic options at translating the findings of this dissertation to a clinical setting, an important strength of this research. A key limitation in the interpretation of the data I gathered relating to the deletion of the IGF1R locus in AML cells, was the lack of the droplet digital PCR system to quantify deletion at the time of the experiments. It remains possible that I overestimated the amount of deletion I achieved and the lack of a growth phenotype upon Cre induction was a result of

incomplete deletion. An overall limitation of my research is the overall number of samples used to generate this data. Although the majority of experiments were performed across multiple cell lines and PDX samples, some experiments were only done on a limited number of replicates and should be confirmed in future work. A limitation of my MYB western blots results from the lack of a Jurkat positive control, which may skew my results, however I used the same antibody used in the study which precipitated my experiment, suggesting that it would likely have similar results. A limitation of the experiments probing the expression of Bcl-2 family members is the lack of other apoptotic players that could also possibly be regulated by RUNX1 such as Bim, Bad, etc. in addition to other apoptotic pathways through Fas/Fas-ligand. Finally, I will note that a key limitation of my research is that a majority of the data utilizes different cell lines in a variable number of replicates. In interpreting the data, it should be noted that confirmation of the results will be key in better understanding how IGF1R contributes to AML and RUNX1 contributes to T-ALL.

Of important note, the retroviral insertional mutagenesis study in Chapter 3 did not originate as a prospective screen, but was intended to leverage Weng lab banked frozen mouse leukemia material as a resource to discover novel collaborating oncogenes and tumour suppressors. As such, had I designed the study as a prospective screen I may have considered alternate design approaches. It is important to note that if I had a larger cohort of murine leukemias I may have reached a higher number of common insertion sites. However, despite the large number of integrations recovered and the low number of these as being CIS, it remains possible that this was due to biology and not stochastic noise. The use of a stronger allele of NOTCH1, ΔE, compared to the relatively weaker *lck*-N^{IC} may suggest that other contributions to creating a clone are relatively minor, relative to Notch signaling. As such, there would be less need to select for genes specifically required for proliferation and survival. In this regard, it is notable that there is a lack integrations involving genes such as *Myc*, which is presumably at high levels as a downstream target of Notch. At the same time, my study had common insertion sites such as *Ikzf1* and *Nup214/Abl*, which have been found to be mutated in other insertional mutagenesis screens or in other T-ALL

contexts. This suggests that the integrations I was recovering are unlikely to be false positives and are likely to be biologically relevant to leukemogenesis of T-ALL. Interestingly, my study still had integrations at the Ikaros locus, which could be suggestive that these leukemias have required even higher levels of Notch, or it could also suggest that Ikaros may play other undefined roles outside of the Notch pathway in a T-ALL context. Finally, it should be noted that I did not confirm that integrations near the *Runx3* or *Runx1* loci resulted in increased expression. It should be expected based on similar studies above (such as those done in *Myc*) that their orientation suggests the generation of an enhancer. However, I feel that subsequent functional experiments in a broad panel of mouse and human leukemias, supports a role for these genes in supporting growth of T-ALL cells.

5.4 Future directions of research

The choice of using LSK and GMP subsets for the MLL-AF9 experiments was based on existing data showing differences in leukemia stem cell function between different subsets of stem and progenitor cells capacity to initiate leukemia following transduction[217,374]. However, there are other subsets of stem and progenitor cells which have been prospectively sorted and found to have different capacities for self-renewal and differentiation. It could be of interest to look at other progenitor subsets such as common myeloid progenitors (CMP) or common lymphoid progenitors (CLP), or perhaps a more specific stem cell phenotype like the ESLAM subsets ($CD45^+EPCR^+CD48^-CD150^+$) which can define HSC activity at a frequency as high as 1:2[375,359]. Future experiments relating to the deletion of IGF1R in myeloid neoplasias (using an $IGF1R^{lox/lox}$ or $IGF1R^{neo/neo}$ background should seek to employ droplet digital PCR to quantify deletion and attempt to quantify phenotypes associated with leukemias initiating cell activity. In trying to better understand the difference between IGF1R and InsR in contributing to cell growth of AML cells, blocking antibodies, shRNA knockdown or CRISPR-mediated interruption of IGF1R and InsR could be important in delineating the contributions of each to different cell types in mouse, but especially in human AML cells.

To better explore the collaboration of Notch signaling with other pathways, future insertional mutagenesis studies should seek to increase the number of leukemias studied and attempt to perhaps use next-generation sequencing to sequence the cloned out integrations to make this economical. My studies had few integrations into the same locus more than once, as such strengthening the number of CIS will be critical in determining which genes to study next following RUNX family members. However, using literature support and information from other insertional mutagenesis studies, one might be able to study some of the genes which only have 1-2 integrations such as *Runx1*. Additionally, it could be very interesting to confirm genetic collaboration using the more leukemogenic ΔE allele at a lower cell input dose to measure changes in leukemia initiating activity by the addition of a potential collaborator such as RUNX1 or RUNX3. Another alternative is to attempt to initiate leukemias with a strong allele of NOTCH1 on a congenic mouse background which is deficient for RUNX1 or RUNX3 (conditional knockout model).

While the experiments in my dissertation relating to functions of RUNX1 and RUNX3 in established T-ALL cells will provide insight into how *RUNX1* mutations might function, the mutations themselves were not studied. Future work should look at overexpression of mutated *RUNX1* alleles in both disease initiation and disease maintenance. It would be of interest to perhaps introduce *RUNX1* mutations into human T-ALL cells using CRISP-Cas9, which would allow study of endogenous mutations *de novo.* CRISPR could also be used to delete RUNX1 or RUNX3 in human T-ALL cell lines and perhaps also in patient-derived xenografts. I think that the contribution of RUNX3 is perhaps underappreciated from the results of my research and further work should go into how it contributes, as it likely has functions that are overlapping but also separate and distinct from RUNX1. Further experiments interrogating the role of pro- and anti-apoptotic pathways in mediating RUNX1-low apoptosis could help understand how it contributes to leukemic growth. As mentioned previously, interrogation of both Bcl-2 family members as well as apoptotic mechanisms that are Bcl-2-independent could prove useful in determining the mechanism of RUNX1-mediated survival. Confirming the RNA-seq and epigenomic ChIP-seq in other cells, in more replicates would help to better

understand how RUNX1 contributes to remodeling chromatin. I also think that understanding how RUNX1 contributes to local neighbourhood formation and chromatin conformation capture through 4C/5C/Hi-C could help in better understanding how RUNX1 itself regulates the structure of chromatin. We still understand very little about how RUNX1 helps NOTCH1 in regulating dynamic Notch sites, and so trying to understand the timing of this regulation will be critical as well, and knowing the ways in which they both contribute (which co-factors do they each bring) and if they interact with each other. Perhaps reverse ChIP with mass spectrometry could help in understanding which proteins are present at specific loci when RUNX1 and NOTCH1 are depleted or at steady-state conditions[376]. Additionally, the functions of THZ1 should be further explored as it is clear that while it has RUNX1-specific functions, it also has off-target effects. I think that better understanding of the RUNX1-independent functions will be important in understanding if it will work in the clinic or perhaps it may prove toxic to patients if it has too broad of effects. While my experiments focusing on the regulation of PKCθ through RUNX family members showcase a role of RUNX members as mediators of Notch signaling and LIC activity, we need to better understand how PKCθ itself functions. As such, further description of the phosphorylation targets of PKCθ will be important in trying to determine how it regulates leukemia propagation. Finally, my experiments with manipulating RUNX1 and RUNX3 in combination with Notch inhibition through γ-secretase inhibitors point to the intertwined nature of these transcription factors. More work should be done to understand if RUNX family members can contribute to γ-secretase inhibitor resistance, as many T-ALL cell lines and patient-derived xenografts are resistant to pharmacologic Notch inhibition[44].

Notably, it is still not clear which isoforms of RUNX1 are most abundant at the protein level in a more quantitative sense. Additionally, my studies were limited to the canonical isoforms of RUNX1: RUNX1A, RUNX1B, RUNX1C. Some studies have suggested there may be functional roles attributable to non-canonical RUNX1 isoforms through alternate exon usage[377]. Thus, my studies are likely missing certain aspects of RUNX1 biology in T-ALL. Experiments using mass spectrometry to measure absolute abundance of RUNX1 protein isoforms would be useful in determining the ultimate relevance of each

canonical isoform and cloning of novel cDNAs could be useful in determining the relevance of each possible splicing event.

Finally, as a final acknowledgement of a key limitation of my data, I would suggest that wherever possible future work should seek to maximize the use of patient-derived xenograft data whenever possible.

References

1. Beutler E. The treatment of acute leukemia: past, present, and future. *Leukemia*. 2001;15(4):658-661.
2. Medyouf H, Gusscott S, Wang H, et al. High-level IGF1R expression is required for leukemia-initiating cell activity in T-ALL and is supported by Notch signaling. *J Exp Med*. 2011;208(9):1809-1822.
3. Beverly LJ, Capobianco AJ. Perturbation of Ikaros isoform selection by MLV integration is a cooperative event in Notch(IC)-induced T cell leukemogenesis. *Cancer Cell*. 2003;3(6):551-564.
4. Della Gatta G, Palomero T, Perez-Garcia A, et al. Reverse engineering of TLX oncogenic transcriptional networks identifies RUNX1 as tumor suppressor in T-ALL. *Nat Med*. 2012;18(3):436-440.
5. Grossmann V, Kern W, Harbich S, et al. Prognostic relevance of RUNX1 mutations in T-cell acute lymphoblastic leukemia. *Haematologica*. 2011.
6. Zhang JH, Ding L, Holmfeldt L, et al. The genetic basis of early T-cell precursor acute lymphoblastic leukaemia. *Nature*. 2012;481(7380):157-163.
7. Sanda T, Lawton LN, Barrasa MI, et al. Core transcriptional regulatory circuit controlled by the TAL1 complex in human T cell acute lymphoblastic leukemia. *Cancer Cell*. 2012;22(2):209-221.
8. Wang H, Zang C, Taing L, et al. NOTCH1-RBPJ complexes drive target gene expression through dynamic interactions with superenhancers. *Proc Natl Acad Sci U S A*. 2014;111(2):705-710.
9. Wang H, Zou JY, Zhao B, et al. Genome-wide analysis reveals conserved and divergent features of Notch1/RBPJ binding in human and murine T-lymphoblastic leukemia cells. *PNAS*. 2011;108(36):14908-14913.
10. Dohner H, Estey EH, Amadori S, et al. Diagnosis and management of acute myeloid leukemia in adults: recommendations from an international expert panel, on behalf of the European LeukemiaNet. *Blood*. 2010;115(3):453-474.
11. Hills RK, Castaigne S, Appelbaum FR, et al. Addition of gemtuzumab ozogamicin to induction chemotherapy in adult patients with acute myeloid leukaemia: a meta-analysis of individual patient data from randomised controlled trials. *Lancet Oncology*. 2014;15(9):986-996.
12. Gupta V, Tallman MS, Weisdorf DJ. Allogeneic hematopoietic cell transplantation for adults with acute myeloid leukemia: myths, controversies, and unknowns. *Blood*. 2011;117(8):2307-2318.
13. Grimwade D, Hills RK, Moorman AV, et al. Refinement of cytogenetic classification in acute myeloid leukemia: determination of prognostic significance of rare recurring chromosomal abnormalities among 5876 younger adult patients treated in the United Kingdom Medical Research Council trials. *Blood*. 2010;116(3):354-365.
14. Peterson LF, Zhang DE. The 8;21 translocation in leukemogenesis. *Oncogene*. 2004;23(24):4255-4262.
15. Okuda T, Cai Z, Yang S, et al. Expression of a knocked-in AML1-ETO leukemia gene inhibits the establishment of normal definitive hematopoiesis and directly generates dysplastic hematopoietic progenitors. *Blood*. 1998;91(9):3134-3143.

16. Mulloy JC, Cammenga J, MacKenzie KL, Berguido FJ, Moore MA, Nimer SD. The AML1-ETO fusion protein promotes the expansion of human hematopoietic stem cells. *Blood*. 2002;99(1):15-23.
17. Tonks A, Pearn L, Tonks AJ, et al. The AML1-ETO fusion gene promotes extensive self-renewal of human primary erythroid cells. *Blood*. 2003;101(2):624-632.
18. Fenske TS, Pengue G, Mathews V, et al. Stem cell expression of the AML1/ETO fusion protein induces a myeloproliferative disorder in mice. *Proc Natl Acad Sci U S A*. 2004;101(42):15184-15189.
19. de Guzman CG, Warren AJ, Zhang Z, et al. Hematopoietic stem cell expansion and distinct myeloid developmental abnormalities in a murine model of the AML1-ETO translocation. *Mol Cell Biol*. 2002;22(15):5506-5517.
20. Lutterbach B, Hou Y, Durst KL, Hiebert SW. The inv(16) encodes an acute myeloid leukemia 1 transcriptional corepressor. *Proc Natl Acad Sci U S A*. 1999;96(22):12822-12827.
21. Adya N, Stacy T, Speck NA, Liu PP. The leukemic protein core binding factor beta (CBFbeta)-smooth-muscle myosin heavy chain sequesters CBFalpha2 into cytoskeletal filaments and aggregates. *Mol Cell Biol*. 1998;18(12):7432-7443.
22. Kanno Y, Kanno T, Sakakura C, Bae SC, Ito Y. Cytoplasmic sequestration of the polyomavirus enhancer binding protein 2 (PEBP2)/core binding factor alpha (CBFalpha) subunit by the leukemia-related PEBP2/CBFbeta-SMMHC fusion protein inhibits PEBP2/CBF-mediated transactivation. *Mol Cell Biol*. 1998;18(7):4252-4261.
23. Swansbury GJ, Slater R, Bain BJ, Moorman AV, Secker-Walker LM. Hematological malignancies with t(9;11)(p21-22;q23)--a laboratory and clinical study of 125 cases. European 11q23 Workshop participants. *Leukemia*. 1998;12(5):792-800.
24. Mrozek K, Heinonen K, Lawrence D, et al. Adult patients with de novo acute myeloid leukemia and t(9; 11)(p22; q23) have a superior outcome to patients with other translocations involving band 11q23: a cancer and leukemia group B study. *Blood*. 1997;90(11):4532-4538.
25. Byrd JC, Mrozek K, Dodge RK, et al. Pretreatment cytogenetic abnormalities are predictive of induction success, cumulative incidence of relapse, and overall survival in adult patients with de novo acute myeloid leukemia: results from Cancer and Leukemia Group B (CALGB 8461). *Blood*. 2002;100(13):4325-4336.
26. Cancer Genome Atlas Research N. Genomic and epigenomic landscapes of adult de novo acute myeloid leukemia. *N Engl J Med*. 2013;368(22):2059-2074.
27. Shilatifard A. Chromatin modifications by methylation and ubiquitination: implications in the regulation of gene expression. *Annu Rev Biochem*. 2006;75:243-269.
28. Biondi A, Cimino G, Pieters R, Pui CH. Biological and therapeutic aspects of infant leukemia. *Blood*. 2000;96(1):24-33.
29. Huret JL, Dessen P, Bernheim A. An atlas of chromosomes in hematological malignancies. Example: 11q23 and MLL partners. *Leukemia*. 2001;15(6):987-989.
30. Meyer C, Schneider B, Jakob S, et al. The MLL recombinome of acute leukemias. *Leukemia*. 2006;20(5):777-784.
31. Milne TA, Briggs SD, Brock HW, et al. MLL targets SET domain methyltransferase activity to Hox gene promoters. *Mol Cell*. 2002;10(5):1107-1117.
32. Milne TA, Martin ME, Brock HW, Slany RK, Hess JL. Leukemogenic MLL fusion proteins bind across a broad region of the Hox a9 locus, promoting transcription and multiple histone modifications. *Cancer Res*. 2005;65(24):11367-11374.

33. De Braekeleer M, Morel F, Le Bris MJ, Herry A, Douet-Guilbert N. The MLL gene and translocations involving chromosomal band 11q23 in acute leukemia. *Anticancer Res*. 2005;25(3B):1931-1944.
34. Hunger SP, Mullighan CG. Acute Lymphoblastic Leukemia in Children. *N Engl J Med*. 2015;373(16):1541-1552.
35. Marks DI, Paietta EM, Moorman AV, et al. T-cell acute lymphoblastic leukemia in adults: clinical features, immunophenotype, cytogenetics, and outcome from the large randomized prospective trial (UKALL XII/ECOG 2993). *Blood*. 2009;114(25):5136-5145.
36. J.K.C. BMJC. T lymphoblastic leukaemia/lymphoma (ed 4th). Lyon, France: International Agency for Research on Cancer (IARC); 2008.
37. Inaba H, Greaves M, Mullighan CG. Acute lymphoblastic leukaemia. *The Lancet*;381(9881):1943-1955.
38. Coustan-Smith E, Mullighan CG, Onciu M, et al. Early T-cell precursor leukaemia: a subtype of very high-risk acute lymphoblastic leukaemia. *Lancet Oncol*. 2009;10(2):147-156.
39. Rothenberg EV, Moore JE, Yui MA. Launching the T-cell-lineage developmental programme. *Nat Rev Immunol*. 2008;8(1):9-21.
40. Veerman AJ, Kamps WA, van den Berg H, et al. Dexamethasone-based therapy for childhood acute lymphoblastic leukaemia: results of the prospective Dutch Childhood Oncology Group (DCOG) protocol ALL-9 (1997-2004). *Lancet Oncol*. 2009;10(10):957-966.
41. Pui CH, Campana D, Pei DQ, et al. Treating Childhood Acute Lymphoblastic Leukemia without Cranial Irradiation. *New England Journal of Medicine*. 2009;360(26):2730-2741.
42. Ellisen LW, Bird J, West DC, et al. TAN-1, the human homolog of the Drosophila notch gene, is broken by chromosomal translocations in T lymphoblastic neoplasms. *Cell*. 1991;66(4):649-661.
43. Pear WS, Aster JC, Scott ML, et al. Exclusive development of T cell neoplasms in mice transplanted with bone marrow expressing activated Notch alleles. *J Exp Med*. 1996;183(5):2283-2291.
44. Weng AP, Ferrando AA, Lee W, et al. Activating mutations of NOTCH1 in human T cell acute lymphoblastic leukemia. *Science*. 2004;306(5694):269-271.
45. Schmitt TM, Zuniga-Pflucker JC. Induction of T cell development from hematopoietic progenitor cells by delta-like-1 in vitro. *Immunity*. 2002;17(6):749-756.
46. Ng SY, Yoshida T, Zhang J, Georgopoulos K. Genome-wide lineage-specific transcriptional networks underscore Ikaros-dependent lymphoid priming in hematopoietic stem cells. *Immunity*. 2009;30(4):493-507.
47. Chi AWS, Chavez A, Xu LW, et al. Identification of Flt3(+)CD150(-) myeloid progenitors in adult mouse bone marrow that harbor T lymphoid developmental potential. *Blood*. 2011;118(10):2723-2732.
48. Krueger A, von Boehmer H. Identification of a T lineage-committed progenitor in adult blood. *Immunity*. 2007;26(1):105-116.
49. Deangelo DJ, Stone RM, Silverman LB, et al. A phase I clinical trial of the notch inhibitor MK-0752 in patients with T-cell acute lymphoblastic leukemia/lymphoma (T-ALL) and other leukemias. *Journal of Clinical Oncology*. 2006;24(18):357s-357s.
50. Hebert J, Cayuela JM, Berkeley J, Sigaux F. Candidate tumor-suppressor genes MTS1 (p16INK4A) and MTS2 (p15INK4B) display frequent homozygous deletions in primary cells

from T- but not from B-cell lineage acute lymphoblastic leukemias. *Blood*. 1994;84(12):4038-4044.
51. Dik WA, Brahim W, Braun C, et al. CALM-AF10+ T-ALL expression profiles are characterized by overexpression of HOXA and BMI1 oncogenes. *Leukemia*. 2005;19(11):1948-1957.
52. Larmonie NS, Dik WA, Beverloo HB, van Wering ER, van Dongen JJ, Langerak AW. BMI1 as oncogenic candidate in a novel TCRB-associated chromosomal aberration in a patient with TCRgammadelta+ T-cell acute lymphoblastic leukemia. *Leukemia*. 2008;22(6):1266-1267.
53. Van Vlierberghe P, Ambesi-Impiombato A, De Keersmaecker K, et al. Prognostic relevance of integrated genetic profiling in adult T-cell acute lymphoblastic leukemia. *Blood*. 2013;122(1):74-82.
54. Mullighan CG, Goorha S, Radtke I, et al. Genome-wide analysis of genetic alterations in acute lymphoblastic leukaemia. *Nature*. 2007;446(7137):758-764.
55. Remke M, Pfister S, Kox C, et al. High-resolution genomic profiling of childhood T-ALL reveals frequent copy-number alterations affecting the TGF-beta and PI3K-AKT pathways and deletions at 6q15-16.1 as a genomic marker for unfavorable early treatment response. *Blood*. 2009;114(5):1053-1062.
56. Pilozzi E, Muller-Hermelink HK, Falini B, et al. Gene rearrangements in T-cell lymphoblastic lymphoma. *Journal of Pathology*. 1999;188(3):267-270.
57. Szczepanski T, Pongers-Willemse MJ, Langerak AW, et al. Ig heavy chain gene rearrangements in T-cell acute lymphoblastic leukemia exhibit predominant DH6-19 and DH7-27 gene usage, can result in complete V-D-J rearrangements, and are rare in T-cell receptor alpha beta lineage. *Blood*. 1999;93(12):4079-4085.
58. Graux C, Cools J, Michaux L, Vandenberghe P, Hagemeijer A. Cytogenetics and molecular genetics of T-cell acute lymphoblastic leukemia: from thymocyte to lymphoblast. *Leukemia*. 2006;20(9):1496-1510.
59. Han X, Bueso-Ramos CE. Precursor T-cell acute lymphoblastic leukemia/lymphoblastic lymphoma and acute biphenotypic leukemias. *American Journal of Clinical Pathology*. 2007;127(4):528-544.
60. Royer-Pokora B, Loos U, Ludwig WD. TTG-2, a new gene encoding a cysteine-rich protein with the LIM motif, is overexpressed in acute T-cell leukaemia with the t(11;14)(p13;q11). *Oncogene*. 1991;6(10):1887-1893.
61. McGuire EA, Hockett RD, Pollock KM, Bartholdi MF, O'Brien SJ, Korsmeyer SJ. The t(11;14)(p15;q11) in a T-cell acute lymphoblastic leukemia cell line activates multiple transcripts, including Ttg-1, a gene encoding a potential zinc finger protein. *Mol Cell Biol*. 1989;9(5):2124-2132.
62. Xia Y, Brown L, Yang CY, et al. TAL2, a helix-loop-helix gene activated by the (7;9)(q34;q32) translocation in human T-cell leukemia. *Proc Natl Acad Sci U S A*. 1991;88(24):11416-11420.
63. Begley CG, Aplan PD, Davey MP, et al. Chromosomal translocation in a human leukemic stem-cell line disrupts the T-cell antigen receptor delta-chain diversity region and results in a previously unreported fusion transcript. *Proc Natl Acad Sci U S A*. 1989;86(6):2031-2035.

64. Mellentin JD, Smith SD, Cleary ML. lyl-1, a novel gene altered by chromosomal translocation in T cell leukemia, codes for a protein with a helix-loop-helix DNA binding motif. *Cell*. 1989;58(1):77-83.
65. Homminga I, Pieters R, Langerak AW, et al. Integrated transcript and genome analyses reveal NKX2-1 and MEF2C as potential oncogenes in T cell acute lymphoblastic leukemia. *Cancer Cell*. 2011;19(4):484-497.
66. Mansour MR, Abraham BJ, Anders L, et al. Oncogene regulation. An oncogenic super-enhancer formed through somatic mutation of a noncoding intergenic element. *Science*. 2014;346(6215):1373-1377.
67. Chen Q, Yang CY, Tsan JT, et al. Coding sequences of the tal-1 gene are disrupted by chromosome translocation in human T cell leukemia. *J Exp Med*. 1990;172(5):1403-1408.
68. Bernard O, Guglielmi P, Jonveaux P, et al. Two distinct mechanisms for the SCL gene activation in the t(1;14) translocation of T-cell leukemias. *Genes Chromosomes Cancer*. 1990;1(3):194-208.
69. Kwiatkowski N, Zhang T, Rahl PB, et al. Targeting transcription regulation in cancer with a covalent CDK7 inhibitor. *Nature*. 2014;511(7511):616-620.
70. Clappier E, Cuccuini W, Kalota A, et al. The C-MYB locus is involved in chromosomal translocation and genomic duplications in human T-cell acute leukemia (T-ALL), the translocation defining a new T-ALL subtype in very young children. *Blood*. 2007;110(4):1251-1261.
71. Lahortiga I, De Keersmaecker K, Van Vlierberghe P, et al. Duplication of the MYB oncogene in T cell acute lymphoblastic leukemia. *Nat Genet*. 2007;39(5):593-595.
72. O'Neil J, Tchinda J, Gutierrez A, et al. Alu elements mediate MYB gene tandem duplication in human T-ALL. *J Exp Med*. 2007;204(13):3059-3066.
73. Dang CV. MYC on the path to cancer. *Cell*. 2012;149(1):22-35.
74. Nie Z, Hu G, Wei G, et al. c-Myc is a universal amplifier of expressed genes in lymphocytes and embryonic stem cells. *Cell*. 2012;151(1):68-79.
75. Lin CY, Loven J, Rahl PB, et al. Transcriptional amplification in tumor cells with elevated c-Myc. *Cell*. 2012;151(1):56-67.
76. Dose M, Khan I, Guo Z, et al. c-Myc mediates pre-TCR-induced proliferation but not developmental progression. *Blood*. 2006;108(8):2669-2677.
77. Weng AP, Millholland JM, Yashiro-Ohtani Y, et al. c-Myc is an important direct target of Notch1 in T-cell acute lymphoblastic leukemia/lymphoma. *Genes Dev*. 2006;20(15):2096-2109.
78. Palomero T, Lim WK, Odom DT, et al. NOTCH1 directly regulates c-MYC and activates a feed-forward-loop transcriptional network promoting leukemic cell growth. *Proc Natl Acad Sci U S A*. 2006;103(48):18261-18266.
79. Sharma VM, Calvo JA, Draheim KM, et al. Notch1 contributes to mouse T-cell leukemia by directly inducing the expression of c-myc. *Mol Cell Biol*. 2006;26(21):8022-8031.
80. Yashiro-Ohtani Y, Wang H, Zang C, et al. Long-range enhancer activity determines Myc sensitivity to Notch inhibitors in T cell leukemia. *Proc Natl Acad Sci U S A*. 2014;111(46):E4946-4953.
81. Herranz D, Ambesi-Impiombato A, Palomero T, et al. A NOTCH1-driven MYC enhancer promotes T cell development, transformation and acute lymphoblastic leukemia. *Nat Med*. 2014;20(10):1130-1137.

82. Yada M, Hatakeyama S, Kamura T, et al. Phosphorylation-dependent degradation of c-Myc is mediated by the F-box protein Fbw7. *EMBO J*. 2004;23(10):2116-2125.
83. Welcker M, Orian A, Jin J, et al. The Fbw7 tumor suppressor regulates glycogen synthase kinase 3 phosphorylation-dependent c-Myc protein degradation. *Proc Natl Acad Sci U S A*. 2004;101(24):9085-9090.
84. O'Neil J, Grim J, Strack P, et al. FBW7 mutations in leukemic cells mediate NOTCH pathway activation and resistance to gamma-secretase inhibitors. *J Exp Med*. 2007;204(8):1813-1824.
85. Thompson BJ, Buonamici S, Sulis ML, et al. The SCFFBW7 ubiquitin ligase complex as a tumor suppressor in T cell leukemia. *Journal of Experimental Medicine*. 2007;204(8):1825-1835.
86. Asnafi V, Radford-Weiss I, Dastugue N, et al. CALM-AF10 is a common fusion transcript in T-ALL and is specific to the TCR-gamma delta lineage. *Blood*. 2003;102(3):1000-1006.
87. Armstrong SA, Staunton JE, Silverman LB, et al. MLL translocations specify a distinct gene expression profile that distinguishes a unique leukemia. *Nature Genetics*. 2002;30(1):41-47.
88. Faber J, Krivtsov AV, Stubbs MC, et al. HOXA9 is required for survival in human MLL-rearranged acute leukemias. *Blood*. 2009;113(11):2375-2385.
89. Rozovskaia T, Feinstein E, Mor O, et al. Upregulation of Meis1 and HoxA9 in acute lymphocytic leukemias with the t(4 : 11) abnormality. *Oncogene*. 2001;20(7):874-878.
90. Speleman F, Cauwelier B, Dastugue N, et al. A new recurrent inversion, inv(7)(p15q34), leads to transcriptional activation of HOXA10 and HOXA11 in a subset of T-cell acute lymphoblastic leukemias. *Leukemia*. 2005;19(3):358-366.
91. Hatano M, Roberts CW, Minden M, Crist WM, Korsmeyer SJ. Deregulation of a homeobox gene, HOX11, by the t(10;14) in T cell leukemia. *Science*. 1991;253(5015):79-82.
92. Bernard OA, Busson-LeConiat M, Ballerini P, et al. A new recurrent and specific cryptic translocation, t(5;14)(q35;q32), is associated with expression of the Hox11L2 gene in T acute lymphoblastic leukemia. *Leukemia*. 2001;15(10):1495-1504.
93. Ferrando AA, Neuberg DS, Dodge RK, et al. Prognostic importance of TLX1 (HOX11) oncogene expression in adults with T-cell acute lymphoblastic leukaemia. *Lancet*. 2004;363(9408):535-536.
94. Ferrando AA, Neuberg DS, Staunton J, et al. Gene expression signatures define novel oncogenic pathways in T cell acute lymphoblastic leukemia. *Cancer Cell*. 2002;1(1):75-87.
95. Ito Y. RUNX genes in development and cancer: Regulation of viral gene expression and the discovery of RUNX family genes. *Advances in Cancer Research, Vol 99*. 2008;99:33-+.
96. Hilton MJ, Tu XL, Wu XM, et al. Notch signaling maintains bone marrow mesenchymal progenitors by suppressing osteoblast differentiation. *Nature Medicine*. 2008;14(3):306-314.
97. Ito K, Lim ACB, Salto-Tellez M, et al. RUNX3 attenuates beta-catenin/T cell factors in intestinal tumorigenesis. *Cancer Cell*. 2008;14(3):226-237.
98. Pratap J, Wixted JJ, Gaur T, et al. Runx2 transcriptional activation of Indian Hedgehog and a downstream bone metastatic pathway in breast cancer cells. *Cancer Research*. 2008;68(19):7795-7802.
99. Min B, Kim MK, Zhang JW, et al. Identification of RUNX3 as a component of the MST/Hpo signaling pathway. *Journal of Cellular Physiology*. 2012;227(2):839-849.

100. Yagi R, Chen LF, Shigesada K, Murakami Y, Ito Y. A WW domain-containing Yes-associated protein (YAP) is a novel transcriptional co-activator. *Embo Journal*. 1999;18(9):2551-2562.
101. Ito Y, Miyazono K. RUNX transcription factors as key targets of TGF-beta superfamily signaling. *Current Opinion in Genetics & Development*. 2003;13(1):43-47.
102. Huang H, Woo AJ, Waldon Z, et al. A Src family kinase-Shp2 axis controls RUNX1 activity in megakaryocyte and T-lymphocyte differentiation. *Genes & Development*. 2012;26(14):1587-1601.
103. Tahirov TH, Inoue-Bungo T, Morii H, et al. Structural analyses of DNA recognition by the AML1/Runx-1 Runt domain and its allosteric control by CBFbeta. *Cell*. 2001;104(5):755-767.
104. Kim WY, Sieweke M, Ogawa E, et al. Mutual activation of Ets-1 and AML1 DNA binding by direct interaction of their autoinhibitory domains. *Embo Journal*. 1999;18(6):1609-1620.
105. Pozner A, Goldenberg D, Negreanu V, et al. Transcription-coupled translation control of AML1/RUNX1 is mediated by cap- and internal ribosome entry site-dependent mechanisms. *Molecular and Cellular Biology*. 2000;20(7):2297-2307.
106. Levanon D, Groner Y. Structure and regulated expression of mammalian RUNX genes. *Oncogene*. 2004;23(24):4211-4219.
107. Draper JE, Sroczynska P, Tsoulaki O, et al. RUNX1B Expression Is Highly Heterogeneous and Distinguishes Megakaryocytic and Erythroid Lineage Fate in Adult Mouse Hematopoiesis. *Plos Genetics*. 2016;12(1).
108. Yu M, Mazor T, Huang H, et al. Direct Recruitment of Polycomb Repressive Complex 1 to Chromatin by Core Binding Transcription Factors. *Molecular Cell*. 2012;45(3):330-343.
109. Guo H, Friedman AD. Phosphorylation of RUNX1 by Cyclin-dependent Kinase Reduces Direct Interaction with HDAC1 and HDAC3. *Journal of Biological Chemistry*. 2011;286(1):208-215.
110. Huang G, Zhao X, Wang L, et al. The ability of MLL to bind RUNX1 and methylate H3K4 at PU.1 regulatory regions is impaired by MDS/AML-associated RUNX1/AML1 mutations. *Blood*. 2011;118(25):6544-6552.
111. Kitabayashi I, Aikawa Y, Nguyen LA, Yokoyama A, Ohki M. Activation of AML1-mediated transcription by MOZ and inhibition by the MOZ-CBP fusion protein. *EMBO J*. 2001;20(24):7184-7196.
112. Wee HJ, Voon DC, Bae SC, Ito Y. PEBP2-beta/CBF-beta-dependent phosphorylation of RUNX1 and p300 by HIPK2: implications for leukemogenesis. *Blood*. 2008;112(9):3777-3787.
113. Okuda T, van Deursen J, Hiebert SW, Grosveld G, Downing JR. AML1, the target of multiple chromosomal translocations in human leukemia, is essential for normal fetal liver hematopoiesis. *Cell*. 1996;84(2):321-330.
114. Takakura N, Watanabe T, Suenobu S, et al. A role for hematopoietic stem cells in promoting angiogenesis. *Cell*. 2000;102(2):199-209.
115. North TE, de Bruijn MF, Stacy T, et al. Runx1 expression marks long-term repopulating hematopoietic stem cells in the midgestation mouse embryo. *Immunity*. 2002;16(5):661-672.
116. Cai Z, de Bruijn M, Ma X, et al. Haploinsufficiency of AML1 affects the temporal and spatial generation of hematopoietic stem cells in the mouse embryo. *Immunity*. 2000;13(4):423-431.

117. Wang Q, Stacy T, Miller JD, et al. The CBFbeta subunit is essential for CBFalpha2 (AML1) function in vivo. *Cell*. 1996;87(4):697-708.
118. Ichikawa M, Asai T, Saito T, et al. AML-1 is required for megakaryocytic maturation and lymphocytic differentiation, but not for maintenance of hematopoietic stem cells in adult hematopoiesis. *Nat Med*. 2004;10(3):299-304.
119. Growney JD, Shigematsu H, Li Z, et al. Loss of Runx1 perturbs adult hematopoiesis and is associated with a myeloproliferative phenotype. *Blood*. 2005;106(2):494-504.
120. Motoda L, Osato M, Yamashita N, et al. Runx1 protects hematopoietic stem/progenitor cells from oncogenic insult. *Stem Cells*. 2007;25(12):2976-2986.
121. Putz G, Rosner A, Nuesslein I, Schmitz N, Buchholz F. AML1 deletion in adult mice causes splenomegaly and lymphomas. *Oncogene*. 2006;25(6):929-939.
122. Schnittger S, Dicker F, Kern W, et al. RUNX1 mutations are frequent in de novo AML with noncomplex karyotype and confer an unfavorable prognosis. *Blood*. 2011;117(8):2348-2357.
123. Hong D, Gupta R, Ancliff P, et al. Initiating and cancer-propagating cells in TEL-AML1-associated childhood leukemia. *Science*. 2008;319(5861):336-339.
124. Anderson K, Lutz C, van Delft FW, et al. Genetic variegation of clonal architecture and propagating cells in leukaemia. *Nature*. 2011;469(7330):356-361.
125. Jacob B, Osato M, Yamashita N, et al. Stem cell exhaustion due to Runx1 deficiency is prevented by Evi5 activation in leukemogenesis. *Blood*. 2010;115(8):1610-1620.
126. Chen MJ, Yokomizo T, Zeigler BM, Dzierzak E, Speck NA. Runx1 is required for the endothelial to haematopoietic cell transition but not thereafter. *Nature*. 2009;457(7231):887-891.
127. Cai X, Gaudet JJ, Mangan JK, et al. Runx1 loss minimally impacts long-term hematopoietic stem cells. *PLoS One*. 2011;6(12):e28430.
128. Cai X, Gao L, Teng L, et al. Runx1 Deficiency Decreases Ribosome Biogenesis and Confers Stress Resistance to Hematopoietic Stem and Progenitor Cells. *Cell Stem Cell*. 2015;17(2):165-177.
129. Wang CQ, Motoda L, Satake M, et al. Runx3 deficiency results in myeloproliferative disorder in aged mice. *Blood*. 2013;122(4):562-566.
130. Wang CQ, Krishnan V, Tay LS, et al. Disruption of Runx1 and Runx3 leads to bone marrow failure and leukemia predisposition due to transcriptional and DNA repair defects. *Cell Rep*. 2014;8(3):767-782.
131. Satpathy AT, Briseno CG, Cai X, et al. Runx1 and Cbfbeta regulate the development of Flt3+ dendritic cell progenitors and restrict myeloproliferative disorder. *Blood*. 2014;123(19):2968-2977.
132. Wang CQ, Chin DW, Chooi JY, et al. Cbfb deficiency results in differentiation blocks and stem/progenitor cell expansion in hematopoiesis. *Leukemia*. 2015;29(3):753-757.
133. Tober J, Yzaguirre AD, Piwarzyk E, Speck NA. Distinct temporal requirements for Runx1 in hematopoietic progenitors and stem cells. *Development*. 2013;140(18):3765-3776.
134. Hayashi K, Natsume W, Watanabe T, et al. Diminution of the AML1 Transcription Factor Function Causes Differential Effects on the Fates of CD4 and CD8 Single-Positive T Cells. *The Journal of Immunology*. 2000;165(12):6816-6824.
135. Shimizu C, Kawamoto H, Yamashita M, et al. Progression of T cell lineage restriction in the earliest subpopulation of murine adult thymus visualized by the expression of lck proximal promoter activity. *Int Immunol*. 2001;13(1):105-117.

136. Masuda K, Kakugawa K, Nakayama T, Minato N, Katsura Y, Kawamoto H. T cell lineage determination precedes the initiation of TCR beta gene rearrangement. *J Immunol*. 2007;179(6):3699-3706.
137. Taniuchi I, Osato M, Egawa T, et al. Differential requirements for Runx proteins in CD4 repression and epigenetic silencing during T lymphocyte development. *Cell*. 2002;111(5):621-633.
138. Egawa T, Tillman RE, Naoe Y, Taniuchi I, Littman DR. The role of the Runx transcription factors in thymocyte differentiation and in homeostasis of naive T cells. *J Exp Med*. 2007;204(8):1945-1957.
139. Naoe Y, Setoguchi R, Akiyama K, et al. Repression of interleukin-4 in T helper type 1 cells by Runx/Cbf beta binding to the Il4 silencer. *J Exp Med*. 2007;204(8):1749-1755.
140. Setoguchi R, Tachibana M, Naoe Y, et al. Repression of the transcription factor Th-POK by Runx complexes in cytotoxic T cell development. *Science*. 2008;319(5864):822-825.
141. Wong WF, Nakazato M, Watanabe T, et al. Over-expression of Runx1 transcription factor impairs the development of thymocytes from the double-negative to double-positive stages. *Immunology*. 2010;130(2):243-253.
142. Carow B, Gao Y, Coquet J, Reilly M, Rottenberg ME. lck-Driven Cre Expression Alters T Cell Development in the Thymus and the Frequencies and Functions of Peripheral T Cell Subsets. *J Immunol*. 2016;197(6):2261-2268.
143. Kawazu M, Asai T, Ichikawa M, et al. Functional domains of Runx1 are differentially required for CD4 repression, TCRbeta expression, and CD4/8 double-negative to CD4/8 double-positive transition in thymocyte development. *J Immunol*. 2005;174(6):3526-3533.
144. Nishimura M, Fukushima-Nakase Y, Fujita Y, et al. VWRPY motif-dependent and -independent roles of AML1/Runx1 transcription factor in murine hematopoietic development. *Blood*. 2004;103(2):562-570.
145. Vaillant F, Blyth K, Andrew L, Neil JC, Cameron ER. Enforced expression of Runx2 perturbs T cell development at a stage coincident with beta-selection. *J Immunol*. 2002;169(6):2866-2874.
146. Talebian L, Li Z, Guo Y, et al. T-lymphoid, megakaryocyte, and granulocyte development are sensitive to decreases in CBFbeta dosage. *Blood*. 2007;109(1):11-21.
147. Guo Y, Maillard I, Chakraborti S, Rothenberg EV, Speck NA. Core binding factors are necessary for natural killer cell development and cooperate with Notch signaling during T-cell specification. *Blood*. 2008;112(3):480-492.
148. Kueh HY, Yui MA, Ng KK, et al. Asynchronous combinatorial action of four regulatory factors activates Bcl11b for T cell commitment. *Nat Immunol*. 2016;17(8):956-965.
149. Harada Y, Harada H. Molecular pathways mediating MDS/AML with focus on AML1/RUNX1 point mutations. *J Cell Physiol*. 2009;220(1):16-20.
150. Owen CJ, Toze CL, Koochin A, et al. Five new pedigrees with inherited RUNX1 mutations causing familial platelet disorder with propensity to myeloid malignancy. *Blood*. 2008;112(12):4639-4645.
151. Preudhomme C, Renneville A, Bourdon V, et al. High frequency of RUNX1 biallelic alteration in acute myeloid leukemia secondary to familial platelet disorder. *Blood*. 2009;113(22):5583-5587.
152. Nishimoto N, Imai Y, Ueda K, et al. T cell acute lymphoblastic leukemia arising from familial platelet disorder. *Int J Hematol*. 2010;92(1):194-197.

153. Buijs A, Poddighe P, van Wijk R, et al. A novel CBFA2 single-nucleotide mutation in familial platelet disorder with propensity to develop myeloid malignancies. *Blood*. 2001;98(9):2856-2858.
154. Arepally G, Rebbeck TR, Song W, Gilliland G, Maris JM, Poncz M. Evidence for genetic homogeneity in a familial platelet disorder with predisposition to acute myelogenous leukemia (FPD/AML). *Blood*. 1998;92(7):2600-2602.
155. Song WJ, Sullivan MG, Legare RD, et al. Haploinsufficiency of CBFA2 causes familial thrombocytopenia with propensity to develop acute myelogenous leukaemia. *Nat Genet*. 1999;23(2):166-175.
156. Michaud J, Wu F, Osato M, et al. In vitro analyses of known and novel RUNX1/AML1 mutations in dominant familial platelet disorder with predisposition to acute myelogenous leukemia: implications for mechanisms of pathogenesis. *Blood*. 2002;99(4):1364-1372.
157. Beri-Dexheimer M, Latger-Cannard V, Philippe C, et al. Clinical phenotype of germline RUNX1 haploinsufficiency: from point mutations to large genomic deletions. *Eur J Hum Genet*. 2008;16(8):1014-1018.
158. Kirito K, Sakoe K, Shinoda D, Takiyama Y, Kaushansky K, Komatsu N. A novel RUNX1 mutation in familial platelet disorder with propensity to develop myeloid malignancies. *Haematologica*. 2008;93(1):155-156.
159. Churpek JE, Garcia JS, Madzo J, Jackson SA, Onel K, Godley LA. Identification and molecular characterization of a novel 3′ mutation in RUNX1 in a family with familial platelet disorder. *Leuk Lymphoma*. 2010;51(10):1931-1935.
160. van der Crabben S, van Binsbergen E, Ausems M, Poot M, Bierings M, Buijs A. Constitutional RUNX1 deletion presenting as non-syndromic thrombocytopenia with myelodysplasia: 21q22 ITSN1 as a candidate gene in mental retardation. *Leuk Res*. 2010;34(1):e8-12.
161. Jongmans MC, Kuiper RP, Carmichael CL, et al. Novel RUNX1 mutations in familial platelet disorder with enhanced risk for acute myeloid leukemia: clues for improved identification of the FPD/AML syndrome. *Leukemia*. 2010;24(1):242-246.
162. Shinawi M, Erez A, Shardy DL, et al. Syndromic thrombocytopenia and predisposition to acute myelogenous leukemia caused by constitutional microdeletions on chromosome 21q. *Blood*. 2008;112(4):1042-1047.
163. Katzaki E, Morin G, Pollazzon M, et al. Syndromic mental retardation with thrombocytopenia due to 21q22.11q22.12 deletion: Report of three patients. *Am J Med Genet A*. 2010;152A(7):1711-1717.
164. Giambra V, Jenkins CR, Wang H, et al. NOTCH1 promotes T cell leukemia-initiating activity by RUNX-mediated regulation of PKC-theta and reactive oxygen species. *Nat Med*. 2012;18(11):1693-1698.
165. Jalagadugula G, Mao G, Kaur G, Dhanasekaran DN, Rao AK. Platelet protein kinase C-theta deficiency with human RUNX1 mutation: PRKCQ is a transcriptional target of RUNX1. *Arterioscler Thromb Vasc Biol*. 2011;31(4):921-927.
166. Miyoshi H, Shimizu K, Kozu T, Maseki N, Kaneko Y, Ohki M. t(8;21) breakpoints on chromosome 21 in acute myeloid leukemia are clustered within a limited region of a single gene, AML1. *Proc Natl Acad Sci U S A*. 1991;88(23):10431-10434.

167. Moorman AV, Ensor HM, Richards SM, et al. Prognostic effect of chromosomal abnormalities in childhood B-cell precursor acute lymphoblastic leukaemia: results from the UK Medical Research Council ALL97/99 randomised trial. *Lancet Oncol*. 2010;11(5):429-438.
168. Harewood L, Robinson H, Harris R, et al. Amplification of AML1 on a duplicated chromosome 21 in acute lymphoblastic leukemia: a study of 20 cases. *Leukemia*. 2003;17(3):547-553.
169. Grossmann V, Haferlach C, Weissmann S, et al. The molecular profile of adult T-cell acute lymphoblastic leukemia: mutations in RUNX1 and DNMT3A are associated with poor prognosis in T-ALL. *Genes Chromosomes Cancer*. 2013;52(4):410-422.
170. Mok MM, Du L, Wang CQ, et al. RUNX1 point mutations potentially identify a subset of early immature T-cell acute lymphoblastic leukaemia that may originate from differentiated T-cells. *Gene*. 2014;545(1):111-116.
171. Cleveland SM, Goodings C, Tripathi RM, et al. LMO2 induces T-cell leukemia with epigenetic deregulation of CD4. *Exp Hematol*. 2014;42(7):581-593 e585.
172. Hnisz D, Weintraub AS, Day DS, et al. Activation of proto-oncogenes by disruption of chromosome neighborhoods. *Science*. 2016;351(6280):1454-1458.
173. Wong WF, Looi CY, Kon S, et al. T-cell receptor signaling induces proximal Runx1 transactivation via a calcineurin-NFAT pathway. *European Journal of Immunology*. 2014;44(3):894-904.
174. Medyouf H, Alcalde H, Berthier C, et al. Targeting calcineurin activation as a therapeutic strategy for T-cell acute lymphoblastic leukemia. *Nature Medicine*. 2007;13(6):736-741.
175. Shimizu K, Yamagata K, Kurokawa M, Mizutani S, Tsunematsu Y, Kitabayashi I. Roles of AML1/RUNX1 in T-cell malignancy induced by loss of p53. *Cancer Science*. 2013;104(8):1033-1038.
176. Pollak MN, Schernhammer ES, Hankinson SE. Insulin-like growth factors and neoplasia. *Nat Rev Cancer*. 2004;4(7):505-518.
177. Baker J, Liu JP, Robertson EJ, Efstratiadis A. Role of insulin-like growth factors in embryonic and postnatal growth. *Cell*. 1993;75(1):73-82.
178. Bendall SC, Stewart MH, Menendez P, et al. IGF and FGF cooperatively establish the regulatory stem cell niche of pluripotent human cells in vitro. *Nature*. 2007;448(7157):1015-1021.
179. Ivanova NB, Dimos JT, Schaniel C, Hackney JA, Moore KA, Lemischka IR. A Stem Cell Molecular Signature. *Science*. 2002;298(5593):601-604.
180. Barbieri M, Bonafe M, Franceschi C, Paolisso G. Insulin/IGF-I-signaling pathway: an evolutionarily conserved mechanism of longevity from yeast to humans. *Am J Physiol Endocrinol Metab*. 2003;285(5):E1064-1071.
181. De Meyts P. Insulin and its receptor: structure, function and evolution. *Bioessays*. 2004;26(12):1351-1362.
182. Garofalo RS. Genetic analysis of insulin signaling in Drosophila. *Trends Endocrinol Metab*. 2002;13(4):156-162.
183. Belfiore A, Frasca F, Pandini G, Sciacca L, Vigneri R. Insulin receptor isoforms and insulin receptor/insulin-like growth factor receptor hybrids in physiology and disease. *Endocr Rev*. 2009;30(6):586-623.
184. Benyoucef S, Surinya KH, Hadaschik D, Siddle K. Characterization of insulin/IGF hybrid receptors: contributions of the insulin receptor L2 and Fn1 domains and the alternatively

spliced exon 11 sequence to ligand binding and receptor activation. *Biochem J*. 2007;403(3):603-613.
185. LeRoith D. Editorial: Insulin-Like Growth Factor I Receptor Signaling-Overlapping or Redundant Pathways? *Endocrinology*. 2000;141(4):1287-1288.
186. Kavran JM, McCabe JM, Byrne PO, et al. How IGF-1 activates its receptor. *Elife*. 2014;3.
187. Dews M, Prisco M, Peruzzi F, Romano G, Morrione A, Baserga R. Domains of the insulin-like growth factor I receptor required for the activation of extracellular signal-regulated kinases. *Endocrinology*. 2000;141(4):1289-1300.
188. Sell C, Rubini M, Rubin R, Liu JP, Efstratiadis A, Baserga R. Simian virus 40 large tumor antigen is unable to transform mouse embryonic fibroblasts lacking type 1 insulin-like growth factor receptor. *Proc Natl Acad Sci U S A*. 1993;90(23):11217-11221.
189. Myal Y, Shiu RP, Bhaumick B, Bala M. Receptor binding and growth-promoting activity of insulin-like growth factors in human breast cancer cells (T-47D) in culture. *Cancer Res*. 1984;44(12 Pt 1):5486-5490.
190. Gallagher EJ, LeRoith D. Minireview: IGF, Insulin, and Cancer. *Endocrinology*. 2011;152(7):2546-2551.
191. Baier TG, Ludwig WD, Schonberg D, Hartmann KK. Characterisation of insulin-like growth factor I receptors of human acute lymphoblastic leukaemia (ALL) cell lines and primary ALL cells. *Eur J Cancer*. 1992;28A(6-7):1105-1110.
192. Karrman K, Kjeldsen E, Lassen C, et al. The t(X;7)(q22;q34) in paediatric T-cell acute lymphoblastic leukaemia results in overexpression of the insulin receptor substrate 4 gene through illegitimate recombination with the T-cell receptor beta locus. *Br J Haematol*. 2009;144(4):546-551.
193. Baier TG, Jenne EW, Blum W, Schonberg D, Hartmann KK. Influence of antibodies against IGF-I, insulin or their receptors on proliferation of human acute lymphoblastic leukemia cell lines. *Leuk Res*. 1992;16(8):807-814.
194. Huang Z, Fang Z, Zhen H, Zhou L, Amin HM, Shi P. Inhibition of type I insulin-like growth factor receptor tyrosine kinase by picropodophyllin induces apoptosis and cell cycle arrest in T lymphoblastic leukemia/lymphoma. *Leuk Lymphoma*. 2014;55(8):1876-1883.
195. Leclerc GM, Leclerc GJ, Fu G, Barredo JC. AMPK-induced activation of Akt by AICAR is mediated by IGF-1R dependent and independent mechanisms in acute lymphoblastic leukemia. *J Mol Signal*. 2010;5:15.
196. Chapuis N, Tamburini J, Cornillet-Lefebvre P, et al. Autocrine IGF-1/IGF-1R signalling is responsible for constitutive PI3K/Akt activation in acute myeloid leukemia: therapeutic value of neutralizing anti-IGF-1R antibody. *Haematologica*. 2010;95(3):415-423.
197. Doepfner KT, Spertini O, Arcaro A. Autocrine insulin-like growth factor-I signaling promotes growth and survival of human acute myeloid leukemia cells via the phosphoinositide 3-kinase//Akt pathway. *Leukemia*. 2007;21(9):1921-1930.
198. Tazzari PL, Tabellini G, Bortul R, et al. The insulin-like growth factor-I receptor kinase inhibitor NVP-AEW541 induces apoptosis in acute myeloid leukemia cells exhibiting autocrine insulin-like growth factor-I secretion. *Leukemia*. 2007;21(5):886-896.
199. Wahner Hendrickson AE, Haluska P, Schneider PA, et al. Expression of Insulin Receptor Isoform A and Insulin-like Growth Factor-1 Receptor in Human Acute Myelogenous Leukemia:

Effect of the Dual-Receptor Inhibitor BMS-536924 In vitro. *Cancer Res*. 2009;69(19):7635-7643.
200. Gu TL, Nardone J, Wang Y, et al. Survey of activated FLT3 signaling in leukemia. *PLoS One*. 2011;6(4):e19169.
201. Chapuis N, Lacombe C, Tamburini J, Bouscary D, Mayeux P. Insulin Receptor A and IGF-1R in AML – Letter. *Cancer Research*. 2010;70(17):7010.
202. Wahner Hendrickson AE, Haluska P, Erlichman C, et al. Insulin Receptor A and IGF-IR in AML – Response. *Cancer Research*. 2010;70(17):7010.
203. Fire A, Xu S, Montgomery MK, Kostas SA, Driver SE, Mello CC. Potent and specific genetic interference by double-stranded RNA in Caenorhabditis elegans. *Nature*. 1998;391(6669):806-811.
204. Elbashir SM, Harborth J, Lendeckel W, Yalcin A, Weber K, Tuschl T. Duplexes of 21-nucleotide RNAs mediate RNA interference in cultured mammalian cells. *Nature*. 2001;411(6836):494-498.
205. Hannon GJ, Rossi JJ. Unlocking the potential of the human genome with RNA interference. *Nature*. 2004;431(7006):371-378.
206. Amarzguioui M, Rossi JJ, Kim D. Approaches for chemically synthesized siRNA and vector-mediated RNAi. *FEBS Lett*. 2005;579(26):5974-5981.
207. Brummelkamp TR, Bernards R, Agami R. A system for stable expression of short interfering RNAs in mammalian cells. *Science*. 2002;296(5567):550-553.
208. Paddison PJ, Caudy AA, Bernstein E, Hannon GJ, Conklin DS. Short hairpin RNAs (shRNAs) induce sequence-specific silencing in mammalian cells. *Genes Dev*. 2002;16(8):948-958.
209. Sarnow P, Jopling CL, Norman KL, Schutz S, Wehner KA. MicroRNAs: expression, avoidance and subversion by vertebrate viruses. *Nat Rev Microbiol*. 2006;4(9):651-659.
210. Silva JM, Li MZ, Chang K, et al. Second-generation shRNA libraries covering the mouse and human genomes. *Nat Genet*. 2005;37(11):1281-1288.
211. Sauer B, Henderson N. Site-specific DNA recombination in mammalian cells by the Cre recombinase of bacteriophage P1. *Proc Natl Acad Sci U S A*. 1988;85(14):5166-5170.
212. Orban PC, Chui D, Marth JD. Tissue- and site-specific DNA recombination in transgenic mice. *Proc Natl Acad Sci U S A*. 1992;89(15):6861-6865.
213. Gu H, Marth JD, Orban PC, Mossmann H, Rajewsky K. Deletion of a DNA polymerase beta gene segment in T cells using cell type-specific gene targeting. *Science*. 1994;265(5168):103-106.
214. Kuhn R, Schwenk F, Aguet M, Rajewsky K. Inducible gene targeting in mice. *Science*. 1995;269(5229):1427-1429.
215. Capecchi MR. Generating mice with targeted mutations. *Nat Med*. 2001;7(10):1086-1090.
216. Huntly BJ, Gilliland DG. Leukaemia stem cells and the evolution of cancer-stem-cell research. *Nat Rev Cancer*. 2005;5(4):311-321.
217. Krivtsov AV, Twomey D, Feng Z, et al. Transformation from committed progenitor to leukaemia stem cell initiated by MLL-AF9. *Nature*. 2006;442(7104):818-822.
218. Muntean AG, Hess JL. The Pathogenesis of Mixed-Lineage Leukemia. *Annual Review of Pathology: Mechanisms of Disease*. 2012;7(1):null.

219. Corral J, Lavenir I, Impey H, et al. An Mll-AF9 fusion gene made by homologous recombination causes acute leukemia in chimeric mice: a method to create fusion oncogenes. *Cell*. 1996;85(6):853-861.
220. Somervaille TCP, Cleary ML. Identification and characterization of leukemia stem cells in murine MLL-AF9 acute myeloid leukemia. *Cancer Cell*. 2006;10(4):257-268.
221. Martin ME, Milne TA, Bloyer S, et al. Dimerization of MLL fusion proteins immortalizes hematopoietic cells. *Cancer Cell*. 2003;4(3):197-207.
222. Chen W, Kumar AR, Hudson WA, et al. Malignant transformation initiated by Mll-AF9: gene dosage and critical target cells. *Cancer Cell*. 2008;13(5):432-440.
223. Barabe F, Kennedy JA, Hope KJ, Dick JE. Modeling the initiation and progression of human acute leukemia in mice. *Science*. 2007;316(5824):600-604.
224. Jo SY, Granowicz EM, Maillard I, Thomas D, Hess JL. Requirement for Dot1l in murine postnatal hematopoiesis and leukemogenesis by MLL translocation. *Blood*. 2011;117(18):4759-4768.
225. Kuntimaddi A, Achille NJ, Thorpe J, et al. Degree of recruitment of DOT1L to MLL-AF9 defines level of H3K79 Di- and tri-methylation on target genes and transformation potential. *Cell Rep*. 2015;11(5):808-820.
226. Nguyen AT, Taranova O, He J, Zhang Y. DOT1L, the H3K79 methyltransferase, is required for MLL-AF9-mediated leukemogenesis. *Blood*. 2011;117(25):6912-6922.
227. Wang Y, Krivtsov AV, Sinha AU, et al. The Wnt/{beta}-Catenin Pathway Is Required for the Development of Leukemia Stem Cells in AML. *Science*. 2010;327(5973):1650-1653.
228. Holzenberger M, Leneuve P, Hamard G, et al. A targeted partial invalidation of the insulin-like growth factor I receptor gene in mice causes a postnatal growth deficit. *Endocrinology*. 2000;141(7):2557-2566.
229. Akashi K, Traver D, Miyamoto T, Weissman IL. A clonogenic common myeloid progenitor that gives rise to all myeloid lineages. *Nature*. 2000;404(6774):193-197.
230. Pollak M. The insulin and insulin-like growth factor receptor family in neoplasia: an update. *Nat Rev Cancer*. 2012;12(3):159-169.
231. Wittman M, Carboni J, Attar R, et al. Discovery of a 1H-Benzoimidazol-2-yl)-1H-pyridin-2-one (BMS-536924) Inhibitor of Insulin-like Growth Factor I Receptor Kinase with in Vivo Antitumor Activity. *Journal of Medicinal Chemistry*. 2005;48(18):5639-5643.
232. Carboni JM, Wittman M, Yang Z, et al. BMS-754807, a small molecule inhibitor of insulin-like growth factor-1R/IR. *Molecular Cancer Therapeutics*. 2009;8(12):3341-3349.
233. Lehne G, Grasmo-Wendler UH, Berner JM, et al. Upregulation of stem cell genes in multidrug resistant K562 leukemia cells. *Leuk Res*. 2009;33(10):1379-1385.
234. Abe S, Funato T, Takahashi S, et al. Increased expression of insulin-like growth factor i is associated with Ara-C resistance in leukemia. *Tohoku J Exp Med*. 2006;209(3):217-228.
235. Gal H, Amariglio N, Trakhtenbrot L, et al. Gene expression profiles of AML derived stem cells; similarity to hematopoietic stem cells. *Leukemia*. 2006;20(12):2147-2154.
236. Xie J, Chen X, Zheng J, et al. IGF-IR determines the fates of BCR/ABL leukemia. *J Hematol Oncol*. 2015;8:3.
237. Whelan JT, Ludwig DL, Bertrand FE. HoxA9 induces insulin-like growth factor-1 receptor expression in B-lineage acute lymphoblastic leukemia. *Leukemia*. 2008;22(6):1161-1169.

238. Guenther MG, Lawton LN, Rozovskaia T, et al. Aberrant chromatin at genes encoding stem cell regulators in human mixed-lineage leukemia. *Genes Dev*. 2008;22(24):3403-3408.
239. Triplett TA, Cardenas KT, Lancaster JN, et al. Endogenous dendritic cells from the tumor microenvironment support T-ALL growth via IGF1R activation. *Proc Natl Acad Sci U S A*. 2016;113(8):E1016-1025.
240. Weisberg E, Nonami A, Chen Z, et al. Upregulation of IGF1R by mutant RAS in leukemia and potentiation of RAS signaling inhibitors by small-molecule inhibition of IGF1R. *Clin Cancer Res*. 2014;20(21):5483-5495.
241. Zhang J, Huang FF, Wu DS, et al. SUMOylation of insulin-like growth factor 1 receptor, promotes proliferation in acute myeloid leukemia. *Cancer Lett*. 2015;357(1):297-306.
242. Duesberg PH, Vogt PK. Differences between the ribonucleic acids of transforming and nontransforming avian tumor viruses. *Proc Natl Acad Sci U S A*. 1970;67(4):1673-1680.
243. Stehelin D, Varmus HE, Bishop JM, Vogt PK. DNA related to the transforming gene(s) of avian sarcoma viruses is present in normal avian DNA. *Nature*. 1976;260(5547):170-173.
244. Steffen D. Proviruses are adjacent to c-myc in some murine leukemia virus-induced lymphomas. *Proc Natl Acad Sci U S A*. 1984;81(7):2097-2101.
245. Shen H, Suzuki T, Munroe DJ, et al. Common sites of retroviral integration in mouse hematopoietic tumors identified by high-throughput, single nucleotide polymorphism-based mapping and bacterial artificial chromosome hybridization. *J Virol*. 2003;77(2):1584-1588.
246. Uren AG, Mikkers H, Kool J, et al. A high-throughput splinkerette-PCR method for the isolation and sequencing of retroviral insertion sites. *Nat Protoc*. 2009;4(5):789-798.
247. de Ridder J, Uren A, Kool J, Reinders M, Wessels L. Detecting statistically significant common insertion sites in retroviral insertional mutagenesis screens. *PLoS Comput Biol*. 2006;2(12):e166.
248. Sarver AL, Erdman J, Starr T, Largaespada DA, Silverstein KA. TAPDANCE: an automated tool to identify and annotate transposon insertion CISs and associations between CISs from next generation sequence data. *BMC Bioinformatics*. 2012;13:154.
249. Keng VW, Villanueva A, Chiang DY, et al. A conditional transposon-based insertional mutagenesis screen for genes associated with mouse hepatocellular carcinoma. *Nat Biotechnol*. 2009;27(3):264-274.
250. Bergemann TL, Starr TK, Yu H, et al. New methods for finding common insertion sites and co-occurring common insertion sites in transposon- and virus-based genetic screens. *Nucleic Acids Res*. 2012;40(9):3822-3833.
251. Vaillant F, Blyth K, Terry A, et al. A full-length Cbfa1 gene product perturbs T-cell development and promotes lymphomagenesis in synergy with myc. *Oncogene*. 1999;18(50):7124-7134.
252. Hacein-Bey-Abina S, Von Kalle C, Schmidt M, et al. LMO2-associated clonal T cell proliferation in two patients after gene therapy for SCID-X1. *Science*. 2003;302(5644):415-419.
253. Robey E, Chang D, Itano A, et al. An activated form of Notch influences the choice between CD4 and CD8 T cell lineages. *Cell*. 1996;87(3):483-492.
254. Fowlkes BJ, Robey EA. A reassessment of the effect of activated Notch1 on CD4 and CD8 T cell development. *J Immunol*. 2002;169(4):1817-1821.
255. Dumortier A, Jeannet R, Kirstetter P, et al. Notch activation is an early and critical event during T-Cell leukemogenesis in Ikaros-deficient mice. *Mol Cell Biol*. 2006;26(1):209-220.

256. Medyouf H, Gao X, Armstrong F, et al. Acute T-cell leukemias remain dependent on Notch signaling despite PTEN and INK4A/ARF loss. *Blood*. 2010;115(6):1175-1184.
257. Cuypers HT, Selten G, Quint W, et al. Murine leukemia virus-induced T-cell lymphomagenesis: integration of proviruses in a distinct chromosomal region. *Cell*. 1984;37(1):141-150.
258. Ochman H, Gerber AS, Hartl DL. Genetic applications of an inverse polymerase chain reaction. *Genetics*. 1988;120(3):621-623.
259. McAleer MA, Coffey AJ, Dunham I. DNA rescue by the vectorette method. *Methods Mol Biol*. 2003;226:393-400.
260. Hui EK, Wang PC, Lo SJ. Strategies for cloning unknown cellular flanking DNA sequences from foreign integrants. *Cell Mol Life Sci*. 1998;54(12):1403-1411.
261. Devon RS, Porteous DJ, Brookes AJ. Splinkerettes--improved vectorettes for greater efficiency in PCR walking. *Nucleic Acids Res*. 1995;23(9):1644-1645.
262. Matthaei KI. Genetically manipulated mice: a powerful tool with unsuspected caveats. *J Physiol*. 2007;582(Pt 2):481-488.
263. Ryan MD, King AM, Thomas GP. Cleavage of foot-and-mouth disease virus polyprotein is mediated by residues located within a 19 amino acid sequence. *J Gen Virol*. 1991;72 (Pt 11):2727-2732.
264. de Felipe P. Skipping the co-expression problem: the new 2A "CHYSEL" technology. *Genet Vaccines Ther*. 2004;2(1):13.
265. Donnelly ML, Luke G, Mehrotra A, et al. Analysis of the aphthovirus 2A/2B polyprotein 'cleavage' mechanism indicates not a proteolytic reaction, but a novel translational effect: a putative ribosomal 'skip'. *J Gen Virol*. 2001;82(Pt 5):1013-1025.
266. de Felipe P, Luke GA, Hughes LE, Gani D, Halpin C, Ryan MD. E unum pluribus: multiple proteins from a self-processing polyprotein. *Trends in Biotechnology*. 2006;24(2):68-75.
267. Holst J, Szymczak-Workman AL, Vignali KM, Burton AR, Workman CJ, Vignali DAA. Generation of T-cell receptor retrogenic mice. *Nature Protocols*. 2006;1(1):406-417.
268. Bettini ML, Bettini M, Nakayama M, Guy CS, Vignali DAA. Generation of T cell receptor-retrogenic mice: improved retroviral-mediated stem cell gene transfer. *Nature Protocols*. 2013;8(10):1837-1840.
269. Kim JH, Lee SR, Li LH, et al. High Cleavage Efficiency of a 2A Peptide Derived from Porcine Teschovirus-1 in Human Cell Lines, Zebrafish and Mice. *Plos One*. 2011;6(4).
270. Szymczak AL, Workman CJ, Wang Y, et al. Correction of multi-gene deficiency in vivo using a single 'self-cleaving' 2A peptide-based retroviral vector (vol 22, pg 589, 2004). *Nature Biotechnology*. 2004;22(12):1590-1590.
271. Bosch MK, Nerbonne JM, Ornitz DM. Dual Transgene Expression in Murine Cerebellar Purkinje Neurons by Viral Transduction In Vivo. *Plos One*. 2014;9(8).
272. de Felipe P, Luke GA, Brown JD, Ryan MD. Inhibition of 2A-mediated 'cleavage' of certain artificial polyproteins bearing N-terminal signal sequences. *Biotechnology Journal*. 2010;5(2):213-223.
273. Chan HY, Sivakamasundari V, Xing X, et al. Comparison of IRES and F2A-Based Locus-Specific Multicistronic Expression in Stable Mouse Lines. *Plos One*. 2011;6(12).
274. Chiang MY, Xu ML, Histen G, et al. Identification of a conserved negative regulatory sequence that influences the leukemogenic activity of NOTCH1. *Molecular and Cellular Biology*. 2006;26(16):6261-6271.

275. Kong J, Zhu F, Stalker J, Adams DJ. iMapper: a web application for the automated analysis and mapping of insertional mutagenesis sequence data against Ensembl genomes. *Bioinformatics*. 2008;24(24):2923-2925.
276. Akagi K, Suzuki T, Stephens RM, Jenkins NA, Copeland NG. RTCGD: retroviral tagged cancer gene database. *Nucleic Acids Res*. 2004;32(Database issue):D523-527.
277. Graux C, Cools J, Melotte C, et al. Fusion of NUP214 to ABL1 on amplified episomes in T-cell acute lymphoblastic leukemia. *Nat Genet*. 2004;36(10):1084-1089.
278. Selten G, Cuypers HT, Zijlstra M, Melief C, Berns A. Involvement of c-myc in MuLV-induced T cell lymphomas in mice: frequency and mechanisms of activation. *EMBO J*. 1984;3(13):3215-3222.
279. Corcoran LM, Adams JM, Dunn AR, Cory S. Murine T lymphomas in which the cellular myc oncogene has been activated by retroviral insertion. *Cell*. 1984;37(1):113-122.
280. Stewart M, Terry A, Hu M, et al. Proviral insertions induce the expression of bone-specific isoforms of PEBP2alphaA (CBFA1): evidence for a new myc collaborating oncogene. *Proc Natl Acad Sci U S A*. 1997;94(16):8646-8651.
281. Wotton S, Stewart M, Blyth K, et al. Proviral insertion indicates a dominant oncogenic role for Runx1/AML-1 in T-cell lymphoma. *Cancer Res*. 2002;62(24):7181-7185.
282. Stewart M, MacKay N, Cameron ER, Neil JC. The common retroviral insertion locus Dsi1 maps 30 kilobases upstream of the P1 promoter of the murine Runx3/Cbfa3/Aml2 gene. *J Virol*. 2002;76(9):4364-4369.
283. Li J, Shen H, Himmel KL, et al. Leukaemia disease genes: large-scale cloning and pathway predictions. *Nat Genet*. 1999;23(3):348-353.
284. Mikkers H, Allen J, Knipscheer P, et al. High-throughput retroviral tagging to identify components of specific signaling pathways in cancer. *Nat Genet*. 2002;32(1):153-159.
285. Suzuki T, Shen H, Akagi K, et al. New genes involved in cancer identified by retroviral tagging. *Nat Genet*. 2002;32(1):166-174.
286. Kim R, Trubetskoy A, Suzuki T, Jenkins NA, Copeland NG, Lenz J. Genome-based identification of cancer genes by proviral tagging in mouse retrovirus-induced T-cell lymphomas. *J Virol*. 2003;77(3):2056-2062.
287. Lund AH, Turner G, Trubetskoy A, et al. Genome-wide retroviral insertional tagging of genes involved in cancer in Cdkn2a-deficient mice. *Nat Genet*. 2002;32(1):160-165.
288. Shin MS, Fredrickson TN, Hartley JW, Suzuki T, Akagi K, Morse HC, 3rd. High-throughput retroviral tagging for identification of genes involved in initiation and progression of mouse splenic marginal zone lymphomas. *Cancer Res*. 2004;64(13):4419-4427.
289. Blyth K, Cameron ER, Neil JC. The RUNX genes: gain or loss of function in cancer. *Nat Rev Cancer*. 2005;5(5):376-387.
290. Tanaka T, Tanaka K, Ogawa S, et al. An acute myeloid leukemia gene, AML1, regulates hemopoietic myeloid cell differentiation and transcriptional activation antagonistically by two alternative spliced forms. *EMBO J*. 1995;14(2):341-350.
291. Moriarity BS, Largaespada DA. Sleeping Beauty transposon insertional mutagenesis based mouse models for cancer gene discovery. *Curr Opin Genet Dev*. 2015;30:66-72.
292. Dupuy AJ, Akagi K, Largaespada DA, Copeland NG, Jenkins NA. Mammalian mutagenesis using a highly mobile somatic Sleeping Beauty transposon system. *Nature*. 2005;436(7048):221-226.

293. Berquam-Vrieze KE, Nannapaneni K, Brett BT, et al. Cell of origin strongly influences genetic selection in a mouse model of T-ALL. *Blood*. 2011;118(17):4646-4656.
294. Sauvageau M, Miller M, Lemieux S, Lessard J, Hebert J, Sauvageau G. Quantitative expression profiling guided by common retroviral insertion sites reveals novel and cell type-specific cancer genes in leukemia. *Blood*. 2008;111(2):790-799.
295. Hwang HC, Martins CP, Bronkhorst Y, et al. Identification of oncogenes collaborating with p27(Kip1) loss by insertional mutagenesis and high-throughput insertion site analysis. *Proceedings of the National Academy of Sciences of the United States of America*. 2002;99(17):11293-11298.
296. Golub TR, Barker GF, Bohlander SK, et al. Fusion of the TEL gene on 12p13 to the AML1 gene on 21q22 in acute lymphoblastic leukemia. *Proc Natl Acad Sci U S A*. 1995;92(11):4917-4921.
297. Harada H, Harada Y, Niimi H, Kyo T, Kimura A, Inaba T. High incidence of somatic mutations in the AML1/RUNX1 gene in myelodysplastic syndrome and low blast percentage myeloid leukemia with myelodysplasia. *Blood*. 2004;103(6):2316-2324.
298. Osato M. Point mutations in the RUNX1/AML1 gene: another actor in RUNX leukemia. *Oncogene*. 2004;23(24):4284-4296.
299. Zhao LJ, Wang YY, Li G, et al. Functional features of RUNX1 mutants in acute transformation of chronic myeloid leukemia and their contribution to inducing murine full-blown leukemia. *Blood*. 2012;119(12):2873-2882.
300. Kundu M, Compton S, Garrett-Beal L, et al. Runx1 deficiency predisposes mice to T-lymphoblastic lymphoma. *Blood*. 2005;106(10):3621-3624.
301. Gilliland DG, Griffin JD. The roles of FLT3 in hematopoiesis and leukemia. *Blood*. 2002;100(5):1532-1542.
302. Palii CG, Perez-Iratxeta C, Yao Z, et al. Differential genomic targeting of the transcription factor TAL1 in alternate haematopoietic lineages. *EMBO J*. 2011;30(3):494-509.
303. Sarbassov DD, Guertin DA, Ali SM, Sabatini DM. Phosphorylation and regulation of Akt/PKB by the rictor-mTOR complex. *Science*. 2005;307(5712):1098-1101.
304. Giambra V, Jenkins CE, Lam SH, et al. Leukemia stem cells in T-ALL require active Hif1alpha and Wnt signaling. *Blood*. 2015;125(25):3917-3927.
305. D'Astolfo DS, Pagliero RJ, Pras A, et al. Efficient intracellular delivery of native proteins. *Cell*. 2015;161(3):674-690.
306. Yost AJ, Shevchuk OO, Gooch R, et al. Defined, serum-free conditions for in vitro culture of primary human T-ALL blasts. *Leukemia*. 2013;27(6):1437-1440.
307. Gusscott S, Jenkins CE, Lam SH, Giambra V, Pollak M, Weng AP. IGF1R Derived PI3K/AKT Signaling Maintains Growth in a Subset of Human T-Cell Acute Lymphoblastic Leukemias. *PLoS One*. 2016;11(8):e0161158.
308. Mansour MR, Reed C, Eisenberg AR, et al. Targeting oncogenic interleukin-7 receptor signalling with N-acetylcysteine in T cell acute lymphoblastic leukaemia. *Br J Haematol*. 2015;168(2):230-238.
309. Zuurbier L, Petricoin EF, 3rd, Vuerhard MJ, et al. The significance of PTEN and AKT aberrations in pediatric T-cell acute lymphoblastic leukemia. *Haematologica*. 2012;97(9):1405-1413.
310. You D, Xin J, Volk A, et al. FAK mediates a compensatory survival signal parallel to PI3K-AKT in PTEN-null T-ALL cells. *Cell Rep*. 2015;10(12):2055-2068.

311. Li H, Durbin R. Fast and accurate long-read alignment with Burrows-Wheeler transform. *Bioinformatics*. 2010;26(5):589-595.
312. Butterfield YS, Kreitzman M, Thiessen N, et al. JAGuaR: junction alignments to genome for RNA-seq reads. *PLoS One*. 2014;9(7):e102398.
313. Mortazavi A, Williams BA, McCue K, Schaeffer L, Wold B. Mapping and quantifying mammalian transcriptomes by RNA-Seq. *Nat Methods*. 2008;5(7):621-628.
314. Lorzadeh A, Bilenky M, Hammond C, et al. Nucleosome Density ChIP-Seq Identifies Distinct Chromatin Modification Signatures Associated with MNase Accessibility. *Cell Rep*. 2016;17(8):2112-2124.
315. Ramirez F, Dundar F, Diehl S, Gruning BA, Manke T. deepTools: a flexible platform for exploring deep-sequencing data. *Nucleic Acids Res*. 2014;42(Web Server issue):W187-191.
316. Gu Z, Eils R, Schlesner M. Complex heatmaps reveal patterns and correlations in multidimensional genomic data. *Bioinformatics*. 2016;32(18):2847-2849.
317. Dobin A, Davis CA, Schlesinger F, et al. STAR: ultrafast universal RNA-seq aligner. *Bioinformatics*. 2013;29(1):15-21.
318. Benjamini Y, Hochberg Y. Controlling the False Discovery Rate - a Practical and Powerful Approach to Multiple Testing. *Journal of the Royal Statistical Society Series B-Methodological*. 1995;57(1):289-300.
319. Storey JD. The positive false discovery rate: A Bayesian interpretation and the q-value. *Annals of Statistics*. 2003;31(6):2013-2035.
320. Auer PL, Doerge RW. A Two-Stage Poisson Model for Testing RNA-Seq Data. *Statistical Applications in Genetics and Molecular Biology*. 2011;10(1).
321. Law CW, Chen YS, Shi W, Smyth GK. voom: precision weights unlock linear model analysis tools for RNA-seq read counts. *Genome Biology*. 2014;15(2).
322. Anders S, Huber W. Differential expression analysis for sequence count data. *Genome Biology*. 2010;11(10).
323. Hayashi K, Natsume W, Watanabe T, et al. Diminution of the AML1 transcription factor function causes differential effects on the fates of CD4 and CD8 single-positive T cells. *J Immunol*. 2000;165(12):6816-6824.
324. Huang G, Shigesada K, Ito K, Wee HJ, Yokomizo T, Ito Y. Dimerization with PEBP2beta protects RUNX1/AML1 from ubiquitin-proteasome-mediated degradation. *EMBO J*. 2001;20(4):723-733.
325. Nolden L, Edenhofer F, Haupt S, et al. Site-specific recombination in human embryonic stem cells induced by cell-permeant Cre recombinase. *Nat Methods*. 2006;3(6):461-467.
326. Kundu M, Compton S, Garrett-Beal L, et al. Runx1 deficiency predisposes mice to T-lymphoblastic lymphoma. *Blood*. 2005;106(10):3621-3624.
327. Zenatti PP, Ribeiro D, Li W, et al. Oncogenic IL7R gain-of-function mutations in childhood T-cell acute lymphoblastic leukemia. *Nat Genet*. 2011;43(10):932-939.
328. Lee J, Hoi CS, Lilja KC, et al. Runx1 and p21 synergistically limit the extent of hair follicle stem cell quiescence in vivo. *Proc Natl Acad Sci U S A*. 2013;110(12):4634-4639.
329. Goyama S, Schibler J, Cunningham L, et al. Transcription factor RUNX1 promotes survival of acute myeloid leukemia cells. *J Clin Invest*. 2013;123(9):3876-3888.
330. Mansour MR, Sanda T, Lawton LN, et al. The TAL1 complex targets the FBXW7 tumor suppressor by activating miR-223 in human T cell acute lymphoblastic leukemia. *J Exp Med*. 2013;210(8):1545-1557.

331. Terriente-Felix A, Li JH, Collins S, et al. Notch cooperates with Lozenge/Runx to lock haemocytes into a differentiation programme. *Development*. 2013;140(4):926-937.
332. Coustan-Smith E, Mullighan CG, Onciu M, et al. Early T-cell precursor leukaemia: a subtype of very high-risk acute lymphoblastic leukaemia. *The Lancet Oncology*. 2009;10(2):147-156.
333. Gutierrez A, Kentsis A, Sanda T, et al. The BCL11B tumor suppressor is mutated across the major molecular subtypes of T-cell acute lymphoblastic leukemia. *Blood*. 2011;118(15):4169-4173.
334. Winter SS, Jiang Z, Khawaja HM, et al. Identification of genomic classifiers that distinguish induction failure in T-lineage acute lymphoblastic leukemia: a report from the Children's Oncology Group. *Blood*. 2007;110(5):1429-1438.
335. Burns CE, Traver D, Mayhall E, Shepard JL, Zon LI. Hematopoietic stem cell fate is established by the Notch–Runx pathway. *Genes & Development*. 2005;19(19):2331-2342.
336. Garg V, Muth AN, Ransom JF, et al. Mutations in NOTCH1 cause aortic valve disease. *Nature*. 2005;437(7056):270-274.
337. Spender LC, Whiteman HJ, Karstegl CE, Farrell PJ. Transcriptional cross-regulation of RUNX1 by RUNX3 in human B cells. *Oncogene*. 2005;24(11):1873-1881.
338. Taniuchi I, Littman DR. Epigenetic gene silencing by Runx proteins. *Oncogene*. 2004;23(24):4341-4345.
339. Weng AP, Nam Y, Wolfe MS, et al. Growth suppression of pre-T acute lymphoblastic leukemia cells by inhibition of notch signaling. *Mol Cell Biol*. 2003;23(2):655-664.
340. Townsend EC, Murakami MA, Christodoulou A, et al. The Public Repository of Xenografts Enables Discovery and Randomized Phase II-like Trials in Mice. *Cancer Cell*. 2016;29(4):574-586.
341. Herskowitz I. Functional inactivation of genes by dominant negative mutations. *Nature*. 1987;329(6136):219-222.
342. de Sousa Abreu R, Penalva LO, Marcotte EM, Vogel C. Global signatures of protein and mRNA expression levels. *Mol Biosyst*. 2009;5(12):1512-1526.
343. Vogel C, Marcotte EM. Insights into the regulation of protein abundance from proteomic and transcriptomic analyses. *Nature Reviews Genetics*. 2012;13(4):227-232.
344. Fingar DC, Salama S, Tsou C, Harlow E, Blenis J. Mammalian cell size is controlled by mTOR and its downstream targets S6K1 and 4EBP1/eIF4E. *Genes & Development*. 2002;16(12):1472-1487.
345. Doidy J, Li Y, Neymotin B, et al. "Hit-and-Run" transcription: de novo transcription initiated by a transient bZIP1 "hit" persists after the "run". *BMC Genomics*. 2016;17:92.
346. Zenatti PP, Ribeiro D, Li W, et al. Oncogenic IL7R gain-of-function mutations in childhood T-cell acute lymphoblastic leukemia. *Nat Genet*. 2011;43(10):932-939.
347. Ribeiro D, Melao A, Barata JT. IL-7R-mediated signaling in T-cell acute lymphoblastic leukemia. *Adv Biol Regul*. 2013;53(2):211-222.
348. Treanor LM, Zhou S, Janke L, et al. Interleukin-7 receptor mutants initiate early T cell precursor leukemia in murine thymocyte progenitors with multipotent potential. *Journal of Experimental Medicine*. 2014;211(4):701-713.
349. Bailis W, Pear WS. Notch and PI3K: how is the road traveled? *Blood*. 2012;120(7):1349-1350.

350. Yokoyama K, Yokoyama N, Izawa K, et al. In vivo leukemogenic potential of an interleukin 7 receptor alpha chain mutant in hematopoietic stem and progenitor cells. *Blood*. 2013;122(26):4259-4263.
351. Stewart M, Terry A, O'Hara M, Cameron E, Onions D, Neil JC. til-1: a novel proviral insertion locus for Moloney murine leukaemia virus in lymphomas of CD2-myc transgenic mice. *J Gen Virol*. 1996;77 (Pt 3):443-446.
352. Cameron ER, Blyth K, Hanlon L, et al. The Runx genes as dominant oncogenes. *Blood Cells Molecules and Diseases*. 2003;30(2):194-200.
353. Borland G, Kilbey A, Hay J, et al. Addiction to Runx1 is partially attenuated by loss of p53 in the E mu-Myc lymphoma model. *Oncotarget*. 2016;7(17):22973-22987.
354. Jacobs PT, Cao L, Samon JB, et al. Runx Transcription Factors Repress Human and Murine c-Myc Expression in a DNA-Binding and C-Terminally Dependent Manner. *Plos One*. 2013;8(7).
355. Telfer JC, Hedblom EE, Anderson MK, Laurent MN, Rothenberg EV. Localization of the domains in Runx transcription factors required for the repression of CD4 in thymocytes. *Journal of Immunology*. 2004;172(7):4359-4370.
356. Telfer JC, Rothenberg EV. Expression and function of a stem cell promoter for the murine CBF alpha 2 gene: Distinct roles and regulation in natural killer and T cell development. *Developmental Biology*. 2001;229(2):363-382.
357. Maser RS, Choudhury B, Campbell PJ, et al. Chromosomally unstable mouse tumours have genomic alterations similar to diverse human cancers. *Nature*. 2007;447(7147):966-U963.
358. Palomero T, Sulis ML, Cortina M, et al. Mutational loss of PTEN induces resistance to NOTCH1 inhibition in T-cell leukemia. *Nature Medicine*. 2007;13(10):1203-1210.
359. Yilmaz OH, Valdez R, Theisen BK, et al. Pten dependence distinguishes haematopoietic stem cells from leukaemia-initiating cells. *Nature*. 2006;441(7092):475-482.
360. Herranz D, Ambesi-Impiombato A, Sudderth J, et al. Metabolic reprogramming induces resistance to anti-NOTCH1 therapies in T cell acute lymphoblastic leukemia. *Nat Med*. 2015;21(10):1182-1189.
361. Sarmento LM, Huang H, Limon A, et al. Notch1 modulates timing of G1-S progression by inducing SKP2 transcription and p27 Kip1 degradation. *J Exp Med*. 2005;202(1):157-168.
362. Barata JT, Cardoso AA, Nadler LM, Boussiotis VA. Interleukin-7 promotes survival and cell cycle progression of T-cell acute lymphoblastic leukemia cells by down-regulating the cyclin-dependent kinase inhibitor p27(kip1). *Blood*. 2001;98(5):1524-1531.
363. Tsukiyama T, Ishida N, Shirane M, et al. Down-regulation of p27Kip1 expression is required for development and function of T cells. *J Immunol*. 2001;166(1):304-312.
364. Dohda T, Maljukova A, Liu L, et al. Notch signaling induces SKP2 expression and promotes reduction of p27Kip1 in T-cell acute lymphoblastic leukemia cell lines. *Exp Cell Res*. 2007;313(14):3141-3152.
365. Fujii M, Hayashi K, Niki M, et al. Overexpression of AML1 renders a T hybridoma resistant to T cell receptor-mediated apoptosis. *Oncogene*. 1998;17(14):1813-1820.
366. Malumbres M. Cyclin-dependent kinases. *Genome Biol*. 2014;15(6):122.
367. Zhang T, Kwiatkowski N, Olson CM, et al. Covalent targeting of remote cysteine residues to develop CDK12 and CDK13 inhibitors. *Nat Chem Biol*. 2016;12(10):876-884.
368. Moellering RE, Cornejo M, Davis TN, et al. Direct inhibition of the NOTCH transcription factor complex. *Nature*. 2009;462(7270):182-188.

369. Armstrong F, Brunet de la Grange P, Gerby B, et al. NOTCH is a key regulator of human T-cell acute leukemia initiating cell activity. *Blood*. 2009;113(8):1730-1740.
370. Tatarek J, Cullion K, Ashworth T, Gerstein R, Aster JC, Kelliher MA. Notch1 inhibition targets the leukemia-initiating cells in a Tal1/Lmo2 mouse model of T-ALL. *Blood*. 2011.
371. Nishimoto N, Arai S, Ichikawa M, et al. Loss of AML1/Runx1 accelerates the development of MLL-ENL leukemia through down-regulation of p19ARF. *Blood*. 2011;118(9):2541-2550.
372. Yu SY, Zhou XY, Steinke FC, et al. The TCF-1 and LEF-1 Transcription Factors Have Cooperative and Opposing Roles in T Cell Development and Malignancy. *Immunity*. 2012;37(5):813-826.
373. Germar K, Dose M, Konstantinou T, et al. T-cell factor 1 is a gatekeeper for T-cell specification in response to Notch signaling. *Proceedings of the National Academy of Sciences of the United States of America*. 2011;108(50):20060-20065.
374. Seita J, Weissman IL. Hematopoietic stem cell: self-renewal versus differentiation. *Wiley Interdiscip Rev Syst Biol Med*. 2010;2(6):640-653.
375. Eaves CJ. Hematopoietic stem cells: concepts, definitions, and the new reality. *Blood*. 2015;125(17):2605-2613.
376. Rusk N. Reverse ChIP. *Nature Methods*. 2009;6(3):187-187.
377. Komeno Y, Yan M, Matsuura S, et al. Runx1 exon 6-related alternative splicing isoforms differentially regulate hematopoiesis in mice. *Blood*. 2014;123(24):3760-3769.

Appendices

Appendix A Integrations cloned from hNOTCH1ΔE murine leukemias.

Closest gene(s)	Number of independent integrations
Ikzf1	3
Nup214/Fam78a/Abl1	3
Runx3	3
Chi3l1/Mybph/Adora1	2
F11r/Slamf7/Slamf1	2
Pten	2
Il12rb1	2
Gga1 (AL592169.14, Sh3bp1)	2
Rhoa, Gpx1, Usp4	2
Smad6	2
IRF2BP2	2
Lfng / Ttyh3	2
Sos2 / Arf6	2
Runx1	1
Slc18a2/Emx2	1
Cpsf1, Slc39a4, Vps28, Nfkbil2	1
Slc25a20	1
Rcc2	1
Mid1	1
Rsbn1l / Ptpn12	1
St3gal1	1
Prune/Fam63a	1
Ppp1r1b / Stard3	1
Pdgfb	1
Ptma	1
AC129309.4/Socs5	1
Ikzf5 /Acadsb	1
Plekhf2	1
Nxn	1
4632415k11Rik / Atp2c2 / Cotl1	1
Pvrl3	1
Elovl6 / EGF	1
Bcl2l12/Irf3/Scaf1	1
5730453I16Rik/Tmem216	1

Closest gene(s)	Number of independent integrations
Zfp740/Itgb7/Rarg	1
Znrf1	1
Tatdn3, Nsl1	1
Pecam1	1
Slc7a7	1
AC155333.5-6	1
Hnrnpf	1
Snx30, AL831738.4-2	1
Igfbp6, Soat2	1
Plag1, Chchd7	1
EG240055 / Neurl1b	1
Bbx	1
Zfp523, Def6	1
R3hdm2 / Gli1	1
Olfr259	1
Ggt1 / Adora2a	1
Lclat1	1
Mettl11a	1
Ednra / Ttc29	1
1700016M24Rik / Bai1	1
Gpr110	1
Frmd8, Slc25a45	1
SNORA17 / Cmah	1
Glrx5 / Dicer1	1
Asprv1 / Mxd1 / Snrpg / Tgfa	1
BC005764, Prtn3, Ela2, Cfd	1
Ikzf3 (Aiolos), U2	1
Myo16 / Irs2	1
Vamp1, Tapbpl, Cd27	1
EG545963, Lmtk3, GM5897	1
Csf2rb2	1
SNORA17 / Ubxn7	1
fndc3a	1
Lancl3, RP23-423L11.7	1
Ubb	1
Npy / Stk31	1
Lmo2	1
Ghitm	1

Closest gene(s)	Number of independent integrations
Rbx1 / EP300	1
Pign / Tnfrsf11a / Zcchc2	1
2610110G12Rik, Mrps18b, Ppp1r10, mmu-mir-1894	1
Myeov2, Otos	1
Ttll5 / Fos / Tgfb3	1
Pdgfrb/Camk2a	1
Ndel1	1
Bach2	1
Mthfd1l, Plekhg1	1
Ptk2b	1
Grasp	1
Fam65b	1
Lgals3bp, Cant1	1
Btd	1
Pitpnc1/Smurf2	1
Il6ra/Nup210l/Ubap2l	1
Ptpn6, Grcc10	1
Golga5, Itpk1	1
Sema7a/Cyp11a1	1
Evi5	1
Ccm2/Camk2b	1
St3gal5/Capg	1
Hemgn/Foxe1/Coro2a	1
Cox6a2/Itgam	1
Hand1	1
REDD1	1
CPT1A	1
Wdr81, mmu-mir-22, Tlcd2	1
Acsf3	1
Ifnar1/Il10rb	1
Heg1	1
Calm1	1
Klf7/Creb1	1
Jakmip1	1
Cxxc5	1
Pts/Bco/Il18	1
Gadd45b, Gng7	1

Closest gene(s)	Number of independent integrations
Rps6ka3	1
Pvrl2	1
Nrarp/Noxa1	1
Pigl	1
PNKP	1
DOCK9	1
Ugt1a10	1
Rtn4r	1
Tbkbp1	1
Arhgdib	1
Rilpl2, AC127339.5, Snrnp35	1
Tox	1
Zer1/Nup188	1
Mmp19, 1110012D08Rik, Dnajc14	1
Rasa2/Zbtb38	1
Rnf43, Supt4h1	1
B4GALT5/Slc9a8	1
Hnmt	1
Dpp10, SNORA17	1
Zfp788	1
Lmo7	1
Taf8/Guca1a	1
Glcci1	1
SNORA17	1
Tacc1/Fgfr1	1
Prdm6/Snx24	1
Ero1l/Psmc6	1
Ppyr1/Fam35a	1
Ctnnbl1	1
Pros1/Epha3	1
Wnt7a/Tmem43/Xpc	1
Fam117a/NGFR	1
Camkk2	1
Plcg1	1

Appendix B RUNX1 depletion remodels H3K27Ac at key target genes.

B.1 *MYC* locus

RUNX1 and NOTCH1 Transcription Factor ChIP-seq binding is depicted as red bars from publically available data[8,9] (GEO accessions: GSE51800, GSE29600). H3K27Ac ChIP-seq is depicted above for the tracks with labels.

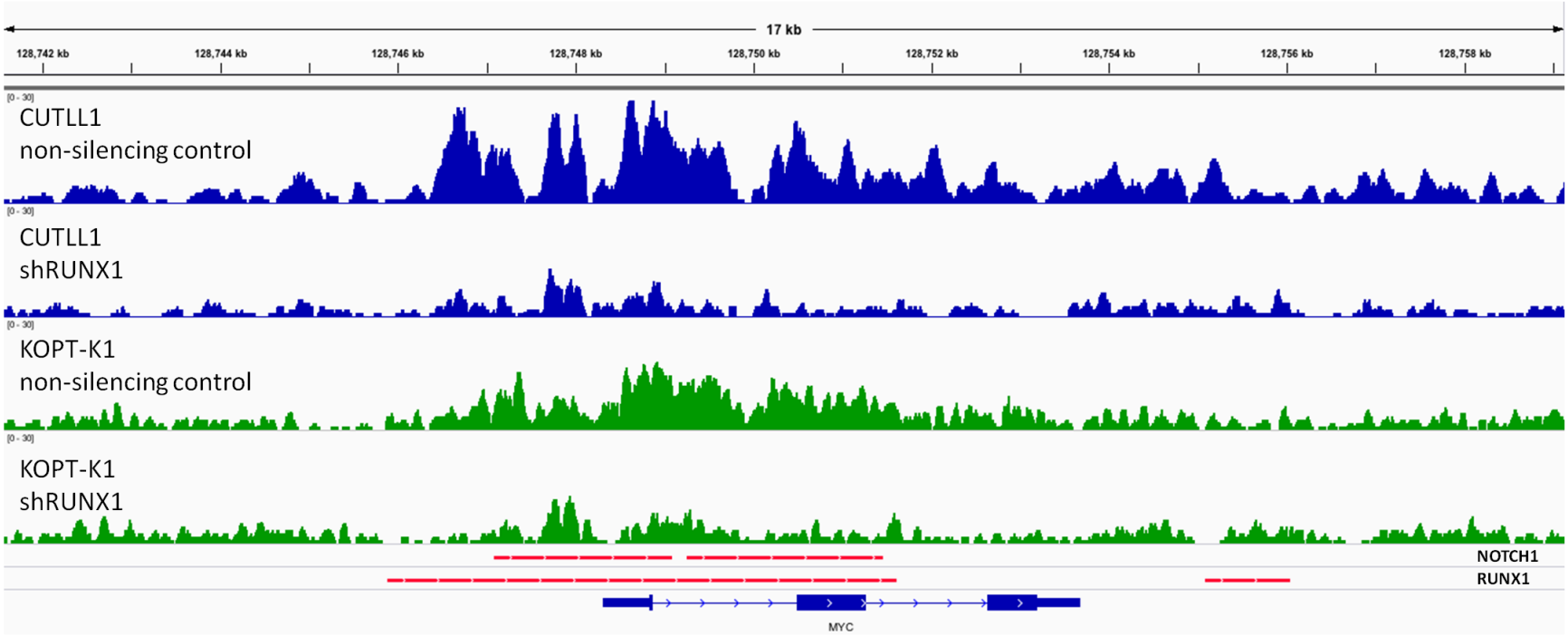

B.2 *IGF1R* locus

RUNX1 and NOTCH1 Transcription Factor ChIP-seq binding is depicted as red bars from publically available data[8,9] (GEO accessions: GSE51800, GSE29600). H3K27Ac ChIP-seq is depicted above for the tracks with labels.

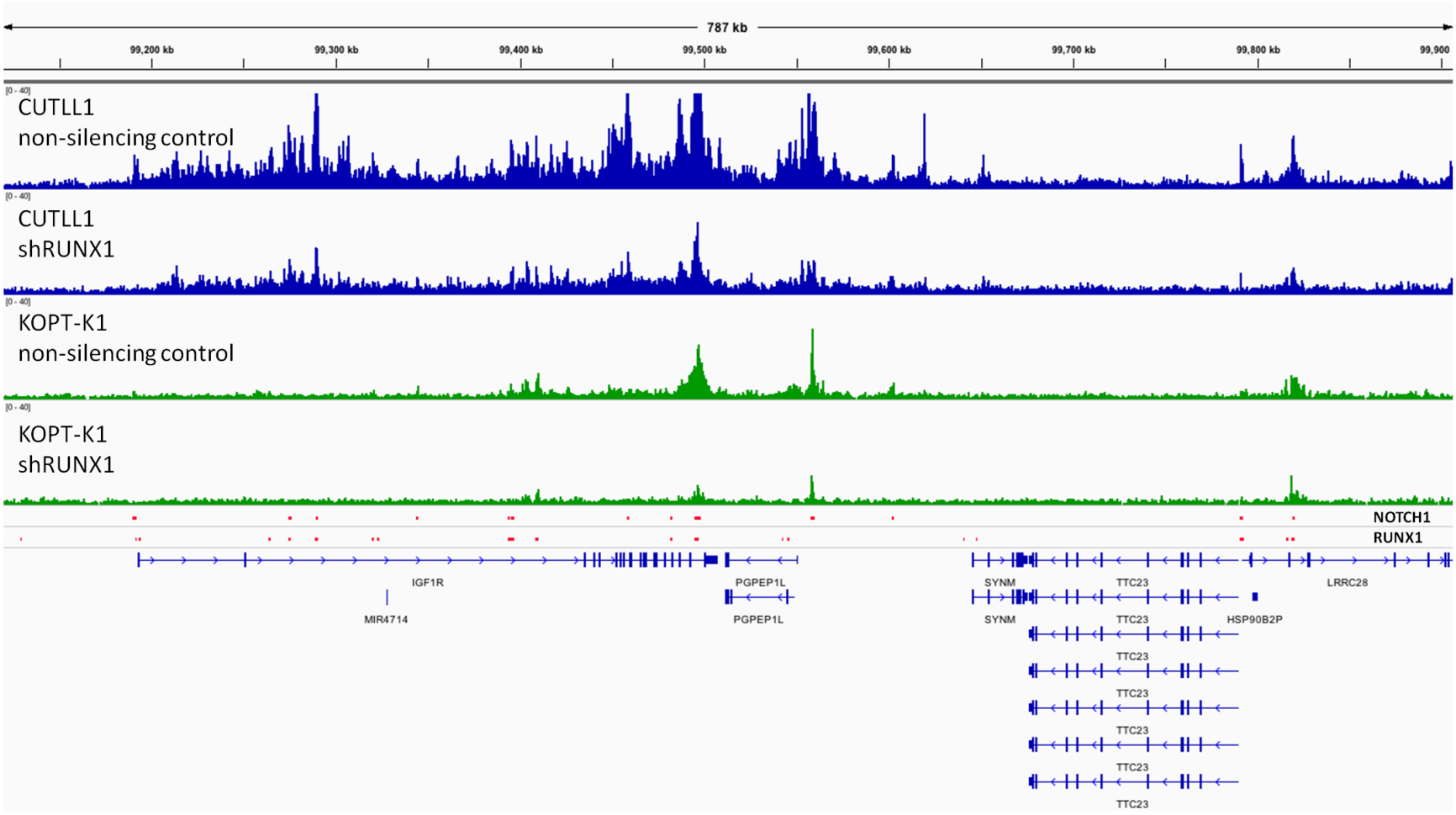

B.3 *IL7R* locus

RUNX1 and NOTCH1 Transcription Factor ChIP-seq binding is depicted as red bars from publically available data[8,9] (GEO accessions: GSE51800, GSE29600). H3K27Ac ChIP-seq is depicted above for the tracks with labels. Enhancers E3 and E5 are also depicted[8].

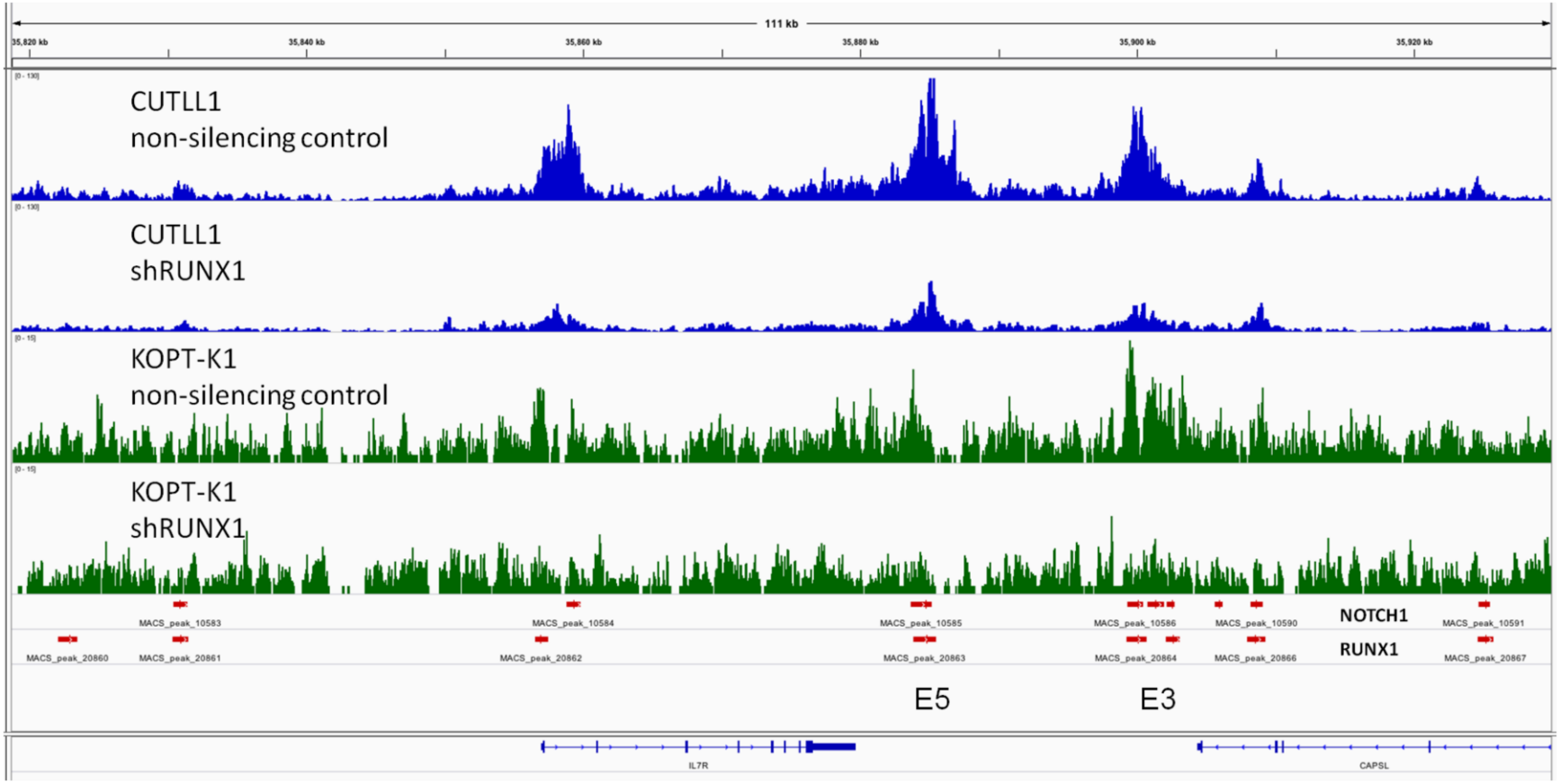

B.4 *DTX1* locus

RUNX1 and NOTCH1 Transcription Factor ChIP-seq binding is depicted as red bars from publically available data[8,9] (GEO accessions: GSE51800, GSE29600). H3K27Ac ChIP-seq is depicted above for the tracks with labels.

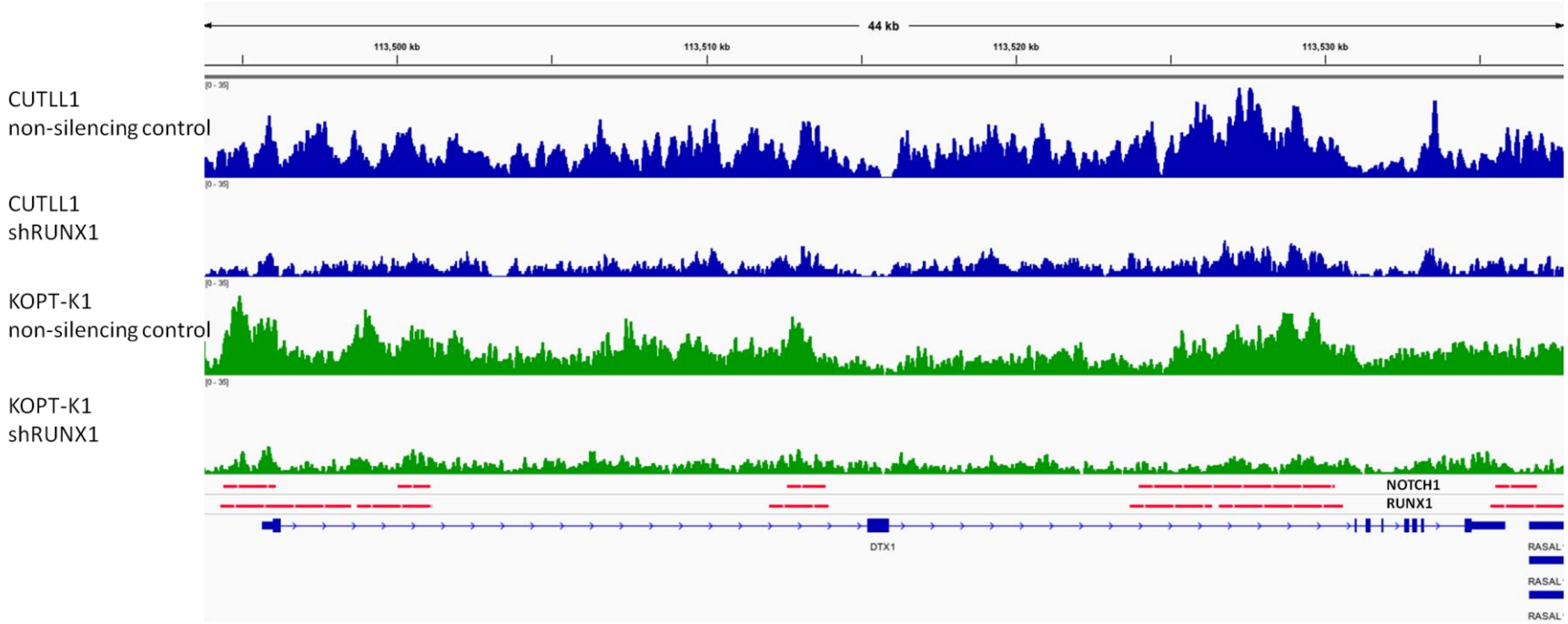

Appendix C Expression Profiling Data.

The data in Appendix C relates to gene expression profiling data from three T-ALL cell lines (HPB-ALL, RPMI 8402, and KOPT-K1) in two conditions, non-silencing control and shRUNX1-58 in duplicates. T-ALL cell lines were transduced with lentiviruses in duplicate. 3 days post-transduction, cells were selected with 1µg/ml Puromycin for 3 further days before RNA isolation for gene expression profiling. The microarrays used were Affymetrix GeneChip® PrimeView™ Human Gene Expression Arrays. All hierarchical clustering was done using average linkage using a Euclidean distance metric. Tables of differentially expressed genes are sorted by fold change from highest to lowest.

C.1 Hierarchical clustering of all samples with no filters

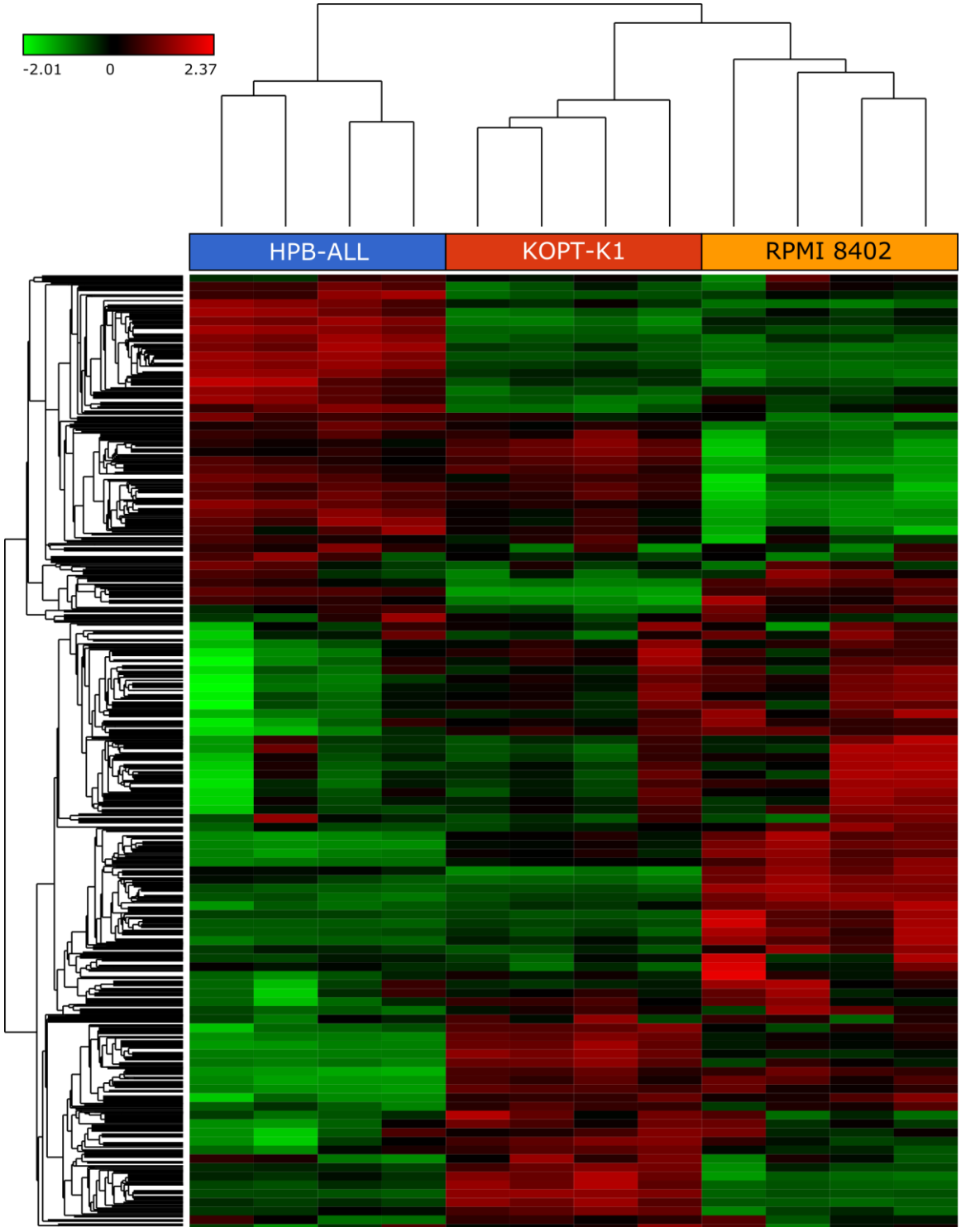

C.2 Principal components analysis of gene expression profiling data.

Two different angles are shown of the first three principal components with the variance shown in parentheses. Each dot is representative of one sample, with smaller dots representing controls and the larger dots representing shRUNX1-58 samples.

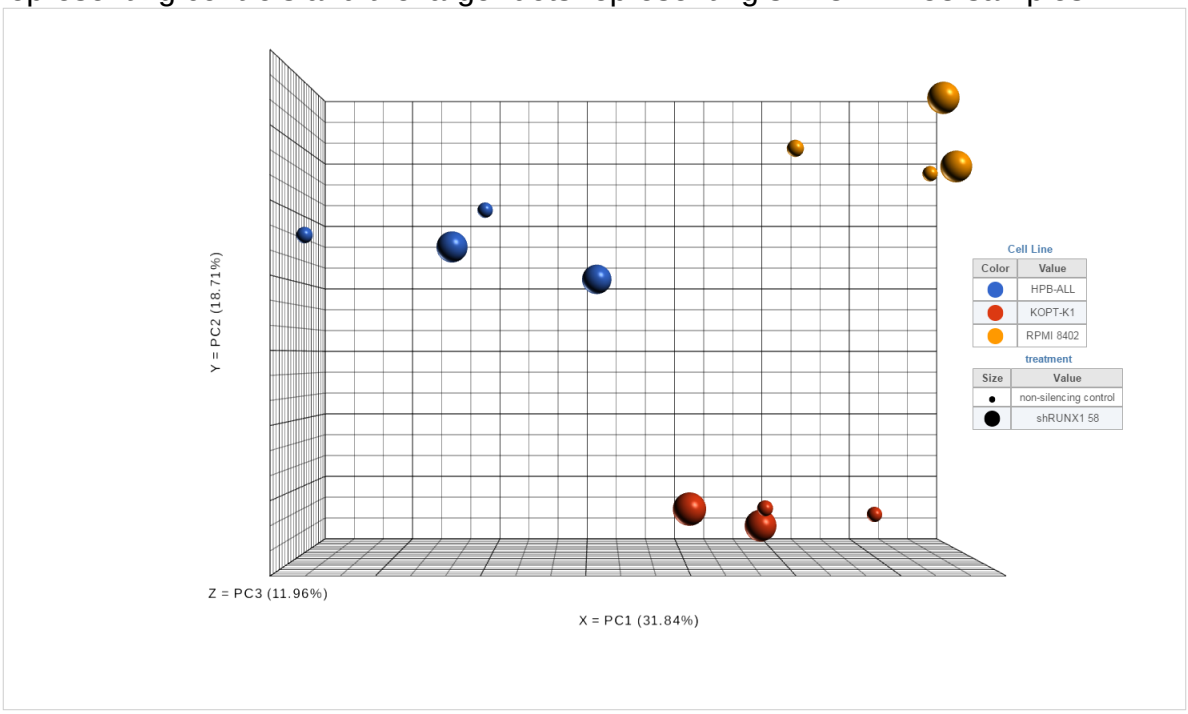

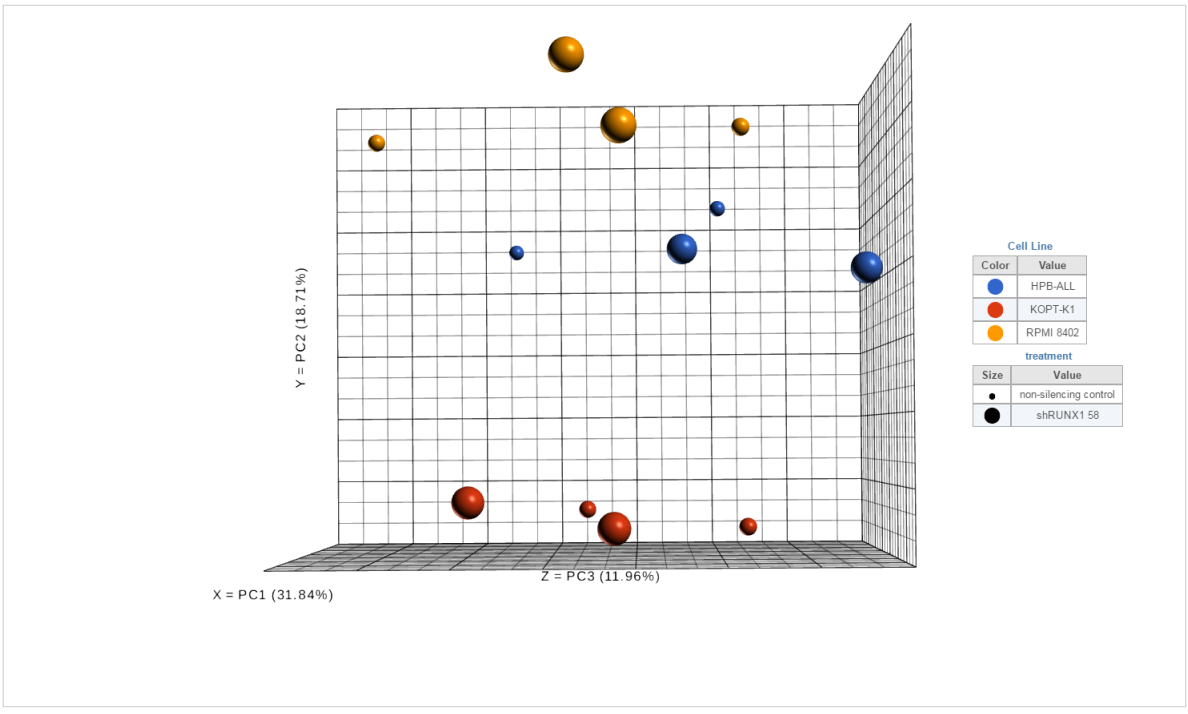

C.3 Genes downregulated upon RUNX1 knockdown in HPB-ALL, RPMI-8402, and KOPT-K1

non-silencing control vs. shRUNX1-58 filtered by FDR cutoff of 0.01

Gene	P-value	FDR	Fold change
PGK1P2	6.82E-09	2.49E-05	2.58
SNRPC	1.83E-07	9.91E-05	2.49
YWHAEP4	3.48E-06	7.05E-04	2.43
PGK1	1.01E-10	1.41E-06	2.37
PDIA3	1.65E-07	9.91E-05	2.29
COX7A2L	9.90E-09	2.77E-05	2.25
RP11-516A11.1	2.95E-07	1.31E-04	2.23
CDC25A	5.09E-07	2.01E-04	2.20
H3F3AP6	1.14E-07	9.91E-05	2.19
PDIA3P1	7.37E-07	2.51E-04	2.19
ATP6V0E1P3	1.48E-07	9.91E-05	2.16
BTF3L4P3	3.86E-08	5.39E-05	2.15
ATP6V0E1	9.66E-08	9.00E-05	2.13
ATP6V0E1P2	9.90E-07	3.01E-04	2.07
RP11-349N19.2	5.88E-08	6.79E-05	2.06
YWHAEP5	6.32E-08	6.79E-05	2.00
TSPAN7	1.45E-06	3.89E-04	1.99
YWHAEP1	1.63E-07	9.91E-05	1.99
SNRPBP1	6.89E-05	6.25E-03	1.98
RP4-536B24.2	9.61E-07	2.98E-04	1.97
BTF3L4P4	2.37E-06	5.43E-04	1.97
RP11-578C11.2	2.26E-07	1.09E-04	1.94
YWHAE	7.14E-09	2.49E-05	1.94
SRP9P1	1.95E-08	3.94E-05	1.94
AC005102.1	3.95E-07	1.67E-04	1.89
DCBLD2	2.23E-06	5.31E-04	1.89
POM121	5.63E-08	6.79E-05	1.88
SLC7A5	6.66E-07	2.45E-04	1.88
KIF1BP	4.66E-05	4.82E-03	1.88
UBE2V2P3	1.03E-05	1.56E-03	1.87
CD3G	3.76E-10	2.63E-06	1.86
PPIF	1.43E-06	3.89E-04	1.86
TCEA1P2	2.51E-07	1.17E-04	1.86
PPA2	3.79E-06	7.47E-04	1.84
ZNF462	2.09E-05	2.81E-03	1.83
POM121C	1.98E-08	3.94E-05	1.83
NRAS	4.15E-07	1.70E-04	1.82
LZTFL1	9.74E-06	1.50E-03	1.81
PTGES3P1	1.94E-06	4.93E-04	1.81
DBF4P1	2.26E-08	3.94E-05	1.81
SRP9	1.46E-07	9.91E-05	1.80
MAGT1	4.78E-06	8.26E-04	1.79
PTGES3P2	1.33E-07	9.91E-05	1.79
AAAS	4.14E-06	7.93E-04	1.78
G3BP2	2.57E-08	3.98E-05	1.78
YWHAEP7	1.89E-06	4.90E-04	1.75
MTND5P8	2.24E-06	5.31E-04	1.73
H3F3AP5	1.88E-07	9.91E-05	1.73
ACSL4	1.91E-07	9.91E-05	1.71
ZDHHC4	2.18E-05	2.82E-03	1.70
PKMP2	3.75E-05	4.11E-03	1.69
PLEKHB2	1.41E-06	3.89E-04	1.66
MOSPD1	3.06E-05	3.57E-03	1.66
MAPK6	2.96E-06	6.26E-04	1.64
DDI2	6.43E-05	5.99E-03	1.64
PSMD5	4.60E-06	8.12E-04	1.64
ALYREF	6.93E-07	2.49E-04	1.64
SF3B2	8.44E-07	2.70E-04	1.63
RP11-760D2.7	1.33E-07	9.91E-05	1.62
RANBP9	3.93E-06	7.63E-04	1.62
TIMP2	2.93E-05	3.50E-03	1.61
RP11-773H22.4	2.95E-06	6.26E-04	1.61
ISY1	4.65E-06	8.12E-04	1.61
STARD7	2.75E-06	6.11E-04	1.60
TM9SF2	8.14E-07	2.70E-04	1.59
PTGES3P3	5.21E-06	8.78E-04	1.58
TMBIM6	2.99E-07	1.31E-04	1.57
SLC20A1P1	5.79E-07	2.19E-04	1.57
DIABLO	4.38E-06	8.06E-04	1.56
MYO7B	2.54E-05	3.09E-03	1.56

Gene	P-value	FDR	Fold change
MAPK6PS4	2.95E-05	3.50E-03	1.55
SNRPB	2.13E-05	2.81E-03	1.55
RPRD1B	2.37E-06	5.43E-04	1.55
RMND5A	8.48E-08	8.47E-05	1.54
KIF3A	4.12E-05	4.43E-03	1.54
NOP10	6.50E-05	6.01E-03	1.54
TMEM38B	1.17E-05	1.74E-03	1.53
ANTXR1	4.30E-05	4.56E-03	1.52
DBF4	1.59E-07	9.91E-05	1.51
TMA16P1	2.00E-05	2.72E-03	1.51
ITGA6	8.64E-05	7.33E-03	1.50
XPO7	1.08E-06	3.21E-04	1.50
RP11-747H12.5	2.11E-05	2.81E-03	1.50
VPS26BP1	8.49E-05	7.28E-03	1.50
UBE3C	4.53E-05	4.72E-03	1.49
PKM	2.81E-06	6.14E-04	1.49
ZFP91-CNTF	3.16E-05	3.65E-03	1.49
KPNA3	4.28E-06	7.98E-04	1.49
ELK4	1.92E-05	2.63E-03	1.49
SEH1L	7.48E-05	6.56E-03	1.49
CTDSPL2	5.09E-06	8.68E-04	1.48
RP3-337H4.10	7.31E-05	6.51E-03	1.48
N4BP1	6.15E-05	5.81E-03	1.48
CD3D	2.05E-07	1.02E-04	1.47
GLRX	2.67E-05	3.22E-03	1.47
TCEA1	7.13E-06	1.12E-03	1.47
XPO5	2.37E-05	2.93E-03	1.46
BAG4	9.88E-05	8.03E-03	1.46
MYL12A	3.76E-05	4.11E-03	1.46
CSNK1G1	7.15E-06	1.12E-03	1.46
NAT10	3.24E-05	3.71E-03	1.45
CENPF	5.76E-05	5.55E-03	1.45
PFAS	4.61E-06	8.12E-04	1.45
HNRNPA3P14	7.70E-05	6.69E-03	1.45
TUSC3	6.29E-05	5.90E-03	1.45
C12orf57	8.99E-05	7.44E-03	1.44
ATP6V1A	5.00E-05	5.09E-03	1.43
AC004980.10	1.47E-06	3.89E-04	1.43
SMARCD1	1.58E-05	2.24E-03	1.42
ANAPC13	6.54E-05	6.01E-03	1.42
EIF5B	2.30E-05	2.89E-03	1.42
RAB8B	8.82E-05	7.39E-03	1.42
TMA16	1.26E-05	1.82E-03	1.42
AC009506.2	1.23E-04	9.34E-03	1.41
CAPZA1	2.30E-05	2.89E-03	1.41
CHEK1	2.58E-06	5.82E-04	1.41
ZNF280C	7.45E-05	6.56E-03	1.41
MYH10	3.20E-06	6.68E-04	1.40
BNIP2	2.47E-05	3.03E-03	1.40
IFI6	7.20E-05	6.50E-03	1.40
RTN4	2.02E-06	5.03E-04	1.39
ACOX1	3.69E-05	4.11E-03	1.39
PTGES3	5.19E-07	2.01E-04	1.39
UCP2	1.53E-05	2.18E-03	1.38
RP11-419M24.5	2.18E-05	2.82E-03	1.38
HMGB3	5.15E-05	5.09E-03	1.38
SMC1A	3.71E-05	4.11E-03	1.38
PHF6	5.23E-05	5.11E-03	1.38
GBAS	3.52E-05	4.00E-03	1.38
SORT1	1.87E-05	2.59E-03	1.37
ZDHHC20	6.47E-06	1.05E-03	1.37
GTF2I	1.22E-05	1.77E-03	1.37
MCFD2	1.10E-04	8.72E-03	1.36
SLA	3.69E-05	4.11E-03	1.36
IMPDH2	9.28E-05	7.58E-03	1.36
CDC42P6	1.18E-04	9.22E-03	1.35
GAPDHP17	1.15E-05	1.72E-03	1.35
BUB3	5.17E-05	5.09E-03	1.34
IDH1	1.18E-05	1.74E-03	1.34
KIF20A	5.40E-06	8.98E-04	1.34
NUCKS1	5.67E-06	9.33E-04	1.33
EIF2S3	1.73E-05	2.42E-03	1.33
MYL12AP1	1.27E-04	9.57E-03	1.33
SEPHS1P6	1.15E-04	9.10E-03	1.33
SARAF	5.16E-05	5.09E-03	1.33
CD164	3.41E-06	7.01E-04	1.32
NUCKS1P1	4.21E-05	4.50E-03	1.32
BUB1	3.99E-05	4.32E-03	1.30
ATP1B3	1.20E-04	9.24E-03	1.30

Gene	P-value	FDR	Fold change
DLGAP5	6.74E-05	6.16E-03	1.28
SSRP1	8.83E-05	7.39E-03	1.28
LEPROTL1	2.36E-05	2.93E-03	1.27
SACM1L	6.12E-05	5.81E-03	1.24
UCK2	8.88E-05	7.39E-03	1.24
TAF15	1.30E-04	9.70E-03	1.18
ITM2A	4.49E-05	4.72E-03	1.14

C.4 Genes upregulated upon RUNX1 knockdown in all three cell lines (HPB-ALL, RPMI-8402, and KOPT-K1)

non-silencing control vs. shRUNX1-58 filtered by FDR cutoff 0.01

Gene	P-value	FDR	Fold change
RP11-592H6.3	6.54E-06	1.05E-03	2.29
FLT1	7.50E-05	6.56E-03	2.28
CASP10	1.10E-04	8.72E-03	2.10
ABCD3	3.65E-06	7.29E-04	1.99
DYNLRB1	1.78E-07	9.91E-05	1.99
BHLHE40	1.31E-06	3.82E-04	1.97
DNTT	4.54E-06	8.12E-04	1.77
YPEL5	7.20E-07	2.51E-04	1.70
ERG	2.25E-05	2.89E-03	1.70
ACTG2	1.04E-04	8.36E-03	1.70
ARRDC3	1.02E-04	8.27E-03	1.68
FAM65B	5.80E-05	5.55E-03	1.63
NPC2	8.51E-07	2.70E-04	1.61
SDCBPP2	4.23E-06	7.98E-04	1.60
SS18	1.44E-06	3.89E-04	1.59
UGP2	7.65E-06	1.19E-03	1.56
SDCBPP3	2.06E-06	5.05E-04	1.55
KDM1B	1.24E-04	9.35E-03	1.53
HSD17B10	5.56E-05	5.39E-03	1.50
PNRC1	4.81E-05	4.95E-03	1.48
TMED4	3.02E-05	3.54E-03	1.47
NBPF3	5.02E-05	5.09E-03	1.47
GTF2H1	1.18E-04	9.22E-03	1.47
STRADB	5.08E-05	5.09E-03	1.44
SOCS2	1.20E-04	9.24E-03	1.44
PREPL	9.22E-05	7.58E-03	1.34
GATSL3	7.87E-05	6.79E-03	1.32
UBA6-AS1	1.23E-04	9.34E-03	1.31
NDUFB5	8.66E-05	7.33E-03	1.29
LINC01578	7.26E-05	6.51E-03	1.29
NCOA1	1.20E-04	9.24E-03	1.26
GAS5	1.31E-04	9.75E-03	1.22

C.5 Hierarchical clustering of KOPT-K1 samples

Filtered by a FDR of 0.01 with a fold change of 1.5 or more

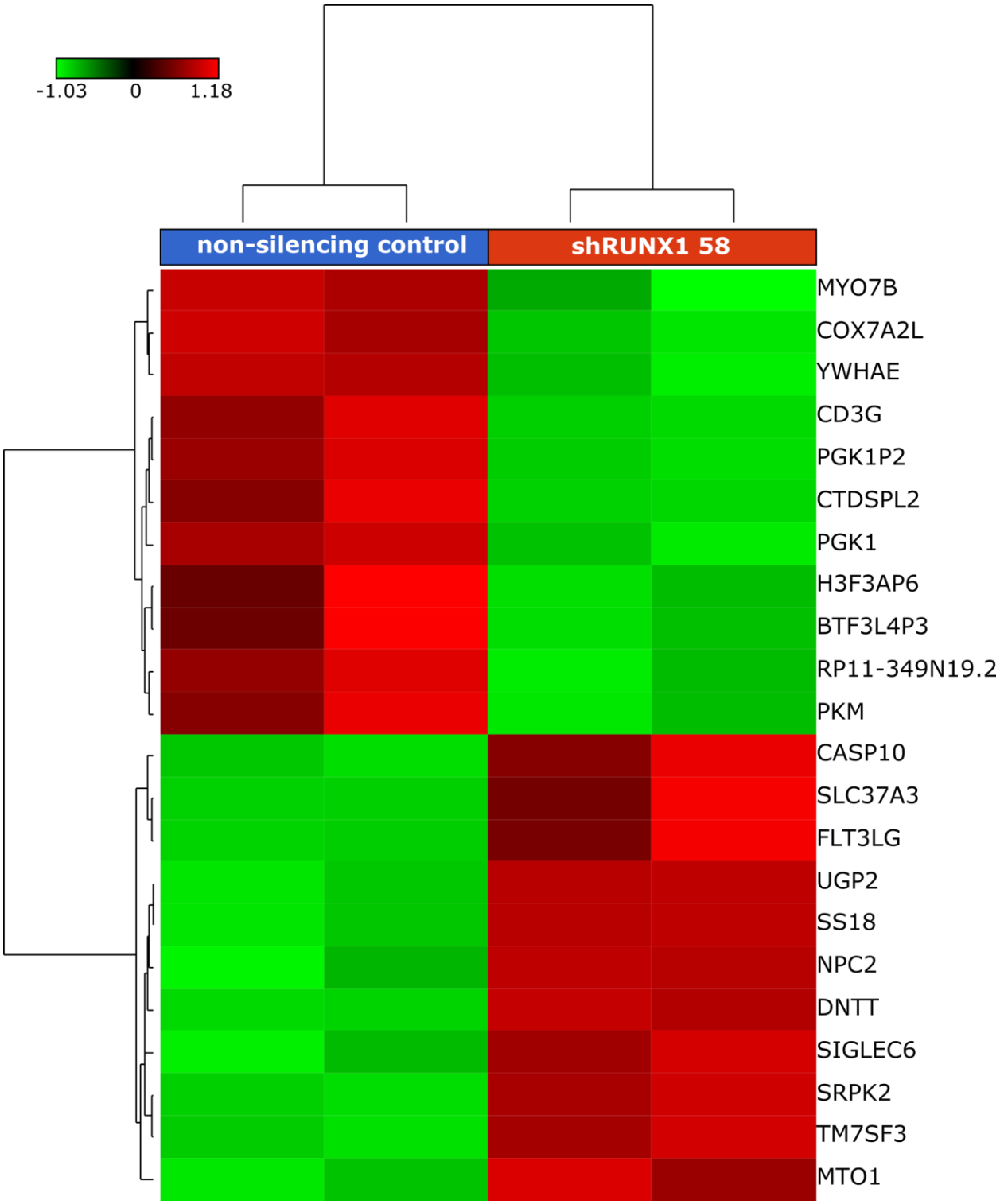

C.6 Genes downregulated upon RUNX1 knockdown in KOPT-K1 samples

non-silencing control vs. shRUNX1-58 filtered by FDR cutoff 0.01 with a fold change of 1.5 or more

Gene	P-value	FDR	Fold change
PGK1P2	3.38E-06	3.94E-03	2.50
H3F3AP6	7.62E-06	6.27E-03	2.42
COX7A2L	6.77E-06	5.91E-03	2.36
PGK1	3.93E-07	1.83E-03	2.32
BTF3L4P3	1.50E-05	9.51E-03	2.28
RP11-349N19.2	1.54E-06	3.00E-03	2.09
PKM	4.59E-06	4.94E-03	1.96
YWHAE	6.34E-06	5.91E-03	1.89
CD3G	1.29E-06	3.00E-03	1.75
MYO7B	1.46E-05	9.51E-03	1.68
CTDSPL2	1.27E-05	8.88E-03	1.60

C.7 Genes upregulated upon RUNX1 knockdown in KOPT-K1 samples

non-silencing control vs. shRUNX1-58 filtered by FDR cutoff 0.01 with a fold change of 1.5 or more

Gene	P-value	FDR	Fold change
DNTT	1.19E-08	1.66E-04	4.67
SIGLEC6	2.04E-06	3.00E-03	4.08
CASP10	8.98E-06	6.61E-03	2.33
FLT3LG	1.40E-06	3.00E-03	2.17
MTO1	8.23E-06	6.39E-03	1.96
NPC2	8.49E-07	2.97E-03	1.87
SS18	2.31E-06	3.00E-03	1.87
SLC37A3	1.84E-06	3.00E-03	1.83
UGP2	2.98E-07	1.83E-03	1.75
TM7SF3	2.36E-06	3.00E-03	1.68
SRPK2	5.00E-06	5.00E-03	1.65

C.8 Hierarchical clustering of HPB-ALL samples

Filtered by a FDR of 0.01 with a fold change of 1.5 or more

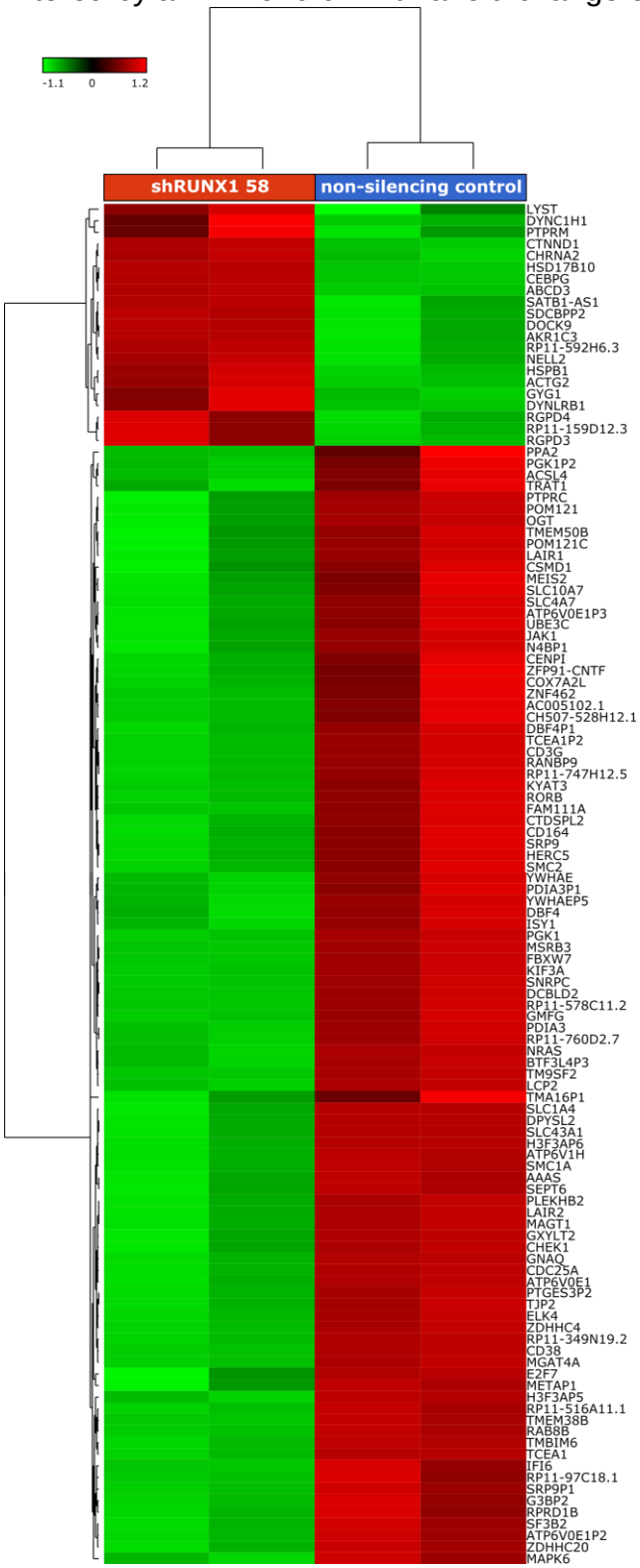

C.9 Genes downregulated by RUNX1 knockdown in HPB-ALL samples

non-silencing control vs. shRUNX1-58 filtered by FDR cutoff 0.01 with a fold change of 1.5 or more

Gene	P-value	FDR	Fold change
CD38	1.82E-06	1.49E-03	4.31
ATP6V0E1P2	2.78E-07	7.19E-04	3.36
RP11-349N19.2	2.40E-08	2.45E-04	3.00
H3F3AP6	7.75E-07	1.22E-03	3.00
PDIA3	1.30E-06	1.26E-03	2.77
ATP6V0E1	7.57E-06	2.86E-03	2.63
CH507-528H12.1	4.73E-05	6.88E-03	2.57
PDIA3P1	1.90E-05	4.74E-03	2.53
SNRPC	2.80E-05	5.01E-03	2.52
PGK1P2	5.21E-06	2.34E-03	2.41
ATP6V0E1P3	5.27E-05	7.29E-03	2.39
PGK1	3.09E-07	7.19E-04	2.37
RP11-578C11.2	2.54E-07	7.19E-04	2.35
MAGT1	1.13E-06	1.26E-03	2.27
DCBLD2	8.66E-07	1.22E-03	2.27
RP11-516A11.1	1.74E-05	4.73E-03	2.25
COX7A2L	1.30E-05	4.04E-03	2.24
AAAS	4.01E-05	6.10E-03	2.24
SRP9P1	3.16E-06	1.91E-03	2.21
PTPRC	1.04E-05	3.37E-03	2.21
KYAT3	2.55E-06	1.78E-03	2.18
HERC5	2.24E-05	4.74E-03	2.16
DPYSL2	6.59E-06	2.63E-03	2.15
ELK4	1.30E-06	1.26E-03	2.15
CDC25A	6.33E-05	8.20E-03	2.14
H3F3AP5	8.75E-07	1.22E-03	2.13
SRP9	1.35E-06	1.26E-03	2.09
BTF3L4P3	3.95E-05	6.07E-03	2.09
RANBP9	1.67E-06	1.46E-03	2.07
PPA2	2.40E-05	4.80E-03	2.04
ZDHHC4	3.31E-05	5.49E-03	2.02
TCEA1P2	1.99E-05	4.74E-03	2.01
AC005102.1	8.35E-05	9.42E-03	1.99
SLC4A7	2.98E-05	5.14E-03	1.98
SLC43A1	5.00E-06	2.34E-03	1.98
MAPK6	8.51E-06	3.05E-03	1.96
ATP6V1H	6.14E-05	8.10E-03	1.96
ACSL4	4.05E-06	2.18E-03	1.95
N4BP1	3.07E-05	5.24E-03	1.95
G3BP2	6.37E-06	2.62E-03	1.93
PLEKHB2	4.79E-05	6.91E-03	1.93
TMEM38B	8.17E-07	1.22E-03	1.93
RORB	2.12E-05	4.74E-03	1.91
PTGES3P2	1.98E-05	4.74E-03	1.91
TM9SF2	7.17E-06	2.78E-03	1.90
RP11-747H12.5	1.64E-05	4.59E-03	1.89
YWHAEP5	3.57E-05	5.61E-03	1.89
JAK1	5.36E-06	2.34E-03	1.89
GNAQ	3.40E-05	5.49E-03	1.87
SLC10A7	3.37E-05	5.49E-03	1.87
MEIS2	5.88E-05	7.90E-03	1.87
IFI6	2.76E-05	5.01E-03	1.86
CENPI	2.83E-05	5.01E-03	1.85
E2F7	2.58E-05	4.89E-03	1.84
POM121C	3.27E-06	1.91E-03	1.84
CTDSPL2	9.80E-07	1.25E-03	1.83
POM121	1.52E-05	4.45E-03	1.82
OGT	9.04E-06	3.16E-03	1.82
YWHAE	1.19E-05	3.78E-03	1.82
RP11-97C18.1	2.05E-05	4.74E-03	1.82
ZNF462	2.29E-05	4.74E-03	1.80
KIF3A	3.21E-06	1.91E-03	1.79
FBXW7	1.77E-05	4.73E-03	1.79
SMC1A	2.06E-06	1.51E-03	1.78
ZFP91-CNTF	2.09E-05	4.74E-03	1.77
UBE3C	1.38E-05	4.21E-03	1.77
LCP2	5.22E-06	2.34E-03	1.77
RAB8B	3.71E-06	2.07E-03	1.76

Gene	P-value	FDR	Fold change
ISY1	6.46E-05	8.28E-03	1.75
SLC1A4	2.81E-05	5.01E-03	1.74
DBF4P1	3.53E-05	5.61E-03	1.74
NRAS	2.26E-05	4.74E-03	1.74
MSRB3	3.20E-05	5.38E-03	1.74
LAIR2	5.68E-05	7.71E-03	1.73
CD3G	1.91E-06	1.49E-03	1.71
SF3B2	2.31E-05	4.74E-03	1.71
TMA16P1	6.90E-05	8.53E-03	1.71
TMEM50B	7.81E-05	9.10E-03	1.70
TMBIM6	2.12E-05	4.74E-03	1.69
GXYLT2	7.27E-05	8.84E-03	1.68
MGAT4A	3.23E-06	1.91E-03	1.67
SMC2	4.55E-05	6.69E-03	1.66
FAM111A	5.09E-06	2.34E-03	1.65
RPRD1B	6.26E-05	8.18E-03	1.64
TCEA1	1.99E-05	4.74E-03	1.63
GMFG	2.55E-05	4.89E-03	1.60
CSMD1	5.10E-05	7.27E-03	1.60
DBF4	1.53E-05	4.45E-03	1.59
RP11-760D2.7	5.15E-05	7.27E-03	1.58
TRAT1	2.92E-05	5.11E-03	1.57
CD164	9.66E-06	3.26E-03	1.56
CHEK1	2.59E-05	4.89E-03	1.56
LAIR1	2.22E-05	4.74E-03	1.54
METAP1	2.44E-05	4.80E-03	1.54
SEPT6	7.46E-05	8.84E-03	1.52
TJP2	7.79E-05	9.10E-03	1.51
ZDHHC20	5.21E-05	7.28E-03	1.51

C.10 Genes upregulated by RUNX1 knockdown in HPB-ALL samples

non-silencing control vs. shRUNX1-58 filtered by FDR cutoff 0.01 with a fold change of 1.5 or more

Gene	P-value	FDR	Fold change
RP11-592H6.3	7.35E-05	8.84E-03	3.03
ACTG2	2.21E-07	7.19E-04	2.53
ABCD3	3.51E-08	2.45E-04	2.49
CHRNA2	5.61E-06	2.38E-03	2.40
AKR1C3	1.64E-05	4.59E-03	2.13
DYNLRB1	6.63E-05	8.43E-03	2.09
RGPD3	1.87E-05	4.74E-03	2.02
SATB1-AS1	9.78E-06	3.26E-03	2.01
DYNC1H1	4.98E-06	2.34E-03	1.87
NELL2	2.76E-05	5.01E-03	1.85
RP11-159D12.3	3.62E-05	5.62E-03	1.75
HSD17B10	3.42E-05	5.49E-03	1.74
SDCBPP2	5.68E-05	7.71E-03	1.74
DOCK9	6.09E-05	8.10E-03	1.71
RGPD4	6.84E-05	8.53E-03	1.69
CEBPG	2.38E-05	4.80E-03	1.69
GYG1	2.21E-05	4.74E-03	1.66
CTNND1	8.34E-06	3.05E-03	1.63
PTPRM	8.04E-05	9.21E-03	1.62
LYST	6.87E-05	8.53E-03	1.60
HSPB1	4.11E-05	6.18E-03	1.51

C.11 Hierarchical clustering of RPMI 8402 samples

Filtered by a FDR of 0.01 with a fold change of 1.5 or more

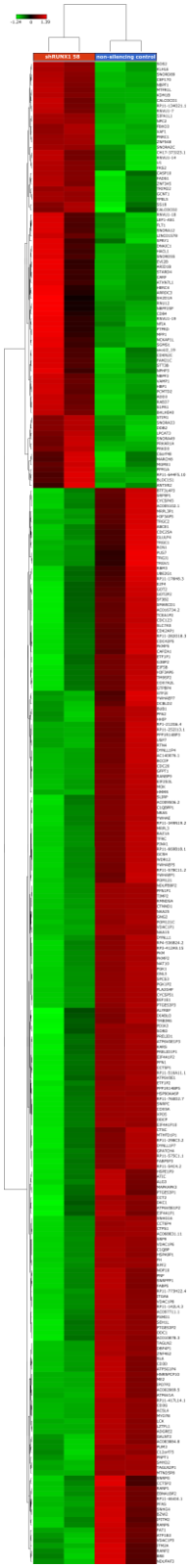

C.12 Genes downregulated by RUNX1 knockdown in RPMI 8402 samples

non-silencing control vs. shRUNX1-58 filtered by FDR cutoff 0.01 with a fold change of 1.5 or more

Gene	P-value	FDR	Fold change
TRGJ1	1.08E-05	2.55E-03	3.84
TRGV1	3.43E-06	1.55E-03	3.78
TRGC2	6.15E-07	7.84E-04	3.53
TRGC1	1.89E-06	1.06E-03	3.48
ITGA6	9.93E-07	8.99E-04	3.31
CD3G	8.99E-10	1.26E-05	3.01
MTND5P8	9.72E-08	4.53E-04	2.95
PKMP2	2.59E-06	1.39E-03	2.85
CD3D	2.95E-08	2.06E-04	2.80
PGK1P2	1.15E-06	9.45E-04	2.74
SNRPC	1.23E-05	2.56E-03	2.65
ITM2A	5.76E-07	7.84E-04	2.63
RP11-176H8.3	1.74E-04	8.52E-03	2.62
RP4-536B24.2	2.37E-05	3.33E-03	2.58
CDC25A	8.78E-06	2.27E-03	2.56
GOT2P2	1.16E-04	6.95E-03	2.47
PFN1P1	8.25E-07	8.87E-04	2.46
PGK1	2.11E-07	7.37E-04	2.43
PPP1R14BP5	5.73E-05	5.02E-03	2.42
FABP5P3	1.35E-05	2.66E-03	2.38
ATP6V0E1P3	4.16E-05	4.16E-03	2.38
PLA2G4F	1.26E-05	2.56E-03	2.36
POM121	5.09E-07	7.84E-04	2.34
NOP10	2.13E-05	3.28E-03	2.31
ETF1P1	8.89E-05	6.22E-03	2.28
RP11-516A11.1	1.37E-05	2.66E-03	2.24
LZTFL1	1.11E-04	6.86E-03	2.23
AC005102.1	1.92E-05	3.22E-03	2.22
YWHAEP5	3.98E-06	1.64E-03	2.21
ADGRE2	7.48E-07	8.71E-04	2.20
PKMP5	4.03E-05	4.10E-03	2.19
POM121C	2.72E-07	7.61E-04	2.18
ZNF462	1.44E-06	1.02E-03	2.17
AC016734.2	9.51E-05	6.30E-03	2.17
SNHG4	5.20E-06	1.82E-03	2.16
DYNLL1P4	6.21E-05	5.29E-03	2.16
SLC7A5	8.26E-05	6.08E-03	2.14
YWHAEP1	1.43E-05	2.73E-03	2.13
ATP6V0E1	5.63E-05	5.01E-03	2.13
E2F4	1.10E-04	6.81E-03	2.11
HHIP	2.25E-04	9.74E-03	2.11
PKM	1.66E-06	1.02E-03	2.10
BTF3L4P3	3.84E-05	4.03E-03	2.09
COX7A2L	2.79E-05	3.64E-03	2.07
YWHAE	1.58E-06	1.02E-03	2.07
CYCSP51	1.37E-06	1.02E-03	2.07
TIMP2	9.85E-07	8.99E-04	2.06
RP11-773H22.4	1.76E-06	1.02E-03	2.06
DBF4P1	2.96E-06	1.50E-03	2.05
ETF1P2	2.71E-05	3.61E-03	2.02
PUS7	1.86E-04	8.89E-03	2.02
PTGES3P1	5.01E-05	4.63E-03	2.02
PPP1R14BP3	1.23E-05	2.56E-03	2.01
RP3-412A9.15	7.64E-06	2.09E-03	2.00
TFRC	5.79E-07	7.84E-04	2.00
GNG2	1.03E-06	8.99E-04	1.98
GOT2	7.65E-05	5.78E-03	1.97
PPA2	3.41E-05	3.96E-03	1.97
ATP6V0E1P2	6.42E-05	5.38E-03	1.97
DYNLL1P7	5.39E-05	4.83E-03	1.96
MRPL3P1	1.50E-05	2.83E-03	1.95
RCN1	2.51E-05	3.47E-03	1.95
BRE	6.89E-05	5.51E-03	1.94
RP11-578C11.2	3.22E-06	1.50E-03	1.94
RANP2	1.93E-04	9.16E-03	1.92
PTGES3P3	7.28E-06	2.04E-03	1.92
SRP9	4.56E-06	1.72E-03	1.92
PTGES3P2	1.71E-05	3.06E-03	1.91
CTNND1	5.13E-07	7.84E-04	1.91

Gene	P-value	FDR	Fold change
NRAS	5.10E-06	1.82E-03	1.90
FAT1	3.68E-06	1.56E-03	1.90
KARS	4.45E-05	4.35E-03	1.90
SLA	6.12E-06	1.99E-03	1.89
SORD	1.70E-04	8.51E-03	1.88
YWHAEP7	4.41E-05	4.35E-03	1.88
SEH1L	2.38E-05	3.33E-03	1.88
NAT10	6.71E-06	2.04E-03	1.88
FABP5	1.15E-05	2.55E-03	1.85
ODC1	1.16E-05	2.55E-03	1.85
GCSH	2.91E-05	3.73E-03	1.85
SRP9P1	3.75E-05	4.02E-03	1.84
NDUFB9P2	3.14E-05	3.96E-03	1.84
C1QBP	1.67E-06	1.02E-03	1.84
GPATCH4	2.12E-04	9.55E-03	1.83
MYO7B	3.59E-06	1.56E-03	1.83
SNHG16	1.17E-05	2.55E-03	1.83
H3F3AP6	2.06E-04	9.39E-03	1.83
PDIA3	1.33E-04	7.57E-03	1.83
CDC42P5	5.70E-05	5.02E-03	1.82
VDAC1P8	3.93E-05	4.04E-03	1.81
RBM3	1.45E-04	7.82E-03	1.81
CDK2AP1	2.07E-05	3.24E-03	1.81
CCT6P4	1.61E-04	8.28E-03	1.81
AC068831.11	3.88E-05	4.04E-03	1.80
PNPT1	3.42E-05	3.96E-03	1.80
GNL3	6.03E-06	1.99E-03	1.79
HSPE1P9	3.62E-05	3.96E-03	1.79
ODCP	5.79E-05	5.02E-03	1.79
RP11-464I4.1	2.08E-05	3.24E-03	1.79
HNRNPCP10	3.62E-05	3.96E-03	1.78
TAGLN2P1	1.57E-05	2.92E-03	1.78
RP11-669B18.1	9.70E-05	6.36E-03	1.77
XPO5	2.22E-05	3.32E-03	1.77
RANP1	6.91E-06	2.04E-03	1.76
AC097711.1	5.52E-06	1.88E-03	1.76
RP1-212G6.4	9.30E-05	6.22E-03	1.76
SMYD2	2.31E-05	3.32E-03	1.75
RP11-575C1.1	3.27E-05	3.96E-03	1.75
G3BP2	2.55E-05	3.47E-03	1.75
PRELID1P1	1.47E-04	7.92E-03	1.75
RP11-282O18.3	1.54E-04	8.09E-03	1.74
CYCSP45	1.91E-04	9.07E-03	1.74
TAGLN2	1.23E-05	2.56E-03	1.74
PNP	1.51E-04	8.00E-03	1.73
RP11-760D2.7	8.01E-06	2.11E-03	1.73
SNRPFP1	2.23E-05	3.32E-03	1.72
ALG3	2.00E-04	9.32E-03	1.72
AC009506.2	1.93E-05	3.22E-03	1.72
EBNA1BP2	1.02E-05	2.55E-03	1.72
WDR12	2.28E-05	3.32E-03	1.72
CCT5P2	1.08E-04	6.79E-03	1.72
RP11-349N19.2	3.35E-05	3.96E-03	1.71
VDAC1P1	1.02E-04	6.57E-03	1.71
EIF4A1P10	3.52E-05	3.96E-03	1.70
MAPKAPK3	2.14E-04	9.55E-03	1.70
C1QBPP1	1.63E-04	8.34E-03	1.69
PFAS	1.14E-05	2.55E-03	1.69
EIF2S3L	2.07E-05	3.24E-03	1.69
EIF5B	4.95E-05	4.63E-03	1.68
AC083884.8	6.21E-05	5.29E-03	1.68
TCEA1P2	2.35E-04	9.97E-03	1.68
PFN1	2.84E-05	3.68E-03	1.68
EIF4A1P2	1.24E-04	7.31E-03	1.68
CTSC	5.14E-05	4.70E-03	1.68
HSP90AA6P	1.82E-04	8.83E-03	1.68
DIABLO	2.37E-04	9.99E-03	1.67
NDUFAF3	1.43E-04	7.79E-03	1.67
DYNLL1	3.23E-05	3.96E-03	1.66
RPF2	9.11E-05	6.22E-03	1.66
SLIRP	1.76E-04	8.61E-03	1.66
AC010878.3	1.98E-04	9.28E-03	1.66
PUM3	1.70E-04	8.51E-03	1.66
CCT2	5.03E-05	4.63E-03	1.66
ATP6V1A	3.59E-05	3.96E-03	1.65
ALYREF	2.04E-04	9.39E-03	1.65
NAA15	4.35E-06	1.69E-03	1.65

Gene	P-value	FDR	Fold change
SPCS3	1.75E-05	3.06E-03	1.65
AC140076.1	7.24E-05	5.59E-03	1.64
RP11-142L4.3	2.78E-05	3.64E-03	1.64
GTPBP4	2.00E-04	9.32E-03	1.64
DCBLD2	1.10E-04	6.83E-03	1.64
RP11-54C4.2	8.01E-05	5.96E-03	1.64
PRELID1	1.58E-04	8.18E-03	1.63
C12orf75	1.81E-05	3.13E-03	1.63
H3F3AP5	6.97E-05	5.51E-03	1.62
RP11-417L14.1	6.30E-06	2.00E-03	1.61
EIF4A1P1	1.61E-04	8.30E-03	1.61
NAA25	3.41E-05	3.96E-03	1.61
SMARCD1	1.50E-04	7.98E-03	1.61
SNRPG	7.62E-05	5.78E-03	1.61
CDC20	9.20E-05	6.22E-03	1.61
HSPA9P1	4.81E-05	4.54E-03	1.61
MRPL3	1.11E-05	2.55E-03	1.60
RP11-252I13.1	6.96E-05	5.51E-03	1.60
TM9SF2	1.14E-04	6.92E-03	1.60
RMND5A	3.46E-05	3.96E-03	1.60
EEF1E1	7.70E-05	5.79E-03	1.60
ACSL4	1.15E-04	6.95E-03	1.59
IFITM2	2.38E-04	9.99E-03	1.59
FH	2.22E-04	9.68E-03	1.59
BZW2	1.30E-04	7.52E-03	1.59
VDAC1P6	1.70E-04	8.51E-03	1.59
ATIC	4.05E-05	4.10E-03	1.59
ATP5G1P4	2.19E-04	9.67E-03	1.58
USP7	1.02E-05	2.55E-03	1.58
VDAC1P3	1.51E-04	8.00E-03	1.58
COX5A	1.73E-04	8.52E-03	1.57
TMBIM6	7.32E-05	5.62E-03	1.57
ABCE1	8.80E-05	6.21E-03	1.57
RP11-298C3.2	1.18E-04	7.01E-03	1.57
RANBP9	1.56E-04	8.13E-03	1.57
GALNT2	4.11E-05	4.13E-03	1.56
ATP1B3	7.13E-05	5.54E-03	1.56
MTHFD1P1	2.20E-04	9.68E-03	1.55
MOK	1.09E-04	6.81E-03	1.55
PSMD1	6.77E-05	5.51E-03	1.55
SF3B2	1.34E-04	7.57E-03	1.55
RANP6	2.28E-04	9.81E-03	1.54
CAPZA1	9.25E-05	6.22E-03	1.54
LCK	7.96E-05	5.95E-03	1.54
DKC1	1.65E-04	8.44E-03	1.53
CDC123	1.72E-04	8.52E-03	1.53
CCT5P1	1.69E-04	8.51E-03	1.53
PINX1	1.15E-04	6.94E-03	1.53
GLULP4	2.13E-04	9.55E-03	1.53
GTF2I	8.08E-05	5.97E-03	1.52
BCCIP	2.11E-04	9.53E-03	1.52
RTN4	2.09E-05	3.24E-03	1.52
HMMR	1.06E-04	6.73E-03	1.52
GFPT1	1.36E-04	7.57E-03	1.52
BAZ1A	8.56E-05	6.17E-03	1.51
BUB1	3.79E-05	4.02E-03	1.51
IPO7P2	2.17E-04	9.62E-03	1.51
UBE2G1	2.04E-04	9.39E-03	1.51
CTPS1	1.35E-04	7.57E-03	1.50
ME2	1.24E-04	7.31E-03	1.50
AC002069.5	1.08E-04	6.79E-03	1.50

C.13 Genes upregulated by RUNX1 knockdown in RPMI 8402 samples

non-silencing control vs. shRUNX1-58 filtered by FDR cutoff 0.01 with a fold change of 1.5 or more

Gene	P-value	FDR	Fold change
CD84	1.74E-05	3.06E-03	3.29
RNU12	6.37E-05	5.36E-03	2.85
STARD4	7.84E-06	2.11E-03	2.54
FLT1	6.89E-05	5.51E-03	2.47
PTPRD	2.00E-05	3.24E-03	2.45
KDM1B	6.17E-07	7.84E-04	2.43
ADD3	3.20E-06	1.50E-03	2.39
SPRY1	9.24E-05	6.22E-03	2.36
ANTXR2	1.26E-05	2.56E-03	2.30
SH2D1A	3.92E-05	4.04E-03	2.28
TRIM22	3.62E-05	3.96E-03	2.22
U1	1.03E-04	6.62E-03	2.20
Mar-08	9.32E-05	6.22E-03	2.17
EVI2B	1.13E-04	6.90E-03	2.12
BHLHE40	6.87E-06	2.04E-03	2.10
NBPF25P	1.39E-04	7.65E-03	2.06
LEF1-AS1	7.31E-06	2.04E-03	2.05
S1PR1	6.34E-05	5.36E-03	2.05
ARRDC3	2.31E-04	9.87E-03	2.04
SNORA2C	2.23E-05	3.32E-03	2.01
snoU2_19	3.79E-05	4.02E-03	2.01
GCNT1	1.36E-04	7.57E-03	2.00
ARID1B	1.66E-05	3.01E-03	2.00
SNORA12	8.72E-05	6.20E-03	1.98
NCKAP1L	2.27E-05	3.32E-03	1.98
SNORA33	1.16E-05	2.55E-03	1.98
ZNF345	2.59E-05	3.48E-03	1.97
NFIA	1.16E-04	6.95E-03	1.96
XAF1	7.12E-05	5.54E-03	1.94
VAMP1	1.47E-06	1.02E-03	1.93
CARF	4.68E-05	4.50E-03	1.92
RNVU1-7	5.02E-05	4.63E-03	1.90
BLOC1S1	1.34E-05	2.66E-03	1.90
CDKN2C	3.32E-05	3.96E-03	1.89
CASP10	9.96E-05	6.47E-03	1.89
YPEL5	1.94E-05	3.22E-03	1.85
NPHP3	1.18E-04	7.01E-03	1.83
SGMS1	1.05E-04	6.70E-03	1.83
RNVU1-14	1.56E-04	8.13E-03	1.82
CH17-373J23.1	1.56E-04	8.13E-03	1.82
RP11-644F5.10	3.49E-05	3.96E-03	1.77
NBPF3	4.68E-06	1.72E-03	1.77
NBPF1	4.15E-06	1.66E-03	1.76
PNRC1	1.15E-05	2.55E-03	1.75
NPC2	3.04E-06	1.50E-03	1.74
RP11-134O21.1	6.73E-05	5.51E-03	1.72
RNVU1-18	4.57E-05	4.44E-03	1.72
RNVU1-19	1.95E-04	9.19E-03	1.69
ATXN7L1	9.66E-05	6.36E-03	1.68
RAB37	4.72E-05	4.50E-03	1.68
MGME1	1.85E-04	8.89E-03	1.67
DNAJC1	7.59E-05	5.78E-03	1.66
HACL1	1.36E-04	7.57E-03	1.66
PPM1A	3.72E-05	4.02E-03	1.65
FRS2	2.14E-04	9.55E-03	1.64
SNORD55	1.33E-04	7.57E-03	1.64
CALCOCO1	2.36E-05	3.33E-03	1.63
FBXO3	9.22E-05	6.22E-03	1.62
CALCOCO2	2.05E-04	9.39E-03	1.62
SS18	2.53E-05	3.47E-03	1.62
SIPA1L1	8.31E-05	6.08E-03	1.61
HERC4	2.07E-04	9.39E-03	1.61
PCMTD2	7.07E-05	5.54E-03	1.59
C6orf48	1.13E-04	6.90E-03	1.59
PRKD3	2.22E-04	9.68E-03	1.59
HBP1	5.78E-05	5.02E-03	1.59
LPCAT3	2.93E-05	3.73E-03	1.58
SOS2	6.59E-05	5.48E-03	1.58
CEP170	8.56E-05	6.17E-03	1.58

Gene	P-value	FDR	Fold change
ZNF548	5.36E-05	4.83E-03	1.57
MPP1	2.04E-04	9.39E-03	1.57
SNORD89	3.56E-05	3.96E-03	1.56
STT3B	1.35E-04	7.57E-03	1.56
MTFR1L	1.02E-04	6.57E-03	1.56
DDB2	4.74E-05	4.50E-03	1.55
LINC01578	9.26E-05	6.22E-03	1.55
FADS1	1.43E-04	7.80E-03	1.55
PRKAR1A	7.30E-06	2.04E-03	1.54
STIM1	1.65E-05	3.01E-03	1.54
FAM21C	1.83E-04	8.83E-03	1.51
KLHL6	4.44E-05	4.35E-03	1.51
SNORA49	5.32E-05	4.83E-03	1.51